RADIOLOGY AND ONCOLOGY

vol.46 no.3
september 2012

SKRAJŠAN POVZETEK GLAVNIH ZNAČILNOSTI ZDRAVILA

Ime zdravila ALIMTA 100 mg prašek za koncentrat za raztopino za infundiranje in ALIMTA 500 mg prašek za koncentrat za raztopino za infundiranje **Kakovostna in količinska sestava** ALIMTA 100 mg: vsaka viala vsebuje 100 mg pemetrekseda (v obliki dinatrijevega pemetrekseda). Po pripravi vsebuje vsaka viala 25 mg/ml pemetrekseda. Pomožne snovi: Vsaka viala vsebuje približno 11 mg natrija, manitol, klorovodikova kislina, natrijev hidroksid. ALIMTA 500 mg: vsaka viala vsebuje 500 mg pemetrekseda (v obliki dinatrijevega pemetrekseda). Po pripravi vsebuje vsaka viala 25 mg/ml pemetrekseda. Pomožne snovi: Vsaka viala vsebuje približno 54 mg natrija, manitol, klorovodikova kislina, natrijev hidroksid. **Terapevtske indikacije:** ALIMTA je v kombinaciji s cisplatinom indicirana za zdravljenje bolnikov z neresektabilnim malignim plevralnim mezoteliomom, ki jih še nismo zdravili s kemoterapijo. ALIMTA je v kombinaciji s cisplatinom indicirana kot zdravljenje prvega izbora za bolnike z lokalno napredovalim ali metastatskim nedrobnoceličnim karcinomom pljuč, ki nima pretežno ploščatocelične histologije. ALIMTA je indicirana kot monoterapija za zdravljenje lokalno napredovalega ali metastatskega nedrobnoceličnega pljučnega karcinoma, ki nima pretežno ploščatocelične histologije pri bolnikih, pri katerih bolezen ni napredovala neposredno po kemoterapiji na osnovi platine. ALIMTA je indicirana kot monoterapija za zdravljenje drugega izbora bolnikov z lokalno napredovalim ali metastatskim nedrobnoceličnim pljučnim karcinomom, ki nima pretežno ploščatocelične histologije. **Odmerjanje in način uporabe:** *Odmerjanje:* ALIMTO smemo dajati le pod nadzorom zdravnika, usposobljenega za uporabo kemoterapije za zdravljenje raka. ALIMTA v kombinaciji s cisplatinom Priporočeni odmerek ALIMTE je 500 mg/m2 telesne površine (TP), dan kot intravenska infuzija v 10 minutah prvi dan vsakega 21-dnevnega ciklusa. Priporočeni odmerek cisplatina je 75 mg/m2 TP, infundiran v dveh urah približno 30 minut po zaključku infuzije pemetrekseda prvi dan vsakega 21 dnevnega ciklusa. Bolniki morajo prejeti zadostno antiemetično zdravljenje, pred in/ali po prejemanju cisplatina jih moramo tudi ustrezno hidrirati. *ALIMTA kot samostojno zdravilo* Priporočeni odmerek ALIMTE je 500 mg/m2 TP, dan kot intravenska infuzija v 10 minutah prvi dan vsakega 21 dnevnega ciklusa. *Režim premedikacije* Da zmanjšamo incidenco in resnost kožnih reakcij, dajemo kortikosteroid dan pred dajanjem pemetrekseda, na dan dajanja pemetrekseda in naslednji dan. Kortikosteroid naj ustreza 4 mg deksametazona, danega peroralno dvakrat dnevno. Za zmanjšanje toksičnosti morajo bolniki dnevno jemati tudi peroralno folno kislino ali multivitaminski pripravek, ki jo vsebuje (350 do 1000 mikrogramov). V sedmih dneh pred prvim odmerkom pemetrekseda morajo vzeti vsaj pet odmerkov folne kisline, odmerjanje pa morajo nadaljevati ves čas zdravljenja in še 21 dni po zadnjem odmerku pemetrekseda. Bolniki morajo prejeti tudi intramuskularno injekcijo vitamina B12 (1000 mikrogramov) v tednu pred prvim odmerkom pemetrekseda in enkrat vsake tri cikluse zatem. Kasnejše injekcije vitamina B12 lahko dajemo isti dan kot pemetreksed. **Kontraindikacije:** Preobčutljivost za zdravilno učinkovino ali katerokoli pomožno snov. Dojenje. Sočasno cepljenje proti rumeni mrzlici. **Posebna opozorila in previdnostni ukrepi:** Pemetreksed lahko zavre delovanje kostnega mozga, kar se kaže kot nevtropenija, trombocitopenija in anemija (ali pancitopenija). Mielosupresija običajno predstavlja toksičnost za omejitev odmerka. Pri bolnikih, ki pred zdravljenjem niso prejemali kortikosteroidov, so poročali o kožnih reakcijah. Uporabe pemetrekseda pri bolnikih z očistkom kreatinina < 45 ml/min ne priporočamo. Bolniki z blagim do zmernim popuščanjem delovanja ledvic naj se izogibajo jemanju nesteroidnih protivnetnih zdravil (NSAID), denimo, ibuprofena in acetilsalicilne kisline 2 dni pred dajanjem pemetrekseda, na dan dajanja in še 2 dni po dajanju pemetrekseda. Vsi bolniki, ki jih lahko zdravimo s pemetreksedom, naj se izogibajo jemanju NSAID-ov z dolgimi razpolovnimi časi izločanja vsaj 5 dni pred dajanjem pemetrekseda, na dan dajanja in še vsaj 2 dni po dajanju pemetrekseda. Poročali so o resnih ledvičnih primerih, vključno z akutno ledvično odpovedjo, s pemetreksedom samim ali v povezavi z drugimi kemoterapevtiki. Pri bolnikih s klinično pomembno tekočino tretjega prostora moramo razmisliti o drenaži izliva pred dajanjem pemetrekseda. Kot posledico toksičnosti pemetrekseda v kombinaciji s cisplatinom za prebavila so opažali hudo dehidracijo, zato moramo bolnike pred prejemanjem terapije in/ali po njej ustrezno hidrirati, prejeti morajo zadostno antiemetično zdravljenje. Občasno so v kliničnih študijah pemetrekseda, običajno ob sočasnem dajanju z drugo citotoksično učinkovino, poročali o resnih srčnožilnih dogodkih, vključno z miokardnim infarktom in možganskožilnimi dogodki. Odsvetujemo uporabo živih oslabljenih cepiv. Spolno zrelim moškim odsvetujemo zaploditev otroka v času zdravljenja in še 6 mesecev zatem. Priporočamo ukrepe proti zanositvi ali vzdržnost. Zaradi možnosti, da zdravljenje s pemetreksedom povzroči trajno neplodnost, naj se moški pred začetkom zdravljenja posvetujejo o shranjevanju semena. Ženske v rodni dobi morajo v času zdravljenja s pemetreksedom uporabljati učinkovito kontracepcijo. Poročali so o primerih radiacijske pljučnice pri bolnikih, ki so jih zdravili z radiacijo pred, med ali po zdravljenju s pemetreksedom. Poročali so o radiacijskem izpuščaju pri bolnikih, ki so se zdravili z radioterapijo pred tedni ali leti. **Medsebojno delovanje z drugimi zdravili in druge oblike interakcij:** Sočasno dajanje nefrotoksičnih zdravil (denimo, aminoglikozidov, diuretikov zanke, spojin platine, ciklosporina) lahko potencialno povzroči zakasnjeni očistek pemetrekseda. Sočasno dajanje snovi, ki se tudi izločajo s tubulno sekrecijo (denimo, probenecid, penicilin), lahko potencialno povzroči zakasnjeni očistek pemetrekseda. Pri bolnikih z normalnim delovanjem ledvic lahko visoki odmerki nesteroidnih protivnetnih zdravil (NSAID-i, denimo, ibuprofen) in acetilsalicilna kislina v visokih odmerkih zmanjšajo eliminacijo pemetrekseda in tako lahko povečajo pojavnost neželenih učinkov pemetrekseda. Pri bolnikih z blagim do zmernim popuščanjem delovanja ledvic se moramo izogibati sočasnemu dajanju pemetrekseda z NSAID-i (denimo, ibuprofenom) ali acetilsalicilne kisline v visokih odmerkih 2 dni pred dajanjem pemetrekseda, na dan dajanja in še 2 dni po dajanju pemetrekseda. Sočasnemu dajanju NSAID-ov z daljšimi razpolovnimi časi s pemetreksedom se moramo izogibati vsaj 5 dni pred dajanjem pemetrekseda, na dan dajanja in še vsaj 2 dni po dajanju pemetrekseda.Velika različnost med posamezniki v koagulacijskem statusu v času bolezni ter možnost medsebojnega delovanja med peroralnimi antikoagulacijskimi učinkovinami ter kemoterapijo proti raku zahtevata povečano pogostnost spremljanja INR. **Kontraindicirana sočasna uporaba:** Cepivo proti rumeni mrzlici: tveganje za smrtno generalizirano bolezen po cepljenju. **Odsvetovana sočasna uporaba:** Živa oslabljena cepiva (razen proti rumeni mrzlici): tveganje za sistemsko, potencialno smrtno bolezen. **Neželeni učinki** Klinične študije malignega plevralnega mezotelioma *Zelo pogosto:* znižani nevtrofilci/granulociti, znižani levkociti, znižan hemoglobin, znižani trombociti, nevropatija-senzorna, diareja, bruhanje, stomatitis/faringitis, slabost, anoreksija, zaprtje, izpuščaj, alopecija, povišan kreatinin, znižan očistek kreatinina, utrujenost. *Pogosti:* dehidracija, motnje okusa, konjuktivitis, dispepsija. Klinične študije nedrobnoceličnega pljučnega karcinoma - ALIMTA monoterapija, zdravljenje 2. izbora: *Zelo pogosti:* znižan nevtrofilci/granulociti, znižani levkocitit, znižan hemoglobin, diareja, bruhanje, stomatitis/faringitis, slabost, anoreksija, izpuščaj/luščenje, utrujenost. *Pogosti:* znižani trombociti, zaprtje, povišanje SGPT (ALT), povišanje SGOT (AST), srbenje, alopecija, povišana telesna temperatura. Klinične študije nedrobnoceličnega pljučnega karcinoma - ALIMTA v kombinaciji s cisplatinom, zdravljenje 1. izbora: *Zelo pogosti:* znižan hemoglobin, znižani nevtrofilci/granulociti, znižani levkocitit, znižani trombociti, slabost, bruhanje, anoreksija, zaprtje, stomatitis/faringitis, diareja brez kolostomije, alopecija, izpuščaj/luščenje, povišan kreatinin, utrujenost. *Pogosti:* nevropatija-senzorična, motnje okusa, dispepsija/zgaga. Klinične študije nedrobnoceličnega pljučnega karcinoma - ALIMTA monoterapija, vzdrževalno in nadaljevalno zdravljenje: *Zelo pogosti:* znižan hemoglobin, slabost, anoreksija, utrujenost. *Pogosti:* znižani levkociti, znižani nevtrofilci, nevropatija-senzorična, bruhanje, mukozitis/stomatitis, povišanje ALT (SGPT), povišanje AST (SGOT), izpuščaj/luščenje, bolečina. Občasno so v kliničnih študijah pemetrekseda poročali o primerih resnih srčnožilnih in možganskožilnih dogodkov, vključno z miokardnim infarktom, angino pektoris, cerebrovaskularnim insultom in prehodnimi ishemičnimi atakami; primerih kolitisa ter o primerih intersticijske pljučnice z respiratorno insuficience, primerih edema, o ezofagitisu/radiacijskem ezofagitisu in o primerih sepse. Redkeje pa o primerih potencialno resnega hepatitisa in pancitopenije. Po uvedbi zdravila na trg so poročali o primerih akutne odpovedi ledvic s pemetreksedom samim ali v povezavi z drugimi kemoterapevtiki, primerih radiacijske pljučnice pri bolnikih, ki so jih zdravili z radiacijo pred, med ali po njihovem zdravljenju s pemetreksedom, primerih radiacijskega izpuščaja pri bolnikih, ki so se v preteklosti zdravili z radioterapijo, o primerih periferne ishemije, ki je včasih vodila v nekrozo okončin, redkih primerih buloznih stanj, kot sta Stevens-Johnsonov sindrom in toksična epidermalna nekroliza, ki so bila v nekaterih primerih usodna in o redkih primerih hemolitične anemije. **Imetnik dovoljenja za promet** Eli Lilly Nederland B.V., Grootslag 1 5, NL 3991 RA, Houten, Nizozemska. Datum zadnje revizije besedila 24.10.2011. **Način izdaje zdravila:** H. SAMO ZA STROKOVNO JAVNOST.

Podrobnejše informacije o zdravilu Alimta, so dostopne na spletni strani Evropske agencije za zdravila EMA http://www.ema.europa.eu in na lokalnem predstavništvu.

SIALM00025

Eli Lilly Farmacevtska družba, d.o.o.
Brnčičeva 41G, 1231 Ljubljana - Črnuče, Slovenija
Telefon: +386 (0)1 5800 010
Faks: +386 (0)1 5691 705

RADIOLOGY AND ONCOLOGY

September 2012
Vol. 46 No. 3
Pages 179-270
ISSN 1318-2099
UDC 616-006
CODEN: RONCEM

Publisher
Association of Radiology and Oncology

Affiliated with
Slovenian Medical Association – Slovenian Association of Radiology, Nuclear Medicine Society,
Slovenian Society for Radiotherapy and Oncology, and Slovenian Cancer Society
Croatian Medical Association – Croatian Society of Radiology
Societas Radiologorum Hungarorum
Friuli-Venezia Giulia regional groups of S.I.R.M.
Italian Society of Medical Radiology

Aims and scope
Radiology and Oncology is a journal devoted to publication of original contributions in diagnostic and interventional radiology, computerized tomography, ultrasound, magnetic resonance, nuclear medicine, radiotherapy, clinical and experimental oncology, radiobiology, radiophysics and radiation protection.

Editorial office

Radiology and Oncology
Zaloška cesta 2
P. O. Box 2217
SI-1000 Ljubljana
Slovenia
Phone: +386 1 5879 369
Phone/Fax: +386 1 5879 434
E-mail: gsersa@onko-i.si

Reader for English

Vida Kološa

Secretary

Mira Klemenčič

Zvezdana Vukmirović

Design

Monika Fink-Serša, Samo Rovan, Ivana Ljubanović

Layout

Matjaž Lužar

Printed by

Tiskarna Ozimek, Slovenia

Published quarterly in 600 copies

Beneficiary name: DRUŠTVO RADIOLOGIJE IN ONKOLOGIJE
Zaloška cesta 2
1000 Ljubljana
Slovenia

Beneficiary bank account number: SI56 02010-0090006751
IBAN: SI56 0201 0009 0006 751
Our bank name: Nova Ljubljanska banka, d.d.,
Ljubljana, Trg republike 2,
1520 Ljubljana; Slovenia

SWIFT: LJBASI2X

Subscription fee for institutions EUR 100, individuals EUR 50

The publication of this journal is subsidized by the Slovenian Book Agency.

Indexed and abstracted by:
Science Citation Index Expanded (SciSearch®)
Journal Citation Reports/Science Edition
Scopus
PubMed
PubMed Central
EMBASE/Excerpta Medica
DOAJ
Open J-gate
Chemical Abstracts
Biomedicina Slovenica
Summon by Serial Solutions (ProQuest)

This journal is printed on acid- free paper

On the web: ISSN 1581-3207
http://versitaopen.com/ro
http://www.radioloncol.com
http://versita.com/science/medicine/ro/
http://www.onko-i.si/radioloncol/

contents

nuclear medicine

radiology

experimental oncology

clinical oncology

RADIOLOGY AND ONCOLOGY is covered in Science Citation Index Expanded (SciSearch®),Journal Citation Reports/Science Edition, Scopus,

PubMed, PubMed Central, DOAJ, EMBASE/Excerpta Medica, Open J-gate, Chemical Abstracts, Biomedicina Slovenica, Summon by Serial Solutions (ProQuest)

research article

Imaging primary prostate cancer with 11C-Choline PET/CT: relation to tumour stage, Gleason score and biomarkers of biologic aggressiveness

Ji Chen[1], Yong Zhao[1], Xin Li[2], Peng Sun[1], Muwen Wang[1], Ridong Wang[3], Xunbo Jin[1]

[1] Department of Minimally Invasive Urology center, Provincial Hospital Affiliated to Shandong University, Jinan, People's Republic of China

[2] Department of PET/CT Center, Provincial Hospital Affiliated to Shandong University, Jinan, People's Republic of China

[3] Center for Addiction and Mental Health, University of Toronto, Toronto, Canada

Radiol Oncol 2012; 46(3): 179-188.

Received 15 October 2011
Accepted 3 May 2012

Correspondence to:
1. Xunbo Jin: Provincial Hospital Affiliated to Shandong University, 324 Jingwu Road, Jinan, Shandong Province, 250021, People's Republic of China; Phone: +86 531 66953273; Fax: +86 531 87068707; E-mail: dochj@foxmail.com
2. Muwen Wang: Provincial Hospital Affiliated to Shandong University, 324 Jingwu Road, Jinan, Shandong Province, 250021, People's Republic of China;Phone: +86 531 87938911; Fax: +86 531 87904002;E-mail: wangmuwen@sdu.edu.cn

Disclosure: No potential conflicts of interest were disclosed.

Background. As a significant overlap of 11C-Choline standardized uptake value (SUV) between prostate cancer and benign prostate hyperplasia (BPH) tissue, controversy exists regarding the clinical value of 11C-Choline PET/CT scan in primary prostate cancer. In this study, the SUVmax of the prostate lesions and the pelvic muscles were measured and their ratios (SUVmax-P/M ratio) were calculated. Then we evaluated whether the tracer 11C-Choline uptake, quantified as SUVmax-P/M ratio, correlated with tumour stage, Gleason score, and expression levels of several biomarkers of aggressiveness.

Methods. Twenty-six patients with primary prostate cancer underwent 11C-Choline PET/CT. Tumour specimens from these patients were graded histopathologically, and immunnohistochemistry for Ki-67, CD31, androgen receptor (AR), Her-2/neu, Bcl-2, and PTEN were performed.

Results. Both SUVmax and SUVmax-P/M ratio showed no significant difference between patients with tumour stage II and III, but significantly elevated in patients with tumour stage IV. SUVmax-P/M ratio was also significantly higher in lesions with Gleason score of 4+3 or higher versus less than or equal to 3+4. SUVmax-P/M ratio was found significantly correlated with expression levels of Ki-67 and CD31. In addition, a higher SUVmax-P/M ratio was demonstrated in Her-2/neu positive subgroup than negative subgroup. At the same time, Gleason score and expression levels of these biomarkers showed no significant association with SUVmax.

Conclusions. Using the parameter SUVmax-P/M ratio, 11C-Choline PET/CT may be a valuable non-invasive imaging technology in the diagnosis of primary prostate cancer.

Key words: prostate cancer; aggressiveness; PET/CT; choline

Introduction

Prostate cancer is one of the most common malignancies in males and the second leading cause of death in American men.[1] The incidence of prostate cancer increases directly with age; however, this tumour shows variable biologic behaviour, from a clinically silent, indolent intra-prostatic tumour to an aggressive malignancy and causes death in a relatively small proportion of men.[2] Therefore, identifying aggressiveness early in the disease process could be beneficial for therapeutic decision mak-

ing.[3-5] The development of prognostic markers that can accurately predict outcome is crucial to identify patients who could benefit from aggressive therapy.

In recent years, positron emission tomography combined with computed tomography (PET/CT), which allows image fusion of metabolic and anatomical information, has been reported as a non-invasive, whole-body imaging modality commonly used in the evaluation of many neoplasms including prostate cancer.[6,7] PET/CT can provide more information than conventional tumour seeking procedures. This technique shows molecular function and activity that are not available with conventional imaging such as ultrasound and magnetic resonance imaging. In fact, clinical studies performed on several malignant tumours other than prostate cancer have shown that hypermetabolic tumours usually have high tracer uptake and a poor prognosis.[8-13]

The aim of the present study was to evaluate whether the use of 11C-Choline PET/CT would provide a non-invasive metabolic parameter that is associated with the biologic aggressiveness of prostate cancer. Gleason score and tumour stage were selected for analysis. Several molecular biomarkers of key prostate cancer pathogenic pathways including Ki-67 (proliferation), Bcl-2(apoptosis), CD31 (angiogenesis), Her-2/neu (oncogene), PTEN (anti-oncogene), and AR (androgen receptor) were also involved in this study. These data would further confirm the association between 11C-Choline uptake and prostate cancer allowing the integration of this tool into clinical practice.

Patients and methods

This study was approved by the institutional review board of Provincial hospital affiliated to Shandong University, and written consent was obtained from all participants. Twenty-six patients with initial diagnosis of prostate cancer between April 2007 and March 2010 at our center were included in this study. Patients were excluded from this study if they had received antiandrogen therapy before PET/CT. All patients underwent ultrasound-guided transrectal biopsy of their tumour and histologically proved carcinomas. To avoid false positive accumulation of choline caused by existence of inflammatory cells, scanning was performed before histological intervention. And the results of PET/CT scan were taken as reference for biopsy. Patients were staged based on the 2002 American Joint Committee Cancer Staging Manual.[14]

11C-Choline PET/CT

PET/CT studies were performed the same as previously described in detail.[15] 11C-Choline was synthesized according to the solid-phase method in a modified commercial synthesis module (TRACElab, FXc; GE Healthcare). Five minutes after injection of 7.4 MBq/kg of 11C-Choline, PET images were acquired in the supine position over 2 bed positions from the upper pelvis through the midthigh. For patients with a serum prostate specific antigen (PSA) >10 ng/ml, whole body PET/CT imaging was performed (6 bed positions). The parameters of the multidetector helical CT scan were 140 kV, 80 mA, 0.8 seconds per tube rotation, slice thickness of 5mm, pitch of 6, and table speed of 11.25 mm/s. CT and PET images were matched and fused into transaxial, sagittal, and coronal images. The 11C-Choline maximal standardized uptake value (SUVmax) was determined using a circular (1 cm diameter) region of interest. The SUVmax of the prostate lesions (target) and the pelvic muscles (nontarget) were measured and their ratios (P/M) were calculated. The PET/CT findings were compared with histopathologic and immunohistochemical results.

Immunohistochemistry

All samples were taken at the sites selected with direct reference to the PET/CT scan results. As tumour stage of our cohort ranged from II to IV, for the patients who could not receive radical resection, biopsies at the site of abnormal uptake in PET/CT scan were selected for analysis. For immunohistochemical staining, paraffin sections (5-μm thickness) on glass slides coated with poly-L-lysine were deparaffinized in turpentine, hydrated, and then placed in phosphate-buffered saline (PH 7.6). Antigen retrieval was performed by boiling for 15 minutes in 0.01mol/L citrate buffer (PH 6.0). Sections were treated with 3% hydrogen peroxide for 10 minutes to quench endogenous peroxidase activity, rinsed with deionized water, and washed with phosphate-buffered saline. The primary antibodies used included mouse monoclonal antibodies against Ki-67 nuclear antigen (MIB-1), CD31 (JC/70A), AR (AR441), Her-2/neu (CB11), Bcl-2 (Bcl-2-100), and PTEN (28H6). All these antibodies were purchased from ZSGB-BIO (Beijing, China) and diluted at 1:50 dilution. Sections were incubated with the first antibodies overnight at 4°C in a moist chamber and then were washed three times with phosphate-buffered saline. Detection of the antibodies was performed

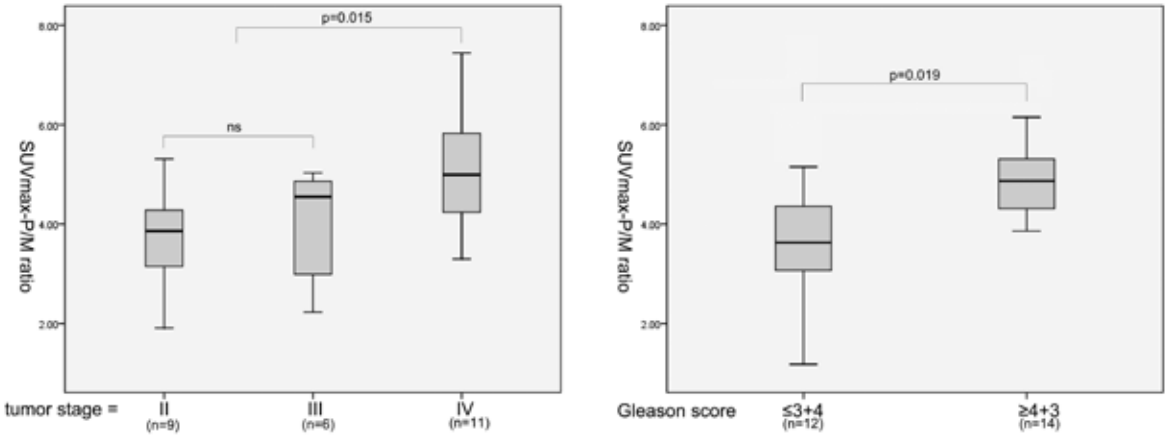

FIGURE 1. 11C-Choline uptake (measured as SUVmax-P/M ratio) according to tumour stage and Gleason score. SUVmax-P/M ratio was significantly higher in patients with tumour stage or Gleason score > 7(3+4).

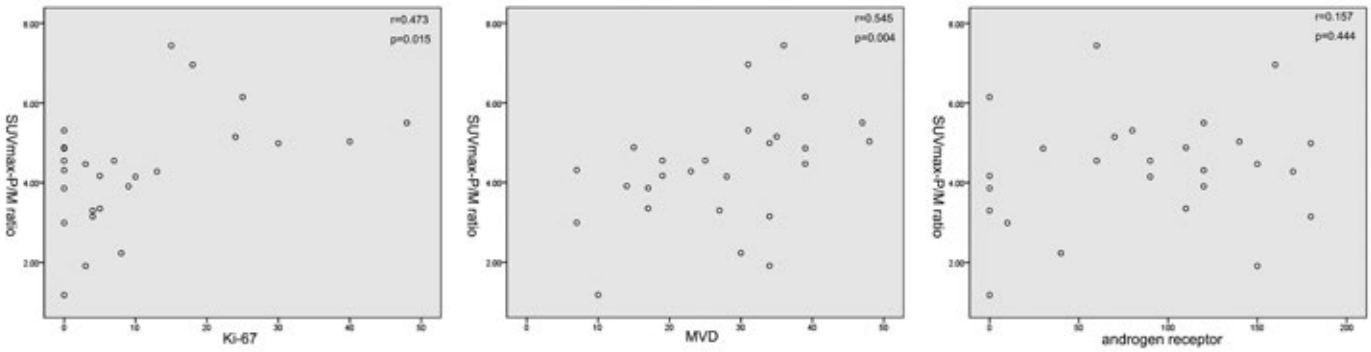

FIGURE 2. Correlation between 11C-Choline uptake (measured as SUVmax-P/M ratio) and expression of Ki-67, CD31 and AR.A statistically significant correlation was found between SUVmax-P/M ratio and expression levels of Ki-67 and CD31.

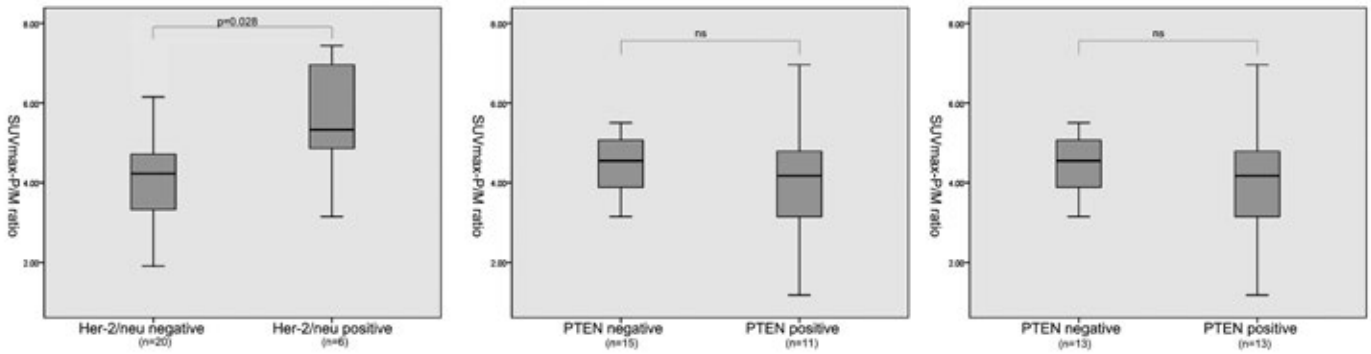

FIGURE 3. 11C-Choline uptake (measured as SUVmax-P/M ratio) according to expression of Her-2/neu, Bcl-2, and PTEN. SUVmax-P/M ratio was significantly higher in patients with Her-2/neu positive staining.

with a non-biotin horseradish peroxidase detection system, PV9000 Polymer Detection System (ZSGB-BIO, Beijing, China). After incubation with the polyperoxidase-anti-mouse/rabbit IgG for 30 minutes at room temperature, the tissue sections were washed with phosphate-buffered saline. Diaminobenzidinetetrahydrochloridechromogen was added for 3 minutes at room temperature, which causes brown precipitate at the antigen site. Sections were counterstained with hematoxylin, dehydrated, and then coverslipped with permount mounting medium.

Each slide was scored by two independent observers who were blinded to the clinicopatho-

TABLE 1. Clinicopathological characteristics of 26 patients with prostatic carcinoma

No.	Age	GS	Stage*	SUVmax	SUVmax-P/M ratio	Initial treatment
1	77	7	IV	6.42	5.5	Antiandrogen therapy
2	74	6	II	3.25	1.91	Radical resection
3	60	7	III	4.86	2.99	Radical resection
4	79	9	II	19.10	5.31	Antiandrogen therapy
5	68	7	IV	4.66	3.30	Antiandrogen therapy
6	69	7	II	5.26	4.15	Radical resection
7	70	5	II	3.31	1.18	Radical resection
8	59	7	III	5.05	4.55	Radical resection
9	63	8	IV	6.49	4.88	Antiandrogen therapy
10	56	9	IV	21.05	6.15	Antiandrogen therapy
11	63	7	II	4.01	4.28	Radical resection
12	63	8	IV	8.23	4.31	Antiandrogen therapy
13	81	7	III	11.58	5.03	Antiandrogen therapy
14	59	9	IV	9.38	7.44	Antiandrogen therapy
15	68	7	IV	24.65	5.15	Antiandrogen therapy
16	68	7	II	5.11	4.47	Radical resection
17	62	6	II	7.58	3.35	Radical resection
18	59	5	IV	4.49	6.96	Antiandrogen therapy
19	63	9	III	14.15	2.23	Radical resection
20	59	9	II	6.39	4.55	Radical resection
21	76	7	IV	8.26	4.99	Antiandrogen therapy
22	64	7	II	1.69	3.15	Radical resection
23	78	7	III	17.83	4.86	Radiotherapy
24	66	5	IV	19.96	3.91	Antiandrogen therapy
25	70	9	II	3.11	3.86	Radical resection
26	58	6	IV	19.11	4.17	Antiandrogen therapy

GS = Gleason Score; SUV = standardized uptake value; *Based on American Joint Committee on Cancer prostate cancer staging system (2002)

logical data of the patients. Approximately 600 neoplastic cells were evaluated on each slide. The results of Ki-67 immunohistochemistry were expressed as the percentage of tumour cells with positive nuclear staining. Expression of PTEN (nuclear staining) was considered to be positive if there was staining of area of the epithelial component of the tumour. Staining of AR (nuclear staining), Her-2/neu (membranous staining), and Bcl-2 (cytoplasmic staining) were scored by evaluating the percentage of staining positively and the intensity of staining. Staining intensity was defined as 0, negative or weak; 1, moderate; or 2, strong. The level of immunohistochemical staining of AR was scored semiquantitatively as the product of the staining intensity score and the percentage of tumour cells with positive staining.[16] As to the staining level of Her-2/neu and Bcl-2, either moderate or strong staining intensity in >10% of tumour cells was considered as positive expression.[17]

To investigate microvessel density (MVD), the number of vessels was counted on a ×400 magnification field (0.15mm^2) in areas of the most intense neovascularization marked by CD31 expression in vascular endothelium from each sample. As in a previous report, any single cell or spot that stained by the CD31 was counted as a vessel. MVD was expressed as the absolute number of microvessels per ×400 field for each case.[17]

Statistical analysis

Statistical analysis was performed using SPSS for Windows 17.0 software (SPSS, Inc., Chicago, IL,

USA). The relationship between SUVmax-P/M ratio and Gleason score, tumour stage, expression levels of Her-2/neu, Bcl-2, PTEN were evaluated using the Mann-Whitney rank sum test. Correlation between MVD, expression levels of Ki-67, AR and SUVmax-P/M ratio was analysed using Spearman's rank correlation test. Probability values of <0.05 indicated a statistically significant difference.

Results

Patients' characteristics are listed in Table 1. The mean age of the patients was 67.1 years (range, 56-81 years). There were 10 patients with stage II, 5 patients with stage III, and 11 patients with stage IV. Fourteen patients had a Gleason score ≥7 (4+3). As initial treatment, 12 patients were treated with radical prostatectomy, 13 patients antiandrogen therapy, and 1 patient radiotherapy. The mean value of SUVmax of the primary tumours in 26 patients was 9.42 ± 6.70 (ranged from 1.69 to 24.65), whereas the mean SUVmax-P/M ratios was 4.33 ± 1.41 (ranged from 1.18 to 7.44). Using 2.3 (SUVmax-P/M raito) as a criterion for differentiating malignant from benign prostatic lesions in our cohort, the sensitivity of 11C-Choline PET/CT imaging was 88.6% (23/26). The mean value of Ki-67 labeling index and AR index was 10.4±13.1 (ranged from 0 to 48) and 86.5 ± 61.8 (ranged from 0 to 180). The mean rate of MVD as assessed by CD31 was 26.4 ± 11.8 (ranged from 7 to 48). Positive expression of Her-2/neu, Bcl-2 and PTEN was recognized in 6, 13, and 11 patients, respectively.

Association of several clinicopathological factors and expression levels of these molecular markers was then analysed. The mean SUVmax in stages II, III, and IV were 5.88 ± 4.96, 10.69 ± 5.69, and 12.06 ± 7.50. The mean SUVmax-P/M ratio in stages II, III, and IV were 3.62 ± 1.26, 3.93 ± 1.25, and 5.16 ± 1.28. Both SUVmax-P/M ratio and SUVmax showed no significant difference between patients with tumour stage II and III (p-value 0.113 and 0.328, respectively), but significantly elevated in patients with tumour stage IV (p-value 0.036 and 0.015, respectively). Furthermore, SUVmax-P/M ratio was also significantly higher in patients with Gleason score of 4+3 or higher versus less than or equal to 3+4 (Figure 1). The correlation coefficients for SUVmax-P/M ratio with Ki-67 and MVD were 0.503 and 0.545, and the P values for both of these two biomarkers correlations were <0.05 (Figure 2). As shown in Figure 3, SUVmax-P/M raito was higher in Her-2/neu positive subgroup than negative subgroup. In contrast, neither Gleason score nor expression levels of the biomarkers involved in the study associated with SUVmax.

Figure 4 and Figure 5 showed PET/CT imaging and immunohistochemistry results from two patients (patient 17 and patient 1). Patient 1, with tumour stage IV and a Gleason score of 7(4+3), demonstrated relatively higher expression levels of Ki-67, CD31, AR, PTEN and Her-2/neu. However, a higher SUVmax was found in patient 17 (7.58 versus 6.42). At the same time, uptake of 11C-Choline in patient 17 was also higher than in patient 1 (2.26 versus 1.17), which resulted in a relatively lower SUVmax-P/M ratio in patient 17 (3.35 versus 5.50).

Discussion

PET is a whole-body non-invasive imaging technique that has great diagnostic value because it can identify damage by counting metabolic activity which is not available with other conventional imaging modalities. PET/CT, which combines a morphological imaging technique with a metabolic diagnostic technique, allows image fusion of metabolic and anatomical information and shows increasing usefulness in clinical oncology for disease staging, prognostic stratification, therapy planning, monitoring treatment and early detection of recurrence. The most used radiotracer in oncology, 18F-Fluorodeoxyglucose (18F-FDG), has shown to be an accurate tracer for tumour detection in many types of malignant tumours including breast cancer, colorectal cancer, esophageal cancer, melanoma, lung cancer, liver cancer, Wilms' tumour, and sarcoma.[6] However, use of this tracer is disappointing in detection of prostate cancer because of its physiologic urinary excretion and the low glucose metabolism of prostate cancer cells.[19]

Due to the limitation of 18F-FDG, alternative tracers for molecular imaging of prostate cancer have been introduced. Choline is a substrate for the synthesis of phosphatidylcholine, which is an essential component of all cell membranes. As carcinogenesis is characterized by enhanced cell proliferation that lead to increased membrane or fatty acid demands, the uptake of choline could reflect proliferative activity. Thus, choline labelled with 11C or 18F has been introduced for molecular imaging of prostate cancer. 11C-Choline PET/CT has been reported to give clear images of the pelvic region, prostate cancer, and pelvic lymph node metastases due to lower urinary excretion, while 18F-Choline PET/CT is more useful for pos-

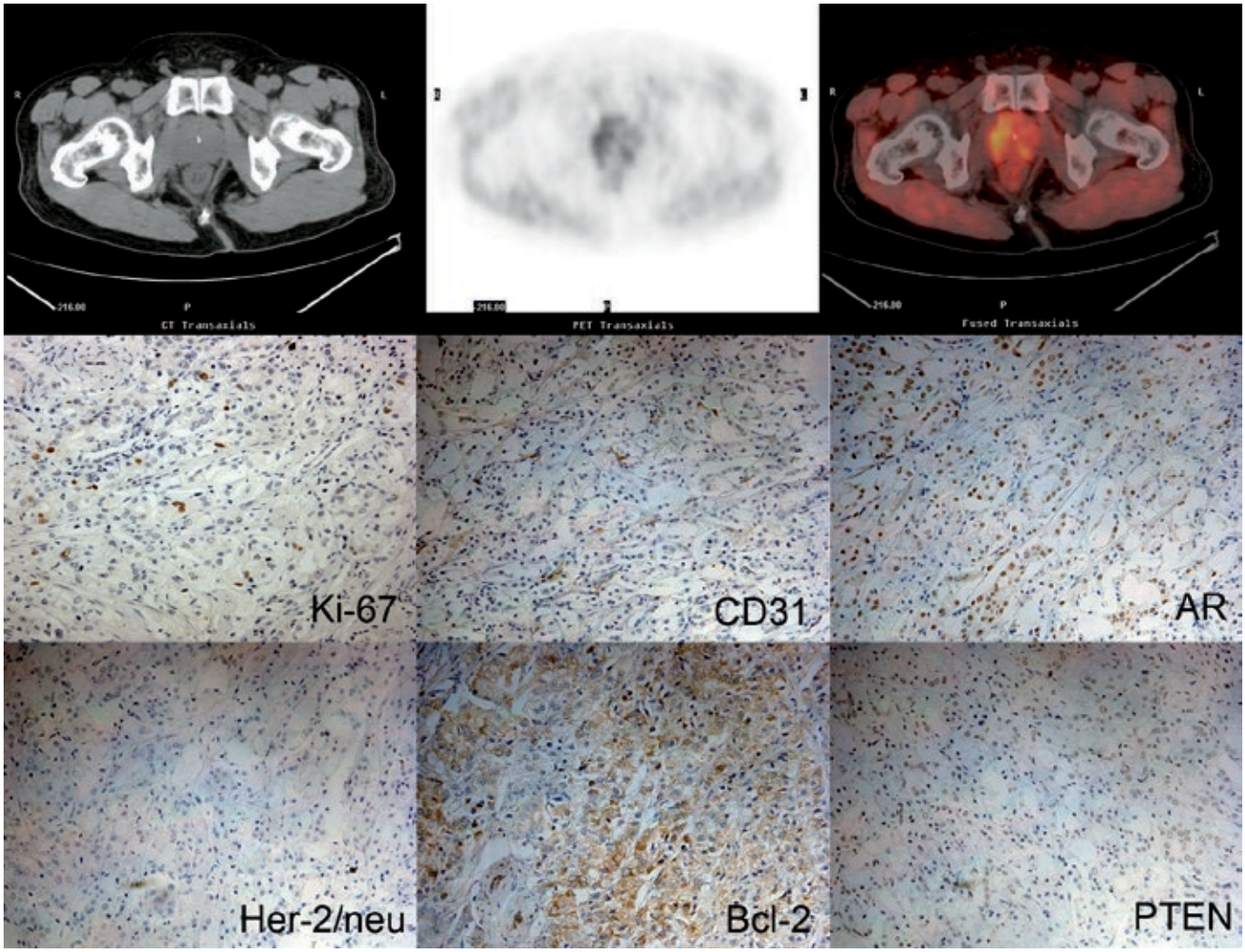

FIGURE 4. 11C-Choline PET/CT images and immunohistochemistry images form patient No. 17.

sible distribution to centers lacking in on-site cyclotron.[20]

The diagnostic value of 11C-Choline PET/CT in imaging prostate cancer with increasing PSA after first-line treatment has been investigated by several authors, and this technique demonstrated to be more helpful than conventional imaging modalities in the detection of lymph node and distant metastases.[21-27] However, its use for primary prostate cancer remains controversial. The results of different studies varied considerably. Some authors reported a significant overlap of 11C-Choline SUVmax between prostate cancer and benign prostate hyperplasia (BPH) tissue[22,27], while some other studies showed that 11C-Choline PET was effective in differentiating malignant from benign prostate lesions.[28-31]

In our previous study on the usefulness of 11C-Choline PET/CT in detecting prostate cancer in patients with an elevated serum PSA level, we also found some BPH patients with rather higher prostate SUVmax. Moreover, it seemed that high SUVmax in these patients were usually accompanied with high muscle SUVmax. On the other hand, SUV methodology is affected by many factors such as patient size, time between tracer injection and PET/CT scan. So we calculated SUVmax-P/M ratios in all patients and the subsequent results demonstrated that there was a significant statistical difference in SUVmax-P/M raitos between malignant and benign lesions of prostate. Using 2.3 (SUVmax-P/M ratio) as a criterion, 11C-Choline PET/CT showed a sensitivity of 90.48%, a specificity of 85.71%, an accuracy of 87.76%, a positive

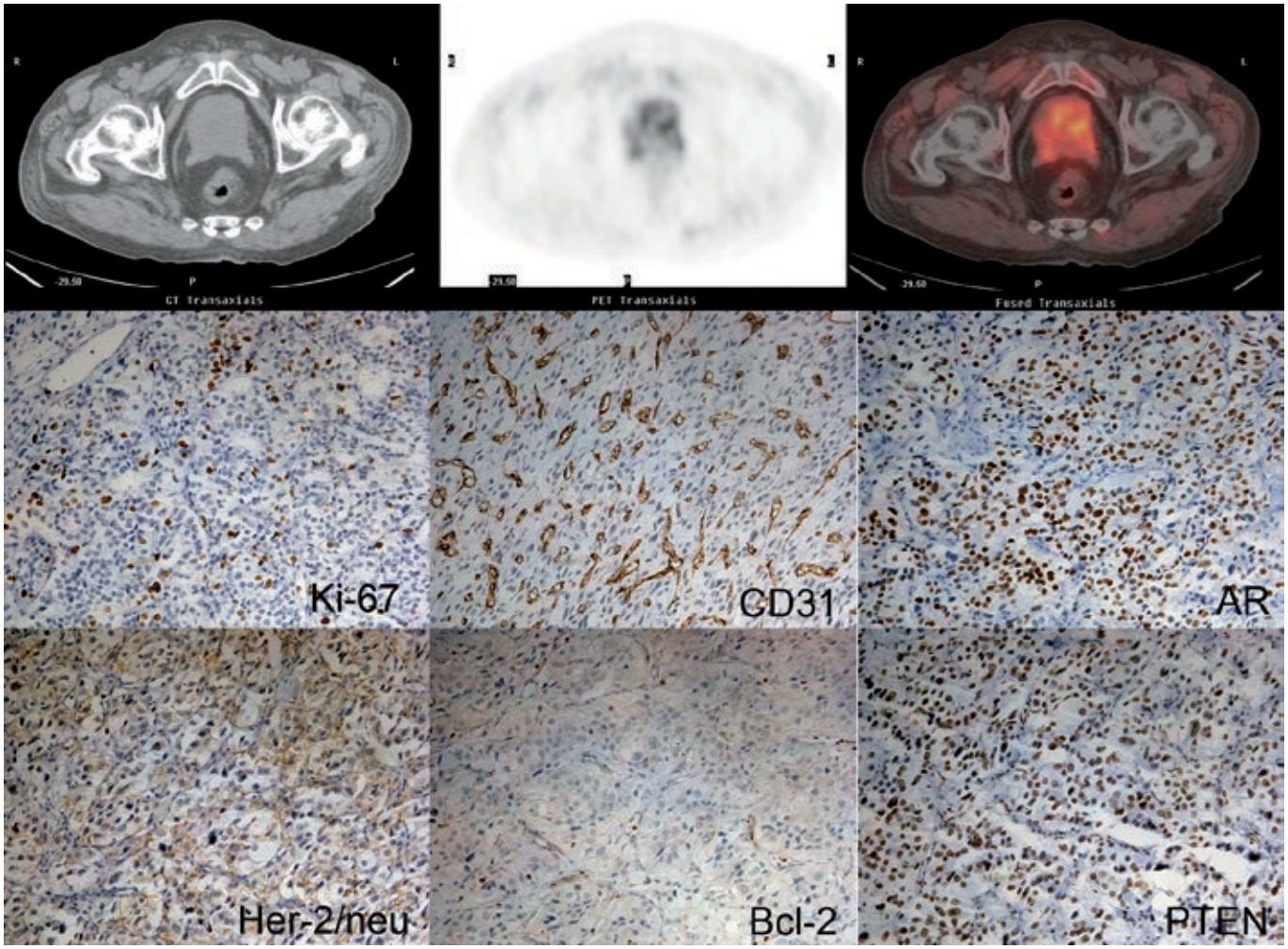

FIGURE 5. 11C-Choline PET/CT images and immunohistochemistry images form patient No. 1.

predictive value of 82.61%, and a negative predictive value of 92.31%.[14]

As PET/CT is of limited clinical value if used only as a tumour seeking procedure, this study was conducted to evaluate the relationship between clincopathological parameters, molecular biomarkers of aggressiveness and 11C-Choline PET/CT imaging. In fact, several investigators also focused their attention on the relationship between 11C-Choline uptake in PET scans and biologic behaviour of primary prostate cancer in the last few years. However, like the usefulness of 11C-Choline PET in detecting primary prostate cancer, the association between 11C-Choline uptake and tumour biologic behaviour remains confusing. Sutinen *et al.* reported that no correlation could be demonstrated between the tumour uptake of 11C-Choline and the histological grade, Gleason score, volume of the prostate or PSA.[32] These data were confirmed by Farsad *et al.*,[27] and Giovacchini *et al.*.[22] Yamaguchi *et al.* observed significant linear correlations between SUVmax and serum PSA, while no significant correlations were found between SUVmax and Gleason score, or between SUVmax and tumour grade.[33] Reske *et al.*,[31] in agreement with another study by Breeuwsma *et al.*,[34] reported that tumoral 11C-Choline uptake was related to tumour stage and no correlation was found between SUV and either the Gleason score or pre-operative serum PSA. In addition, Breeuwsma *et al.* compared the uptake of 11C-Choline with the amount of Ki-67 staining and demonstrated no relationship.[34]

However, it seems that these studies were restricted to the exclusive evaluation of apparent tumour SUV (mean or maximum). As a significant overlap of 11C-Choline uptake in PET imaging

between malignant and benign lesions of prostate, the parameter SUV alone may not serve as a marker of tumour biologic behaviour. According to a more recent study by Piert *et al*. [35], in which the radioactivity concentrations of the tumour (T) and benign prostate background (B) were measured and their ratios (T/B) were calculated, high Gleason score (≥4+3) and Ki-67 index (≥5%) were significantly associated with an increased SUV T/B ratio in 11C-Choline PET/CT imaging. However, as the author mentioned in the study, it is difficult to define the true location of benign prostate tissue, which serve as radioactivity background.

In the light of our previous study, SUVmax-P/M ratio was added to express 11C-Choline uptake in the present study. And this parameter seems to be much more valuable than SUVmax in 11C-Choline PET/CT imaging of prostate cancer. Our results indicated that 11C-Choline SUVmax-P/M ratio was significantly associated with clinical tumour stage and Gleason score. The Gleason system is the most widely used grading of prostate carcinoma that ranges from 1 (well differentiated) to 5 (poorly differentiated). The Gleason score is the sum of the most prevalent and second most prevalent grade and prostate cancer could be classified as well and moderately differentiated (Gleason score 2-7) and poorly differentiated (8-10).[36] A low Gleason score is associated with a more indolent malignancy with a good prognosis whereas a high Gleason score is indicative of an aggressive biologic behaviour and an increased risk of occult systemic disease.[37] As there were 11 patients with a Gleason score of 7 in our cohort, we chose 7(3+4) as the cut-off Gleason score in the analysis and demonstrated a significantly elevated SUVmax-P/M ratio in poorly differentiated prostatic carcinoma.

The molecular biomarkers involved in this study included Ki-67, CD31, AR, Her-2/neu, Bcl-2, and PTEN. Among these markers, Ki67, CD31 and Her-2/neu showed association with SUVmax-P/M ratio, whereas expression levels of the remaining 3 proteins showed no association. Our results might suggest an association between aggressiveness of prostate cancer and upregulation of choline metabolism in tumour tissue. The nuclear antigen Ki-67 is a well-established molecular marker of proliferation in prostate cancer. As aggressive tumours have a higher proliferation rate compared with insignificant tumours, indicators of proliferation may be expected to be good predictors of clinical outcome. Several studies have already suggested that Ki-67 is a useful marker by significantly correlating with biologic aggressiveness and prognosis in prostate cancer.[15,38-40] Our results, in agreement with the study by Piert *et al*.,[35] demonstrate that 11C-Choline uptake measured by PET/CT could reflect proliferative activity of prostate cancer. CD31 is a pan-endothelial marker that can be used as a marker for the determination of vascular density. Angiogenesis is a fundamental process by which new blood vessels are formed, and it is essential for tumour growth by providing nutrients and eliminating metabolic waste products. It has been proposed as a promising prognostic marker in prostate cancer by several investigators.[41-42] Our results demonstrated angiogenesis may promote 11C-Choline uptake by enhanced tracer delivery. As to Her-2/neu, since Slamon *et al*.,[43] firstly reported that its overexpression was associated with high risk of relapse and death in breast cancer, the role of the Her-2/neu oncogene in prostate cancer progression and metastasis has been investigated. Her-2/neu expression is reported associated with unfavourable tumour phenotype, rapid tumour cell proliferation, PSA biochemical recurrence and poor prognosis.[44-45] In addition, a higher expression level of Her-2/neu was reported in hormone-refractory prostate cancer.[46-47] A study by Craft N *et al.* demonstrated that Her-2/neu overexpression provides an alternative mechanism for the activation of AR signalling pathways with low levels of testosterone, thereby contributing to androgen independent growth.[48] It seems that expression rate of this biomarker in the present study was rather higher than the results reported by the researchers mentioned above. However, most of these studies were performed on radical prostatectomy specimens, while our cohort included patients with advanced prostate cancer who were not suitable for radical surgery. In fact, positive expression of Her-2/neu was recognized in 4 of 9 patients with tumour stage IV, while only 2 of 12 patients with relatively early stage. This may contribute to a higher SUVmax-P/M ratio in Her-2/neu positive subgroup, as this parameter was significantly correlated with tumour stage in our cohort.

This study has certain limitations. Firstly, the results from the small sample size will be questionable. A larger study with long-term follow-up in subgroups receiving different therapy would be necessary to determine directly whether SUVmax-P/M ratio is independent with respect to other well-known clinical and biologic prognostic variables in prostate cancer. Secondly, despite we selected prostate samples with reference to PET/CT results; we do not know for certain whether the specific tumour assessed by immunohistochemis-

try and pathology was accurately identified on imaging. Our study was not about assessing tumour localization by PET/CT. Nevertheless, our data showed that as the SUV-max P/M ratio increased, so did level of clincopathological and molecular markers in the representative tumour lesion assessed. Another limitation is that specimens in our study were obtained through different methods. And for the patients obtaining samples through biopsy, only those with an adequate specimen for immunohistochemical analysis could be included. These may bias to verify the results of our study. In addition, as some patients' serum PSA tests were not performed at our center, we did not take this parameter into analysis. Further studies are needed to investigate the relationship between these parameters and 11C-Choline uptake.

Conclusions

This pilot study indicates that the 11C-Choline uptake in primary prostate cancer normalized by pelvic muscle does correlate with Gleason score, tumour stage and expression of several tumour biomarkers. These findings confirm that PET/CT could be used as a non-invasive diagnostic modality that can provide information currently available only through pathological examination of tumour tissues. Because Gleason score and biomarkers involved in the study are prognostic markers of prostate cancer, the SUVmax-P/M ratio determined by 11C-Choline PET/CT may offer important biological information about prostate cancer. We might be able to pretherapeutically evaluate the biologic aggressiveness of primary prostate cancer by means of 11C-Choline PET/CT scan, and monitoring the SUVmax-P/M ratio would be informative for work-up and management of primary prostate cancer.

Acknowledgments

Sources of support: Shandong Province Government grant 2009QW014 (Jin) and BS2009YY028 (Wang).

Reference

1. Jemal A, Siegel R, Xu J, Ward E. Cancer statistics. *CA Cancer J Clin* 2010; **60:** 277-300.
2. Brawley OW, Ankerst DP, Thompson IM. Screening prostate cancer. *CA Cancer Clin* 2009; **59:** 264-73.
3. Albersen PC. A challenge to contemporary management of prostate cancer. *Nat Clin Pract Urol* 2009; **6:** 12-3.
4. Avazpour I, Roslan RE, Bayat P, Saripan MI, Nordin AJ, Abdullah RSAR. Segmenting CT images of bronchogenic carcinoma with bone metastases using PET intensity markers approach. *Radiol Oncol* 2009; **43:** 180-6.
5. Rojnik M, Jevnikar Z, Mirkovic B, Janes D, Zidar N, Kikelj D, et al. Cathepsin H indirectly regulates morphogenetic protein-4 (BMP-4) in various human cell lines. *Radiol Oncol* 2011; **45:** 259-66.
6. Ben-Haim S, Ell P. 18f-FDG PET and PET/CT in the evaluation of cancer treatment response. *J Nucl Med* 2009; **50:** 88-99.
7. Farsad M, Schiavina R, Franceschelli A, Sanguedolce F, Castellucci P, Bertaccini A, et al. Positron emission tomography in imaging and staging prostate cancer. *Cancer Biomarkers* 2008; **4:** 277-84.
8. Westerterp M, Sloof GW, Hoekstra OS, Ten Kate FJ, Meijer GA, Reitsma JB, et al. 18FDG uptake in oesophageal adenocarcinoma: linking biology and outcome. *J Cancer Res Clin Oncol* 2008; **134:** 227-36.
9. Gu J, Yamamoto H, Fukunaga H, Danno K, Takemasa I, Ikeda M, et al. Correlation of Glut-1 overexpression, tumor size, and depth of invasion with 18F-2-fluoro-2-deoxy-D-glucose uptake by positron emission tomography in colorectal cancer. *Dig Dis Sci* 2006; **51:** 2198-205.
10. Ueda S, Kondoh N, Tsuda H, Yamamoto S, Asakawa H, Fukatsu K, et al. Expression of centromere protein F (CENP-F) associated with higher FDG uptake on PET/CT, detected by cDNA microarray, predicts high-risk patients with primary breast cancer. *BMC Cancer* 2008; **8:** 384.
11. Nakamura H, Hirata T, Kitamura H, Nishikawa J. Correlation of the standardized uptake value in FDG-PET with the expression level of cell-cycle-related molecular biomarkers in resected non-small cell lung cancers. *Ann Thorac Cardiovasc Surg* 2009; **15:** 304-10.
12. Backes H, Ullrick R, Neumaier B, Kracht L, Wienhard K, Hacobs AH. Noninvasive quantification of tumour proliferation in patients with high-grade glioma. *Eur J Nucl Mol Imaging* 2009; **36:** 1960-7.
13. Kawai N, Zhen HN, Miyake K, Yamamaoto Y, Nishiyama Y, Tamiya T. Prognostic value of pretreatment 18F-FDG PET in patients with primary central system lymphoma: SUV-based assessment. *J Neuroncol* 2010; **100:** 225-32.
14. American Joint Committee on Cancer. Prostate. In: Greene FL, Page DL, Fleming ID, editors. *AJCC Cancer staging manual*. 6th edition. New York: Springer; 2002. p. 309-16.
15. Li X, Liu Q, Wang M, Jin X, Liu Q, Yao S, et al. C-11 choline PET/CT imaging for differenting malignant from benign prostate lesions. *Clin Nucl Med* 2008; **10:** 671-6.
16. Shukla-Dave A, Hricak H, Ishill N, Moskowitz CS, Drobnjak M, Reuter VE, et al. Prediction of prostate cancer recurrence using magnetic resonance imaging and molecular profiles. *Clin Cancer Res* 2009; **15:** 3842-9.
17. Zellweger T, Ninck C, Bloch M, Mirlacher M, Koivisto PA, Helin HJ, et al. Expression patterns of potential therapeutic targets in prostate cancer. *Int J Cancer* 2005; **113:** 619-28.
18. Veltri RW, Isharwal S, Miller MC, Epstein JI, Mangold LA, Humphreys E, et al. Long term assessment of prostate cancer progression free survival: evaluation of pathological parameters, nuclear shape and molecular biomarkers of pathogenesis. *Prostate* 2008; **68:** 1806-15.
19. Shreve PD, Grossman HB, Gross MD, Wahl RL. Metastatic prostate cancer: initial fingdings of PET with 2-deoxy-2[F-18]fluoro-D-glucose. *Radiology* 1996; **199:** 751-6.
20. Hodolic M. Role of F-choline PET/CT in evaluation of patients with prostate carcinoma. *Radiol Oncol* 2011; **45:** 17-21.
21. Hara T. 11C-choline and 2-deoxy-2-[18F]fluoro-D-glucose in tumor imaging with positron emission tomography. *Mol Imaging Biol* 2002; **4:** 267-73.
22. Giovacchini G, Picchio M, Coradeschi E, Scattoni V, Bettinardi V, Cozzarini C, et al. [11C] Choline uptake with PET/CT for initial diagnosis of prostate cancer: relation to PSA levels, tumour stage, and antiandrogenic therapy. *Eur J Nucl Med Mol Imaging* 2008; **35:** 1065-73.
23. Picchio M, Messa C, Landoni C, Gianolli L, Sironi S, Brioschi M, et al. Value of [11C]choline-positron emission tomography for re-staging prostate cancer: a comparison with [18F] fluorodeoxyglucose-positron emission tomography. *J Urol* 2003; **169:** 1337-40.
24. Scattoni V, Picchio M, Suardi N, Messa C, Freschi M, Roscigno M, et al. Detection of lymphy-node metastases with integrated [11C]choline PET/CT in patients with PSA failure after radical retropubic prostatectomy: results confirmed by open pelvic-retroperitoneal lymphadenectomy. *Eur Urol* 2007; **52:** 423-9.

25. Tuncel M, Souvatzoglou M, Herrmann K, Stollfuss J, Schuster T, Weirich G, et al. [11C]Choline positron emission tomography/computed tomography for staging and restaging of patients with advanced prostate cancer. *Nucl Med Bio* 2008; **35:** 689-95.

26. Reske SN, Blumstein NM, Glatting G. [11C]Choline PET/CT imaging in occult local relapse of prostate cancer after radical prostatectomy. *Eur J NuclMol Imaing* 2008; **35:** 9-17.

27. Farsad M, Schiavina R, Castellucci P, Nanni C, Corti B, Martorana G, et al. Detection and localization of prostate cancer: correlation of 11C-choline PET/CT with histopathologic step-section analysis. *J Nucl Med* 2005; **46:** 1642-9.

28. Hara T, Kosaka N, Kishi H. PET imaging of prostate cancer using carbon-11-choline. *J Nucl Med* 1998; **6:** 990-5.

29. Kotzerke J, Prang J, Neumaier B, Volkmer B, Guhlmann A, Kleinschmidt K, et al. Experience with carbon-11 choline positron emission tomography in prostate carcinoma. *Eur J Nucl Med* 2000; **27:** 1415-9.

30. de Jong IJ, Pruim J, Elsinga PH, Vaalburg W, Mensink HJ. Visualization of prostate cancer with 11C-choline positron emission tomography. *Eur Urol* 2002; **42:** 18-23.

31. Reske SN, Blumstein NM, Neumaier B, Gottfried HW, Finsterbusch F, Kocot D, et al. Imaging prostate cancer with 11C-choline PET/CT. *J Nucl Med* 2006; **47:** 1642-9.

32. Sutinen E, Nurmi M, Roivainen A, Varpula M, Tolvanen T, Lehikoinen P, et al. Kinetics of [(11)C] choline uptake in prostate cancer: a PET study. *Eur J Nucl Mol Imaging* 2004; **31:** 317-24.

33. Yamaguchi T, Lee J, Uemura H, Sasaki T, Takahashi N, Oka T, et al. Prostate cancer: a comparative study of 11C-choline PET and MR imaging combined with proton MR spectroscopy. *Eur J Nucl Mol Imaging* 2005; **32:** 724-8.

34. Breeuwsma AJ, Pruim J, Jongen MM, Suurmeijer AJ, Vaalburg W, Nijman RJ, et al. In vivo uptake of [11C]choline does not correlate with cell proliferation in human prostate cancer. *Eur J Nucl Med Mol Imaging* 2005; **32:** 668-73.

35. Piert M, Park H, Khan A, Siddiqui J, Hussain H, Chenevert T, et al. Detection of aggressive primary prostate cancer with 11C-choline PET/CT using multimodality fusion techniques. *J Nucl Med* 2009; **50:** 1585-93.

36. Han M, Partin AW, Pound CR, Epstein JI, Walsh PC. Long-term biochemical disease-free and cancer-specific survival following anatomic radical retropubic prostatectomy. The 15-year Johns Hopkins experience. *Urol Clin North Am* 2001; **28:** 555-65.

37. Sogani PC, Israel A, Lieberman PH, Lesser ML, Whitmore WF Jr. Gleason grading of prostate cancer: a predictor of survival. *Urology* 1985; **25:** 223-7.

38. Kumar-Sinha C, Chinnaiyan AM. Molecular markers to identify patients at risk for recurrence after primary treatment for prostate cancer. *Urology* 2003; **62(Suppl 1):** 19-35.

39. Quinn DI, Henshall SM, Sutherland RL. Molecular markers of prostate cancer outcome. *Eur J Cancer* 2005; **41:** 858-87.

40. Berney DM, Gopalan A, Kudahetti S, Fisher G, Ambroisine L, Foster CS, et al. Ki-67 and outcome in clinically localised prostate cancer: analysis of conservatively treated prostate cancer patients from the Trans-Atlantic Prostate Group study. *Br J Cancer* 2009; **100:** 888-93.

41. Erbersdobler A, Isbarn H, Dix K, Steiner I, Schlomm T, Mirlacher M, et al. Prognostic value of microvessel density in prostate cancer: a tissue microarray study. *World J Urol* 2010; **28:** 687-92.

42. Silberman MA, Partin AW, Veltri RW, Epstein JI. Tumor angiogenesisi correlates with progression after radical prostatectomy but not with pathologic stage in Gleason sum 5 to 7 adenocarcinoma of the prostate. *Cancer* 1997; **79:** 772-9.

43. Slamon DJ, Clark GM, Wong SG, Levin WJ, Ullrich A, McGuire WL. Human breast cancer: correlation of relapse and survival with amplification of the HER-2/neu oncogene. *Science* 1987; **235:** 177-82.

44. Calvo BF, Levine AM, Marcos M, Collins QF, Iacocca MV, Caskey LS, et al. Human epidermal receptor-2 expression in prostate cancer. *Clin Cancer Res* 2003; **9:** 1087-97.

45. Savinainen KJ, Saramäki OR, Linja MJ, Bratt O, Tammela TL, Isola JJ, et al. Expression and gene copy number analysis of ERBB2 oncogene in prostate cancer. *Am J Pathol* 2002; **160:** 339-45.

46. Signoretti S, Montironi R, Manola J, Altimari A, Tam C, Bubley G, et al. Her-2-neu expression and progression toward androgen independence in human prostate cancer. *J Natl Cancer Inst* 2000; **92:** 1918-25.

47. Edwards J, Traynor P, Munro AF, Pirret CF, Dunne B, Bartlett JM. The role of HER1-HER4 and EGFRvIII in hormone-refractory prostate cancer. *ClinCancer Res* 2006; **12:** 123-30.

48. Minner S, Jessen B, Stiedenroth L, Burandt E, Köllermann J, Mirlacher M, et al. Low level HER2 overexpression is associated with rapid tumor cell proliferation and poor prognosis in prostate cancer. *Clin Cancer Res* 2010; **16:** 1553-60.

research article

The clinical value of combined use of MR imaging and multi-slice spiral CT in limb salvage surgery for orthopaedic oncology patients: initial experience in nine patients

Jie Xu[1], Jun Shen[2], Yue Ding[1], Hui-Yong Shen[1], Zhan-Peng Zeng[1], Ruo-Fan Ma[1], Chun-Hai Li[1], Bertram Barden[3]

[1] Department of Orthopaedic Surgery, Sun Yat-Sen Memorial Hospital of Sun Yat-Sen University, 107 Yanjiangxi Road, 510120, Guangzhou, P. R. China

[2] Department of radiology, Sun Yat-Sen Memorial Hospital of Sun Yat-Sen University, 107 Yanjiangxi Road, 510120, Guangzhou, P. R. China

[3] Department of Orthopaedic Surgery, Düren Hospital, Academic Hospital of University of RWTH Aachen, Roonstr. 30, 52351 Düren, Germany

Radiol Oncol 2012; 46(3): 189-197.

Received 27 October 2011
Accepted 4 December 2011

Correspondence to: Yue Ding, Department of Orthopaedic Surgery, Sun Yat-Sen Memorial Hospital of Sun Yat-Sen University, 107 Yanjiangxi Road, 510120, Guangzhou, P. R. China. Phone: +86 20 81332553; Fax: +86 20 81332792; E-mail: dingyue36@126.com; Bertram Barden, Department of Orthopaedic Surgery, Düren Hospital, Academic Hospital of University of RWTH Aachen, Roonstr. 30, 52351 Düren, Germany. Phone: +49(2421)301307; Fax: +49(2421)301474; E-mail: bertram.barden@krankenhaus-dueren.de

Jie Xu and Jun Shen contrebuted equally to this work.

Disclosure: No potential conflicts of interest were disclosed.

Background. The purpose of this prospective study was to evaluate the value of the combined use of MR imaging and multi-slice spiral CT for limb salvage surgery in orthopaedic oncology patients.

Patients and methods. Nine consecutive patients with lower/upper limb malignant bone tumours (7 osteosarcomas and 2 chondrosarcomas) were treated with limb-salvaging procedures. Preoperative planning including determination of the osteotomy plane and diameters of the prosthesis was performed basing on the preoperative CT and MR images. The histopathology was performed as golden diagnostic criteria to evaluate the accuracy of CT and MR-based determination for tumour's boundary.

Results. The tumour extension measured on MRI was consistent with the actual extension (P>0.05, paired Student's *t* test), while the extension measured on CT imaging was less than the actual extension. The length, offset and alignment of the affected limb were reconstructed accurately after the operation. An excellent functional outcome was achieved in all patients.

Conclusions. In the present study, MRI was found to be superior to CT for determining the tumour extension, combined use of MRI and CT measurement provided high precision for the fit of the prosthesis and excellent functional results.

Key words: limb salvage surgery; magnetic resonance imaging (MRI); computed tomography (CT)

Introduction

Better adjuvant therapy, improved metal implants, and innovative surgical techniques have led surgeons to consider limb salvage surgery as an alternative treatment for malignant bone tumour other than amputation. Orthopaedic oncology patients have a chance for an active, disease-free life after limb salvage surgery. In the first evidence-based study, Simon *et al.* had reported the benefits of limb-salvaging procedures for bone tumours.[1] Their multicentre study reported the rates of local recurrence, metastasis and survival in 227 patients with osteosarcoma in the distal femur and sug-

TABLE 1. Lesion features in six patients

NO.	Primary tumor	Sex	Age(y)	Tumor characteristics			Tumor edge disparity between CT and MR(cm)
				location	Size(cm)*	Size(cm)#	
1	Osteosarcoma	M	20	Proximal Femur	6.5	6.0	0.5
2	Chondrosarcoma	F	29	Proximal Femur	7.1	5.5	1.6
3	Osteosarcoma	F	21	Distal Femur	15.5	13.3	2.2
4	Chondrosarcoma	M	31	Proximal Femur	10.0	4.2	5.8
5	Osteosarcoma	F	19	Proximal Femur	8.5	7.0	1.5
6	Osteosarcoma	F	52	Distal Femur	9.0	7.6	1.4
7	Osteosarcoma	M	41	Distal Femur	12.9	11.0	1.9
8	Osteosarcoma	F	22	Proximal humerus	14.2	12.3	1.9
9	Osteosarcoma	M	22	Proximal humerus	13.0	11.5	1.5

*measured on MRI; #measured on CT imaging.

gested that the Kaplan-Meier curves of the patients without recurrence were not statistically different between limb-salvaging surgery and amputation patients during a 5.5-year follow-up. Limb-salvage surgery was considered as safe as an amputation in the management of patients with high-grade osteosarcoma.

The goal of limb-salvaging surgery is to preserve the function of limbs, prevent tumour recurrence, and enable the rapid administration of chemotherapy or radiotherapy.[2] It can be reached with meticulous technique, detailed operative planning, and the use of endoprosthetic replacements and/or bone grafting. For a successful limb-salvage surgery in high-grade malignant tumour, such as sarcomas, a wide margin is necessary to obtain a local control.[3-5] Since marginal and intralesional margins are related to local recurrence, the reconstruction with limb-salvaging options should be carefully considered. The clinical outcome of the limb-salvage surgery with arthroplasty is closely related to the accuracy of the surgical procedure. To improve the final outcome, one must take into account the length of the osteotomy plane, as well as the alignment of the prosthesis with respect to the mechanical axis in order to keep the balance of the soft tissues. Furthermore, the parameters measured with the 3D imagine must be used during the individual manufacture of implant in order to reconstruct the skeletal structure accurately. Therefore, geometric data (such as length of leg, offset) and morphologic data are required.

Magnetic resonance imaging (MRI) was beneficial for tumour detection and consequently staging of musculoskeletal neoplasia. MRI became an ideal imaging modality for musculoskeletal neoplasia because of superior soft-tissue resolution and multiplanar imaging capabilities and had a significant impact on the ability to appropriately stage lesions and adequately plan for limb-salvage surgery.[6,7] In contrast, multi-slice spiral computed tomography (CT) could provide super three-dimensional morphological delineation of the diseased bone. Theoretically, the complimentary use of these two imaging modalities could give the surgeon a more accurate way to implement preoperative planning than the conventional application of 2D images.

The purpose of this prospective study was to report our initial experience with limb salvage surgery for orthopaedic oncology patients by using both MR imaging and multi-slice spiral CT for preoperative planning.

Patients and methods

Patients and preparation

The study protocol has complied with all relevant national regulations and institutional policies and has been approved by the local institutional ethics

TABLE 2. Functional evaluation according to the 30-point functional classification system of the Musculoskeletal Tumour Society

	Classification(points)						Patients Score
	5	4	3	2	1	0	
Pain	None	Intermediate	Modest	Intermediate	Moderate	Severe	4.5±0.7
Emotional Acceptance	Enthusiastic	Intermediate	Satisfied	Intermediate	Accepts	Dislikes	4.4±0.5
Function	NO Restriction	Intermediate	Recreational Restriction	Intermediate	Partial Disability	Total Disability	4.6±0.5
Supports	None	Intermediate	Brace	Intermediate	One cane, One crutch	Two canes, two crutches	3.8±0.5
Walking Ability	Unlimited	Intermediate	Limited	Intermediate	Inside only	Unable	4.3±0.7
Gait	Normal	Intermediate	Minor Cosmetic problem	Intermediate	Major cosmetic problem. Minor handicap	Major cosmetic problem. Major handicap	3.7±1.0

The score of postoperative functional evaluation was given as the mean and the standard deviation, which showed that excellent or good function was achieved in all patients.

committee. Informed consent was obtained from all patients before the procedure. Patients with malignant bone tumours of lower/upper limb were enrolled in the study.

Preoperative work-up consisted of history and clinical examination, routine laboratory tests and an aesthetic assessment, plain radiography of the limb, 64-slice spiral CT scan of the limb and chest, Technetium-99m bone scan, and, in all of the cases, MRI of the affected limb. Antibiotics were administrated before the surgery. Biopsy was performed for pathological examination. Chemotherapy was commenced 6 weeks before the surgery in those cases which were diagnosed as osteosarcoma and dedifferentiated chondrosarcoma. Patients were classified according to the Enneking staging system.[8,9]

The patients received a detailed narrative of conventional, surgical and amputation options after the limb salvage surgery at their own request. Nine consecutive patients with lower/upper limb malignant tumour of bone (5 women, 4 man, mean age 28.6 years, range: 19-52 years) were treated with limb-salvaging procedures. Lesion size (longitudinal direction), location and histology are summarized in Table 1.

MR imaging

MR images were performed at a 1.5-T superconductive unit (Gyroscan Intera, Philips Medical Systems, Netherlands) and a synergy surface coil was used. The sequences included transverse, sagittal and coronal turbo spin echo T1- and fat-suppressed T2-weighted images. The parameters of these sequences were TR/TE=400 /20 ms for T1-weighted imaging, TR/TE=3500 /120 ms for T2-weighted imaging and a field of view of 480 mm×480 mm for sagittal imaging and 40 mm×40 mm for transverse imaging and 480 mm×480 mm for coronal imaging with a matrix of 512×512, 4-6 signals acquisition and a slice thickness/gap = 5/0.5 mm. Contrast enhanced sagittal, coronal and transverse T1-weighted imaging were obtained after the intravenous injection of gadopentetate dimeglumine (Magnevist, Schering, Berlin, Germany) with a dosage of 0.2 mmol/kg of body weight.

Multi-slice spiral CT

CT scan was performed by using a 64-slice spiral CT (Sensation 64, Siemens Medical Systems, Germany). The raw data obtained using an axial collimation of 64×0.6 mm, a pitch of 1.0, a tubular voltage of 120 KV and a tubular current of 360 mAs, were reconstructed into contiguous 1-mm thick slices with an increment of 0.5 mm and a field of view of 376 mm × 376 mm and a matrix of 512 × 512 by using the standard soft tissue and bone algorithm. These thin-slice images were post-processed by using the techniques of multiplanar reformation (MPR) and volume rendering (VR) to demonstrate the lesion details and perform related measurements.

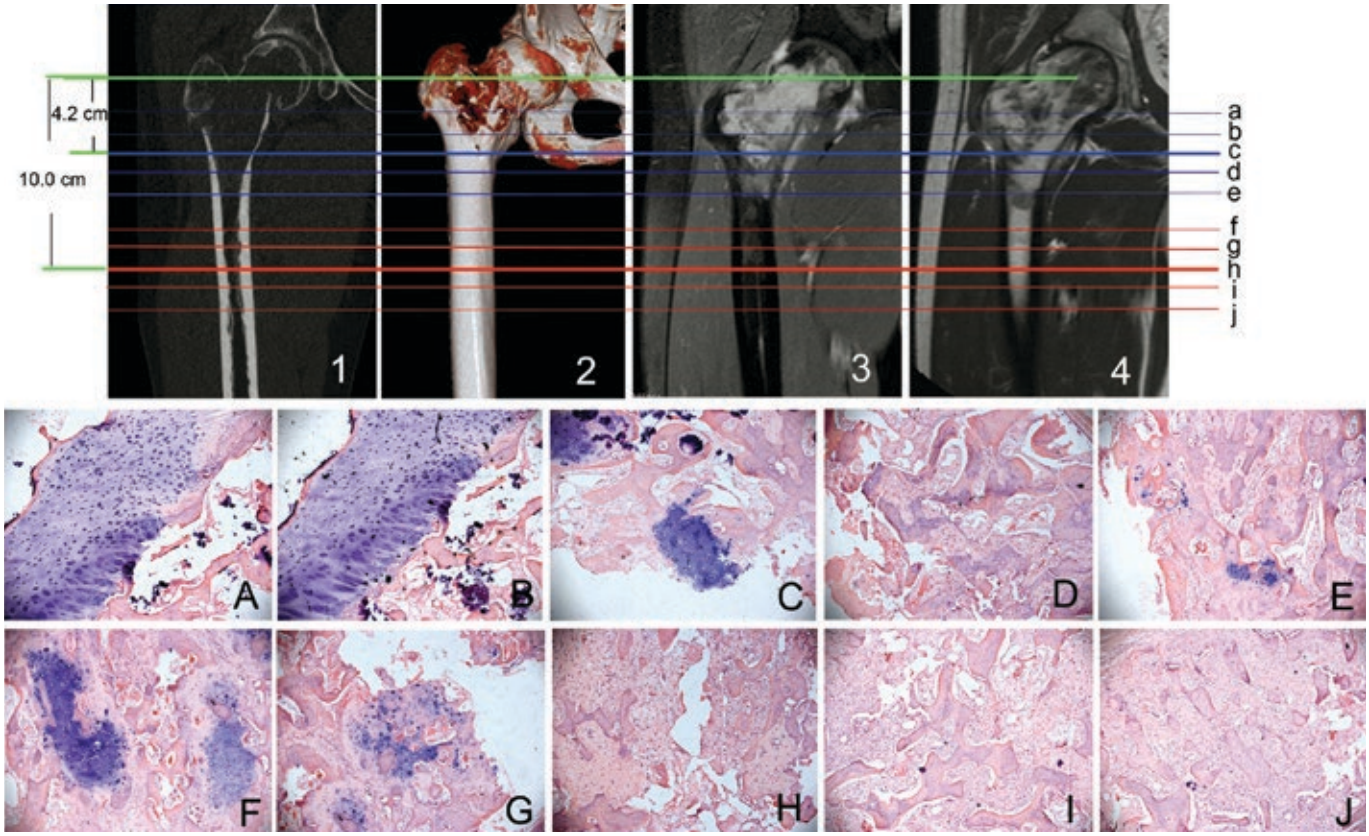

FIGURE 1. CT and MRI determining of tumour extension. A male, 31-year-old patient with chondrosarcoma in the proximal femur. Coronal MPR image (1), Volume rendering image (2) fat-suppressed coronal T1-weighted image (3) and T1-weighted image (4) showed the tumour in the proximal femur. Distance from the rotation centre of femoral head to the tumour margin in orthogonal coronal CT image and coronal T2-weigthted image was 4.2 10.0 cm respectively. The tumour boundary as determined by MRI and CT were in line c and h respectively. Line a, b, d and e represent the plane 1cm, 2cm around tumour and 1cm, 2 cm to the normal tissue distant from the plane determined by CT. Line f, g, i and j were the plane 1cm, 2cm around tumour and 1cm, 2cm to the normal tissue distant from the plane determined by MRI respectively. A-J are corresponding histologic images (HE, ×200) of line a-j. There was no tumour cells found on the plane h, i, j (Figures H, I, J).

Preoperative planning

All preoperative radiographs were evaluated by one radiologist and two consultant orthopaedic surgeons, who were members of the surgical team performing the operations. First, the osteotomy plane was determined separately on CT and MRI. On orthogonal coronal enhanced MR images and CT MPR images, the bulk margin of the tumour in the medullary cavity was defined according to the different signal characteristics or attenuation of the tumour itself and the marrow oedema around the tumour. Then, the maximum distance from the top of the greater trochanter to this tumour margin was measured on orthogonal coronal T1-weigthted MRI images, if the tumour was located in the proximal part of femur. The maximum distance from the knee joint line to the tumour margin was measured for the tumours located in the distal part of femur. The maximum distance was defined as the intramedullary extension of the primary tumour and subsequently was used as a reference for the CT measurement. The osteotomy plane on CT MPR images was defined 30 mm distal from the margin of tumour. This distance was also used to determine the length of the extra medullary part of the prosthesis. After the osteotomy plane had been determined, the detailed shape of the medullary cavity of the preserved part of the femur was assessed using the orthogonal MPR technique for determining the diameter and length of the intra medullary part of prosthesis. Diameters of the medullary cavity at the level of the osteotomy plane and the level of the narrowest plane were measured to determine the diameter of the intra medullary stem of the prosthesis. The length of the intra- medullary stem of the prosthesis should be well matched to the length of medullary cavity of the preserved part of femur, which would be optimal if it had an equal length to the extra medullary part of pros-

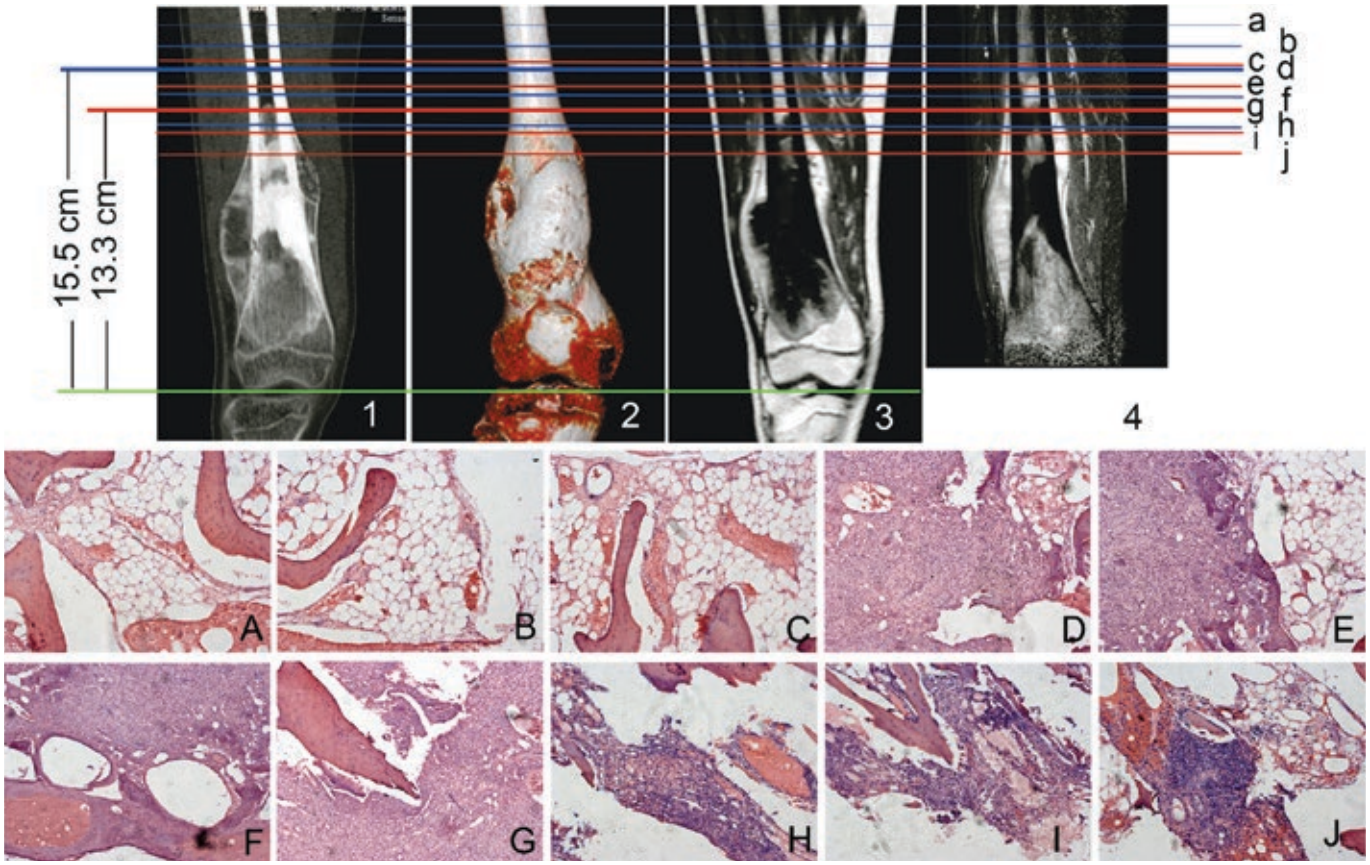

FIGURE 2. CT and MRI determining of tumour extension. A female, 19-year-old patient with osteosarcoma in the distal femur. Coronal MPR image (1), volume rendering CT image (2), coronal enhanced T1-weighted image (3) and fat-suppressed T2-weighted image (4) showed the tumour in the proximal femur . Distance from the gap of the knee to the tumour margin in orthogonal coronal CT image and on orthogonal coronal T2-weigthed image was respectively 7.2 cm and 8.4 cm. The boundary of tumour as determined by MRI and CT were shown in line c and f respectively. Line i, h, d and b were the plane 1cm, 2cm around tumour and 1cm, 2cm to the normal tissue as determined by CT respectively. Line g, e and a were the plane 1cm, 2cm around tumour and 1cm to the normal tissue as determined by MRI. A-J are corresponding histologic images (HE, ×200) of line a-j. No tumour cells were found on the plane a, b, c (Figures A, B, C).

thesis. Finally, the centre axis of the femoral shaft measured on CT was used as a reference. Offset, the distance from the central axis of the femoral shaft and the rotation centre of the femoral head, was the index used to determine the neck length of the prosthesis.

Surgery

All patients underwent en bloc resection and customized prosthetic reconstruction. An anterolateral incision encircling the biopsy scar was used. Limb-salvage surgery consisted of intentional marginal excision, preserving important structures such as major neurovascular bundles, tendons, and ligaments. The osteotomy plane, 30 mm distal from the primary tumour was confirmed based on MRI for all patients. For patients with lesion in the proximal part of femur/humerus, the customized prosthesis was secured using methylmethacrylate cement after the resection. For patients with the tumour in the distal part of the femur, en bloc resection including the tibial plateau was performed and the customized prosthesis was secured using methylmethacrylate cement in both the tibia and femur after the resection. The extensor mechanism was reconstructed by reattachment of the patellar tendon to the slot on the tibial component. After surgery, functional rehabilitation and neoadjuvant chemotherapy were performed.

Postoperative measurement

After surgery, the patients were followed with a mean of 13 months (range, 9 to 20 months). The postoperative assessment of prosthesis was performed on plain radiography. The central axis of the femoral or humeral shaft and offset were

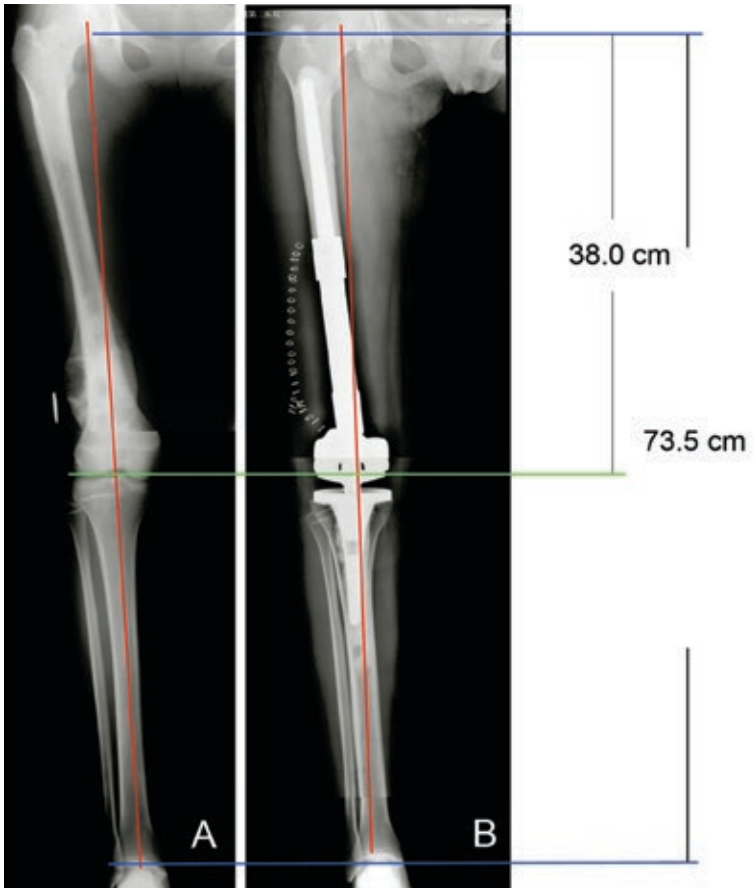

FIGURE 3. Postoperative assessment of prosthesis. A female, 19-year-old patient with osteosarcoma in the distal femur. Preoperative anterior-posterior plain film (A) and postoperative anterior-posterior plain film (B) reveal that the length and alignment were accurate after reconstruction. The red line showed the alignment of lower limb.

defined. The vertical distance from the line between the top of bilateral ischial tuberosities to the femoral condylar plane was assessed to evaluate the change of the length of the lower limbs. The change of the length of the upper limbs was not assessed for those humeral tumour cases. Functional evaluation was performed in all patients using the 30-point functional classification system of the Musculoskeletal Tumour Society.[8]

Statistical analysis

Data were expressed as mean ± SD. All measured values were normally distributed (Kolmogorov-Smirnov test). A paired Student's *t* test was used to evaluate the differences between preoperative planning and post-operative measurements. Values for $p < 0.05$ were considered statistically significant. The statistical analysis was done with SPSS, version 12.0 (SPSS, Inc.).

Results

The mean postoperative functional evaluation score was 23.3 ± 2.7 (range, 15-27) according to Enneking's evaluation. Excellent or good function was achieved in all patients and all patients had preserved stable joint (Table 2). There were no local recurrences, metastases or aseptic loosening determined by bone scan, CT scan, ultrasonic examination and laboratory tests in all patients until the end of the follow-up.

Accuracy of determination for tumour's boundary

To determine the accuracy of tumour boundary defined by MRT and CT, the specimens were collected from 1cm, 2cm proximal to the tumour plane and 1cm, 2cm distal as determined by MRI and CT and were examined for histopathology (Figure 1,2).

There was significant difference in tumour extension between MRI and CT measurements ($P<0.05$). The tumour extension measured on MRI was not statistically different from the actual extension ($P>0.05$), while the extension measured on CT was less than the actual extension (Table 3).

Accuracy of reconstruction of the limb length

Before and after operation, there was no significant difference in the length and offset of affected lower limb (Table 4, Figure 3, 4).

Discussion

The effect of CT combined with MRI on the determination of invasiveness range of malignant bone tumour

Preoperative imaging plays an important role in determining the stage of bone tumours and then an appropriate choice of therapy for affected patients. An appropriate imaging protocol should always begin with plain radiography. If an aggressive or malignant lesion was suspected, further evaluation with cross-sectional imaging such as CT or MR imaging was needed. CT and MRI are imaging methods, often combined in diagnostic procedures of many oncology tumours.[10,11] CT is useful for a detailed assessment of subtle bony lesions and anatomically complex bones. MRI is particularly useful for determining the tumour extension within medullary compartments and is

able to detect tumour involvement of the adjacent muscle compartments, neurovascular structures, and joints. Fat-suppressed T2-weighted imaging proton-density weighted imaging, and contrast-enhanced T1-weighted sequences were frequently used to evaluate neurovascular bundle involvement.[12-13]

Currently, MR imaging has become the modality of choice in the local staging of the primary bone tumour.

Many studies have investigated the accuracy of MRI in determining the infiltration range of osteosarcoma. Sundaram *et al.* first reported that MRI would not overestimate the range of osteosarcoma, compared with histology.[14] Compared with gross and microscopy examination, MRI did not overestimate or underestimate the extent of the tumour, and the false positive and false negative rate were zero. Later, O'Flanagan *et al.* found that MRI could determine the aggression radius of osteosarcoma within the accuracy of 1cm.[15] For high-grade sarcomas, a wide margin is essential to obtain the local control in order to achieve a successful limb-salvage surgery.[16-17] Meyer *et al.* designed the osteotomy plane according to MRI and found that osteotomy plane could be successfully determined by MRI.[18] In the present study, the aggression radius of the tumour determined by MRI and the postoperative histological examination was comparable and MRI is superior to CT for determining the tumour extension. Moreover, we found that the result of MRI was slightly larger than the actual extent. The reasons might be that the low signals of peri-tumour oedema was also assigned to the radius of the tumour, resulting in overestimation of tumour size or the preoperative chemotherapy further reduced the aggression radius of the tumour. This result was consistent with the report of O'Flanagan, who found that the aggression radius of the tumour could be evaluated accurately in coronal and sagittal views of T1-weighted images. In contrast it would be overestimated on T2-weighted or fat-suppressed T2-weighted images because of the presence of the peri-tumour oedema. We suggest that MRI was better to demonstrate peri-tumour oedema in comparison to the histological findings. Since this study does not include a long-term follow-up and a large number of patients, a further study is necessary to determine the eventual effect of MRI osteotomy plane on the long-term survival rate.

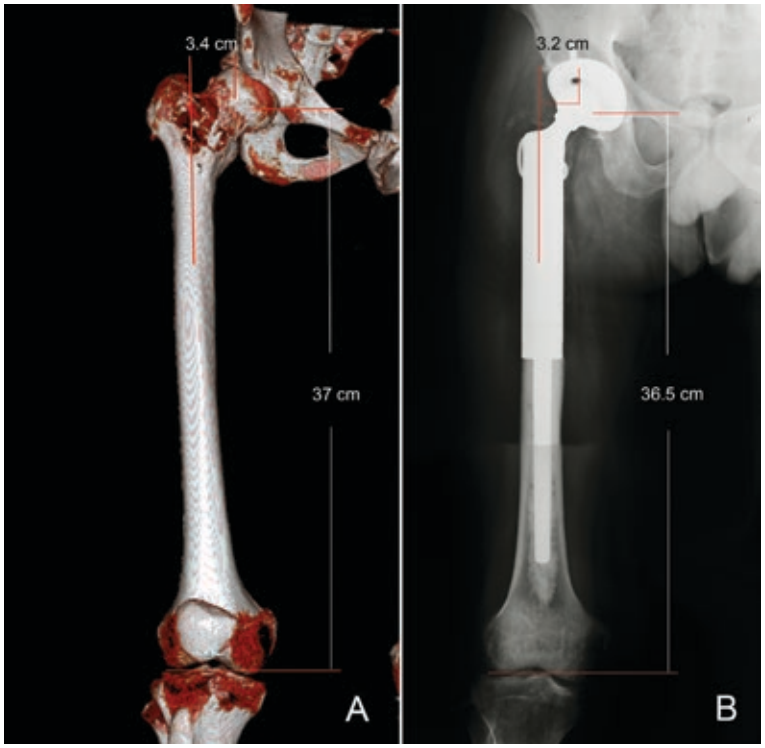

FIGURE 4. Postoperative assessment of prosthesis. A male, 31-year-old patient with chondrosarcoma in the proximal femur. Preoperative volume rendering images (A) and postoperative anterior-posterior plain film (B) demonstrate that the length and offset were accurately reconstructed.

The value of three-dimensional CT in the reconstruction of limbs

There is a huge variety in the human skeleton structure as to the size and shape. Therefore, an implant needs to be custom-made to be more suitable for the patient's bone structure and mechanical requirements. One major challenge is to restore the leg length adequately after the operation.[19] The leg length discrepancy can affect the joint stability, can cause sciatica and low back pain, and inequable stress on the hip.[20] Anja *et al* reported that in 1171 cases of total hip replacement most patients with the length of the difference less than 1 cm walked without limp, while 1/4 patients with more than 2cm difference suffered from claudication.[21] Morrey found that inappropriate eccentricity was one of the factors that could induce dislocation of prosthesis.[22] Therefore, reducing the eccentricity would increase the risk of dislocation. Dorr *et al.* found that both lack of strength of abductor muscles and impingement of the hip, were the important reasons for dislocation.[23] Clinically, many factors could lead to hip dislocation. In the presence of the release of soft tissue around the hip and lack of strength of abductor, the decreased offset

TABLE 3. Accuracy of CT and MRI for determining the tumour extension

	Tumor margin on CT	Tumor margin on MRI	Position from tumor margins on CT				Position from tumor margins on MRI			
			-2cm	-1cm	1cm	2cm	-2cm	-1cm	1cm	2cm
Positive result determined by histopathologic examination	9	7	1	9	9	9	0	1	9	9
Negative result determined by histopathologic examination	0	2	8	0	0	0	9	7	0	0

The specimens were collected from 1cm, 2cm proximal to the tumours and 1cm, 2cm distal as determined by MRI and CT and were examined for histopathology (which were simplified to 1cm, 2cm, -1cm, -2cm respectively). # In 9 cases, which were underestimated by CT, positive result of histopathology was determined on 1-cm-point which was distal from CT-determined boundary. *In 2 cases, which were overestimated by MRI, negative result of histopathology was determined on MR-determined boundary (overestimate).

TABLE 4. Preoperative and postoperative measurements of leg length and offset

No.	Contraleral side		Preoperative planning		Postoperative measurement		Disparity between preoperative and postoperative measurement	
	Leg length (cm)	Offset (cm)	Leg length (cm)	Offset (cm)	Leg length (cm)	Offset (cm)	Leg length (cm)	Offset (cm)
1	39.2	4.1	38.7	4.2	39.4	4.0	0.7	0.2
2	36.0	4.0	37.1	4.2	36.6	4.4	0.5	0.2
3	38.0	3.6	38.0	3.6	38.0	3.6	0.5	0
4	37.3	3.4	37.0	3.4	36.5	3.2	0.5	0.2
5	36.5	3.5	36.0	3.6	35.5	4.0	0.5	0.4
6	37.5	3.7	37.0	3.7	37.2	3.7	0.2	0
7	37.9	3.9	37.7	3.9	37.4	3.9	0.3	0

would significantly increase the incidence of hip impingement syndrome and dislocation, which would increase the instability of the hip joint and may lead to dislocation after slight changes in posture. A smaller offset might lead to excessive loads on prosthesis, and increase the incidence of proximal femoral osteolysis, prosthetic loosening and revision. Theoretically, increasing the offset can reduce the joint reaction force and then may reduce wearing of polyethylene.[24] Each additional 10 mm of the offset can reduce 10% of the abductor force and 10% less force for the acetabular cup. But if the offset is too large, it can easily lead to malposition of the implant, trochanter projections, local bursitis and pain, and also can affect the transfer of stress and lead to the unequal length of limb.

With the advent of multi-slice spiral CT, the development of an individualized prosthesis became realistic. High accuracy of CT provides a reliable basis for designing the individual prostheses. In this study, the three-dimensional reconstruction of CT images was performed. After the osteotomy plane was initially determined on MRI, the detailed morphological parameters were measured on MPR othorgonal planes. The prosthesis was accordingly designed. This combined use of MRI and CT measurement provided high precision for the fit of the prosthesis and excellent functional results.[25]

Conclusions

Preoperative evaluation and planning, meticulous surgical technique, and adequate postoperative management are essential for the bone tumour management. In the present study, MRI was found to be superior to CT for determining the tumour extension; the combined use of MRI and CT measurement provided high precision for the fit of the prosthesis and excellent functional results.

References

1. Simon MA, Aschliman MA, Thomas N, Mankin HJ. Limb-salvage treatment versus amputation for osteosarcoma of the distal end of the femur. 1986. *J Bone Joint Surg Am* 2005; **87:** 2822.
2. Simon MA, Springfield D. *Surgery for bone and soft tissue tumours*. Philadelphia: Lippincott-Raven Publishers; 1998. p. 227-31.
3. Bacci G, Ferrari S, Lari S, Mercuri M, Donati D, Longhi A, et al. Osteosarcoma of the limb: amputation or limb salvage in patients treated by neoadjuvant chemotherapy. *J Bone Joint Surg Br* 2002; **84:** 88-92.
4. Wang TI, Wu PK, Chen CF, Chen WM, Yen CC, Hung GY, et al. The Prognosis of patients with primary osteosarcoma who have undergone unplanned therapy. *Jpn J Clin Oncol* 2011; **41:** 1244-50.
5. Bacci G, Forni C, Longhi A, Ferrari S, Mercuri M, Bertoni F, et al. Local recurrence and local control of non-metastatic osteosarcoma of the extremities: a 27-year experience in a single institution. *J Surg Oncol* 2007; **96:** 118-23.
6. Sanders TG, Parsons TW III. Radiographic imaging of musculoskeletal neoplasia. *Cancer Control* 2001; **8:** 221-31.
7. Cheng EY, Thompson RC Jr. New developments in the staging and imaging of soft-tissue sarcomas. *Instr Course Lect* 2000; **49:** 443-51.
8. Wolf RE, Enneking WF. The staging and surgery of musculoskeletal neoplasms. *Orthop Clin North Am* 1996; **27:** 473-81.
9. Enneking WF, Dunham W, Gebhardt MC, Malawar M, Pritchard DJ. A system for the functional evaluation of reconstructive procedures after surgical treatment of tumours of the musculoskeletal system. *Clin Orthop Relat Res* 1993; **286:** 241-6.
10. Wang XH, Xu MH, Liang H, Xu LS. Comparison of CT and MRI in diagnosis of cerebrospinal leak induced by multiple fractures of skull base. *Radiol Oncol* 2011; **45:** 91-6.
11. Podobnik J, Kocijancic I, Kovac V, Sersa I. 3T MRI in evaluation of asbestos-related thoracic diseases - preliminary results. *Radiol Oncol* 2010; **44:** 92-6.
12. Saifuddin A. The accuracy of imaging in the local staging of appendicular osteosarcoma. *Skeletal Radiol* 2002; **31:** 191-201.
13. Costa FM, Ferreira EC, Vianna EM. Diffusion-weighted magnetic resonance imaging for the evaluation of musculoskeletal tumours. *Magn Reson Imaging Clin N Am* 2011; **19:** 159-80.
14. Sundaram M. The use of gadolinium in the MR imaging of bone tumors. *Semin Ultrasound CT MR* 1997; **18:** 307-11.
15. O'Flanagan SJ, Stack JP, McGee HM, Dervan P, Hurson B. Imaging of intramedullary tumour spread in osteosarcoma. A comparison of techniques. *J Bone Joint Surg Br* 1991; **73:** 998-1001.
16. Bacci G, Forni C, Longhi A, Ferrari S, Mercuri M, Bertoni F, et al. Local recurrence and local control of non-metastatic osteosarcoma of the extremities: a 27-year experience in a single institution. *J Surg Oncol* 2007; **96:** 118-23.
17. Puhaindran ME, Pratt J, Manoso MW, Healey JH, Mintz DN, Athanasian EA. Predictive value of magnetic resonance imaging in determining presence of residual disease after marginal excision of unsuspected soft tissue sarcomas of the hand. *J Hand Surg Am* 2010; **35:** 1479-84.
18. Meyer MS, Spanier SS, Moser M, Scarborough MT. Evaluating marrow margins for resection of osteosarcoma. A modern approach. *Clin Orthop Relat Res* 1999; **363:** 170-5.
19. Austin MS, Hozack WJ, Sharkey PF, Rothman RH. Stability and leg length equality in total hip arthroplasty. *J Arthroplasty* 2003; **18:** 88-90.
20. Sarin VK, Pratt WR, Bradley GW. Accurate femur repositioning is critical during intraoperative total hip arthroplasty length and offset assessment. *J Arthroplasty* 2005; **20:** 887-91.
21. Anja SP. Leg length discrepancies. In: Ochsner PE, editor. *Total hip replacement*. 1st edition. Berlin: Springer; 2002. p. 137-45.
22. Morrey BF. Difficult complications after hip replacement. *Clin Orthop* 1997; **344:** 179-87.
23. Dorr LD,Wan Z. Causes of and treatment protocol for instability of total hip replacement. *Clin Orthop Relat Res* 1998; **355:** 144-51.
24. Schmalzried TP, Shepherd EF, Dorey FJ, Jackson WO, dela Rosa M, Fa'vae F, et al. The John Charnley award. Wear is a function of use, not time. *Clin Orthop Relat Res* 2000; **381:** 36-46.
25. Fan H, Lu Y, Stump A, Reed ST, Baer T, Schunk R, et al. Rapid prototyping of patterned functional nanostructures. *Nature* 2000; **405:** 56-60.

research article

Fluctuating portal velocity tracing with rhythmicity: ultrasonic differential diagnosis and clinical significance

Qingxin Meng[1], Lei Lv[2], Bin Yang[1], Ninghua Fu[1], Guangming Lu[3]

[1] Department of Ultrasound, [2] Department of Cardiology, [3] Department of Medical Imaging, Jinling Hospital, School of Medicine, Nanjing University, Nanjing, Jiangsu Province, China

Radiol Oncol 2012; 46(3): 198-206.

Received 22 October 2011
Accepted 2 January 2012

Correspondence to: Guangming Lu, Department of Medical Imaging, Jinling Hospital, 305 East Zhongshan Road, Nanjing, (210002), Jiangsu, China. Phone: +86-25-80860314, E-mail: prof_meng@yeah.net

Disclosure: No potential conflicts of interest were disclosed.

Background. To evaluate the usefulness of the routine sonographic evaluation of the pattern of fluctuate portal velocity tracings and the hepatic veins for the diagnosis of arterioportal fistula (APF) and cardiogenic trans-sinusoidal shunting (CTS).

Materials and methods. Color Doppler flow imaging and pulsed-wave Doppler (PW) examinations of the portal vein were performed in 282 subjects. The waveforms of the velocity tracings in the portal main trunk and its branches were determined to infer APF or CTS. Suspected cases of APFs or CTSs were always confirmed by echocardiography, contrast-enhanced ultrasound, computed tomography, or digital subtraction angiography findings. The portal maximum velocity (V_{max}), minimum velocity(V_{min}), V_{max}/V_{min}, arterial peak systolic velocity and resistance index, and venous reverse and forward velocities were used to estimate their haemodynamics.

Results. The waveform of the velocity tracing for the draining portal vein of APF was typically arterial-like or diphase, as indicated by a systolic hepatofugal dwarf peak and a diastolic hepatopetal low flat shape. The flow in the affected portal vein was always hepatofugal in an intrahepatic patient, whereas a hepatopetal flow was observed in an extrahepatic APF patient. The waveform of the velocity tracing for the portal vein of CTS patients, especially its intrahepatic branches, showed a typical hump-like shape with or without a transitory hepatofugal tracing. The PW results displayed an increase in the retrograde phase of the hepatic venous flow with increased velocities in the two phases.

Conclusions. Portal velocity tracings should be evaluated during routine detecting for APF or CTS, especially in patients with gastrointestinal upsets.

Key words: velocity tracing; portal hypertension; tricuspid regurgitation; arterioportal fistula; cardiogenic trans-sinusoidal shunting

Introduction

Arterioportal fistula (APF) and cardiogenic trans-sinusoidal shunting (CTS) may both lead to portal hypertension and subsequent esophageal varices with bleeding.[1-6] A timely diagnosis is essential because most cases have curable causes of portal hypertension that require different therapeutic tools.[7,8] However, APF and CTS are often ignored because some patients are asymptomatic or experience equivocal symptoms such as diarrhea, edema, ascites, abdominal pain, and distension. Some APFs exist in patients with liver cirrhosis, whose portal hypertension can be considered the common evolution of cirrhosis; and other patients have the normal internal diameters of portal vein, hepatic vein, and hepatic artery, with indiscoverable focus.[9-12]

APF and CTS can cause variations in hepatic haemodynamics, especially of the portal vein.[13] Ultrasound (US) analysis, which is dynamic, non-invasive, economical, and convenient, can examine

blood vessels in every direction.[14] The haemodynamics determined from the velocity tracings detected via US can easily be analysed[15], but a detecting diagnostic procedure that can be applied during routine examinations has yet to be properly defined. The present study was performed to determine the usefulness of the routine evaluation of portal velocity tracings, in combination with those of the hepatic artery and vein, for APF and CTS diagnosis.

Materials and methods

Patients and controls

Color Doppler flow imaging (CDFI) and pulsed-wave Doppler (PW) studies of the portal vein were performed on 195 patients with APF or CTS. These 195 patients were selected from a consecutive series of APF or CTS diagnoses between January 2002 and December 2010. Among 195 patients, 103 were males and 92 were females. The age distribution ranged from 26 to 67 years, with a mean age of 53 years. The clinical symptoms were the following: edema in 105 patients, abdominal pain and distension in 53 patients, ascites in 32 patients, diarrhea in 17 patients, and malignant hypertension in 3 patients (diastolic pressure>140mmHg). 23 patients were asymptomatic. Among 87 control subjects, 41 were males and 46 were females. The age distribution ranged from 24 to 72 years, with a mean age of 49 years. No significant difference in sex or age distribution between the 195 patients and 87 control subjects.

Standard pre-settings

Two-dimensional images with homogeneous gain could clearly display the vascular lumens. In the CDFI, the blood flow signals exactly suffused the vascular lumen with soft color. The sampling frame steer was consistent with the direction of blood stream, and the sampling gate located at the center of lumen, of which the width was 2 mm, and the correction line paralleled with the direction of bloodstream.

CDFI and PW

All subjects were evaluated by a skilled technician in the morning following an overnight fasting. The patients and control subjects routinely underwent CDFI and PW. The portal maximum velocity (V_{max}), minimum velocity (V_{min}) and V_{max}/V_{min}, arterial peak systolic velocity (*PSV*) and resistance index (*RI*), [$(V_{max}-V_{min}) / V_{max}$], venous reverse velocity (*RV*) and forward velocity (*FV*), and reverse time/forward time [(*RT*)/(*FT*)] were used to estimate their haemodynamics. Each result is the mean of three measurements. The waveforms of the velocity tracings in the main trunk and the branches of the portal vein were determined to infer APF or CTS. A detecting diagnostic procedure is shown in Figure 1.

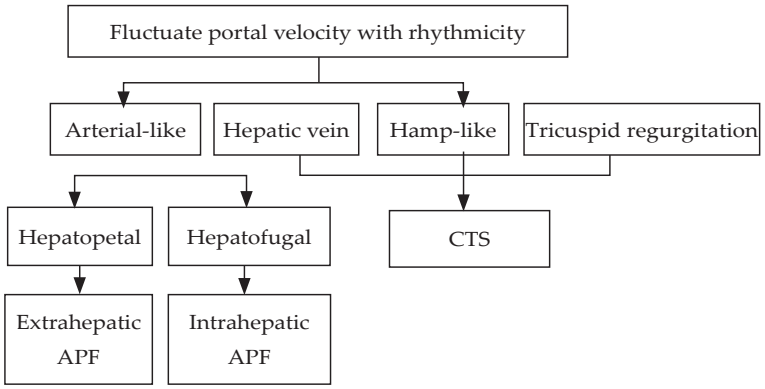

FIGURE 1. Diagnostic procedure for APF or CTS.

Other procedures for confirmed diagnosis

Suspected APF or CTS based on color Doppler US findings were always confirmed by echocardiography, contrast-enhanced US (CEUS), computed tomography (CT), or digital subtraction angiography (DSA) findings.

CEUS was performed using an Acuson Sequoia 512 US scanner equipped with a 3–5 MHz convex transducer and CPS, a contrast-specific CEUS software (Siemens Medical Solutions, Mountain View, CA, USA). Standard pre-settings were used, with adjustment options for individual patients. After the baseline evaluation, SonoVue (Bracco, Milan, Italy) was injected intravenously as a bolus of 2.4 mL, followed by a flush of 5 mL of normal saline. The region of interest set in each JPEG file for the affected portal vein was observed in real-time for about 2 min after the intravenous injection of SonoVue. The entire process was recorded and saved on the hard disk attached to the scanner.

CT scans were performed with a dual-source CT system (Somatom Definition, Siemens Healthcare). Contrast-enhanced triple-phase scans (arterial, portal venous, and equilibrium phases) were obtained after an intravenous bolus injection of 120–150 mL of iopromide (Ultravist 300 mg I/mL, Bayer Schering Pharma) at a rate of 4.0 mL/s using an 18-gauge catheter.

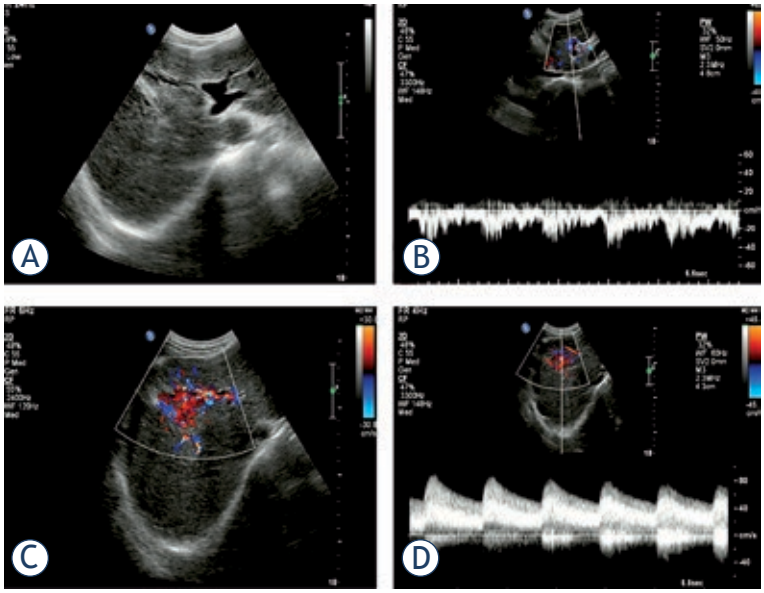

FIGURE 2. US findings for a typical intrahepatic APF. (A) The dilated draining left portal vein. (B) The arterial-like velocity tracing of the draining portal vein with a continuous hepatofugal flow. (C) The turbulent area of APF. (D) The velocity tracing of a feeding artery with fast flow and a low RI.

DSA was performed with femoral catheterisation by the Seldinger technique using a biplane DSA unit with rotational capabilities (Axiom Artis dTA, Siemens Healthcare). Typically, 6–9 mL of nonionic contrast medium (iopromide, Ultravist 300 mg I/mL) was used per acquisition. A baseline DSA of the coeliac trunk and the superior mesenteric artery was performed to visualize the liver vasculature and evaluate the portal vein patency. The common hepatic artery and the right and left hepatic arteries were cannulated, and more superselective cannulations of the feeders to the arteriovenous shunts were performed, if indicated, with or without the use of microcatheters. The arterial and early and late parenchymal phases were evaluated after the acquisition of digitally subtracted images at a rate of one per second. APF was considered in cases where an opacification of one or more portal branches before or during the early parenchymal phase was observed.

Statistical analysis

All values are reported as mean ± standard deviation. Mean comparisons were performed using the t-test for paired samples, as appropriate. Comparisons of coefficients of variation were performed by F-tests. A value of $P < 0.05$ was used as the threshold for the statistical significance. A statistical analysis was performed using SPSS 16.0 software.

Results

US findings

An echo-free focal lesion in continuity with a markedly hypertrophied feeding artery and a dilated draining portal vein, which showed a fast and turbulent flow during the CDFI and PW examinations, (Figure 2) was considered a direct indication of APF. The affected portal vein occasionally showed no enlargement with indiscoverable focal lesions. The waveform of its velocity tracing was typically arterial-like or diphase, as indicated by a systolic hepatofugal dwarf peak and a diastolic hepatopetal low flat shape (Figure 3A).

The right or left branch of the portal vein draining blood from the intrahepatic APF always had a hepatofugal flow, whereas that in the other lobe had a hepatopetal flow. The flow in the main trunk of the portal vein was always hepatopetal with a markedly decreased velocity in an intrahepatic APF patient but with a markedly increased velocity in an extrahepatic APF patient, whose flow directions in the two main branches of the portal vein were hepatopetal (Figures 2, 3A, 4A).

Dynamic CEUS scans showed that microbubbles arrived at the affected portal vein and at its parallel running artery in the early arterial phase 7–10 s after SonoVue injection: the affected portal vein was markedly enhanced by the microbubbles during the arterial phase and became more echogenic than its surrounding parenchyma until the hepatic veins were stained (Figure 3B).

Normal US scans and CDFI always showed normal conditions in the portal vein, hepatic veins, and artery. The hepatic veins were sometimes enlarged. The waveform of the velocity tracing in the portal vein, especially its intrahepatic branches, showed a typical hump-like shape with or without a transitory hepatofugal tracing. PW results displayed an increase in the retrograde phase of hepatic venous flow with increased velocities in the two phases. Echocardiography always exhibited an enlarged right atrium with severe tricuspid regurgitation (Figure 5).

CT findings

The contrast-enhanced CT findings are as follows: (a) earlier enhancement of the affected portal vein compared with the superior mesenteric or splenic vein during the arterial phase or stronger opacification of the affected portal vein compared with that of the superior mesenteric or splenic vein (Figure 3 C); (b) wedge- or irregularly shaped ho-

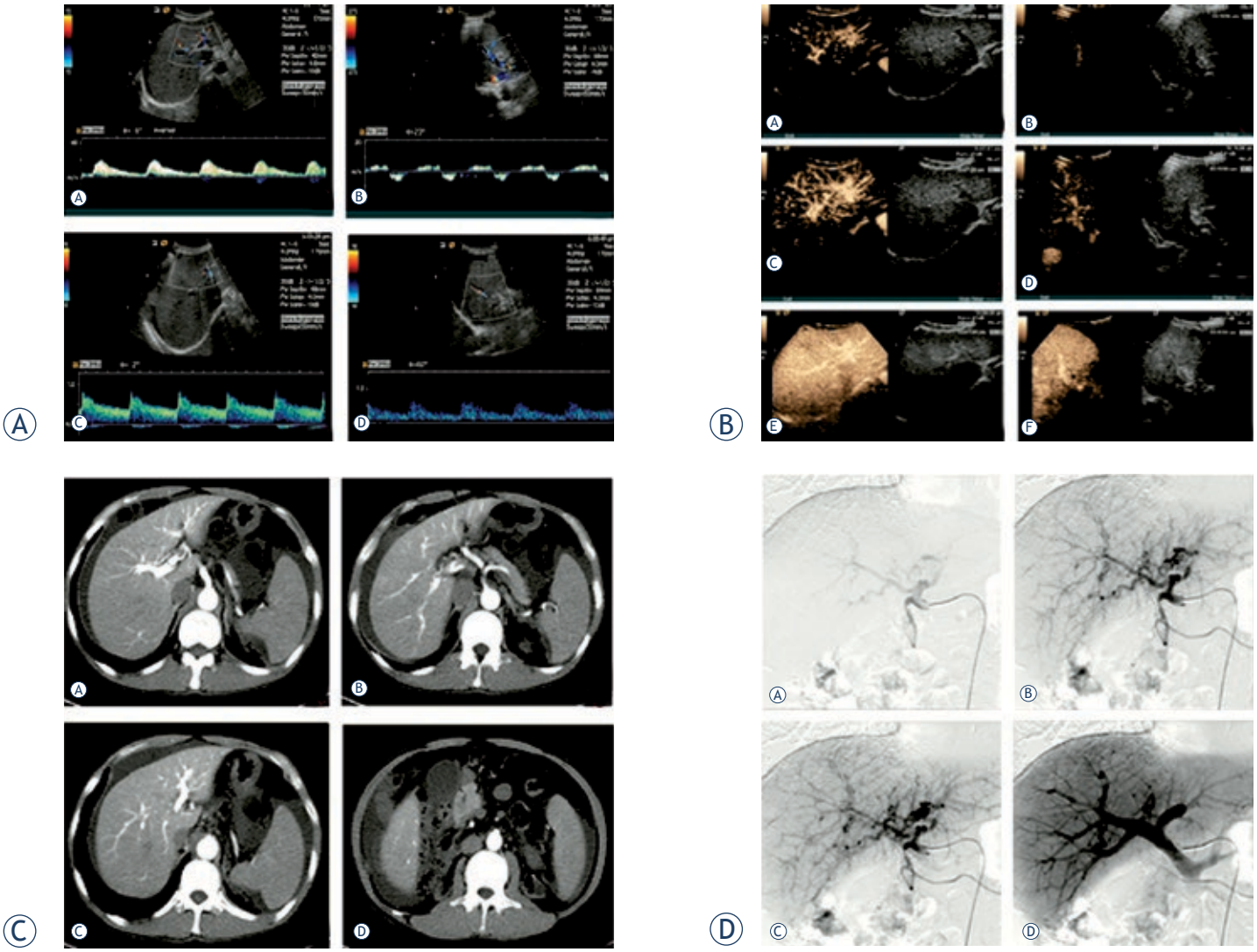

FIGURE 3. Diffuse intrahepatic APFs with indiscoverable focal lesion, confirmed by multimode imaging findings. (A) Color duplex US images of the intrahepatic branches of the portal vein with normal internal diameter shown as typical arterial-like (a: left branch) or diphase velocity (b: right branch) tracings, as indicated by a systolic hepatofugal dwarf peak and a diastolic hepatopetal low flat shape, and that of the enlarged intrahepatic branches of the hepatic artery, which shows high-velocity flow and low resistivity index (c: left branch, d: right branch). (B) Dynamic CEUS scans show that microbubbles arrived at the affected portal vein and at its parallel running artery in the early arterial phase 7–10 s after SonoVue injection (a: left branch, b: right branch), with the affected portal vein markedly enhanced by the microbubbles during the arterial phase (c: left branch, d: right branch) and which became more echogenic than its surrounding parenchyma until the hepatic veins were stained (e: left branch, f: right branch). (C) The contrast-enhanced CT images show an earlier enhancement of the affected portal vein than that of the superior mesenteric vein during the arterial phase (a: right anterior branch, b: right posterior branch, c: left branch, d: the enhancement of the superior mesenteric artery but no enhancement of its parallel running vein). (D) DSA reveals the opacification of the portal vein following its parallel running artery but no visible fistula during the early arterial phase (a: opacification of hepatic artery, b: opacification of peripheric portal vein, c: opacification of left and right branches of portal vein, d: opacification of superior mesenteric and splenic vein).

mogeneous enhancement of the liver parenchyma adjacent to the tumor; and (c) earlier enhancement of the affected superior mesenteric or splenic vein compared that of the portal vein during the arterial phase or stronger opacification of the affected superior mesenteric or splenic vein compared with that of the portal vein (Figure 4 C).

DSA findings

The angiograms demonstrated contrast-filling in the affected portal vein and aneurysmal site of communication between the feeding artery and the draining portal vein during the early arterial phase. Trans-arterial portography revealed a filling defect

TABLE 1. The haemodynamic parameters of the portal vein, hepatic artery, and hepatic vein

Group	Portal vein				Hepatic artery		Hepatic vein		
	V_{max} cm/s	V_{min} cm/s	RI	Direction	PSV cm/s	RI	FV_{max} cm/s	RV_{max} cm/s	RT/FT
Control	33.88±8.89	25.09±6.52	0.26±0.08	hepatopetal	43.46±4.13	0.72±0.05	34.66±5.83	-14.56±6.37	0.21±0.08
Intrahepatic APF	29.71±7.65	5.17±1.34*	0.81±0.05*	hepatofugal	89.34±10.78*	0.53±0.06*	31.23±6.45	-11.69±5.97	0.24±0.07
Extrahepatic APF	30.03±7.12	4.96±1.23*	0.78±0.04*	hepatopetal	41.53±3.96	0.74±0.04	35.79±6.49	-14.56±6.37	0.223±0.06
CTS	11.03±0.64*	-2.84±0.51*	1.26±0.04*	hepatopetal or with brief reverse	45.13±5.42	0.73±0.03	66.16±14.05*	-35.21±10.45*	1.50±0.23*

Note: V_{max}, maximum velocity; V_{min}, minimum velocity; *PSV*, peak systolic velocity; *RI*, resistance index, ($RI = [V_{max} - V_{min}]/V_{max}$); RV_{max}, maximum reverse velocity; FV_{max}, maximum forward velocity; and *RT/FT*, reverse time/forward time.*P < 0.05 versus control.

TABLE 2. Management of APFs and CTSs and clinical outcomes

Type		Cases	Etiology	Management	Outcome(> 6 months)	
					Portal velocity tracing	Symptom
Small APF		5	Liver cirrhosis (3) Biopsy(2)	Follow up (2 closures)	No changes except 2 cases (normal)	Asymptomatic
Intrahepatic APF	Focal	33	Liver cirrhosis (6) Hepatoma (22) Congenital(5)	Embolisation of the feeding artery(28) Ligation:too large(5) or recanalised fistulas(4)	Normalization	Relief or asymptomatic (majority)
	Diffuse	7	Liver cirrhosis (1) No (6)	Embolisation of hepatic artery (7) Ligation: recanalised fistulas (1)	Normalization	Relief or asymptomatic (majority)
Extrahepatic APF	Focal	10	Trauma (10)	Embolisation of the feeding artery (8) Ligation: too large(2) or recanalised fistulas(1)	Normalization	Relief or asymptomatic (majority)
	Diffuse	3	Hypertension (3)	Lowering blood pressure (3)	Normalization	Relief or asymptomatic (majority)
CTS		137	Tricuspid regurgitation (137)	Replacement (127) Repair of tricuspid valve (10)	Normalization	Relief or asymptomatic (majority)

or nonvisualisation in the affected portal of the intrahepatic APF patient. DSA sometimes revealed early pacification of the portal vein and its parallel running artery, but no visible fistula during the arterial phase (Figure 3 D). 137 suspected CTS based on color Doppler US findings were confirmed by echocardiography, 15 APF by CEUS, 27 APF by CT and 51 APF by DSA. The haemodynamic parameters of *Vmax*, *Vmin*, *Vmax/Vmin*, *PSV*, *RI*, *RV*, *FV*, and *RT/FT* are shown in Table 1. Management and clinical outcomes are shown in Table 2.

Discussion

The normal liver receives a dual supply of blood from both the portal vein and the hepatic artery. The main portal vein carries venous blood from the intestines and the spleen, while arteries accompany veins and their terminal branches to join via a capillary network. The main portal vein divides into the right and left branches, and the hepatic artery accompanies the portal vein. The terminal branches of the portal vein and their hepatic arterioles are

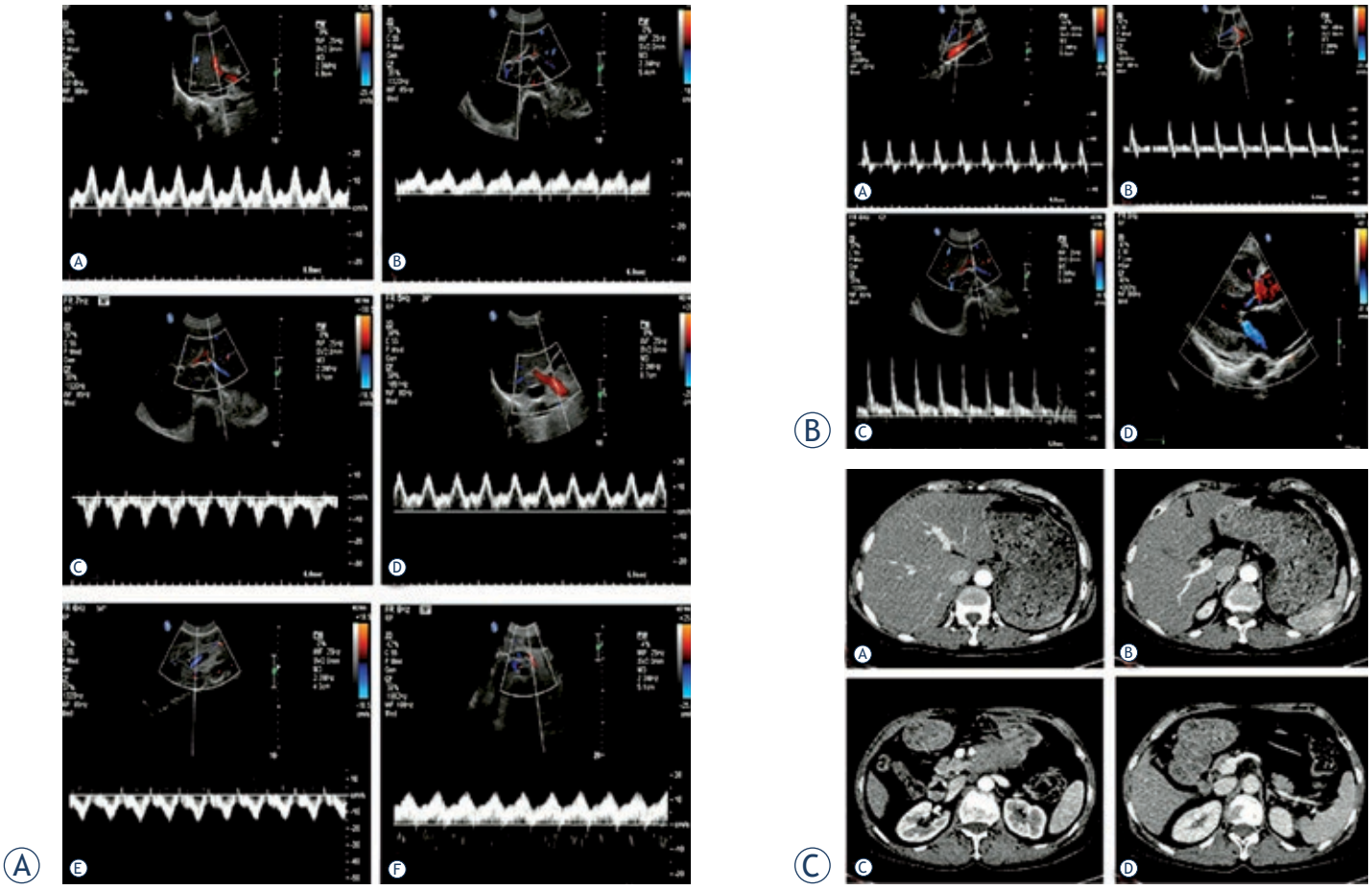

FIGURE 4. Diffuse extrahepatic APFs with indiscoverable focal lesions, confirmed by multimode imaging findings. (A) Color duplex US images of the portal system with normal internal diameter demonstrate typical arterial-like results with a continuous hepatopetal flow (a: right branch, b: left branch, c: sup. segmental brr., d: main trunk, e: superior mesenteric vein, f: splenic vein). (B) High-resistivity of multiple organs (a: triphase velocity tracing of abdominal aorta, b: triphase velocity tracing of hepatic artery, c: velocity tracing of intrahepatic artery with a high *RI*, d: hypertrophic left ventricular wall with aortic and mitral regurgitation). (C) Stronger enhancement of the affected superior mesenteric and splenic vein than that of the portal vein. (a: left branch, b: right posterior branch c: equal enhancement of superior mesenteric vein and its parallel running artery, d: stronger enhancement of the affected splenic vein than that of portal vein).

known as the acinus. Blood perfuses the liver parenchyma through the sinusoids and then enters the terminal hepatic venules, which form sequentially larger veins and drain into the inferior vena cava. The portal and hepatic vein are both without valves, thus their haemodynamics, especially the direction of blood flow, are responsive to change when exposed to variations in vascular pressure. The intrahepatic and extrahepatic terminals of the portal vein are both capillary networks; the intrahepatic terminal branches of the portal vein, and the hepatic artery and vein join the sinusoid. The blood flow directions of the portal vein and the hepatic artery are hepatopetal, but that of the hepatic vein is hepatofugal.[16]

Blood, similar to water, follows the path of least resistance. The normal portal venous flow is typically continuously hepatopetal with minimal variations related to the cardiac or respiratory activity.[17,18] If there is communications between an artery and the portal vein, the arterial blood results in an APF and preferentially flows into the adjacent portal venous system with low resistance rather than into the relatively highly resistant arterial lumen. Consequently, the portal drainage is arterialised, so it shows a hepatic artery-like velocity tracing.

APF can be congenital, post-traumatic, iatrogenic (trans-hepatic intervention or biopsy), neoplastic, or related to ruptured hepatic artery aneurysms.[7,19-22] Trauma and neoplasm are the most common causes of APF.[7] They may be either intra- or extra-hepatic. Intra-hepatic APF can cause the hepatofugal flow of portal drainage in the liver,

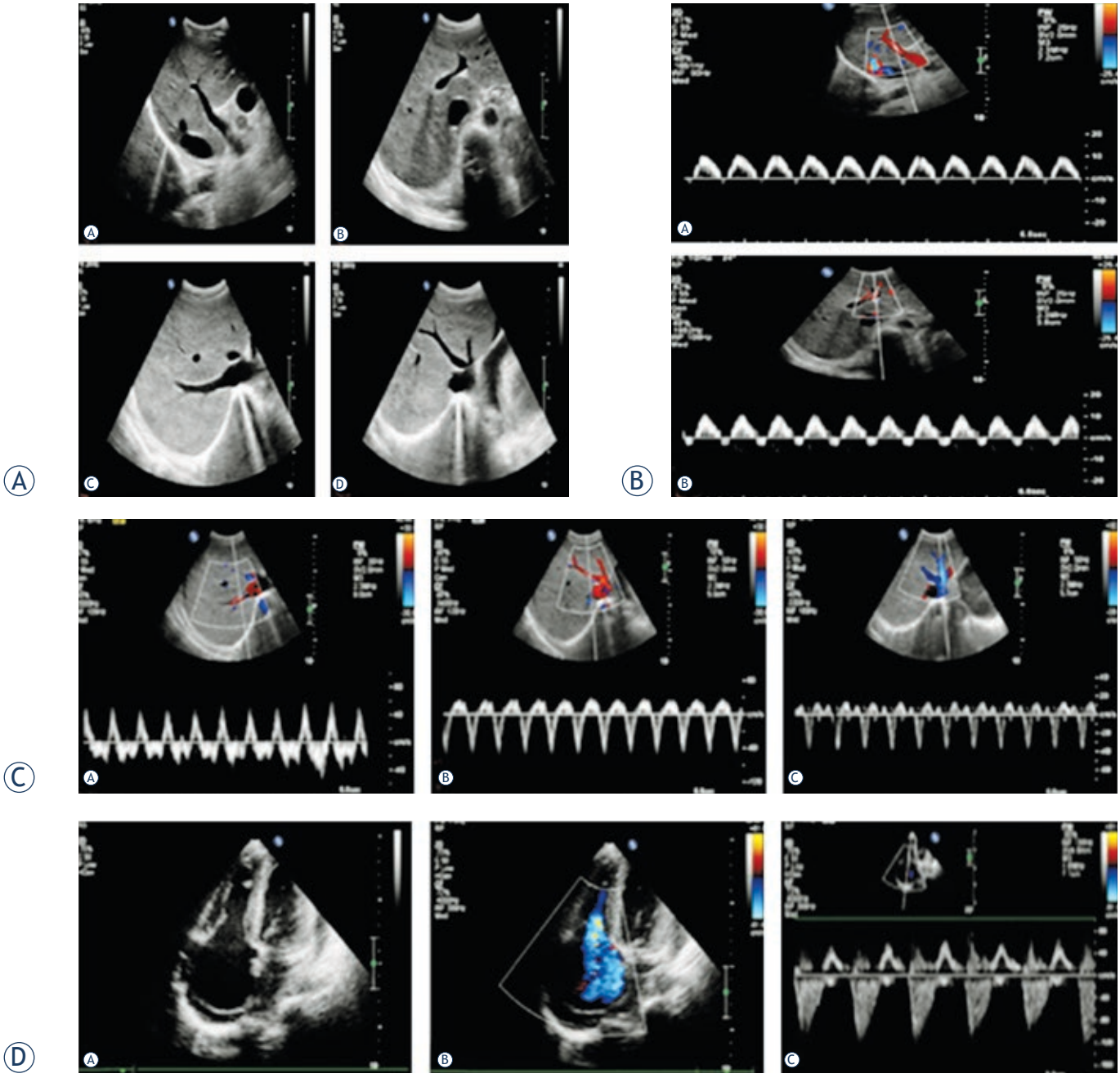

FIGURE 5. CTS with severe tricuspid regurgitation. (A) Normal US scans demonstrate normal internal diameters of the portal and hepatic veins (a: right branch, b: left branch c: right hepatic vein, d: middle and left hepatic vein). (B) The waveform of velocity tracing in the intrahepatic branch of the portal vein shows a typical hump-like shape with a transitory hepatofugal tracing (a: right branch, b: left branch). (C) PW displays an increase of retrograde phase of hepatic venous flow with increased velocities in the two phases (a: right hepatic vein, b: middle hepatic vein, c: left hepatic vein). (D) Echocardiography shows an enlarged right atrium with severe tricuspid regurgitation (a: Normal ultrasound scans, b: CDFI, c: PW).

and extra-hepatic APF can induce the hepatopetal flow.[23]

The portal velocity tracing of CTS is, to a large degree, influenced by the mechanical events in the right atrium.[24] The main factor is increased hepatic venous outflow resistance with subsequent periodic trans-sinusoidal shunting caused by the elevated right atrial pressure with periodic profuse retrograde venous drainage into the hepatic vein via the inferior vena cava.[25] This condition is commonly attributed to tricuspid insufficiency, and rarely, constrictive pericarditis.[26] The pattern is character-

ized by a monophasic hepatopetal flow with peak velocity and gradual diminution of velocity with or without a transitory hepatofugal flow velocity during each cardiac cycle; it exhibits a periodic hump-like velocity tracing. This pattern is associated with periodic portal hypertension and has been found to be predictive of congestive heart failure.

APF or CTS presentation depends particularly on the shunt flow and, thus, its haemodynamic consequences. A fistula blood flow is a direct function of both the size of the vessel supplying it and the diameter of the communication itself.[13,27] Those with small shunts often present as incidental findings in asymptomatic patients with indiscoverable focuses and may close spontaneously. A large or diffuse fistula results in a decrease in the feeding arterial pressure and an increase in the draining portal vein pressure. A large fistula indicates a varicose or saccular vessel with turbulent blood flow adjacent to the portal drainage.

APF can lead to chronic arterial inflow from the portal vein and CTS can facilitate the hepatic venous reflux into the portal vein. The increased blood flow in the portal system is considered to be the cause of portal hypertension.[7,9,28] The increased portal pressure also impairs blood efflux from the spleen and gastrointestinal tract by increasing vascular outflow resistance, which may lead to potential complications.[3,4] Mild to moderate abdominal pain and diarrhea secondary to congestive vascular enteropathy may be some early findings. Signs of more advanced disease include gastro-oesophageal variceal bleeding, splenomegaly, refractory ascites, or other signs of progressive liver failure caused by portal hypertension. APF is one of the main impediments and relative contra-indications to trans-arterial chemo-embolisation, which has been proven to be an effective means of managing unresectable hepatocellular carcinoma (HCC).[19]

The rationale behind AFP treatment is either to overcome existing portal hypertension or to prevent its development. The angiographic embolisation is a simple and effective means of treatment provided that the fistula is not too large and is accessible; it can be performed either via the trans-arterial approach or transvenous approach. The transvenous approach can be considered and used when there are multiple arteriovenous fistulas, or when embolisation via the trans-arterial approach is technically unsuccessful. Closure by embolisation with Gelfoam, steel coils, detachable balloons, n-butyl cyanoacrylate, or bucrylate has proven to be feasible.[2,7,19,22,29] The choice of embolic agent should be based on the underlying mechanism of the shunts and their angio-architecture. The hepatic resection of liver parenchyma containing the AFP and ligation of the feeding artery are reserved for those patients with fistulas that are too large for safe embolization or whose embolised arteries are recanalised.[30]

APF and CTS can be slight and asymptomatic, but they often cause symptoms because of their consequences.[8,10] Both are reversible causes of portal hypertension but utilize different therapeutic procedures. Thus, a correct diagnosis is necessary because only then a definitive therapy can be proposed. The waveform of the velocity tracing of the right and left branches of the portal vein is a reliable indicator that can differentiate the presence of APF or CTS. Its direction can distinguish intrahepatic from extrahepatic APF, and the velocity tracings of the hepatic artery and vein could further support the diagnosis. Therefore, color Doppler US can be proposed for the detecting of APF and CTS. The fistulous mechanism and angio-architecture should be identified in future investigations.

Conclusions

A fluctuating portal velocity tracing with rhythmicity is a reliable indicator for diagnosing APF or CTS. The evaluation of the velocity tracing patterns of the portal and hepatic veins, especially the direction of portal blood flow, should be used for the routine detection for APF and CTS in patients with gastrointestinal symptoms. Timely diagnosis and application of proper measures can relieve portal hypertension caused by APF or CTS.

References

1. Orrego M, Vargas HE, Balan V, Wells C, Harrison ME, Larson J, et al. Portal hypertension due to a splenic arteriovenous fistula: a case report. *Dig Dis Sci* 2006; **51:** 1113-6.
2. Yamagami T, Nakamura T, Nishimura T. Portal hypertension secondary to spontaneous arterio-portal venous fistulas: transcatheter arterial embolization with n-butyl cyanoacrylate and microcoils. *Cardiovasc Intervent Radiol* 2000; **23:** 400-2.
3. Aarts R, Ijland MM, de Blaauw I, Hoogeveen Y, Boetes C, van Proosdij M. Severe gastrointestinal tract bleeding in a two-month-old infant due to congenital intrahepatic arterioportal fistula. *Eur J Radiol* 2006; **59:** 25-8.
4. English WP, Johnson MB, Borman KR, Turner WW Jr. Mesenteric ischemia: an unusual presentation of traumatic intrahepatic arterioportal fistula. *Am Surg* 2001; **67:** 865-67.
5. Meyer MI, Bühler H, Bertschinger P. Arterioportal fistula as a cause of esophageal varices bleeding. *Schweiz Med Wochenschr* 2000; **130:** 42.
6. Raja K, Kochhar R, Sethy PK, Dutta U, Bali HK, Varma JS. An endoscopic study of upper-GI mucosal changes in patients with congestive heart failure. *Gastrointest Endosc* 2004; **60:** 887-93.

7. Tasar M, Gulec B, Bozlar U, Saglam M, Ugurel MS, Ucoz T. Intrahepatic arterioportal fistula and its treatment with detachable balloon and transcatheter embolization with coils and microspheres. *Clin Imaging* 2005; **29:** 325-30.
8. Chan WS, Poon WL, Cho DH, Chiu SS, Luk SH. Transcatheter embolisation of intrahepatic arteriovenous shunts in patients with hepatocellular carcinoma. *Hong Kong Med J* 2010; **16:** 48-55.
9. Ahn JH, Yu JS, Hwang SH, Chung JJ, Kim JH, Kim KW. Nontumorous arterioportal shunts in the liver: CT and MRI findings considering mechanisms and fate. *Eur Radiol* 2010; **20:** 385-94.
10. Capuano G, Pomponi D, Iaccarino V, Budillon G. An unusual case of ascites. *Dig Liver Dis* 2004; **36:** 628-31.
11. Bolognesi M, Sacerdoti D, Bombonato G, Chiesura-Corona M, Merkel C, Gatta A. Arterioportal fistulas in patients with liver cirrhosis: usefulness of color Doppler US for screening. *Radiology* 2000; **216:** 738-43.
12. Lu ZY, Ao JY, Jiang TA, Peng ZY, Wang ZK. A large congenital and solitary intrahepatic arterioportal fistula in an old woman. *World J Gastroenterol* 2009; **15:** 1656-9.
13. Wachsberg RH, Bahramipour P, Sofocleous CT, Barone A. Hepatofugal flow in the portal venous system: pathophysiology, imaging findings, and diagnostic pitfalls. *Radiographics* 2002; **22:** 123-40.
14. Popovic P, Stanisavljevic D, Jeromel M. Percutaneous transcatheter arterial embolization in haemodynamically stable patients with blunt splenic injury. *Radiol Oncol* 2010; 44: 30-3.
15. Meng Q, Ding W, Yang B, Fu N, Lu G. Analysis of peripheral artery velocity tracing in a porcine model. *Radiol Oncol* 2011; **45:** 82-90.
16. Furuta T, Maeda E, Akai H, Hanaoka S, Yoshioka N, Akahane M, Watadani T, Ohtomo K. Hepatic segments and vasculature: projecting CT anatomy onto angiograms. *Radiographics* 2009; **29:** 1-22.
17. Görg C, Riera-Knorrenschild J, Dietrich J. Pictorial review: Colour Doppler ultrasound flow patterns in the portal venous system. *Br J Radiol* 2002; **75:** 919-29.
18. Görg C, Seifart U, Zugmaier G. Color Doppler sonographic signs of respiration-dependent hepatofugal portal flow. *J Clin Ultrasound* 2004; **32:** 62-8.
19. Murata S, Tajima H, Nakazawa K, Onozawa S, Kumita S, Nomura K. Initial experience of transcatheter arterial chemoembolization during portal vein occlusion for unresectable hepatocellular carcinoma with marked arterioportal shunts. *Eur Radiol* 2009; **19:** 2016-23.
20. Sutcliffe R, Mieli-Vergani G, Dhawan A, Corbally M, Karani J, Heaton N. A novel treatment of congenital hepatoportal arteriovenous fistula. *J Pediatr Surg* 2008; **43:** 571-3.
21. Kumar N, de Goyet Jde V, Sharif K, McKiernan P, John P. Congenital, solitary, large, intrahepatic arterioportal fistula in a child: management and review of the literature. *Pediatr Radiol* 2003; **33:** 20-3.
22. Flum AS, Geiger JD, Gemmete JJ, Williams DM, Teitelbaum DH. Management of a traumatic hepatic artery pseudoaneurysm and arterioportal fistula with a combination of a stent graft and coil embolization using flow control with balloon remodeling. *J Pediatr Surg* 2009; **44:** e31-6.
23. Gallego C, Miralles M, Marín C, Muyor P, González G, García-Hidalgo E. Congenital hepatic shunts. *Radiographics* 2004; **24:** 755-72.
24. Loperfido F, Lombardo A, Amico CM, Vigna C, Testa M, Rossi E, et al. Doppler analysis of portal vein flow in tricuspid regurgitation. *J Heart Valve Dis* 1993; **2:** 174-82.
25. Eriksen R, Vegsundvaag J, Hole T, Morstøl TH. Hepatic and renal haemodynamic changes in congestive heart disease. *Tidsskr Nor Laegeforen* 2006; **126:** 743-6.
26. Gorka TS, Gorka W. Doppler sonographic diagnosis of severe portal vein pulsatility in constrictive pericarditis: flow normalization after pericardiectomy. *J Clin Ultrasound* 1999; **27:** 84-8.
27. Pieters PC, Miller WJ, DeMeo JH. Evaluation of the portal venous system: complementary roles of invasive and noninvasive imaging strategies. *Radiographics* 1997; **17:** 879-95.
28. Li WG, Chen YL, Chen JX, Qu L, Xue BD, Peng ZH, et al. Portal venous arterialization resulting in increased portal inflow and portal vein wall thickness in rats. *World J Gastroenterol* 2008; **14:** 6681-8.
29. Hardcastle TC, Reitz D, Hollander D, Rodseth R, Muckart DJ. Posttraumatic intrahepatic pseudoaneurysm in a child managed by coil angioembolization: a case report and literature review. *J Pediatr Surg* 2010; **45:** e1-3.
30. Eickhoff U, Kemen M, Kollig E, Zumtobel V, Senkal M. Post-traumatic intrahepatic arterioportal fistula. *Zentralbl Chir* 2000; **125:** 983-6.

research article

Cathepsin X in serum from patients with colorectal cancer: relation to prognosis

Tjasa Vizin[1], Ib Jarle Christensen[2], Hans Jørgen Nielsen[3,4], Janko Kos[1,5]

[1] Faculty of Pharmacy, University of Ljubljana, Ljubljana, Slovenia
[2] The Finsen Laboratory, Rigshospitalet, DK2200 Copenhagen, Denmark, & Biotech Research and Innovation Centre (BRIC), University of Copenhagen, Copenhagen, Denmark
[3] Department of Surgical Gastroenterology, Hvidovre Hospital, Hvidovre, Denmark
[4] Faculty of Surgery and Anaesthesiology, University of Copenhagen, Copenhagen, Denmark
[5] Department of Biotechnology, Jožef Stefan Institute, Ljubljana, Slovenia

Radiol Oncol 2012; 46(3): 207-212.

Received 26 April 2012
Accepted 6 June 2012

Correspondence to: Professor Janko Kos, PhD, Faculty of Pharmacy, University of Ljubljana, Aškerčeva 7, 1000 Ljubljana, Slovenia. E-mail: janko.kos@ffa.uni-lj.si

Disclosure: No potential conflicts of interest were disclosed.

Background. Up-regulation of lysosomal cysteine protease cathepsin X (Cat X) is associated with disorders of the immune system and neurodegenerative diseases, while its role in the development and progression of cancer is less understood. Enhanced secretion of pro-Cat X was observed in malignant processes, and therefore, the level of total serum Cat X rather than the active enzyme may better reflect the tumour status.

Patients and methods. Seventy-seven patients with colorectal cancer (CRC) were included in a retrospective study. Blood samples were collected prior to therapy. Using ELISA, the values of total Cat X were measured in serum. Groups of healthy persons (n=77), patients with adenomas (n=77) and patients with non-neoplastic findings (n=77) were included.

Results. Significant differences between the group of colorectal patients and the groups of healthy persons, adenoma patients and patients with non-malignant findings could not be shown (p=0.89). Within the group of CRC, higher levels of total Cat X significantly correlated to shorter overall survival (HR=2.08, 95% CI:1.07-4.05, p=0.028).

Conclusions. Total serum Cat X could be a useful prognostic indicator for determining survival of patients with CRC. Increased serum levels of total Cat X may reflect more aggressive tumour cell phenotypes and suggest the involvement of Cat X in processes involved in later stages of tumour progression.

Key words: cysteine cathepsins; cathepsin X; colorectal cancer, prognosis; serum biomarker

Introduction

Cysteine cathepsins have been reported as biomolecules that are involved in development and progression of cancer. The molecules may provide additional diagnostic and prognostic information for cancer patients.[1-3] In particular, increased activity, protein concentration and secretion of cathepsins B and L have been associated with poor patient outcome in various cancer types, including colorectal cancer (CRC).[4] Other cysteine cathepsins, including Cat X have been studied far less in cancer and their role in malignant processes is not clear. Cat X expression is restricted to various cells of the immune system, such as monocytes, macrophages and dendritic cells.[5] It is involved in immune response regulations, such as signal transduction, growth, maturation, adhesion, cell-cell communication, proliferation and migration of immune cells and in phagocytosis.[6-8] By proteolytic cleavage of C-terminal amino acids, Cat X regulates β_2 integrin functions[9], impairs neurotrophic activity of gamma-enolase[10] and the role of chemokine CXCL-12 in adhesion of hematopoietic stem and progenitor cells to osteoblasts.[11] Up-regulation of Cat X was associated also with the inflammatory processes

in patients infected with *Helicobacter pylori*[12], those with multiple trauma[13], inflammatory related neurodegenerative disorders[10], tuberculosis[14] and Huntington's disease.[15]

Several studies support the involvement of Cat X in cancer. First, the gene encoding Cat X is localized on chromosome 20 in region q13, which is frequently amplified in several types of cancer.[16,17] Increased expression of the pro-Cat X and active Cat X was found in tumour and immune cells of prostate cancer[18], gastric cancer[12] and in the most aggressive phenotypes of human malignant melanoma.[19] In immunohistochemical analysis of lung tumours Cat X revealed very faint staining in tumour cells, but positive staining in infiltrated immune cells.[5] Sevenich *et al*. showed that Cat X-deficient and PymT-induced breast cancer transgenic mice had a prolonged tumour-free period for breast cancer compared to Cat X-expressing mice.[20] Furthermore, it was demonstrated that Cat X deficiency leads to accelerated cellular senescence, a powerful tumour suppressor mechanism.[21]

Only few clinical studies related the levels of Cat X with clinico-pathological parameters in cancer patients. As shown by our group, significantly lower levels of active Cat X were found in serum of patients with inflammatory breast cancer compared to non-inflammatory breast cancer.[22] In cyst fluid from epithelial ovarian cancer we did not find a significant correlation of the levels of active Cat X with any clinico-pathological parameter.[23] On the other hand, increased mRNA levels of Cat X in hepatocellular carcinomas significantly correlated with advanced tumour stage.[24]

The aim of the present study was to determine the protein levels of total Cat X (pro-form and active mature form) in serum from patients with CRC in comparison to adenoma patients, patients with non-malignant findings and a group of healthy persons. Further, Cat X levels were related with clinico-pathological parameters, considering especially the correlation with overall survival of the patients.

Materials and methods

Patients

From October 2003 through December 2005, subjects were included in a multi-centre cross sectional study conducted at six Danish hospitals. Eligible for inclusion were subjects (aged 18+ years) undergoing endoscopy following symptoms related to CRC. Subjects previously diagnosed with CRC and subjects unable to give informed consent were excluded from the study. The Regional Ethical Committee and The Danish Data Protection Agency approved the study. Following oral and written consent according to the Helsinki II Declaration 5,165 individuals were included consecutively. Based on this study-population a case-control study was designed including 312 patients representing four diagnostic groups of subjects. The study population was selected in order to test the diagnostic potential of different promising serological markers in CRC. Primarily 77 subjects with pathologically verified colorectal adenocarcinomas (26% RC, n=20 and 74% CC, n=57) were selected at random. These patients underwent surgery and did not receive radio- or chemotherapy. For each of these, a subject with pathologically verified adenomas was randomly selected matching for age, gender and localisation of finding. Then subjects with other (non-malignant) findings were randomly selected and matched as described for the adenomas. Finally, subjects who had no findings at endoscopy and who reported no co-morbidity (healthy persons), were randomly selected and matched to the groups by age and gender. All pathological diagnoses were validated using the Danish National Registry on Pathological Examinations (www.patobank.dk). Patients who were diagnosed with cancer, but did not have the tumour removed were classified according to the clinical information available, and as a result exact tumour staging was not possible in few cases. Similarly for patients diagnosed with adenomas, the type of adenoma was not specified in all cases, either due to incompleteness of the pathological description available or due to loss of specimen during the examination. Previous cancer diagnoses were retrieved from the Danish Cancer Registry. One subject was shown to have a previous CRC and was excluded from the study together with the three matched subjects, leaving a study population of 308 subjects. Descriptive statistics for the matched subjects are given in Table 1.

Sampling

Blood samples were collected at the same day period prior to endoscopy in all subjects, following a standard operating procedure (SOP). At sample collection subjects were non-fasting. All subjects undergoing colonoscopy had completed a bowel preparation. Blood was collected at moderate tourniquet pressure, in 10 ml serum tubes (Vacutainer® Becton-Dickinson, Mountain View, CA, USA), and spun for 10 minutes at 3000 *g* and 4°C within 1

hour following collection. Samples were immediately stored at -80°C and were thawed and refrozen once prior to analysis.

Determination of Cat X

Human total Cat X was analyzed using ELISA, as described.[5] Briefly, microtiter plates (Nunc-IMMUNO™ MODULES, Roskilde, Denmark) were coated with goat polyclonal antibody against human Cat X (R&D SYSTEMS®, Minneapolis, USA), which recognizes pro-form and mature Cat X (2 µg/mL in 100 µL of 1 mM Na_2CO_3, 35 mM $NaHCO_3$, 15 mM NaN_3, pH 9.6). Following incubation over night at 4°C, the plates were washed three times with the washing buffer (0.15 Mm NaCl, 7.5 mM Na_2HPO_4 X $2H_2O$, 2.5 mM NaH_2PO_4 X $2H_2O$, 0.05% Tween® 20 (Sigma-Aldrich Chemie GmbH, Steinheim, Germany), pH 7.2), and blocked with 2% BSA in washing buffer for 1 h. The wells were filled with Cat X standards or serum samples and incubated for 2 h at 37°C. Finally, after washing, 100 µL of horseradish peroxidase-conjugated mouse 3B10 mAb, recognizing the pro-form and mature Cat X (1:1000 dilution) was applied. After 2 h incubation at 37°C, 200 µL of TMB (3,3′,5,5′-tetramethylbenzidine (TMB) Liquid Substrate System, Sigma-Aldrich Chemie GmbH, Steinheim, Germany) in the presence of hydrogen peroxide was added. After 20 minutes the reaction was stopped with 50 µL of 2 M H_2SO_4. The absorbance at 450 nm was measured with a microplate reader (TECAN Saphyre 2, Männedorf, Switzerland) and corrected for the absorbance of controls. Pro-Cat X used as a standard, was prepared and characterized as described.[25] The intra-assay and inter-assay coefficients of variance (CV) were 9.8% and 11.0%, respectively. To determine the linearity of ELISA, serum samples were serially diluted to the levels encompassing the range of the assay. Finally, the samples in a 1:2 dilution were added to the wells of microtiter plate. Detection limit of the assay was 2.0 ng/ml.

Statistical analysis

Statistical analysis was carried out using SAS (v9.2, SAS Institute, Cary, N.C., USA). To identify a diagnostic value of total Cat X, a linear model comparing the level of total Cat X between the four groups was used. Cat X concentrations were log transformed for statistical analysis. P-values less than 5% were considered significant.

For survival analysis, the Kaplan-Meier methods, dichotomizing the values using their respec-

TABLE 1. Subject characteristics

CRC patients	Subjects, n (%)
Gender	
Female	37 (48.0)
Male	40 (52.0)
Age Group	
40+	3 (4)
50+	10 (13)
60+	17 (22)
70+	26 (34)
80+	21 (27)
Localisation	
Right colon	23 (29.9)
Left colon	34 (44.2)
Rectum	20 (26.0)
Cancer Stage	
I	9 (12.5)
II	32 (44.4)
III	16 (22.2)
IV	15 (20.8)
not specified	5 (6.5)
Adenomas	
tubular	45 (58.4)
tubulovillous	16 (20.8)
villous	1 (1.3)
serrat	1 (1.3)
not specified	14 (18.2)
Size	
< 1 cm	41 (53)
> 1 cm	33 (42.8)
not specified	3 (3.8)
Non-malignant finding	
Diverticulosis	72 (93.5)
Haemorrhoids	4 (5.2)
Inflammatory bowel disease	1 (1.3)
Healthy persons	
	77 (100)

TABLE 2. Descriptive statistics for total Cat X concentrations. Values of total Cat X in sera of the colorectal cancer, adenoma, non-malignant findings and the control group of healthy persons.

group	N	median (ng/mL)	minimum (ng/mL)	maximum (ng/mL)	mean (ng/mL)	SD (ng/mL)
colorectal carcinoma	77	16.3	5.9	40.4	17.4	7.0
adenoma	77	17.1	4.1	40.0	17.8	6.5
non-malignant findings	77	17.4	2.0	61.5	18.5	8.7
healthy persons	77	17.1	5.4	99.5	18.8	11.4

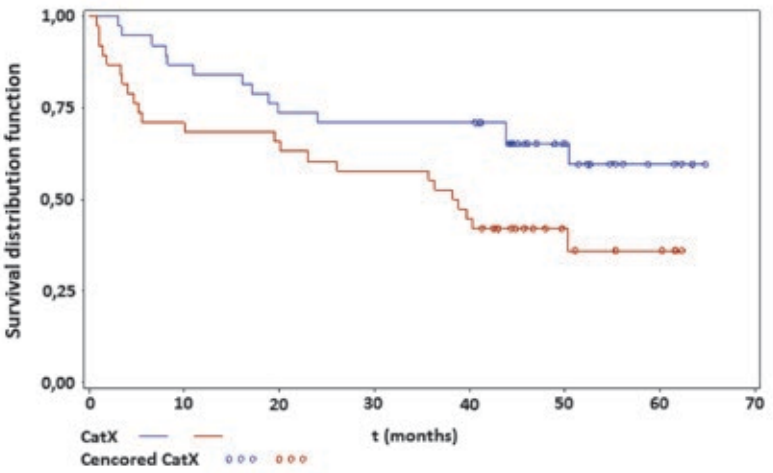

FIGURE 1. Survival analysis of cathepsin X in serum from patients with CRC. The Kaplan-Meier curve dichotomizing by the median shows the association between total Cat X serum concentrations and patient overall survival. Red colour represents a group of patients with high Cat X levels (≥ to median), blue colour represents a group of patients with low Cat X levels (< to median).

tive medians, and Cox regression analysis with the total Cat X values entered as continuous variables in the log scale (base 2), were used. The hazard ratio (HR) for the latter was for a two-fold difference in marker levels.

Results and discussion

CRC is the second most frequent malignant disease in the developed countries.[26,27] Besides carcinoembryonic antigen (CEA), several other serum tumour markers have been suggested for early detection of the disease and for prediction of prognosis[28-31], however, none of them has reached the regular clinical use yet. The levels of serum Cat X, evaluated in this pilot study, revealed no significant difference between CRC patients and control groups, however, higher levels in CRC patients correlated with shorter overall survival and may provide prognostic information.

The levels of total Cat X in the CRC group, adenoma patients, patients with non-malignant findings and the group of healthy persons are shown in Table 2. The results show that there is no significant statistical difference in Cat X levels between the groups (p=0.89).

The survival analysis (Figure 1) shows an association between total Cat X serum concentrations and overall survival of CRC patients. The log rank statistics show that patients with higher serum levels of total Cat X have shorter survival than the patients with lower total Cat X serum levels (p=0.028; HR=2.08 (95% CI: 1.07-4.05)). On the continuous scale the difference was not significant (p=0.19; HR=1.48 (95% CI: 0.83-2.64)).

In immune cells Cat X localizes in lysosomes predominantly as a pro-enzyme. After cell activation, Cat X containing vesicles translocate towards the plasma membrane and Cat X can be secreted into the extracellular space.[32] The similar behaviour was demonstrated also in tumour cells.[5,18] During this process, pro-Cat X can be activated by the other cysteine protease cathepsin L.[33] Enhanced secretion of pro-Cat X rather than the active form seems to be typical for malignant processes, and therefore, the level of total serum Cat X may better reflect the tumour status than the level of the active Cat X alone.[13,22]

The question whether tumour cells or activated immune cells contribute to increased extracellular levels of Cat X remains open. The same holds for the role of Cat X in malignant progression, which cannot be the degradation of extracellular matrix, an event, typical for some other cysteine cathepsins since Cat X acts solely as carboxypeptidase and not as endopeptidase. Based on the results on single and double knock-out mice, Cat X was suggested to compensate the malignant potential of cathepsin B[20,34] enhancing cell adhesion, changing the migration mode[6] or inducing epithelial-mesenchymal transition in tumour cells.[24] Its increased serum levels may reflect more aggressive tumour

cell phenotype which is related to higher risk for relapse and shorter survival of cancer patients.

Our results show that higher levels of total Cat X in serum from CRC patients significantly correlate to shorter overall survival, suggesting the involvement of total Cat X in the late stages of the malignant process. This is in contrast to the results of Sevenich *et al*.[20], which show that in breast cancer transgenic mice model Cat X was associated primarily with the initial stages of the malignant process and less with the tumour progression and metastasis. The authors showed that Cat X deficient mice had a prolonged tumour-free period compared to Cat X-expressing mice, however, only a trend toward reduced metastatic burden was observed. Only a combined loss of cathepsin B and Cat X led to additive effects including a reduction in the number and size of lung metastases. On the other hand, the study by Hidaka *et al.* showed that amplification of the region 20q13.2 correlated with the metastatic potential and tumour progression of CRC[16], suggesting the involvement of Cat X in the later stages of cancer. The latter was proposed also by Wang *et al.*, demonstrating that an upregulation of Cat X expression strongly correlated with advanced clinical stage, shorter overall survival and induced metastatic potential of hepatocellular carcinoma.[24] Moreover, a recent study by Lines *et al.* showed that in pancreatic ductal adenocarcinoma, Cat X expression is downregulated by overexpressed S100P-binding protein, which results in decreased cell adhesion, correlating with lower metastatic potential of pancreatic cancer cells.[35]

Several molecular targets have been proposed either for pro-Cat X or active Cat X which may contribute to progression of cancer. Pro-Cat X binds integrin receptors by RGD motif[36,37] and interacts with heparane sulphate proteoglycans[8] modulating cell adhesion and motility. Active Cat X was shown to cleave C-terminal amino acids of chemokine CXCL-12[11] and beta-2 chain of integrin receptors[6] regulating chemotaxis and a wide range of beta-2 integrin functions, including cell adhesion, proliferation and migration. Active Cat X also cleaves the C-terminal amino acids of gamma-enolase (neuronal specific enolase - NSE)[10], a tumour associated protein, used as a marker for prognosis and response to therapy in lung cancer and neuroblastoma. As shown in our recent studies[38,39], uncleaved NSE regulates proliferation and survival of neuronal cells, whereas the presence of active Cat X significantly impairs the tropic function of gamma-enolase. However, the same effect has not been demonstrated in tumour cells. We may hypothesize that pro-Cat X and active Cat X have the opposite role in malignant progression and the ratio between the pro-Cat X and active Cat X could direct tumour promotive or suppressive action.

To summarize, total serum Cat X could be a useful prognostic indicator to determine overall survival of patients with CRC, serving to optimize therapy and patient care. However, our study based on 77 CRC patients is a preliminary one and a larger group of patients needs to be analysed in a multivariable model to confirm our results.

Acknowledgement

This study was supported by the Research Agency of the Republic of Slovenia [grant n. P4-0127 and J4-4123 (to J.K.)]

References

1. Turk V, Kos J, Turk B. Cysteine cathepsins (proteases)-on the main stage of cancer? *Cancer Cell* 2004; **5:** 409-10.
2. Strojan P. Cysteine cathepsins and stefins in head and neck cancer: an update of clinical studies. *Radiol Oncol* 2008; **42:** 69-81.
3. Ardebili SY, Zajc I, Gole B, Campos B, Herold-Mende C, Drmota S et al. CD133/prominin1 is prognostic for GBM patient's survival, but inversely correlated with cysteine cathepsins' expression in glioblastoma derived spheroids. *Radiol Oncol* 2011; **45:** 102-15.
4. Kos J, Lah TT. Cysteine proteinases and their endogenous inhibitors: target proteins for prognosis, diagnosis and therapy in cancer (review). *Oncol Rep* 1998; **5:** 1349-61.
5. Kos J, Sekirnik A, Premzl A, Zavašnik Bergant V, Langerholc T, Turk B, et al. Carboxypeptidases cathepsins X and B display distinct protein profile in human cells and tissues. *Exp Cell Res* 2005; **306:** 103-13.
6. Kos J, Jevnikar Z, Obermajer N. The role of cathepsin X in cell signalling. *Cell Adh Migr* 2009; **3:** 164-6.
7. Obermajer N, Jevnikar Z, Doljak B, Sadaghiani AM, Bogyo M, Kos J. Cathepsin X-mediated β2-integrin activation results in nanotube outgrowth. *Cell Mol Life Sci* 2009; **66:** 1126-34.
8. Nascimento FD, Rizzi CC, Nantes IL, Stefe I, Turk B, Carmona AK, et al. Cathepsin X binds to cell surface heparan sulfate proteoglycans. *Arch Biochem Biophys* 2005; **436:** 323-32.
9. Obermajer N, Repnik U, Jevnikar Z, Turk B, Kreft M, Kos J. Cysteine protease cathepsin X modulates immune response via activation of β_2 integrins. *Immunology* 2008; **124**: 76-88.
10. Obermajer N, Doljak B, Jamnik P, Fonovič UP, Kos J. Cathepsin X cleaves the C-terminal dipeptide of alpha- and gamma-enolase and impairs survival and neuritogenesis of neuronal cells. *Int J Biochem Cell Biol* 2009; **41:** 1685-96.
11. Staudt DN, Aicher KW, Kalbacher H, Stevanovic S, Carmona KA, Bogyo M, et al. Cathepsin X is secreted by human osteoblasts, digests CXCL-12 and impairs adhesion of hematopoietic stem and progenitor cells to osteoblasts. *Haematol* 2010; **95:** 1452-60.
12. Krueger S, Kalinski T, Hundertmark T, Wex T, Küster D, Peitz U, et al. Up-regulation of cathepsin X in Helicobacter pylori gastritis and gastric cancer. *J Pathol* 2005; **207:** 32-42.
13. Nägler DK, Lechner AM, Oettl A, Kozaczynska K, Scheuber HP, Gippner-Steppert C, et al. An enzyme-linked immunosorbent assay for human cathepsin X, a potential new inflamatory marker. *J Immunol Methods* 2006; **308:** 241-50.

14. Baker AR, Zalwango S, Malone LL, Igo RP Jr, Qiu F, Nsereko M, et al. Genetic susceptibility to tuberculosis associated with cathepsin Z haplotype in a Ugandan household contact study. *Hum Immunol* 2011; **72:** 426-30.

15. Ratovitski T, Chiqhladze E, Waldron E, Hirschhorn RR, Ross CA. Cysteine proteases bleomycin hydrolase and cathepsin Z mediate N-terminal proteolysis and toxicity of mutant huntingtin. *J Biol Chem* 2011; **286:** 12578-89.

16. Hidaka S, Yasutake T, Takeshita H, Kondo M, Tsuji T, Nanashima A, et al. Differences in 20q13.2 Copy Number between Colorectal Cancers with and without liver metastasis. *Clin Cancer Res* 2000; **6:** 2712-7.

17. Bar-Shira A, Pinthus HJ, Rozovsky U, Goldstein M, Sellers RW, Yaron Y, et al. Multiple genes in human 20q13 chromosomal region are involved in an advanced prostate cancer xenograft. *Cancer Res* 2002; **62:** 6803-7.

18. Nägler DK, Krüger S, Kellner A, Ziomek E, Menard R, Buhtz P, et al. Up-regulation of Cathepsin X in prostate cancer and prostatic intraepithelial neoplasia. *Prostate* 2004; **60:** 109-19.

19. Rumpler G, Becker B, Hafner C, McClelland M, Stolz W, Landthaler M, et al. Identification of differentially expressed genes in models of melanoma progression by cDNA array analysis: SPARC, MIF and a novel cathepsin protease characterize aggressive phenotypes. *Exp Dermatol* 2003; **12:** 761-71.

20. Sevenich L, Schurigt U, Sachse K, Gajda M, Werner F, Müller S, et al. Synergistic antitumor effects of combined cathepsin B and cathepsin Z deficiencies on breast cancer progression and metastasis in mice. *PNAS* 2010; **107:** 2497-502.

21. Kraus S, Bunsen T, Schuster S, Cichoń MA, Tacke M, Reinheckel T, et al. Cellular senescence induced by cathepsin X downregulation. *Eur J Cell Biol* 2011; **90:** 678-86.

22. Decock J, Obermajer N, Vozelj S, Hendrickx W, Paridaens R, Kos J. Cathepsin B, cathepsin H, cathepsin X and cystatin C in sera of patients with early-stage and inflammatory breast cancer. *Int J Biol Markers* 2008; **23:** 161-8.

23. Kolwijck E, Kos J, Obermajer N, Span PN, Thomas CM, Massuger LF, et al. The balance between extracellular cathepsins and cystatin C is of importance for ovarian cancer. *Eur J Clin Invest* 2010; **40:** 591-9.

24. Wang J, Chen L, Li Y, Guan XY. Overexpression of Cathepsin Z contributes to tumor metastasis by inducing epithelial-mesenchymal transition of hepatocellular carcinoma. *PLoS ONE* 2011; **6:** e24967.

25. Fonovic PU, Kos J. Efficient removal of Cathepsin L from active Cathepsin X using immunoprecipitation technique. *Acta Chim* 2009; **56:** 985-8.

26. Brenner H, Bouvier AM, Foschi R, Hackl M, Larsen IK, Lemmens V, et al. Progress in colorectal cancer survival in Europe from the late 1980s to the early 21st century: The EUROCARE study. *Int J Cancer* 2011; doi: 10.1002/ijc.26192.

27. Velenik V. Post-treatment surveillance in colorectal cancer. *Radiol Oncol* 2010, **44:** 135-41.

28. Zavoral M, Suchanek S, Zavada F, Dusek L, Muzik J, Seifert B, et al. Colorectal cancer screening in Europe. *World J Gastroenterol* 2009; **15:** 5907-15.

29. Booth RA. Minimally invasive biomarkers for detection and staging of colorectal cancer. *Cancer Lett* 2007; **249:** 87-96.

30. Nielsen HJ, Brünner N, Frederiksen C, Lomholt AF, King D, Jørgensen LN, et al. Plasma tissue inhibitor of metalloproteinases-1 (TIMP-1): a novel biological marker in the detection of primary colorectal cancer. Protocol outlines of the Danish-Australian endoscopy study group on colorectal cancer detection. *Scand J Gastroenterol* 2008; **43:** 242-8.

31. Nielsen HJ, Christensen IJ, Brünner N. A novel prognostic index in colorectal cancer defined by serum carcinoembryonic antigen and plasma tissue inhibitor of metalloproteinases-1. *Scand J Gastroenterol* 2010; **45:** 200-7.

32. Obermajer N, Premzl A, Zavašnik Bergant T, Turk B, Kos J. Carboxypeptidase cathepsin X mediates β_2-integrin-dependent adhesion of differentiated U-937 cells. *Exp Cell Res* 2006; **312:** 2515-27.

33. Nägler DK, Zhang R, Tam W, Sulea T, Purisima EO, Ménard R. Human cathepsin X: A cysteine protease with unique carboxypeptidase activity. *Biochemistry* 1999; **38:** 12648-54.

34. Vasiljeva O, Papazoglou A, Krüger A, Brodoefel H, Korovin M, Deussing J, et al. Tumor cell-derived and macrophage-derived cathepsin B promotes progression and lung metastasis of mammary cancer. *Cancer Res* 2006; **66:** 5242-50.

35. Lines KE, Chelala C, Dmitrovic B, Wijesuriya N, Kocher HM, Marshall JF, et al. S100P-binding protein, S100PBP, mediates adhesion through regulation of cathepsin Z in pancreatic cancer cells. *Am J Pathol* 2012; **180:** 1485-94.

36. Nägler DK, Mènard R: Human cathepsin X: a novel cysteine protease of the papain family with a very short proregion and unique insertions. *FEBS Lett* 1998; **434:** 135-9.

37. Santamaría I, Velasco G, Pendás AM, Fueyo A, López-Otín C. Cathepsin Z, a novel human cysteine proteinase with a short propeptide domain and unique chromosomal location. *J Biol Chem* 1998; **273:** 16816-23.

38. Hafner A, Obermajer N, Kos J. γ-1-syntrophin mediates trafficking of γ-enolase towards the plasma membrane and enhances its neurotrophic activity. *Neurosignals* 2010; **18:** 246-58.

39. Hafner A, Obermajer N, Kos J. γ-Enolase C-terminal peptide promotes cell survival and neurite ougrowth by activation of PI3K/Akt and MAPK/ERK signalling pathways. *Biochem J* 2012; **443:** 439-50.

research article

Contrasting effect of recombinant human erythropoietin on breast cancer cell response to cisplatin induced cytotoxicity

Nina Trost[1], Peter Juvan[1], Gregor Sersa[2], Natasa Debeljak[1,3]

[1] Center for Functional Genomics and Bio-chips, Institute of Biochemistry, Faculty of Medicine, University of Ljubljana, Slovenia
[2] Institute of Oncology, Department of Experimental Oncology, Ljubljana, Slovenia
[3] Medical Center for Molecular Biology, Institute of Biochemistry, Faculty of Medicine, University of Ljubljana, Slovenia

Radiol Oncol 2012; 46(3): 213-225.

Received 26 January 2012
Accepted 18 May 2012

Correspondence to: Assist. Prof. Dr. Nataša Debeljak, Institute of Biochemistry, Faculty of Medicine University of Ljubljana, Vrazov trg 2, SI-1000 Ljubljana, Slovenia. Phone: +386-1-543-7663; Fax: +386-1-543-7641; E-mail: natasa.debeljak@mf.uni-lj.si

Disclosure: No potential conflicts of interest were disclosed.

Background. Human recombinant erythropoietin (rHuEpo) that is used for the treatment of the chemotherapy-induced anaemia in cancer patients was shown to cause detrimental effects on the course of disease due to increased adverse events inflicting patient's survival, potentially related to rHuEpo-induced cancer progression. In this study, we elucidate the effect of rHuEpo administration on breast cancer cell proliferation and gene expression after cisplatin (cDDP) induced cytotoxicity.

Materials and methods. Two breast carcinoma models, MCF-7 and MDA-MB-231 cell lines, were used differing in oestrogen (ER) and progesterone (PR) receptors and *p53* status. Cells were cultured with or without rHuEpo for 24 h or 9 weeks and their growth characteristics after cDDP treatment were assessed together with expression of genes involved in the *p53*-signaling pathway.

Results. Short-term exposure of breast cancer cells to rHuEpo lowers their proliferation and reduces cDDP cytotoxic potency. In contrast, long-term exposure of MCF-7 cells to rHuEpo increases proliferation and predisposes MCF-7 cells to cDDP cytotoxicity, but has no effect on MDA-MB-231 cells. MDA-MB-231 cells show altered level of ERK phosphorylation, indicating involvement of MAPK signalling pathway. Gene expression analysis of *p53*-dependent genes and *bcl-2* gene family members confirmed differences between long and short-term rHuEpo effects, indicating the most prominent changes in *BCL2* and *BAD* expression.

Conclusions. Proliferation and survival characteristics of MCF-7 cells are reversely modulated by the length of the rHuEpo exposure. On the other hand, MDA-MB-231 cells are almost irresponsive to long-term rHuEpo, supposedly due to the mutated *p53* and ER(+)/PR(-) status. The p53 and ER/PR status may predict tumour response on rHuEpo and cDDP treatment.

Key words: breast cancer; erythropoietin; cisplatin; cytotoxicity

Introduction

Erythropoietin (Epo) is a hormone of renal origin that upon its binding to the cognate erythropoietin receptor (EpoR) acts as one of the main regulators of proliferation and differentiation of erythroid progenitors in bone marrow.[1] EpoR expression is not limited only to erythropoietic cells but it is expressed also in a wide variety of non-hematopoietic cells.[1-3] Epo is the only hematopoietic growth factor whose expression is regulated by tissue hypoxia.[4] Accumulating evidence has proven that Epo exerts additional tissue-protective effects for multiple tissues, for example in ischemic and degenerative heart and brain diseases.[5] Expression of EpoR was detected in tumour tissues and question has

arisen whether Epo promotes tumour cell survival and stimulates tumour growth. Direct influences on normal and tumour cell progression therefore require the presence of functional surface EpoR to trigger downstream signalling pathways, namely JAK/STAT5, PI3K/Akt, Ras/MAPK and PKC.[6,7] It was suggested that Epo may exert the pleiotropic mode of action.[8]

Severe anaemia is a frequent side effect of cancer chemotherapy, resulting mainly from chemotherapy induced inhibition of erythroid cell maturation in the bone marrow and interference with the ability of kidney to produce Epo. Onset of anaemia is associated with reduced quality-of-life and is thought to concur with the development of more aggressive cancer phenotypes due to lowered tumour oxygenation.[9] In the early days, rHuEpo was shown to be a safe and effective treatment of choice, improving quality-of-life and reducing the need for blood transfusions.[10,11] However, data from clinical trials in head and neck (ENHANCE)[12] and breast cancer patients (BEST)[13,14] and from subsequent meta-analyses (*e.g.*, EPO-CAN 20, GOG 191 and trials with breast cancer)[15-18] gave conflicting results indicating that rHuEpo treatment is reducing progression-free and overall survival with increasing haemoglobin level over 120 g/L.[19] Breast cancer is the most common cancer among women in the world and as such represents an important health care challenge.[20] Cisplatin (cDDP), a very potent anti-tumour agent, is used for the therapy of several malignancies.[21-23] It shows high activity as first-line chemotherapy in advanced breast cancer.[24] The formation of DNA-cDDP adducts translate cDDP-induced DNA damage to inhibition of DNA synthesis, suppression of RNA transcription causing cell cycle arrest that finally culminates in the activation of apoptosis.[25] Apoptosis is one of the pathways of programmed cell death that is markedly influenced by the variety of genes, among which the most important are the tumour-suppressor gene *p53* and members of the *bcl-2* gene family. Mutations in *p53* have been shown to confer sensitivity to drugs whose toxicity is modulated by nuclear excision repair, such as ERCC1.[26] The main drawback of cDDP based chemotherapy is the occurrence of resistance.[27]

In this study we focused on MCF-7 and MDA-MB-231 breast cancer cell lines in order to address potential effect of Epo on the response of tumour cells to the cDDP cytotoxicity. rHuEpo was reported to stimulate the proliferation of several human breast cancer cell lines that were expressing functional EpoR[28], including both cell lines used in this study. There are several well established genetic differences between the selected cell lines potentially contributing to cell sensitivity to rHuEpo and cDDP. MCF-7 is oestrogen (ER) and progesterone receptor (PR) positive cell line with wild-type *p53*, while MDA-MB-231 cell line is ER-positive but PR-negative with mutated *p53*. Normal p53 function was shown to have positive implications in the propagation of apoptotic cell death. In line with this, ER(+)/PR(-) breast tumours have more aggressive phenotypes and are less sensitive to growth factor deprivation compared to ER(+)/PR(+).[29] Moreover, strong correlations between high *EPOR*, *ER* and *PR* expression were reported and a specific functional association between EpoR and ERα was postulated.[30] Similar studies were performed with different cell types, namely renal carcinoma cells, melanoma, malignant glioma, cervical cancer cells and mesothelioma cells[31-34], reporting contradictory effects of Epo on cell survival after cDDP treatment. However this is the first study focusing on the effects of rHuEpo and cDDP in breast cancer with described genotype (p53, ER/PR status). With cell proliferation, viability and clonogenic assays we evaluated short (24 h, 12 days) and long-term (9 weeks) effect of rHuEpo treatment on MCF-7 and MDA-MB-231 growth characteristics, their sensitivity to cDDP and potential synergism between both treatments. Genes involved in the process of cell apoptosis, specifically those included in the *p53*-signaling pathway and the *bcl-2* gene family, because they mediate majority of cytotoxic stimuli, were analysed with qPCR. Using western blot, we analysed the phosphorylation status of extracellular signal-regulated kinase (ERK, MAPK), protein kinase B (Akt, PI-3K) and signal transducers and activators of transcription 5 (STAT5, Jak/STAT5) proteins that are thought to be activated upon rHuEpo treatment[6,7,35] or were previously shown to be crucial for cDDP induced apoptotic response.[36]

Materials and methods

Cell lines and cell culture pretreatments

MCF-7 and MDA-MB-231 human breast epithelial cells and UT7/Epo human leukemic, an Epo dependent cell line, were maintained in cell culture at 37°C in a humidified 5% (v/v) CO2 atmosphere. MCF-7 and MDA-MB-231 cells were obtained from American Type Culture Collection (ATCC, USA) and were cultured according to the ATCC recommendations. MCF-7 and MDA-MB-231 cells were pretreated with the rHuEpo for 9 weeks (5 and 25

U/mL, Neorecormon, Roche, Germany). In parallel, control cells were cultured in the same conditions, but without rHuEpo. For cell proliferation and cell viability studies, insulin was omitted from the media. cDDP (Pliva, Croatia) was used for cytotoxicity studies (0-200 μM). UT7/Epo cells were kindly provided by C. Lacout (Institute of Cancerology Gustave Roussy, France) and were cultured in alphaMEM medium (Sigma, USA), supplemented with 10% FBS and 2 U/mL rHuEpo and were used as a positive control in western blot analysis.

Proliferation assays

Cell proliferation assays were performed with colorimetric WST-1 reagent (Roche) on 9 weeks rHuEpo pretreated and 24 h treated MCF-7 and MDA-MB-231 cell lines in parallel with control cells that were cultured without rHuEpo. Cells were exposed to cDDP and cell proliferation was assessed as shown in Figure 1A. $4x10^3$ cells per well were seeded in five-plicates on a 96-well plate and left to adhere in the medium. After two days in culture, cells were exposed to varying concentrations of cDDP (0, 1, 3, 10, 30, 60, 100, 120, 150, 180, 200 μM) for 24 h. Cell proliferation was normalized to the proliferation of control cells that were not exposed to cDDP. All experiments were performed three times.

Clonogenic assays (CFAs)

Assay was performed on 9 weeks rHuEpo pretreated and 12 days rHuEpo treated MCF-7 and MDA-MB-231 cells in parallel with control cells that were cultured without rHuEpo. Cells were seeded on 6-well plates at a concentration of 100 cells per well and cultured for 14 days. To address rHuEpo effect, pretreated cells and their controls were cultured in the growth medium without rHuEpo for 14 days (Figure 1B, treatments *b, d, f, h*). rHuEpo and cDDP interaction was evaluated on cells that were exposed to cDDP for 24 h as shown in Figure 1B. Cells were exposed to varying cDDP concentrations (0.01, 0.05, 0.1, 0.5, 1, 6, 10, 12, 18, 20 μM). The medium was changed every 5 days. Colony quantification was done manually and using UviPro analysis system (Uvitec, UK) after crystal violet staining (0.5 %). Colonies were classified as small if containing <100 cells or big otherwise. Surviving fraction of cDDP exposed cells were normalized relative to surviving fraction of non-exposed cells.[25] Experiments were repeated three times in tri-plicates.

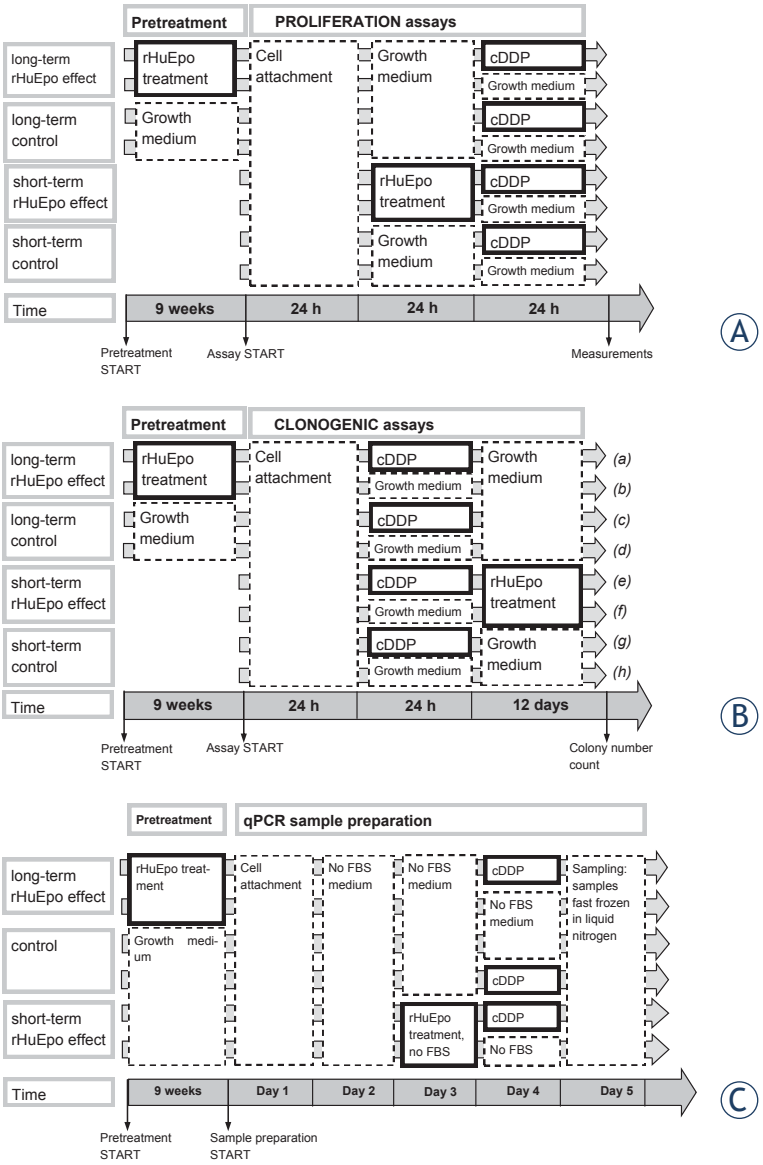

FIGURE 1. Schematic representation of treatment protocols: (A) proliferation, (B) clonogenic, (C) qPCR and western blot assays.

Gene expression analysis

Sample preparation. On day 1, control and rHuEpo pretreated MCF-7 and MDA-MB-231 cells were seeded on 6-well plates in 4 replicates at density $2x10^5$ cells per well (Figure 1C). Medium was changed to serum free medium after 24 h of incubation. Cells were treated with rHuEpo for 24 h on day 3 in order to assess its short-term effect. cDDP treatment was performed on day 4. 10 μM cDDP was used for the treatment of MCF-7 cells and 60 μM for MDA-MB-231 cells. Samples were fast frozen in liquid nitrogen on day 5. RNA was

TABLE 1. Details on genes of interest and reference genes

Gene symbol	Gene Name	Primer sequence	Ref.seq	Amplicon length	Primer Eff
Genes of interest, GOI					
FOS	FBJ murine osteosarcoma viral oncogene homolog	Fw: 5'-CTACCACTCACCCGCAGACT-3' Rev: 5'-AGGTCCGTGCAGAAGTCCT-3'	NM_005252.2	72	2
JUN	jun-proto oncogene	Fw: 5'-CCAAAGGATAGTGCGATGTTT-3' Rev: 5'-CTGTCCCTCTCCACTGCAAC-3'	NM_002228.2	62	2
NFκβ	nuclear factor of kappa light polypeptide gene enhancer in B-cells 1	Fw: 5'-GGTGCCTCTAGTGAAAAGAACAAGA-3' Rev: 5'-GCTGGTCCCACATAGTTGCA-3'	NM_003998.3	68	1.722
TP53	tumor protein p53	Fw: 5'-CCCCAGCCAAAGAAGAAAC-3' Rev: 5'-AACATCTCGAAGCGCTCAC-3'	NM_000546.4	77	1.922
BAD	BCL2-assocciated agonist of cell death	Fw: 5'-GAGTGACGAGTTTGTGGACTCCTT-3' Rev: 5'-TGTGCCCGCGCTCTTC-3'	NM_004322.2	61	2.055
BAX	BCL2-assocciated X protein	Fw: 5'-ATGTTTTCTGACGGCAACTTC-3' Rev: 5'-ATCAGTTCCGGCACCTTG-3'	NM_004324.3	104	1.812
BBC3	BCL2 binding component 3 [PUMA]	Fw: 5'-GACCTCAACGCACAGTACGA-3' Rev: 5'-GAGATTGTACAGGACCCTCCA-3'	NM_001127240.1	84	1.651
BCL2	B-cell CLL/lymphoma 2	Fw: 5'-TCCCTCGCTGCACAAATACTC-3' Rev: 5'-ACGACCCGATGGCCATAGA-3'	NM_000633.2	72	2.117
BCL2L1	BCL2-like 1 [BCL-XL]	Fw: 5'-CTTTTGTGGAACTCTATGGGAACA-3' Rev: 5'-CAGCGGTTGAAGCGTTCCT-3'	NM_138639.1	70	2.023
CASP3	caspase 3, apoptosis-related cysteine peptidase	Fw: 5'-GCCTACAGCCCATTTCTCCAT-3' Rev: 5'-GCGCCCTGGCAGCAT-3'	NM_004346.3	57	2.025
CASP9	caspase 9, apoptosis-related cysteine peptidase	Fw: 5'-GGAAGCCCAAGCTCTTTTTC-3' Rev: 5'-AAGTGGAGGCCACCTCAAA-3'	NM_001229.2	75	1.997
PMAIP1	phorbol-12-myristate-13-acetate-induced protein 1 [NOXA]	Fw: 5'-GGAGATGCCTGGGAAGAAG-3' Rev: 5'-CCTGAGTTGAGTAGCACACTCG-3'	NM_021127.2	94	2.086
EPOR	erythropoietin receptor	Fw: 5'-TTGGAGGACTTGGTGTGTTTC-3' Rev: 5'-AGCTTCCATGGCTCATCCT-3'	NM_000121.2	101	1.813
Reference genes					
Rplp0	ribosomal protein, large, P0	Fw: 5'-TCTACAACCCTGAAGTGCTTGAT-3' Rev: 5'-CAATCTGCAGACAGACACTGG-3'	NM_001002.3	96	2.073
GAPDH	glyceraldehyde-3-phosphate dehydrogenase	Fw: 5'-AGCCACATCGCTCAGACAC-3' Rev: 5'-GCCCAATACGACCAAATCC-3'	NM_002046.3	66	1.999
PpiA	peptidylprolyl isomerase A (cyclophilin A)	Fw: 5'-ATGCTGGACCCAACACAAAT-3' Rev: 5'-TCTTTCACTTTGCCAAACACC-3'	NM_021130.3	97	1.981
YWHAZ	tyrosine 3 – monooxygenase/tryptophan 5 –monooxygenase activation protein	Fw: 5'-GATCCCCAATGCTTCACAAG-3' Rev: 5'-TGCTTGTTGTGACTGATCGAC-3'	NM_003406.2	130	1.833
HPRT1	hypoxanthine phosphoribosyltransferase 1	Fw: 5'-TGACCTTGATTTATTTTGCATACC-3' Rev: 5'-CGAGCAAGACGTTCAGTCCT-3'	NM_000194.2	102	2.013
18S	18S ribosomal RNA	Fw: 5'-GGAGAGGGAGCCTGAGAAAC-3' Rev: 5'-TCGGGAGTGGGTAATTTGC-3'	NR_003286.2	70	1.999
ACTB	actin, beta	Fw: 5'-CCAACCGCGAGAAGATGA-3' Rev: 5'-CCAGAGGCGTACAGGGATAG-3'	NM_001101.3	97	1.938

extracted using TRI Reagent (Sigma) and treated with the DNase I (Roche) according to the manufacturer's instructions. The quality of RNA samples was determined using Agilent bio-analyser (Agilent Technologies, USA) assuring all RNA integrity numbers (RIN) were above 9.8. 1 μg of total RNA was transcribed to cDNA using SuperScript III reverse transcriptase (Invitrogen, USA) according to the manufacturer's instructions.

Primer design and qPCR. Forward and reverse primers were designed to span intron-exon junctions using PrimerExpress software (Applied Biosystems, USA) and their specificity was checked using BLAST algorithm. Primer validation was

performed by analysing slope of the standard curve and the presence of a single peak in the melting curve after qPCR analysis. From the cohort of 7 reference genes (Table 1) two most stable (*Rplp0, GAPDH*) were selected for normalization using GeNorm algorithm.[37] Expression of 13 genes of interest (Table 1) and two selected normalization genes was analysed using SybrGreen chemistry. qPCR was performed on a 384-well platform using LightCycler 480 Real-Time PCR System (Roche). Amplification of specific PCR products was performed in triplicates in a total reaction mixture of 5 μL containing 0.75 μL of cDNA template. Gene expression normalization factors were calculated for each sample based on geometric means of the selected normalization genes.[37] Minimum Information for Publication of Quantitative Real-Time PCR Experiments (MIQE) guidelines were followed in the performance and interpretation of the qPCR reactions.[38]

Western blot analysis

Expression of ERK, Akt and STAT5 proteins and their phosphorylated forms was determined by western blotting in the cell lysates of MCF-7 and MDA-MB-231 cells after rHuEpo treatment and exposure to cDDP. 24 h rHuEpo treated and 9 weeks pretreated cells were together with non-treated cells seeded on 6-well plates in the concentration of $1x10^5$ cells per well and left in culture for 48 h. 24 h before treatments, cells were switched to serum free medium. To assess rHuEpo effect, cells were treated with 5 or 25 U/mL rHuEpo for 15 minutes (similarly as shown in Figure 1C except that rHuEpo treatment was applied instead of cDDP). After treatment, the culture medium was aspirated and samples were fast frozen in liquid nitrogen. To assess rHuEpo and cDDP interaction, cells were exposed to two different concentrations of cDDP for 4 h: 30 and 60 μM for MCF-7 cell line and 60 and 120 μM for MDA-MB-231 (similarly as in Figure 3 except for a shorter cDDP) and fast frozen in liquid nitrogen after culture medium was aspirated.

After treatments, cells were lysed for 10 minutes on ice in lysis buffer as described in Kutuk *et al.*[39] and soluble proteins were recovered in the supernatant following 10 min centrifugation (12000 rpm). Samples of insulin treated (10 μg/mL for 15 min) MCF-7 cells and rHuEpo treated (1 U/mL for 15 min) UT7/Epo cells were used as positive controls. Equal amounts of proteins (10 μg) from each sample were loaded per well. After SDS electrophoresis, proteins were transferred to polyvinylidene difluoride (PVDF) membranes (Immobilon P, Millipore, USA). Membranes were blocked in a blocking solution (5% BSA in 1 mM PBS, 1% Tween-20) for 1 h and incubated in one of the following antibodies and dilutions: anti-ERK (1:1000), anti-Akt (1:600), anti-STAT5 (1:600), anti-P-ERK (1:1000), anti-P-Akt (1:600) and anti-P-STAT5 (1:600). All antibodies were purchased from Cell Signalling Technology and were raised against synthetic peptides in rabbits. Mouse anti-actin antibodies (1:5000, Sigma) were used for loading controls. As a secondary antibody, peroxidase-conjugated anti-rabbit-IgG (1:5000, Sigma) or anti-mouse-IgG (1:5000, Sigma) was used and visualized by chemiluminescence reagent (Pierce ECL Western Blotting Substrate, Thermo Scientific, USA) with CCD camera (FujiFilm, Japan). Membranes were densitometrically analysed using ImageJ software (National Institutes of Health, US)[40] and ratios between phosphorylated proteins to their non-phosphorylated forms were calculated and compared between samples. All experiments were done in duplicates and repeated twice.

Statistical analysis

Statistical analysis of the data was performed using Limma package[41] from Bioconductor analysis tools for R programing language.[42] The effect of EPO treatment, exposure to cDDP and their interaction in cell survival/proliferation assays, western blot and qPCR was assessed by two-way analysis of variance (ANOVA). Multiple-testing correction using false discovery rate (FDR)[43] was employed and $P<0.05$ was considered as statistically significant.

Results

Cell proliferation and survival

rHuEpo effect. Clonogenic assays showed decreased colony number ($p = 0.043$) together with a drop in colony size ($p = 0.0007$) in short-term rHuEpo treated MCF-7 cells (12 days) (Figure 2A and B, short-term), indicating a cytotoxic effect and decreased cell proliferation. Contrary in rHuEpo pretreated MCF-7 cells colony number ($p = 0.002$) and colony size ($p = 0.022$) were increased (Figure 2A and B, long-term), indicating a positive effect on cell proliferation and survival. In MDA-MB-231 cell line, no significant rHuEpo effect was observed (data not shown).

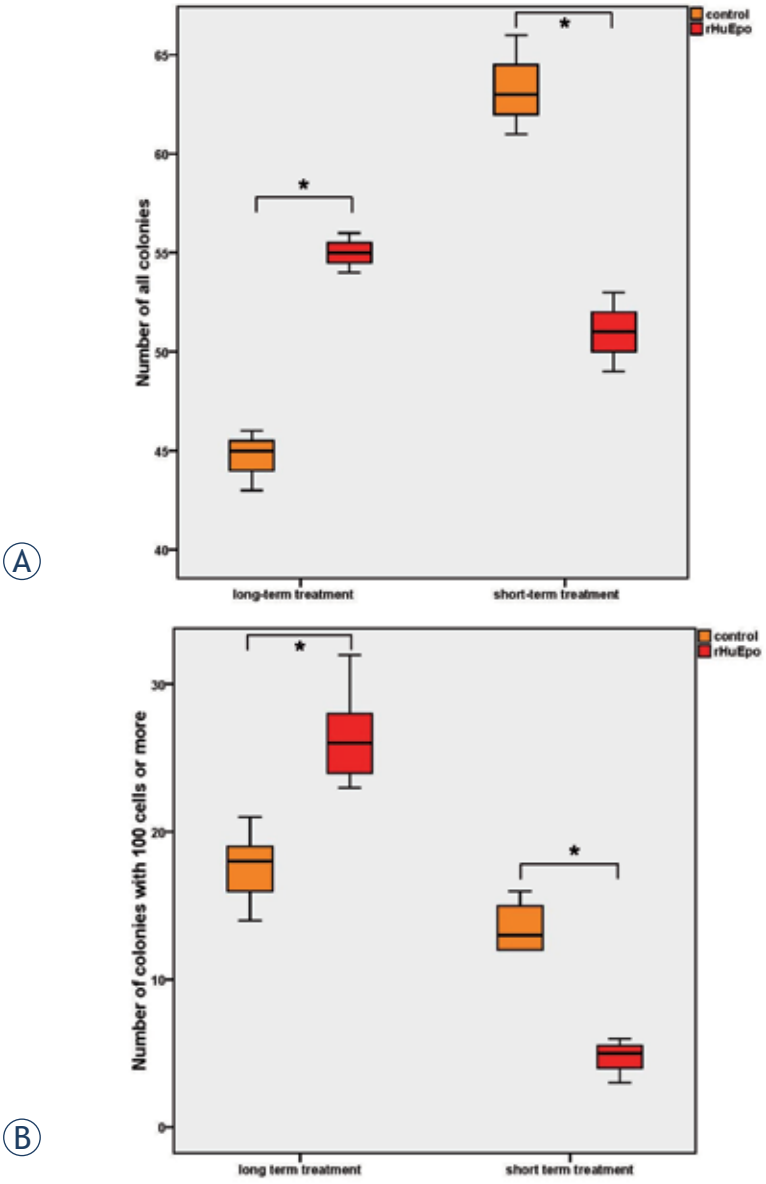

FIGURE 2. Clonogenic assay with short and long-term treated and non-treated MCF-7 cells: (A) Number of all colonies; (B) Number of colonies with 100 cells or more. Asterisk (*) denotes statistical significant differences for Type I error a = 0.05.

Establishment of cDDP inhibitory concentrations that reduced cell survival to 50% (IC50)

The following IC50 concentrations were established for colorimetric assays: 10-30 μM for MCF-7 cell line[44] and 60-100 μM for MDA-MB-231; and clonogenic assays: 0.1-0.5 μM for MCF-7 cell line and 6-10 μM for MDA-MB-231.

rHuEpo and cDDP interaction. Colorimetric WST-1 assays revealed protective effect of short-term rHuEpo treatment for MCF-7 and MDA-MB-231 cells that were exposed to cDDP induced cytotoxicity (Figures 3A and 3C, respectively). Contrary, long-term exposure of cells to rHuEpo sensitized MCF-7 cells to cDDP cytotoxicity but had no effect for the MDA-MB-231 cells (Figures 3B and 3D, respectively). This indicates that the time of Epo exposure is crucial for cell response to cDDP treatment.

Clonogenic assays confirmed protective effect of short-term rHuEpo treatment for the MCF-7 cell response to cDDP cytotoxicity (Figure 4A), while they exposed sensitizing effect for MDA-MB-231 cells (Figure 4C). Long term exposure of cells to EPO predisposed MCF-7 cells to CDDP cytotoxicity (Figure 4B) but not the MDA-MB-231 cells (Figure 4D), as shown by WST-1.

Expression of p53-dependent genes and bcl2-gene family mambers

Expression of 13 genes was measured on control, short-term rHuEpo treated and pretreated MCF-7 and MDA-MB-231 cells that were either exposed to cDDP or not (Figure 1C). qPCR confirmed low *EPOR* expression in all experimental settings with Cq values below 34, a value which was chosen as a cut-off point. *EPOR* expression is therefore not influenced by either increasing confluence of cell cultures or exposure to rHuEpo. Similarly, *CASP3* was not expressed in MCF-7 cells, which is in agreement with Henkels *et al.*[45]

rHuEpo effect. Venn diagrams on Figures 5A and 5B show genes that were differentially expressed upon short and long-term rHuEpo treatments when compared to un-stimulated control cells. In the MCF-7 cell line (Figure 5A), *FOS* and *BCL2L1* were up-regulated and *JUN* was down-regulated after rHuEpo treatment independently of the treatment duration. *BCL2* and *CASP9* were up-regulated after short-term rHuEpo treatment, while long-term treatment down-regulated *BCL2* together with *BAD* and up-regulated *PMAIP1* and *NF-κβ*. In MDA-MB-231 cell line (Figure 5B) several genes were down-regulated after short-term treatment, namely *BAD*, *BAX*, *BBC3* and *PMAIP1*, while the expression of *BCL2L1* was increased. After long-term treatment, only *BAD* was deregulated; in contrast to short-term treatment, its increased expression was observed.

rHuEpo and cDDP interaction. Venn diagrams on Figures 5C and 5D show differentially expressed genes in cells that were exposed to cDDP in comparison to non-exposed control cells with respect to different rHuEpo treatments. In MCF-7 cells (Figure 5C), *BAX* and *BBC3* up-regulation was

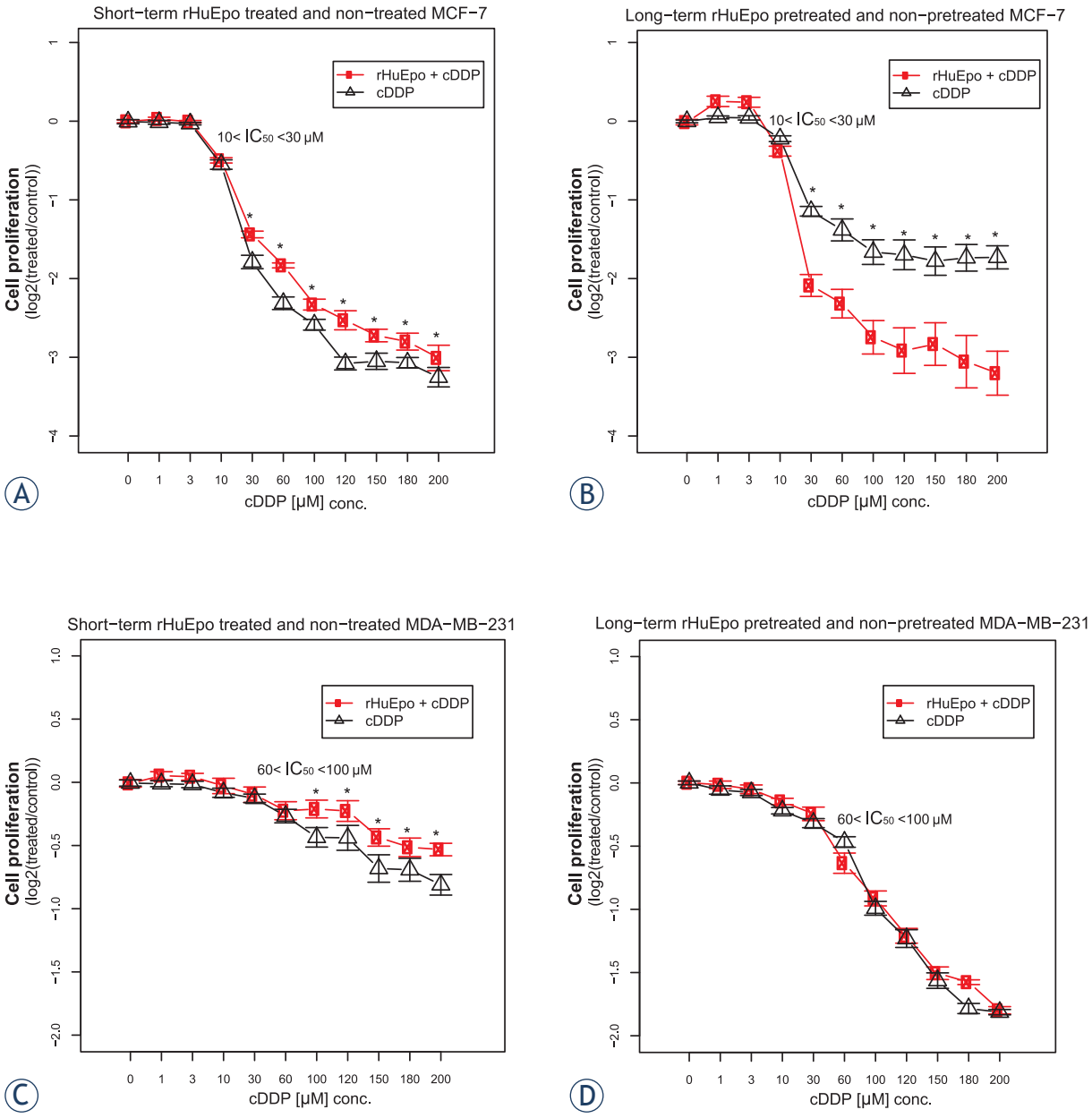

FIGURE 3. Cell proliferation of short (red line, A and C) and long-term (red line, B and D) rHuEpo treated and non-treated cells (black line) after exposure to cDDP, normalized with the proliferation of control cells that were not exposed to cDDP: (A and B) MCF-7; (C and D) MDA-MB-231 cell line. Asterisk (*) denotes statistical significant differences for Type I error α = 0.05.

observed irrespectively of the rHuEpo treatment. *BCL2* was up-regulated in cells that were exposed to cDDP but were not treated with rHuEpo. Exposure of short-term rHuEpo treated cells to cDDP down-regulated several genes, namely *CASP9*, *PMAIP1*, *BCL2L1*, *NF-κβ* and *BCL2*, while *JUN* expression was increased. Long-term rHuEpo treated cells respond to cDDP exposure with *BAD* up-regulation. In MDA-MB-231 cell line (Figure 5D), *FOS*, *CASP9* and *CASP3* were up-regulated and *BCL2L1* was down-regulated after exposure to cDDP irrespectively of the rHuEpo treatment. In short-term rHuEpo treated MDA-MB-231 cells, exposure to cDDP increased the expression of *BAX* and *JUN*. *BAD* up-regulation was shown in short-term treated cells that were exposed to cDDP, while long-term rHuEpo treatment seems to antagonize its up-regulation.

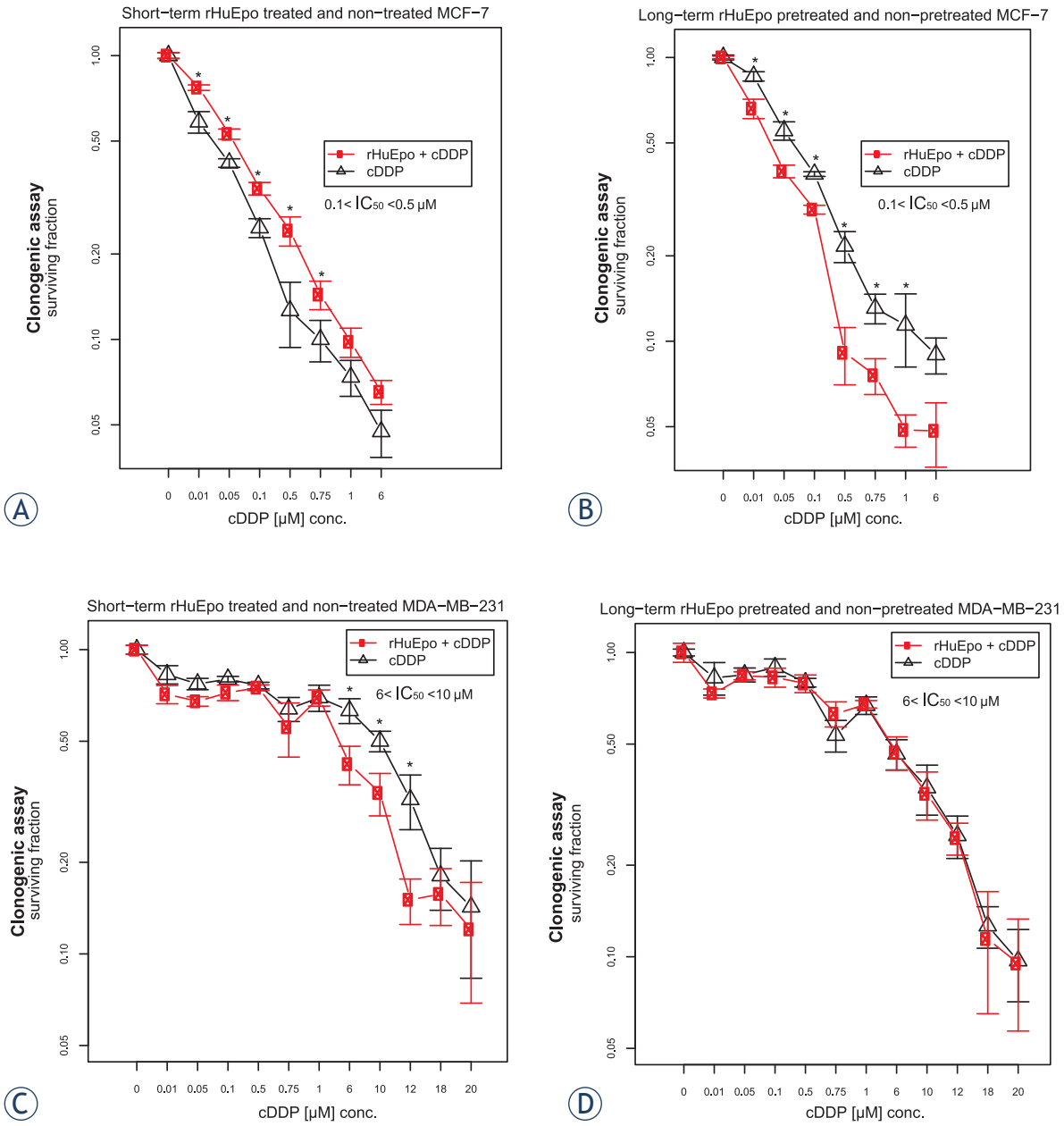

FIGURE 4. Surviving fraction of short (red line, A and C) and long-term (red line, B and D) rHuEpo treated cells after exposure to cDDP: (A and B) MCF-7; (C and D) MDA-MB-231 cell line. Asterisk (*) denotes statistical significant differences for Type I error a = 0.05.

MAPK and PI-3K signalling pathways

In view of the evidence for the expression and functionality of EpoR in MCF-7 and MDA-MB-231 cells, we evaluated the ability of Epo to signal through well-established pathways that are thought to promote cell proliferation and cytoprotection, specifically the ERK, Akt and STAT5. The analysis of MDA-MB-231 cell line is presented on Figure 6. rHuEpo treatment or exposure to cDDP did not promote phosphorylation of ERK, Akt or STAT5 in MCF-7 cells (data not shown). We also confirmed that STAT5 is not expressed in MCF-7 cells, which was already reported by Yamashita *et al.*[46] and is consistent with qPCR data from our laboratory (data not shown).

rHuEpo effect. We were able to detect a low level of ERK phosphorylation in short and long-term rHuEpo treated MDA-MB-231 cells (Figure 6B). Long-term treated cells became less responsive to

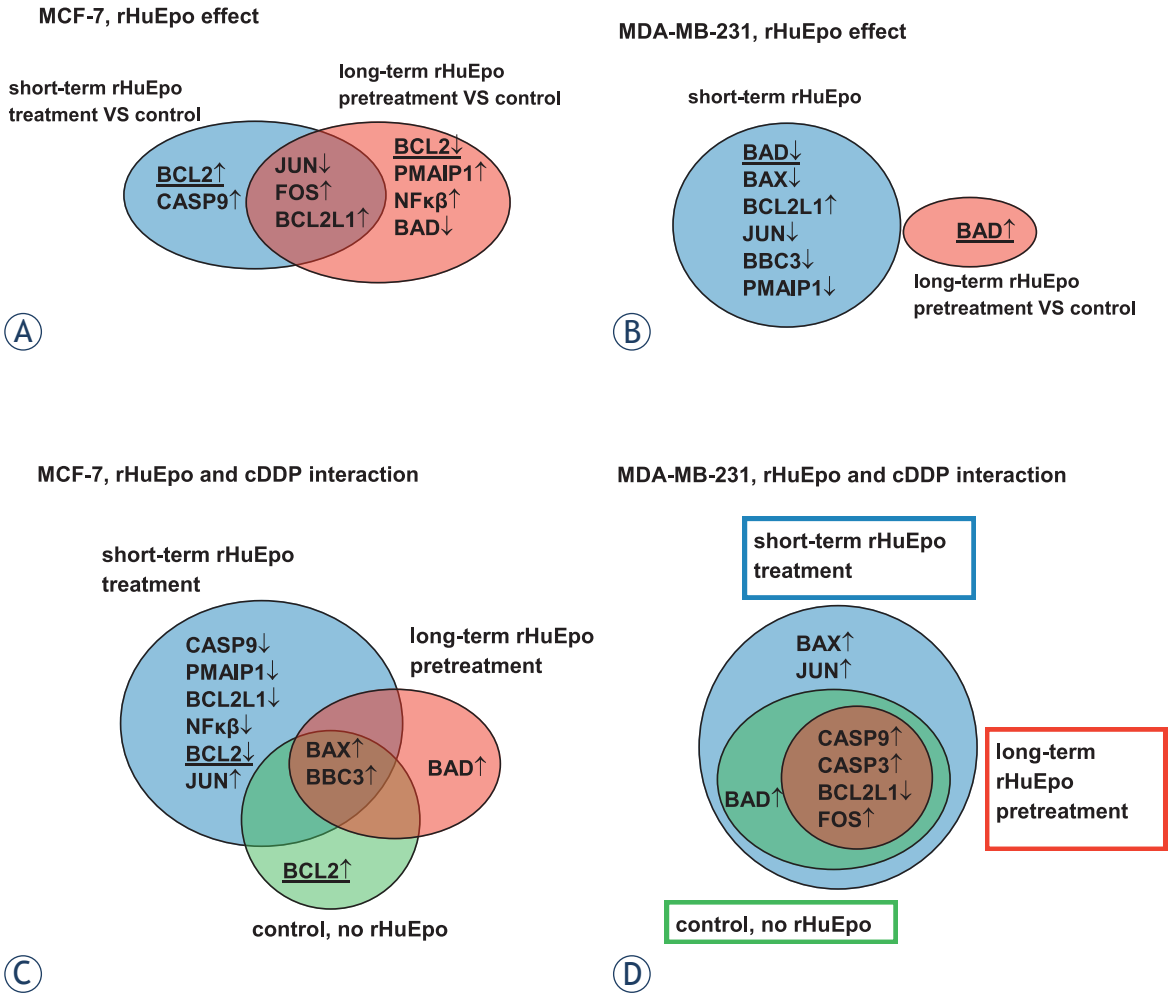

FIGURE 5. (A and B) Venn' diagrams representing differential gene expression at different rHuEpo treatments when compared to non-treated cells: (A) MCF-7; (B) MDA-MB-231 cell line. (C and D) Venn' diagrams representing differential gene expression in cells that were or were not exposed to cDDP at different rHuEpo treatments: (C) MCF-7; (D) MDA-MB-231 cell line. ↑: up-regulation. ↓: down-regulation. Underlined = genes with non-matching direction of change.

the Epo stimulation in comparison to the control cells; there was also a statistically significant difference in ERK phosphorylation between short and long-term treated cells that was approximately 2.5-fold higher in short-term treated cells as measured by densitometry (Figure 6B). rHuEpo was not able to promote phosphorylation of Akt and no STAT5 expression was detected in MDA-MB-231 cells (Figure 6A), the observation that is in agreement with qPCR data from our laboratory (data not shown).

rHuEpo and cDDP interaction. Non-treated MDA-MB-231 cells that were exposed to cDDP for 4 h show an increase in ERK phosphorylation at both cDDP concentrations when compared to cells that were not exposed to cDDP (Figure 6C). After short-term rHuEpo treatment, 120 μM cDDP increased ERK phosphorylation, while 60 μM cDDP decreased the phosphorylation level in comparison with controls (Figure 6C). We could not detect any statistically significant change in the level of ERK phosphorylation after long-term rHuEpo treatment when compared to non-treated and short-term treated cells (data not shown).

Discussion

Clinical trials with rHuEpo have shown decreased anaemia and improved quality-of-life for cancer patients receiving chemotherapy. In spite of these beneficial effects, rHuEpo was shown to cause detrimental effects on patient well-being, decreased loco-regional control of disease progression and de-

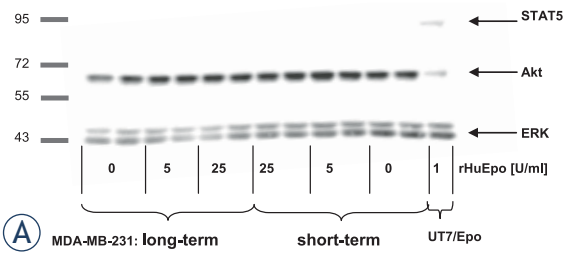

FIGURE 6. Involvement of MAPK (ERK), PI-3K (Akt) and Jak/STAT5 (STAT5) signaling pathways in Epo signaling for MDA-MB-231 cell line. (A) Expression of ERK, Akt and STAT5 proteins in short and long-term rHuEpo treated cells. (B) ERK phosphorylation (p-ERK) in short and long-term rHuEpo treated MDA-MB-231cells. p-ERK to ERK ratios after rHuEpo treatment (5, 25 U/mL) were compared with non-treated samples. Table shows densitometry ratios and corresponding standard deviations (SD). (C) ERK phosphorylation (p-ERK) in short-term rHuEpo treated or non-treated cells after the exposure to cDDP. p-ERK to ERK ratios after exposure to cDDP (60, 120 μM/mL) were compared to samples that were not exposed to cDDP. Table shows densitometry ratios and corresponding standard deviations (SD). Asterisk (*) denotes statistical significant differences (p-ERK to ERK ratio) for Type I error α = 0.05. UT7/Epo cells were used as positive controls for Epo signaling.

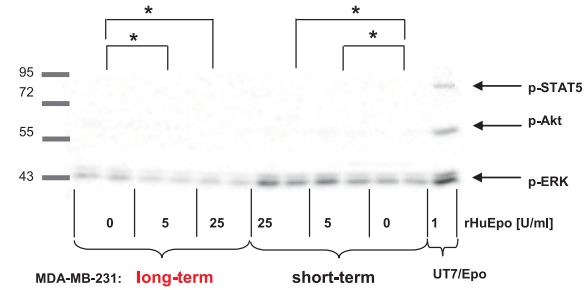

rHuEpo concentration [U/mL]	p-ERK to ERK ratio			
	long-term		short-term	
	Mean	SD	Mean	SD
0	1.00	0.05	1.00	0.07
5	0.61	0.16	1.20	0.07
25	0.86	0.11	1.40	0.15

B

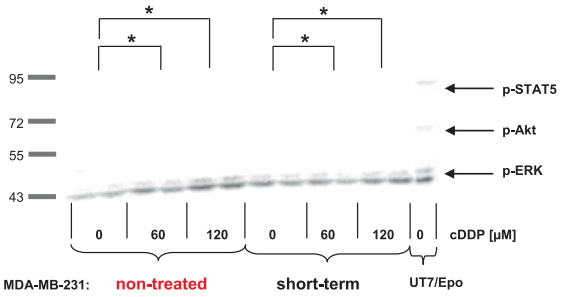

cDDP concentration [μM/mL]	p-ERK to ERK ratio			
	non-treated		short-term	
	Mean	SD	Mean	SD
0	1.00	0.07	1.00	0.06
60	1.33	0.07	0.83	0.09
120	1.53	0.21	1.52	0.07

C

creased over-all survival.[15-18] Mechanisms of the observed adverse clinical effects have remained elusive, but the most frequently considered hypothesis is the binding of cancer cell EpoR with exogenously administered rHuEpo. EpoR activation is considered to influence cancer cell growth in terms of stimulated proliferation, decreased apoptosis and increased resistance to therapy. It was reported that AP-1 (FOS and JUN) transcription factor is critical for the growth and proliferation of breast cancer cells[47] and is also involved in the stimulation of NF-κβ transactivation activity.[48] In erythroid cells, Epo was reported to co- or posttranslationally increase AP-1 activity.[49] We therefore performed rHuEpo treatment of MCF-7 and MDA-MB-231 cells in order to assess the effect of rHuEpo treatment on cell proliferation and its potential to synergize with cDDP in suppression of breast cancer cell growth. We showed that MCF-7 and MDA-MB-231 cells express *EPOR* mRNA and on the basis of previous reports we consider the protein functional.[28] The effect of time duration to rHuEpo exposure (long, short-term) was also addressed.

rHuEpo effect. The effect on MCF-7 cell proliferation and cytotoxicity seems to be influenced by the length of rHuEpo treatment. Clonogenic assays showed decreased number and size of colonies for short-term rHuEpo treated MCF-7 cells, while on the other hand colony number and size were increased with long-term stimulated cells (Figure 2). Surprisingly, rHuEpo in MCF-7 cells failed to elicit phosphorylation of ERK and Akt, therefore the activation of MAPK and PI-3K signalling cascades that are indicative for EpoR activation[6,7] could not be confirmed in this treatment conditions. Results could also suggest that other signalling pathways may be involved. qPCR results (Figure 5) showed up-regulation of *BCL2* gene in short-term rHuEpo treated cells and down-regulation of this gene after long-term treatment, indicating involvement of *BCL2* in the proliferative and cytotoxic response to Epo. Additional up-regulation of *PMAIP1* gene was shown for long-term rHuEpo treated MCF-7 cells. Results suggest that in addition to genes involved in the cell sensitivity to apoptotic stimuli (*BCL2*, *PMAIP1*), Epo also modulates genes involved in cell

proliferation (*FOS*, *NF-κβ*). Consequently, when growth conditions are near optimal, cells proliferate more rapidly, but as soon as an apoptotic stimulus is involved, cell survival is diminished. Using MDA-MB-231 cell line, no change in the proliferation level of rHuEpo treated cells was observed despite low level of ERK phosphorylation. Signalling through the growth factor receptor tyrosine kinase pathway in PR(-) tumours was indicated previously.[28] ERK phosphorylation was significantly reduced after long-term treatment, indicating that cells are non-responsive to Epo stimulation, probably due to saturation of MAPK signalling pathway or regulation of cytosolic phospholipase A2.[50]

Furthermore, qPCR data show that short-term rHuEpo up-regulates *BCL2L1* and down-regulates *BAD*, *BAX*, *PMAIP1* and *BBC3*. In line with this, rHuEpo treatment did not trigger Akt phosphorylation which was previously shown to act as an activator of apoptotic process.[51,52] Comparable proliferation rate and survival of rHuEpo treated and control MDA-MB-231 cells and the presence of activated ERK in all treatment groups may indicate, that lack of rHuEpo effect on the proliferation of MDA-MB-231 cells is due to auto-activating mutations or alteration in gene expression that result in constitutive activation of signalling pathways that drive proliferation at the nearly maximal rate.[53]

rHuEpo and cDDP interaction. Given the controversy of reports explaining Epo role in the cytoprotection of cancer cells,[31,34,54] we addressed effects of rHuEpo treatment and exposure to cDDP and their potential interaction. p53 modulates cell response to cDDP by transcriptional activation of *BAX*, *PMAIP1* and *BBC3* and consequent suppression of *BCL2* expression.[55] Therefore we investigated, whether difference in *p53* status could influence cell response to rHuEpo and cDDP. Using both types of survival assays, we detected attenuated anti-proliferative, apoptotic or senescence-promoting effects of cDDP with short-term rHuEpo treated MCF-7 cells (Figure 3A and 4A). On the other hand, survival of long-term rHuEpo treated cells was significantly lower after the exposure to cDDP (Figure 3B and 4B), particularly at higher cDDP concentrations. rHuEpo pretreatment seems to render MCF-7 cells to be more sensitive to the cytotoxic effect of cDDP. Together with this, qPCR analysis exposed differential gene expression for short and long-term rHuEpo effects (Figure 5C). Results therefore suggest that MCF-7 cell response to cDDP depends on the length of rHuEpo exposure. Furthermore, no significant change in ERK and Akt activation was shown after cDDP treatment which is crucial for the induction of apoptosis.[51,52] These results indicate that Epo may modulate cell response to cDDP through deregulation of ERK and Akt expression. In MDA-MB-231 cell line, clonogenic assays, but not colorimetric ones (Figure 3C and 4C), suggest poorer cell proliferation and survival for short-term treated cells and are in agreement with qPCR results which exposed promoted anti-survival genotype that was evident from the up-regulation of several pro-apoptotic genes (Figure 5D). Clonogenic assays may be more informative because they measure cell number together with cell capacity to form colonies over longer periods of time, while on the other hand colorimetric assays are short-term and only measure cell activity of superoxide dismutase (SOD). Surprisingly, we could not confirm any effect of long-term rHuEpo exposure on the level of proliferation, clonogenicity, qPCR or western blot in this cell line (Figure 3D, 4D, 5D and 6). MDA-MB-231 cells with the mutated *p53* have disrupted apoptotic machinery that could aid to cell un-responsiveness to cytoprotective and proliferative effect of rHuEpo The lack of cell response could also be explained in terms of more aggressive phenotypes for ER(+)/PR(-) tumours[29] and the postulated correlations to the expression of EpoR and steroid receptors.[30,56]

Conclusions

Our study showed that Epo has a contrasting action in breast cancer biology that depends on the duration of exposure to rHuEpo, presence of cytotoxic stimuli, ER/PR and *p53* status. The correlation between ER/PR and Epo was shown previously.[30,56-58] Our study indicates that besides ER/PR status, also p53 is involved in Epo induced tumour response.

Proliferation and survival characteristics of MCF-7, cells with ER(+)/PR(+) status and wild type *p53*, are opposite during short or long term rHuEpo exposure. Prolonged exposure to rHuEpo drives MCF-7 cells to increased proliferation and induced sensitivity to cDDP. In contrast, MDA-MB-231 cells with ER(+)/PR(-) status and mutated *p53* are almost irresponsive to rHuEpo exposure. Functional p53 and ER(+)/PR(+) status seems to be crucial for long-term rHuEpo driven modification of cancer cells. Interestingly, in MCF-7 *in vitro* assay (with optimal growth conditions) prolonged rHuEpo exposure during cDDP chemotherapy is beneficial, while rHuEpo treatment alone is not. These results have to be verified in a setup representing *in vivo* conditions (tumour hypoxia, treatment regime, …).

Furthermore, Epo is involved in transcription regulation of *BAX*, *PMAIP1*, *BBC3* and *BCL2*, results suggesting its involvement in p53-modulated cell response to cDDP. Epo also modulates the expression of *NF-κβ*, *FOS* and *JUN* transcription factors and in MDA-MB-231 cells reduces MAPK kinase signal transduction.

To conclude, ER/PR and p53 genetic signature may be used to predict the beneficial or maleficent effect of rHuEpo supportive therapy in the individual patient. Whole-genome expression studies need to be employed in order to identify the main components of Epo/EpoR signal transduction that modulate cell proliferation and cell sensitivity to cytotoxic stimuli.

Acknowledgement

Authors thank Miroslava Lavrič for the help with clonogenic assays. The authors thank Dr. Toni Petan and Dr Igor Križaj for kindly providing the cell lines. Authors acknowledge the financial support of the Slovenian Research Agency.

References

1. Sytkowski JA. *Erythropoietin: Blood, Brain and Beyond*. Boston: *Wiley-VCH*; 2004.
2. Jelkmann W, Wagner K. Beneficial and ominous aspects of the pleiotropic action of erythropoietin. *Ann Hematol* 2004; **83:** 673-86.
3. Debeljak N, Sytkowski AJ. Erythropoietin: new approaches to improved molecular designs and therapeutic alternatives. *Curr Pharm Des* 2008; **14:** 1302-10.
4. Lacombe C, Mayeux P. The molecular biology of erythropoietin. *Nephrol Dial Transplant* 1999; **14:** 22-8.
5. Sytkowski AJ. The neurobiology of erythropoietin. *Cell Mol Neurobiol* 2011; **31:** 931-7.
6. Jelkmann W, Bohlius J, Hallek M, Sytkowski AJ. The erythropoietin receptor in normal and cancer tissues. *Crit Rev Oncol Hemat* 2008; **67:** 39-61.
7. Debeljak N, Sytkowski AJ. EpoR. *UCSD-Nature Molecule Pages* 2007. (doi: 10.1038/mp.a000863.01)
8. Arcasoy MO. The non-haematopoietic biological effects of erythropoietin. *Br J Haematol* 2008; **141:** 14-31.
9. Vaupel P, Thews O, Hoeckel M. Treatment resistance of solid tumors: role of hypoxia and anemia. *Med Oncol* 2001; **18:** 243-59.
10. Chang J, Couture F, Young S, McWatters KL, Lau CY. Weekly epoetin alfa maintains hemoglobin, improves quality of life, and reduces transfusion in breast cancer patients receiving chemotherapy. *J Clin Oncol* 2005; **23:** 2597-605.
11. Velenik V, Oblak I, Kodre V. Managing anemia with epoetin alfa in patients with rectal cancer. *Radiol Oncol* 2005; **39:** 133-40.
12. Henke M, Laszig R, Rube C, Schafer U, Haase KD, Schilcher B, et al. Erythropoietin to treat head and neck cancer patients with anaemia undergoing radiotherapy: randomised, double-blind, placebo-controlled trial. *Lancet* 2003; **362:** 1255-60.
13. Leyland-Jones B. Breast cancer trial with erythropoietin terminated unexpectedly. *Lancet Oncol* 2003; **4:** 459-60.
14. Leyland-Jones B, Semiglazov V, Pawlicki M, Pienkowski T, Tjulandin S, Manikhas G, et al. Maintaining normal hemoglobin levels with epoetin alfa in mainly nonanemic patients with metastatic breast cancer receiving first-line chemotherapy: a survival study. *J Clin Oncol* 2005; **23:** 5960-72.
15. Bohlius J, Schmidlin K, Brillant C, Schwarzer G, Trelle S, Seidenfeld J, et al. Recombinant human erythropoiesis-stimulating agents and mortality in patients with cancer: a meta-analysis of randomised trials. *Lancet* 2009; **373:** 1532-42.
16. Glaspy J, Crawford J, Vansteenkiste J, Henry D, Rao S, Bowers P, et al. Erythropoiesis-stimulating agents in oncology: a study-level meta-analysis of survival and other safety outcomes. *Br J Cancer* 2010; **102:** 301-15.
17. Ludwig H, Crawford J, Osterborg A, Vansteenkiste J, Henry DH, Fleishman A, et al. Pooled analysis of individual patient-level data from all randomized, double-blind, placebo-controlled trials of darbepoetin alfa in the treatment of patients with chemotherapy-induced anemia. *J Clin Oncol* 2009; **27:** 2838-47.
18. Tonelli M, Hemmelgarn B, Reiman T, Manns B, Reaume MN, Lloyd A, et al. Benefits and harms of erythropoiesis-stimulating agents for anemia related to cancer: a meta-analysis. *CMAJ* 2009; **180:** E62-71.
19. Sytkowski AJ. Does erythropoietin have a dark side? Epo signaling and cancer cells. *Sci STKE* 2007; **2007:** pe38.
20. Fodor J, Major T, Tóth J, Sulyok Z, Polgár C. Comparison of mastectomy with breast-conserving surgery in invasive lobular carcinoma: 15-Year results. *Rep Pract Oncol Radiother.* 2011; **16:** 227-31.
21. Lekic M, Kovac V, Triller N, Knez L, Sadikov A, Cufer1 T. Outcome of small cell lung cancer (SCLC) patients with brain metastases in a routine clinical setting. *Radiol Oncol* 2012; 46(3): 213-225.; **46:** 54-9.
22. Małecki K, Gliński B, Mucha-Małecka A, Ryś J, Kruczak A, Roszkowski K, et al. Prognostic and predictive significance of p53, EGFr, Ki-67 in larynx preservation treatment. *Rep Pract Oncol Radiother.* 2010; **15:** 87-92.
23. Kovač V, Smrdel U. Meta-analyses of clinical trials in patients with non-small cell lung cancer. *Neoplasma* 2004; **51:** 334-40.
24. Martin M. Platinum compounds in the treatment of advanced breast cancer. *Clin Breast Cancer* 2001; **2:** 190-208.
25. Todorovic V, Sersa G, Flisar K, Cemazar M. Enhanced cytotoxicity of bleomycin and cisplatin after electroporation in murine colorectal carcinoma cells. *Radiol Oncol* 2009; **43:** 264-73.
26. Erčulj N, Kovač V, Hmeljak J, Dolžan V. The influence of platinum pathway polymorphisms on the outcome in patients with malignant mesothelioma. *Ann Oncol* 2012; **23:** 961-7.
27. Siddik ZH. Cisplatin: mode of cytotoxic action and molecular basis of resistance. *Oncogene* 2003; **22:** 7265-79.
28. Acs G, Acs P, Beckwith SM, Pitts RL, Clements E, Wong K, et al. Erythropoietin and erythropoietin receptor expression in human cancer. *Cancer Res* 2001; **61:** 3561-5.
29. Cui X, Schiff R, Arpino G, Osborne CK, Lee AV. Biology of progesterone receptor loss in breast cancer and its implications for endocrine therapy. *J Clin Oncol* 2005; **23:** 7721-35.
30. Larsson AM, Jirstrom K, Fredlund E, Nilsson S, Ryden L, Landberg G, et al. Erythropoietin receptor expression and correlation to tamoxifen response and prognosis in breast cancer. *Clin Cancer Res* 2009; **15:** 5552-9.
31. Belenkov AI, Shenouda G, Rizhevskaya E, Cournoyer D, Belzile JP, Souhami L, et al. Erythropoietin induces cancer cell resistance to ionizing radiation and to cisplatin. *Mol Cancer Ther* 2004; **3:** 1525-32.
32. Kumar SM, Zhang G, Bastian BC, Arcasoy MO, Karande P, Pushparajan A, et al. Erythropoietin receptor contributes to melanoma cell survival in vivo. *Oncogene* 2011.
33. Li J, Vesey DA, Johnson DW, Gobe G. Erythropoietin reduces cisplatin-induced apoptosis in renal carcinoma cells via a PKC dependent pathway. *Cancer Biol Ther* 2007; **6:** 1944-50.
34. Palumbo C, Battisti S, Carbone D, Albonici L, Alimandi M, Bei R, et al. Recombinant erythropoietin differently af fects proliferation of mesothelioma cells but not sensitivity to cisplatin and pemetrexed. *Cancer Chemother Pharmacol* 2008; **61:** 893-901.
35. Shi Z, Hodges VM, Dunlop EA, Percy MJ, Maxwell AP, El-Tanani M, et al. Erythropoietin-induced activation of the JAK2/STAT5, PI3K/Akt, and Ras/ERK pathways promotes malignant cell behavior in a modified breast cancer cell line. *Molecular cancer research : MCR* 2010; **8:** 615-26.

36. Hayakawa J, Ohmichi M, Kurachi H, Kanda Y, Hisamoto K, Nishio Y, et al. Inhibition of BAD phosphorylation either at serine 112 via extracellular signal-regulated protein kinase cascade or at serine 136 via Akt cascade sensitizes human ovarian cancer cells to cisplatin. *Cancer Res* 2000; **60:** 5988-94.

37. Vandesompele J, De Preter K, Pattyn F, Poppe B, Van Roy N, De Paepe A, et al. Accurate normalization of real-time quantitative RT-PCR data by geometric averaging of multiple internal control genes. *Genome Biol* 2002; **3:** RESEARCH0034.

38. Bustin SA, Benes V, Garson JA, Hellemans J, Huggett J, Kubista M, et al. The MIQE guidelines: minimum information for publication of quantitative real-time PCR experiments. *Clin Chem* 2009; **55:** 611-22.

39. Kutuk O, Arisan ED, Tezil T, Shoshan MC, Basaga H. Cisplatin overcomes Bcl-2-mediated resistance to apoptosis via preferential engagement of Bak: critical role of Noxa-mediated lipid peroxidation. *Carcinogenesis* 2009; **30:** 1517-27.

40. Abramoff MD, Magelhaes PJ, Ram SJ. Image Processing with ImageJ. *Biophotonics International* 2004; **11:** 36-42.

41. Smyth GK. Limma: linear models for microarray data. In: Robert Gentleman VJC, Wolfgang Huber, Rafael A. Irizarry, Sandrine Dudoit editor. *Bioinformatics and Computational Biology Solutions Using R and Bioconductor*. New York: Springer; 2005. p. 397-420.

42. (2008) RDCT. *R: A language and environment for statistical computing*. Vienna: R Fundation for Statistical Computing; 2011.

43. Benjamini Y, Hochberg Y. Controlling the False Discovery Rate - a Practical and Powerful Approach to Multiple Testing. *R Stat Soc Series B Stat Methodol* 1995; **57:** 289-300.

44. Zager V, Cemazar M, Hreljac I, Lah TT, Sersa G, Filipic M. Development of human cell biosensor system for genotoxicity detection based on DNA damage-induced gene expression. *Radiol Oncol* 2010; **44:** 42-51.

45. Henkels KM, Turchi JJ. Cisplatin-induced apoptosis proceeds by caspase-3-dependent and -independent pathways in cisplatin-resistant and -sensitive human ovarian cancer cell lines. *Cancer Res* 1999; **59:** 3077-83.

46. Yamashita H, Nevalainen MT, Xu J, LeBaron MJ, Wagner KU, Erwin RA, et al. Role of serine phosphorylation of Stat5a in prolactin-stimulated beta-casein gene expression. *Mol Cell Endocrinol* 2001; **183:** 151-63.

47. Lu CH, Shen Q, DuPre E, Kim H, Hilsenbeck S, Brown PH. cFos is critical for MCF-7 breast cancer cell growth. *Oncogene* 2005; **24:** 6516-24.

48. Perkins ND. Achieving transcriptional specificity with NF-kappa B. *Int J Biochem Cell B* 1997; **29:** 1433-48.

49. Patel HR, Sytkowski AJ. Erythropoietin activation of AP1 (Fos/Jun). *Exp Hematol* 1995; **23:** 619-25.

50. Mariggio S, Bavec A, Natale E, Zizza P, Salmona M, Corda D, et al. Galpha13 mediates activation of the cytosolic phospholipase A2alpha through fine regulation of ERK phosphorylation. *Cellular signalling* 2006; **18:** 2200-8.

51. Schnellmann RG, Zhuang SG. A death-promoting role for extracellular signal-regulated kinase. *J Pharmacol Exp Ther* 2006; **319:** 991-7.

52. Marone R, Cmiljanovic V, Giese B, Wymann MP. Targeting phosphoinositide 3-kinase: moving towards therapy. *Biochim Biophys Acta* 2008; **1784:** 159-85.

53. Gewirtz DA, Di X, Walker TD, Sawyer ST. Erythropoietin fails to interfere with the antiproliferative and cytotoxic effects of antitumor drugs. *Clin Cancer Res* 2006; **12:** 2232-8.

54. Sigounas G, Sallah S, Sigounas VY. Erythropoietin modulates the anticancer activity of chemotherapeutic drugs in a murine lung cancer model. *Cancer Lett* 2004; **214:** 171-9.

55. Zhang L, Yu J. PUMA, a potent killer with or without p53. *Oncogene* 2008; **27:** S71-S83.

56. Pelekanou V, Kampa M, Kafousi M, Dambaki K, Darivianaki K, Vrekoussis T, et al. Erythropoietin and its receptor in breast cancer: correlation with steroid receptors and outcome. *Cancer Epidemiol Biomarkers Prev* 2007; **16:** 2016-23.

57. Pelekanou V, Notas G, Sanidas E, Tsapis A, Castanas E, Kampa M. Testosterone membrane-initiated action in breast cancer cells: Interaction with the androgen signaling pathway and EPOR. *Molec Oncol* 2010; **4:** 135-49.

58. Notas G, Kampa M, Pelekanou V, Castanas E. Interplay of estrogen receptors and GPR30 for the regulation of early membrane initiated transcriptional effects: A pharmacological approach. *Steroids* 2011.

research article

The antitumor efficiency of combined electrochemotherapy and single dose irradiation on a breast cancer tumor model

Elham Raeisi[1,2], Seyed Mahmoud Reza Aghamiri[3], Azin Bandi[3], Negar Rahmatpour[3], Seyed Mohammad Firoozabadi[1], Sedigheh Amini Kafi-Abad[4], Lluis M Mir[5,6,7]

[1] Department of Medical Physics, Faculty of Medical Science, Tarbiat Modares University, Tehran, Iran
[2] Faculty of Science, University of Geneve, Geneve, Switzerland
[3] Division of Radiation Medicine, Shahid Beheshti University, Tehran, Iran
[4] Department of Immunohematology, Research Center of Iranian Blood Transfusion Organization (IBTO), Tehran, Iran
[5] CNRS, Orsay, Laboratoire de Vectorologie et Therapeutiques Anticancereuses, UMR 8203, 91405 Orsay cedex, France
[6] Universite Paris-Sud, Laboratoire de Vectorologie et Therapeutiques Anticancereuses, UMR 8203, 91405 Orsay cedex, France
[7] Institute Gustave Roussy, Laboratoire de Vectorologie et Therapeutiques Anticancereuses, UMR 8203, 114 rue E. Vaillant, 94805 Villejuif cedex, France

Radiol Oncol 2012; 46(3): 226-232.

Received 2 December 2011
Accepted 30 December 2011

Correspondence to: Seyed Mahmoud Reza Aghamiri; Division of Radiation Medicine, Shahid Beheshti University, Evin Street, Po. Box: 19839-63113, Tehran, Iran. Phone: +982122431819; Fax +982122431780; E-mail: SMR-Aghamiri@sbu.ac.ir; Lluis M Mir; CNRS UMR 8203, Institut Gustave Roussy, 114 rue E. Vaillant, 94805 Villejuif cedex, France. Phone: +33142114792; Fax +33142115245; E-mail: luismir@igr.fr;

Disclosure: No potential conflicts of interest were disclosed.

Background. The aim of this study was to investigate the antitumor effectiveness of electrochemotherapy with cisplatin combined with suboptimal radiotherapy doses. Tumor radiosensitization was evaluated on large invasive ductal carcinoma tumors in Balb/C mice.

Materials and methods. Tumors of an average volume of 630 mm^3 were treated with cisplatin, electric pulses, radiotherapy, electrochemotherapy, alone as well as in appropriate combinations. Tumors were irradiated with Cobalt-60 γ-rays at doses 3 Gy and 5 Gy in combination with electrochemotherapy using cisplatin. Controls included each of the treatments alone as well as the combination of the radiotherapy with electric pulses alone or with cisplatin alone. Antitumor effectiveness was evaluated by tumor growth delay, tumor-doubling time, inhibition ratio and the objective response rates.

Results. As anticipated, electrochemotherapy was more effective than the treatment with cisplatin alone or the application of the electric pulses alone. When treatments were combined with tumor irradiation at either 3 or 5 Gy, the combination with electrochemotherapy was more effective: at 5 Gy, 2 animals out of 8 were in complete remission 100 days later. In general the higher 5 Gy dose of γ-radiation was more effective than the lower one of 3 Gy.

Conclusions. The results of our study demonstrate that irradiation doses, 3 Gy or 5 Gy, increase the antitumor effectiveness of electrochemotherapy with cisplatin on invasive ductal carcinoma tumors. Good antitumor results were achieved in experimental tumors with a size comparable to clinical lesions, demonstrating that this three-modality combined treatment is useful for the treatment of large lesions even at sub-optimal radiotherapy doses.

Key words: cisplatin; irradiation; electroporation; invasive ductal carcinoma; multimodalities

Introduction

Cisplatin is an anti-cancer chemotherapeutic drug that is administered to treat a large number of cancers such as those of the ovary, head and neck, cervix and bladder, carcinomas as well as small-cell and non-small-cell lung cancers.[1-5] However, resistance to cisplatin is a clinical problem for the treatment of some tumors.[6] After an initial response to chemotherapy, tumors subsequently show the

minimal responsiveness to cisplatin.[1,2,7] Besides direct cytotoxic effects, cisplatin has also the potential to enhance radiation-induced cell killing.[8-10] Cisplatin as a radiosensitizer increases the damage to the nuclear DNA of malignant cells, enhancing the anti-neoplastic efficacy of the radiotherapy.[9,10] The combination of cisplatin and radiation is a common treatment modality with synergistic effects for cancers.[4,5,8,9,11] Several *in vitro* and *in vivo* studies have shown higher response rates, prolonged mean survival, increased survival rates, longer local recurrence-free survival rates, and considerable organ preservation with the use of cisplatin in combination with external radiotherapy.[8-11] Indeed, it has been proven that cisplatin enhances the cytotoxicity of radiation on cells *in vitro*, on experimental tumors *in vivo* and in solid tumors in the clinic.[12-14]

Many studies have been performed to potentiate cisplatin antitumor effectiveness. One way to increase the radiosensitizing effect of cisplatin can result from the increase of the cisplatin intracellular accumulation. Several studies have been conducted using different drug delivery systems to increase the amount of cisplatin in the tumor cells.[8,14-18] Electropermeabilization is a physical method that uses short and intense electric pulses to facilitate drug delivery into the cells.[19,20] Electrochemotherapy (ECT) combines the administration of specific chemotherapeutic drugs (bleomycin or cisplatin) with the application of electric pulses to the tumors to locally increase drug uptake and thus drug effectiveness.[17,21] Electrochemotherapy with bleomycin and cisplatin was elaborated *in vitro*, *in vivo* and in clinical trials.[15,16,21-25] Besides permeability, electroporation has other effects like a transient and reversible reduction of the blood flow.[26] This reduction may contribute to the entrapment of the drug in the tumor, thereby providing more time for the drug to act. As this effect would reduce drug wash-out from the tumor, it could play a role in antitumor efficiency.

It has been demonstrated that the electroporation of tumors increases the radiosensitizing effect of cisplatin on small experimental tumors.[27,28] The enhanced radiosensitizing effect of cisplatin is actually due to the increased electroporation-mediated cisplatin delivery into the tumor cells.[29] These initial studies used an already efficient dose of radiotherapy (RT) which was delivered to SA-1 fibrosarcoma transplanted in mice, combined to electrochemotherapy using cisplatin as well as small tumors in mice.[27]

The aim of the present study was to evaluate the efficiency of electrochemotherapy with cisplatin combined with a single radiotherapy dose on an animal model tumor of breast adenocarcinoma to determine the potentialities of this combination. Two sub-optimal radiotherapy conditions, 3 Gy or 5 Gy, unable to generate long term partial responses in this tumor model, were applied in these combinations. Moreover, it was decided to treat very large experimental tumors, of an average volume of 630 mm^3, to assess the efficacy of the treatment alone or in combination in a preclinical model exploring the possibility of efficiently treating large lesions.

Materials and methods

Mice and tumors

Female Balb/C mice, purchased from the Pasteur Institute (Tehran, Iran) were maintained at 25°C with natural day/night cycle for 10 days for adaptation. Mice were 6–8 weeks old at the beginning of the experiments. A fragment (4 mm^3) of a spontaneous mouse mammary tumor (an invasive ductal carcinoma) was transplanted subcutaneously into the flank of each animal.[30,31] Two weeks after the implantation, when the tumors reached approximately 630 mm^3 in volume (12-15 mm in diameter), the mice were randomly divided into the experimental groups (8-10 animals for each control and each experimental group). The study was approved by the local Research and Medical Ethics Committee, in accordance with the Shahid Beheshti University of Medical Sciences Guidelines for the Care and Use of Laboratory Animals.

Cisplatin

Cisplatin (50 mg/ml, Ebewe Pharma, Austria) was diluted with 0.9% NaCl the day of the treatment. Cisplatin at a dose of 8 mg/kg was injected intratumorally and the injected volume was adjusted to deliver 0.02 ml of this cisplatin solution per gram of body weight.

Electrochemotherapy

Two flat stainless steel plates were mounted on a caliper to serve as 20 x 20 mm parallel electrodes. A distance between electrodes was adjusted by rolling of the caliper depending on the tumor size. The voltage value was then set in an ECT-SBDC device (with a maximal output voltage of 1400 V) to gen-

TABLE 1. Tumor growth after treatment with three modalities; cisplatin, electric pulses and local γ-radiation or combination on invasive ductal carcinoma tumor model

Experimental groups	n	DT days, Mean±SE	GD days, mean	Inhibition ratio (%)	CR number
Control	8	4.6±0.5		0	0
CDDP	8	10.6±1.21	5.5	33	0
EP	8	6.6±0.5	2.0	32	0
ECT	10	20.1±1.2	15.5	61	0
IR (3 Gy)	9	15.7±1.4	11.1	63	0
CDDP + IR (3 Gy)	9	15.9±2.4	11.3	61	0
EP + IR (3 Gy)	8	13.4±2.1	8.8	51	0
ECT + IR (3 Gy)	10	30.3±2.6	25.7	76	0
IR (5 Gy)	8	25.2±1.1	20.6	70	0
CDDP + IR (5 Gy)	8	25.6±1.2	21.0	75	0
EP + IR (5 Gy)	8	22.4±1.4	17.8	59	0
ECT + IR (5 Gy)	8	43.2±1.5	38.6	87	2

CDDP = cisplatin; EP = electric pulses; ECT = electrochemotherapy; IR = irradiation; n = number of mice in the experimental group; DT = tumor doubling time; GD = growth delay; PR = partial response; CR = complete response

erate electric pulses with a voltage to distance ratio of 1000 V/cm. The electrodes and the ECT-SBDC device were designed in the electromagnetic laboratory of the Medical Physics department of Tarbiat Modares University, Tehran, Iran. Eight square-wave electric pulses (two trains of 4 pulses) of 1000 V/cm amplitude, with a pulse duration of 100μs and repetition frequency 1 Hz, were delivered by the two parallel electrodes which were placed on the skin at the opposite sides of the tumor. An optimal contact between the electrodes and the skin was assured by means of a conductive gel. In all the electrochemotherapy groups, mice were treated with the electric pulses 1 min after the cisplatin injection.

Radiotherapy

A cobalt-60 unit (Theraton 780, Canada) was used to locally deliver a single dose of 3 Gy or 5 Gy at a dose rate of 0.6 Gy/min (3 Gy in 5 min) or 0.71 Gy/min (5 Gy in 7 min). Irradiation was performed frontally. As the smallest field covered by the Cobalt beam was 4 x 4 cm^2, the mouse's body around the tumor was shielded using lead blocks so as to leave only the tumor exposed to the irradiation beam.

Study protocol

The experimental groups included: untreated tumors as controls, tumors treated with cisplatin, electric pulses or radiotherapy alone, tumors treated by electrochemotherapy (that is cisplatin injection followed by the local application of electroporative electric pulses) and tumors treated with the combination of cisplatin or electric pulses and radiotherapy. In the combination of cisplatin or electroporation with local radiotherapy, tumor-bearing mice were irradiated 30 min after the cisplatin injection or the electric pulses delivery, to provide the time to cisplatin to enter the cells.

Treatment evaluation

Tumor growth was monitored, every three days, by measuring two mutually orthogonal tumor diameters (e1 being the larger tumor diameter and e2 the largest diameter orthogonal to e1). Tumors were rather spherical and tumor volumes were calculated by the formula $V= \pi/6 \times e1 \times e2^2$. From the tumor growth curves, tumor-doubling time (DT) was determined for each individual tumor. Tumor growth delay (GD) was calculated by subtracting the mean tumor volume doubling time of the untreated tumors (control) from the mean tumor volume doubling time of each experimental group. Inhibition ratio, expressed in percent, was calculated at day 30 after the treatment by the formula [1-(treated tumor average volume/untreated tumor average volume)] x100%. Partial response (PR) was a decrease by more than 50% of the tumor volume. Complete response (CR) was the absence of tumor for more than 100 days.

Normalized volumes at day N for each animal were calculated by dividing the tumor volume Vn at day N after the treatment by the average tumor volume V0 at day 0 that is at the day of the treatment (Vn/V0).

Statistical analysis

All data were tested for normality of distribution. The ANOVA test with repeated measures was used to evaluate statistical significance of differences between experimental and control groups at different times. A p-value<0.05 was considered significant in the statistical tests (*p <0.05).

Results

As shown in Table 1 and Figure 1, cisplatin (at a dose of 8 mg/kg) as a single treatment delayed the tumor growth up to 5.5 days with an inhibition ratio of 33%. Tumors that were treated with electric pulses alone (8 pulses, 1000 V/cm, 100µs duration, at 1 Hz repetition frequency) displayed a tumor growth delay of only 2 days with an inhibition ratio of 32% (Table 1) and with no partial or complete responders with neither of both treatment modalities.

In the electrochemotherapy group, in which tumors were exposed to electric pulses 1 min after the cisplatin injection, a prolonged tumor growth delay (up to 15.5 days) was observed (p <0.05). The inhibition ratio reached 61% (Table 1). Thus, electrochemotherapy was more effective than either cisplatin alone or the application of electric pulses alone, with moreover 30% partial response for the first 9 days (p <0.05).

With local irradiation alone (Table 1 and Figures 1 and 2), the higher dose (5 Gy) resulted in a growth delay up to 20.6 days. Tumors irradiated with a single dose of 3 Gy resulted in a tumor growth delay of 11.1 days and an inhibition ratio of 63% (Table 1). Some partial responses (25%) were observed within the 15 days that followed the administration of 5 Gy, but only 11% with 3 Gy.

When the administration of cisplatin was combined with local irradiation performed 30 min after the drug injection, the treatment of tumors resulted in tumor growth delays and inhibition ratios of 11.3 days and 61% respectively with a 3 Gy radiation and of 21.0 days and 75% with a 5 Gy irradiation (Table 1). These results demonstrate that a dose of 5 Gy was more effective. This is also borne out by the fact that 25% partial responses were observed

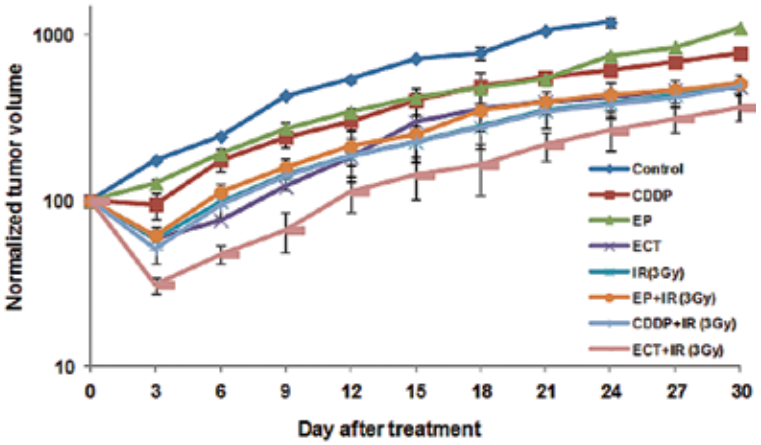

FIGURE 1. Tumor growth curves in untreated tumors or after treatment with CDDP (CDDP), electric pulses (EP) only, irradiation (IR) only, electrochemotherapy (ECT) and the combinations of CDDP or electric pulses and radiotherapy. Data are mean ± SE of at least 8 animals for each of the experimental groups. Irradiation of tumor was 3Gy.

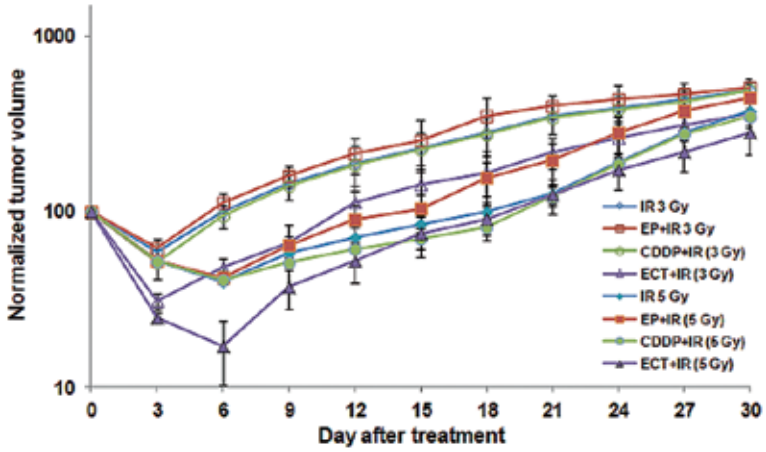

FIGURE 2. Tumor growth curves for invasive ductal carcinoma tumors after treatment with radiotherapy (IR) only, electrochemotherapy (ECT), combination of CDDP or electric pulses and radiotherapy at dose of 3 Gy in comparison to 5 Gy. Data are mean ± SE of at least 8 animals for each of the experimental groups.

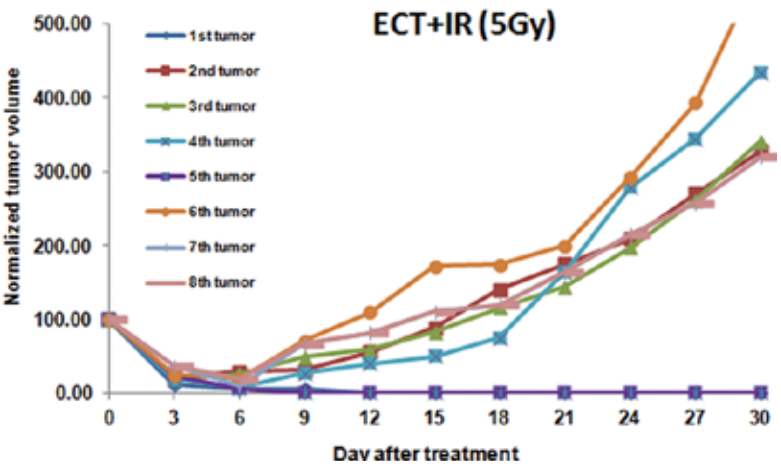

FIGURE 3. Individual tumor growth curves of tumors treated by the combination of electrochemotherapy (ECT) and radiotherapy at the dose of 5 Gy.

for up to 15 days with the 3 Gy irradiation, whereas only 11% partial responses were recorded up to 12 days following the combination of cisplatin and 3 Gy irradiation ($p < 0.05$).

When electric pulses were combined with local irradiation delivered 30 min after the electric pulses application, an improved antitumor effect was not observed compared to irradiation alone. Tumor growth delays of 8.8 days and inhibition ratio of 51% after 3 Gy and of 17.8 days and 59% after 5 Gy were scored (Table 1). With 5 Gy, one partial response (12.5%) was achieved for 15 days with no partial responders after 3 Gy.

Irradiation of tumors pretreated with electrochemotherapy prolonged the tumor growth delay up to 25.7 days and 38.6 days at 3 Gy and 5 Gy respectively. The inhibition ratio reached 76% for the 3 Gy irradiation and 87% for 5 Gy. Ten per cent of partial responses after 30 days were observed with electrochemotherapy followed by 3 Gy, though without complete responders. In contrast, the electrochemotherapy with a 5 Gy irradiation resulted in a higher percentage of partial regressions (37% of the tumors were still in partial response 30 days after the treatment). Moreover, 25% of the mice were still in complete remission 100 days after the treatment (Table 1 and Figure 3). Again, the combination with 5 Gy was significantly ($p < 0.05$) more efficient than the combination with 3 Gy. Even in this group, no body weight loss or skin desquamation was reported. Only a hair loss was observed in all the groups that were irradiated, locally at the level of the irradiation site.

In summary, in all the cases, the combination with γ- radiation resulted in a larger antitumor efficacy than without the combination with γ-rays.

Discussion

In this study, the therapeutic effects of cisplatin, electroporation, γ-radiation and combination of these treatments were evaluated in a murine invasive ductal carcinoma tumor model. Our data confirm and extend previous findings[16-18] showing that the delivery to tumors of electric pulses and cisplatin enhances the cisplatin-induced radiosensitization.

Electroporation combined with cisplatin has shown a significant effectiveness both *in vitro* and *in vivo*, as well as in clinical studies in the treatment of patients with cutaneous tumor nodules.[15-18,24,25] Although the increased radiosensitizing effect of cisplatin using electroporation has been shown in EAT carcinoma and LPB sarcoma cells[27,28], data on radiosensitization for large tumors, of a size closer to clinical situations, have not yet been reported. In this study, this issue was addressed and using local γ-radiation with single doses of 3 Gy or 5 Gy of Cobalt-60 γ-rays in combination with electrochemotherapy with cisplatin on large invasive ductal carcinoma tumors as a model for the treatment of large breast tumors.

Our study confirms that electrochemotherapy was more effective than individual treatments using cisplatin or electric pulses alone which is consistent with previous reports.[16-18,27,28] When electrochemotherapy with cisplatin was combined with local irradiation, the antitumor efficiency was doubled. This three-modality therapy was better than electrochemotherapy, cisplatin combined with local tumor irradiation and electric pulses combined with irradiation. In addition, some tumors were still in complete remission 100 days after the treatment at single dose of 5 Gy. It is important to highlight that the irradiation doses used in the present study (a single 3 Gy or 5 Gy dose) are lower than the doses used in the previous experimental studies with cisplatin reported here above.[27,28] Indeed, Sersa *et al*. used a dose of 15 Gy for electrochemotherapy with cisplatin combined with irradiation on the EAT tumor animal model.[27] However, there are studies that demonstrated an increase of the tumor curability dose (TCD50) for both cisplatin (being 1.6) and bleomycin (1.9).[32,33]

This study concentrated on electrochemotherapy with cisplatin, as cisplatin is a radiosentizer, with the aim also to show that electrochemotherapy can radiosensitize the tumors. However, the initial goal was to determine whether electrochemotherapy efficacy could be increased by irradiation even in large tumors. Indeed, using about the same dose rate 2.2 Gy/min (10-20 Gy), Sersa *et al*. showed that efficacy of electrochemotherapy with bleomycin (a molecule considered a radiomimetic but not a radiosensitizer) was increased with irradiation, on SA-1 and CaNT tumor models.[32]

Finally it is important to report that our results are also in agreement with two clinical studies[34,35] reporting that electrochemotherapy in combination with irradiation is an effective and safe treatment for tumors of various origins in patients, thus on lesions of a size at least comparable to those treated in this study.

In conclusion the results of this study demonstrate that electrochemotherapy with cisplatin radiosensitized the tumors to a single low irradiation dose (3 Gy or 5 Gy of Cobalt-60 γ-rays) on invasive

ductal carcinoma tumors. Moreover, this three-modality combined treatment was useful for the treatment of large lesions even at sub-optimal doses of irradiation. Complete response of very large tumors could be achieved after a single session with the combined multimodality treatment.

Acknowledgements

This work was supported by the Radiation Medicine Department, Shahid Beheshti University, Tehran, Iran. Authors would like to thank Novin Medical Radiation Institute (NMRI), Tehran, Iran especially Dr. Zahmatkesh and Dr. Akhlaghpour for providing us with Cobalt-60 therapy system. We also thank Professor Ahmadiani, Neuroscience Research Center, Shahid Beheshti University, Medical Sciences, Tehran, Iran. One of the authors (ER) would like to thanks the ABC Laboratory from the European Scientific Institute, 74160 Archamps, France, where the present manuscript was completed. Also, we would like to thank Prof. Miralbell from Dept. of Radiation Oncology, University Hospital, Geneve, Switzerland for help in editing the manuscript.

References

1. Gately DP, Howell SB. Cellular accumulation of the anticancer agent CDDP: a review. *Br J Cancer* 1993; **67:** 1171-6.
2. Kelland L. The resurgence of platinum-based cancer chemotherapy. *Nat Rev Cancer* 2007; **7:** 573-84.
3. Lekic M, Kovac V, Triller N, Knez L, Sadikov A, Cufer T. Outcome of small cell lung cancer (SCLC) patients with brain metastases in a routine clinical setting. *Radiol Oncol* 2012; 46(3): 226-232.; **46:** 54-9.
4. Malecki K, Glinski B, Mucha-Malecka A, Rys J, Kruczak A, Roszkowski K, et al. Prognostic and predictive significance of p53, EGFr, Ki-67 in larynx preservation treatment. *Rep Pract Oncol Radiother.* 2010; **15:** 87-92.
5. Kovac V, Smrdel U. Meta-analyses of clinical trials in patients with non-small cell lung cancer. *Neoplasma* 2004; **51:** 334-40.
6. Erculj N, Kovac V, Hmeljak J, Dolzan V. The influence of platinum pathway polymorphisms on the outcome in patients with malignant mesothelioma. *Ann Oncol* 2012; **23:** 961-7.
7. Kelland LR. Preclinical perspectives on platinum resistance. *Drugs* 2000; **59:** 1-8.
8. Begg AC, Deurloo MJ, Kop W, Bartelink H. Improvement of combined modality therapy with CDDP and radiation using intratumoral drug administration in murine tumors. *Radiother Oncol* 1994; **31:** 129-37.
9. Sharma VM, Wilson WR. Radiosensitization of advanced squamous cell carcinoma of the head and neck with CDDP during concomitant radiation therapy. *Eur Arch Otorhinolaryngol* 1999; **256:** 462-5.
10. Bergs JWJ, Franken NAP, Cate RT, Bree CV, Haveman J. Effects of CDDP and γ-irradiation on cell survival, the induction of chromosomal aberrations and apoptosis in SW-1573 cells. *Mutat Res* 2006; **594:** 148-54.
11. Ning S, Yu N, Brown DM, Kanekal S, Knox SJ. Radiosensitization by intratumoral administration of CDDP in a sustained-release drug delivery system. *Radiother Oncol* 1999; **50:** 215-23.
12. Strojan P, Katarina K, Lojze S, Erika S, Igor F, Boris J, Aleksandar A, Marjan B, Branko Z. Concomitant chemoradiotherapy with Mitomycin C and Cisplatin in advanced unresectable carcinoma of the head and neck: Phase I-II Clinical Study. *Int J Radiat Oncol Biol Phys* 2008; **72:** 365-72.
13. Carde P, Laval F. Effect of cis-dichlorodiammineplatinum (II) and X-rays on mammalian cell survival. *Int J Radiat Oncol Biol Phys* 1981; **7:** 929-33.
14. Geldof AA, Slotman BJ. Radiosensitizing effect of CDDP in prostate cancer cell lines. *Cancer Lett* 1996; **101:** 233-9.
15. Melvik JE, Pettersen EO, Gordon PB, Seglen PO. Increase in cis- dichlorodiammineplatinum (II) cytotoxicity upon reversible electro-permeabilization of the plasma membrane in cultured human NHIK 3025 cells. *Eur J Cancer Clin Oncol* 1986; **22:** 1523-30.
16. Cemazar M, Miklavcic D, Vodovnik L, Jarm T, Rudolf Z, Stabuc B, et al. Improved therapeutic effect of electrochemotherapy with cisplatin by intratumoral drug administration and changing of electrode orientation for electromeatabilization on EAT tumor model in mice. *Radiol Oncol* 1995; **29:** 121-7.
17. Sersa G, Cemazar M, Miklavcic D. Antitumor effectiveness of electrochemotherapy with cis-diamminedichloroplatinum (II) in mice. *Cancer Res* 1995; **55:** 3450-5.
18. Sersa G, Cemazar M, Semrov D, Miklavcic D. Changing electrode orientation improves the efficacy of electrochemotherapy of solid tumors in mice. *Bioelectrochem Bioenerg* 1996; **39:** 61-6.
19. Mir LM, Orlowski S. The basis of electrochemotherapy. In: Jaroszeski MJ, Heller R, Gilbert R, editors. *Electrochemotherapy, Electrogentherapy, and Transdermal Drug Delivery. Electrically Mediated Delivery of Molecules to Cells.* Totowa: Humana Press; 2000. p. 99–117.
20. Silve A, Mir LM. Clinical aspects of electroporation. In: Kee ST, Gehl J, Lee EW, editors. *Cell electropermeabilization and cellular uptake of small molecules: the ECT concept.* New York; Springer; 2011. p. 69-82.
21. Mir LM, Orlowski S, Belehradek J Jr, Paoletti C. Electrochemotherapy potentiation of antitumor effect of bleomycin by local electric pulses. *Eur J Cancer* 1991; **27:** 68-72.
22. Marty M, Sersa G, Garbay JR, Gehl J, Collins CG, Snoj M, et al. Electrochemotherapy—an easy, highly effective and safe treatment of cutaneous and subcutaneous metastases: results of ESOPE (European Standard Operating Procedures of Electrochemotherapy) study. *EJC Suppl* 2006; **4:** 3-13.
23. Sersa G, Stabuc B, Cemazar M, Jancar B, Miklavcic D, Rudolf Z. Electrochemotherapy with CDDP: potentiation of local CDDP antitumor effectiveness by application of electric pulses in cancer patients. *Eur J Cancer* 1998; **34:** 1213-8.
24. Cemazar M, Sersa G, Miklavcic D, Scancar J, Dolzan, Golouh R, et al . Increased platinum accumulation in SA-1 tumor cells after in vivo electrochemotherapy with CDDP. *Br J Cancer* 1999; **79:** 1386-91.
25. Sersa G, Stabuc B, Cemazar M, Miklavcic D, Rudolf Z. Electrochemotherapy with cisplatin: clinical experience in malignant melanoma patients. *Clin Cancer Res* 2000; **6:** 863-7.
26. Jarm T, Cemazar M, Miklavcic D, Sersa G. Antivascular effects of electrochemotherapy: implications in treatment of bleeding metastases. *Expert Rev Anticancer Ther* 2010; **10:** 729-46.
27. Sersa G, Kranjc S, Cemazar M. Improvement of combined modality therapy with CDDP and radiation using electroporation of tumors. *Int J Radiat Oncol Biol Phys* 2000; **46:** 1037-41.
28. Kranjc S, Cemazar M, Grosel A, Scancar J, Sersa G. Electroporation of LPB sarcoma cells *in vitro* and tumors *in vivo* increases the radiosensitizing effect of CDDP. *Anticancer Res* 2003; **23:** 275-82.
29. Kranjc S, Cemazar M, Grosel A, Pipan Z, Sersa G. Effect of electroporation on radiosensitization with cisplatin in two cell lines with different chemo- and radiosensitivity. *Radio Oncol* 2003; **37:** 101-7.
30. Hassan ZM, Yaraee R, Chazanfari T, Safar Kejad AH, Nozari B. Immunomodulatory affect of R10 fraction of garlic extract on natural killer activity. *Int J Immunopharmaco* 2003; **3:** 1483-9.
31. Raeisi E, Firoozabadi SMP, Hajizadeh S, Rajabi H, Hassan Z M. The effect of high-frequency electric pulses on tumor blood flow in vivo. *J Membrane Biol* 2010; **236:** 163-66.

32. Kranjc S, Tevz G, Vidic S, Cemazar M, Sersa G. Radiosensitizing effect of electrochemotherapy in a fractionated radiation regimen in radiosensitive murine sarcoma and radioresistant adenocarcinoma tumor model. *Radiat Res* 2009; **172:** 677-85.

33. Sersa G, Kranjc S, Cemazar M. Advanced electroporation techniques in biology and medicine. In: Pakhomov A, Miklavcic D, Marko MS, editors. *Combined modality therapy: electrochemotherapy with tumor irradiation.* CRC Press; 2010. p. 441-452.

34. Sersa G, Cemazar M, Rudolf Z, Fras AP. Adenocarcinoma skin metastases treated by electrochemotherapy with cisplatin combined with radiation. *Radiol Oncol* 1999; **33:** 291-6.

35. Skarlatos I, Kyrgias G, Mosa E, Provatopoulou X, Spyrou M, Theodorou K, et al. Electrochemotherapy in cancer patients: first clinical trial in Greece. *In Vivo* 2011; **25:** 265-74.

research article

miR-548c-5p inhibits proliferation and migration and promotes apoptosis in CD90+ HepG2 cells

Lin Fang[1], Hai-Bing Zhang[2], Hua Li[1], Yong Fu[2], Guang-Shun Yang[1,2]

[1] Department of Laboratory Centre, Shanghai Tenth People's Hospital, Tongji University School of Medicine, Shanghai. China
[2] 5th Department of Liver Surgery, Eastern Hepatobiliary Surgery Hospital, Second Military Medical University, Shanghai, China

Radiol Oncol 2012; 46(3): 233-241.

Received 13 September 2011
Accepted 1 February 2012

Correspondence to: Guang-Shun Yang, MD, Department of Laboratory Centre, Shanghai Tenth People's Hospital, Tongji University School of Medicine, 301 Yan Chang Road, Shanghai 200072, China. Phone: +86-21-66301057; Fax: +86-21-66301057; E-mail: docyang@yeah.net

Disclosure: No potential conflicts of interest were disclosed.

Background. Since the introduction of the theory of tumour stem cells (TSCs), the liver cancer stem cell (LCSC)-like cells have become one of the focuses in the research on liver cancer.

Materials and methods. In this study, CD90+ cells were applied as the possible LCSC-like cells, and the miRNA and gene expression were analyzed in the CD90+ HepG2 cells. The pilot study showed miR-548c-5p exerted potential effect on the CD90+ HepG2 cells and was thereafter applied for the further study. CD90+ HepG2 cells were assigned to miR-548c-5p mimic transfection group and control group. MTT assay was performed to detect the proliferation of CD90+ HepG2 cells. The migration and invasion abilities were examined by wound healing assay and transwell migration assay, respectively. A detection of apoptosis was performed by fluorescence microscopy.

Results. Our results showed that *caspase-3* and *bcl-2* were down-regulated while *caspase-8* was up-regulated in the CD90+ HepG2 cells. Moreover, the miR-548c-5p transfection could down-regulate the expression of *β-catenin, Tg737, bcl-2, bcl-XL*, and *caspase-3*, inhibit the proliferation, migration and invasion and promote the apoptosis of the CD90+ HepG2 cells.

Conclusions. Our findings indicate the imbalance between apoptosis and anti-apoptosis in the LCSC-like cells, which influence the biological features of LCSC-like cells. miRNA plays a regulatory role in the LCSC-like cells among which miR-548c-5p might be a suppressor.

Key words: liver cancer stem cells; miR-548c-5p; apoptosis; NF-κB, *β-catenin*

Introduction

The pathogenesis of primary liver cancer remains unclear. Since the introduction of the theory of tumour stem cells (TSCs), the liver cancer stem cells (LCSC) have become one of the focuses in the research on liver cancer. The theory of LCSC concerns the tumour formation and biological features at the cellular level and the new explanations for the development and progression of tumours, which provide a new direction for the future research on liver cancer.[1-5] However, there is no report on the existence of LCSCs in tumour tissues.

There is a difficulty in the isolation and biological investigations of LCSCs, due to the absence of specific marker for LCSCs. Studies have revealed that CD90 could be used as a possible surface marker of LCSCs.[6-8] When CD90+ cells isolated from liver cancer cell lines and liver tissues of liver cancer patients were inoculated into severe combined immunodeficiency (SCID) rats, animals developed cancer showing that these cells were carcinogenic.[6] The diagnosis of primary liver cancer was also confirmed by pathological evaluation. CD90+ cells were also detected in liver cancer patients[7], suggesting that CD90 could be used

as a valuable surface marker of LCSCs, and as the target of gene diagnosis and therapy. CD133 has been also considered a specific surface marker of LCSCs, because $CD133^+$ cells have biological features of LCSCs.[9-11] Side population (SP) cells refer to normal stem cells whose membrane contains ATP-binding cassette transporter, which can expel Hoechst33342 dye from the inside to the outside of the membrane effectively, while these characteristics are absent in the non-SP cells. It has been demonstrated that 100 SP cells isolated from liver cancer cells were enough for carcinogenesis, while non-SP cells had no carcinogenic ability, and SP could be used as a method to isolate LCSC-like cells.[12] However, LCSC-like cells isolated by the above method are by no mean true LCSCs. In the present study, $CD90^+$ cells were used as the possible LCSC-like cells for the further study.

The expression of multiple tumour suppressor genes is abnormal in the liver cancer, of which *p53* and *Tg737* are believed to be closely associated with the occurrence of liver cancer by affecting the LCSC -like cells.[13,14] The Wnt and NF-κB signalling pathways play important roles in regulating the LCSC-like cells.[15,16] Apoptosis plays an essential role in not only the growth and development of cancer cells but in various diseases including tumours, immune diseases, infectious diseases and neurological diseases. Anti-apoptosis is an important process in the development and progression of tumours, and apoptosis also exists in liver cancer cells.[17,18]

miRNAs are a group of endogenous non-protein-encoding single-stranded low-molecular-weight RNA with a length of about 20-25 nt, widely existing in the eukaryotes. miRNAs play important roles in the cell proliferation, differentiation and apoptosis.[19] However, the specific role of miRNAs in the LCSC-like cells is still poorly understood.

In the present study, CD90 was used as a possible marker for LCSC-like cells, and these LCSC-like cells were isolated from liver cancer cells HepG2, and changes in the expression of miRNAs, cancer-inhibiting genes and apoptosis-related genes were determined. Our results showed the difference in expressions of miR-548c-5p, miR-145, miR-375, miR-874, miR-155, miR-198 and miR-1289 between $CD90^+$ HepG2 cells and $CD90^-$ HepG2 cells, of which our pilot study revealed miR-548c-5p could affect the proliferation and promote the apoptosis of the $CD90^+$ HepG2 cells. Thus, miR-548c-5p was further studied, hoping to gain a preliminary understanding of the effect of miR-548c-5p on the $CD90^+$ LCSC-like cells and provide evidence for the understanding of biological features of LCSC-like cells.

Materials and methods

Cell line and culture

Human liver cancer cell line HepG2 (Shanghai Institutes for Biological Sciences of the Chinese Academy of Sciences, China) was maintained in monolayer cultures in high glucose Dulbecco's Modified Eagle Medium (DMEM; Gibco, USA) containing 10% (v/v) foetal bovine serum (FBS; Gibco, USA) and 1% (v/v) penicillin (Weihui Biotechnology Co. Ltd., China) at 37°C in a humidified atmosphere of 5% CO_2. Cells in the exponential growth phase were harvested and a cell suspension was prepared at a density of 3.0×10^4 cells/mL and added into 96-well plates for transfection.

Screening of $CD90^+$ HepG2 cells

After the addition of PE-labelled anti-human $CD90^+$ monoclonal antibody (BD Biosciences, USA), the cells were mixed with EasySep® PE Selection Cocktail and cultured by addition of EasySep® magnetic beads (Baitong Co., Ltd, China). The $CD90^+$ cells were isolated from the HepG2 cells by magnetic activated cell sorting (MACS; Baitong Co., Ltd, China).

Detection of gene and miRNA expression by real-time-PCR assay

Total RNA was extracted from the $CD90^+$ HepG2 cells with TRIzol (Invitrogen, USA) and cDNA was synthesized from 2 μg of total RNA using Moloney murine leukaemia virus (MMLV) reverse transcriptase (Promega, USA). Real-time PCR was performed on ABI 7300 Real-time PCR System (Applied Biosystems, USA). The expression of the related genes (*p65*, *β-catenin*, *p53*, *Tg737*, *bcl-2*, *bcl-XL*, *caspase-3* and *caspase-8*) was analyzed using SYBR ExScript real-time PCR Kit (Tiangen Biotech Co., Ltd., China). Briefly, 20 μL of reaction mix was prepared. Thermal cycle conditions were as follows: 95°C for 30 s; 40 cycles of 95°C for 5 s and 60°C for 32 s. The expression levels of target genes were determined by using the $2^{-\Delta\Delta Ct}$ method. GAPDH was used as an endogenous control. A detection was carried out in triplicates.

miRNA was extracted with TRIzol similar to total RNA isolation for miRNA reverse transcription and amplification followed by the detection of ex-

pressions of miR-155, miR-198, miR-373, miR-548c-5p, miR-1289, miR-145, miR-375, miR-874, miR-1183 and miR-1324 using SYBR chemistry (Tiangen Biotech Co., Ltd, China).

The expression of selected genes and miRNAs in $CD90^+$ HepG2 cells was compared to those in $CD90^-$ HepG2 cells. The relative expression of the mRNA was calculated with the following formula:

ΔCT=CT sample - CT endogenous control

Relative expression $=2^{-\Delta CT\ (CD90+)}/2^{-\Delta CT\ (CD90-)}\times 100\%$

Cell transfection and detection of selected genes

$CD90^+$ HepG2 cells were assigned to miR-548c-5p group and control group. Cells in miR-548c-5p group were transfected with miR-548c-5p mimics (GenePharma. Co., Ltd, China) according to manufacturer's instructions. Cells in the control group were exposed to neither Lipofect transfection reagent nor miR-548c-5p mimics. miR-548c-5p mimics were mixed with Lipofect transfection reagent (Promega, Madison, WI, USA) followed by 10 min incubation. The concentration of miR-548c-5p mimics was diluted to 50 nmol/L before transfection. Cells were incubated with 100 μl of transfection mixture and collected 24 h and 48 h later for the use in further assays. All transfections were carried out in triplicates. miRNA was extracted at 24 h and 48 h after the transfection and the miR-548c-5p expression was detected by real time-PCR to verify the transfection efficiency. Total RNA was extracted from the transfected $CD90^+$ HepG2 cells which highly express miR-548c-5p, and real time-PCR was employed to detect the mRNA expression of related genes (*p65, β-catenin, p53, Tg737, bcl-2, bcl-XL, caspase-3* and *caspase-8*).

Caspase-3, bcl-2 and bcl-xl protein expression

Total protein was extracted at 48 h after the transfection with Total Protein Extraction Kit (BioChain, USA) according to manufacturer's instructions. In brief, 100 μg of proteins in each group was subjected to 10% SDS/PAGE and transferred onto PVDF membranes (Millipore, USA). The membranes were subsequently incubated with rabbit anti-caspase-3, bcl-2 and bcl-xl antibodies (1:800; Santa Cruz Biotechnology, USA), and rabbit anti-β-actin (1:1,000; Santa Cruz Biotechnology, USA). After the incubation with horseradish peroxidase conjugated secondary anti-rabbit antibody (1:5,000-10,000; Santa Cruz Biotechnology, USA), visualization was performed with an enhanced chemiluminescence kit (Supersignal West Pico Chemiluminescent Substrate Kit, Pierce, USA) followed by exposure to X-ray film (Kodak, USA). β-actin served as an endogenous control. Experiment was performed three times.

MTT assay

MTT assay was performed to detect the proliferation of $CD90^+$ HepG2 cells. miR-548c-5p mimics were independently diluted to 20, 40, 60, 80 and 100 nmol for the transfection. The transfected cells were maintained in the 96-well plate at 37°C in humidified air with 5% CO_2. In brief, MTT solution (5 mg/ml; Sigma, USA) was prepared with PBS and stored at 4°C. At 24, 48 and 72 h after the transfection, 20 μl of MTT was added to each well followed by incubation at 37°C for 5 h. After the addition of 150 μl of DMSO to each well to dissolve crystals, optical density (OD) was measured at 490 nm. The experiment was performed in quadruplicates. The inhibition rate (IR) of transfected $CD90^+$ HepG2 cells was calculated as follows: IR = (1-OD treated / OD untreated) × 100%.

Wound healing assay

In the *in vitro* wound healing assay, transfected $CD90^+$ HepG2 cells were grown in 6-well plates until the cell confluence reached about 80%. Then, a scratch was made in each well using a sterile pipette tip, and cells were then maintained at 37°C in an atmosphere with 5% CO_2. Wound healing was observed under a light microscope and images were captured at the same site at 0, 12, 24 and 48 h after scratching to observe the process of wound healing. The experiments were repeated twice and representative photographs are shown.

Invasion assay

A transwell invasion assay was performed in miR-548c-5p mimics group and control group with CHEMICON Cell Invasion Assay Kit (Chemicon, USA). Transwell chambers were pre-coated with Matrigel. Cells were added to the Transwell system 48 h after the transfection. The lower chambers were filled with 500 μl of DMEM containing 15% FBS. The Transwell system was placed in the 24-well plate followed by the incubation for 48 h at 37°C in an atmosphere with 5% CO_2. After removing the Matrigel and cells in the upper chambers, the membrane was stained with 0.1% crystal vio-

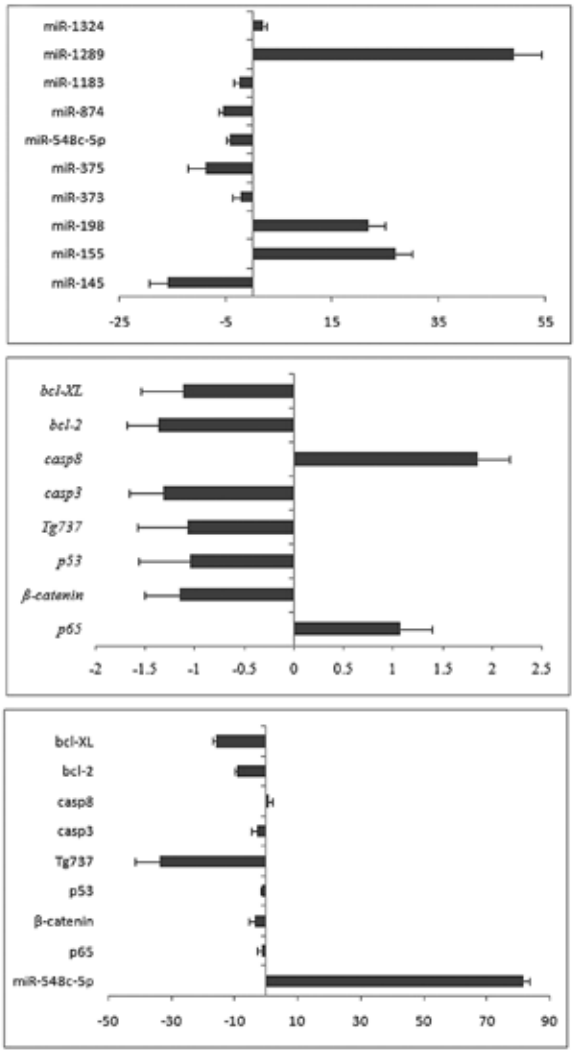

FIGURE 1. miRNA and gene expressions in CD90⁺ HepG2 cells as compared to CD90- HepG2 cells. (A) Fold-change in miRNA expressions in CD90+ HepG2 cells. (B) Fold-change in expression of target genes in CD90⁺ HepG2 cells. (C) Fold-change in expression of target genes 48 h after miR-548c-5p transfection as compared to un-transfected CD90⁺ HepG2 cells. Bars represent the mean value. Positive fold change represents up-regulation and negative fold change represents down-regulation.

let and observed under a microscope. Five fields were randomly selected from each membrane, and the number of cells penetrating the membrane was counted at a magnification of ×400. The invasion ability was expressed as the number of invading cells. The invasion of each group was assayed in triplicates. The experiment was repeated three times.

Detection of apoptosis by fluorescence microscopy

CD90⁺ HepG2 cells were collected at 48 h after the transfection with miR-548c-5p by centrifugation at 300× g for 5 min at room temperature. Cells were washed once in cold PBS, and gently re-suspended in Annexin V Incubation Reagent (Trevigen, USA). Annexin V Incubation Reagent was prepared according to the manufacturer's instructions. Cells were incubated in dark for 15 min at room temperature, then washed once in 1× Binding Buffer (Trevigen), and re-suspended in 100 μl of 1× Binding Buffer. Cell suspension was added onto cover slip and dried for a few minutes. Before the cell suspension completely dried, a drop of fluorescence mounting media (Trevigen, USA) was added onto the cover slip. Cells were observed under a fluorescence microscope (Olympus, Japan) at 540 nm to detect cells positive for propidium iodide and at 490 nm to detect cells positive for Annexin V-FITC.

Statistical analysis

SPSS version 13.0 software program was employed for the statistical analysis. Data were expressed as mean ± standard error (SEM). A statistical analysis was performed by using one way analysis of variance followed by least significant difference (LSD) post-hoc test. A two-tailed Student's paired t-test was also performed to compare the differences between 2 groups. A value of $P<0.05$ was considered statistically significant.

Results

miRNA expression in CD90⁺ HepG2 cells

Differences in miRNA expression in CD90+ HepG2 cells and in CD90- HepG2 cells were observed (Figures 1A). The expression of miR-548c-5p, miR-145, miR-375 and miR-874 decreased significantly in the CD90⁺ cells ($P<0.05$) when compared with CD90⁻ cells, while the expression of miR-155, miR-198 and miR-1289 were higher in the CD90⁺ cells than those in the CD90⁻ cells ($P<0.05$). However, there was no marked difference in the expression of miR-373, miR-1183 and miR-1324 between two groups.

Expression of p65, ß-catenin, p53, Tg737, bcl-2, bcl-XL, caspase-3 and caspase-8 in CD90⁺ cells

The expression of *caspase-3* and *bcl-2* was significantly down-regulated, and that of *caspase-8* markedly up-regulated in the CD90⁺ cells when compared with the CD90⁻ cells (both $P<0.05$). There

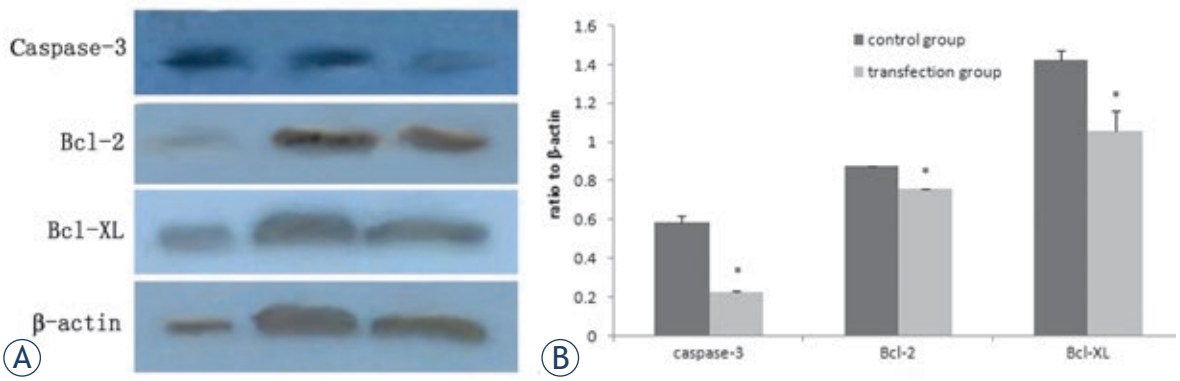

FIGURE 2. Protein expression of caspase-3, bcl-2 and bcl-xl after miR-548c-5p transfection. (A) Western blot assay demonstrated decreased OD of caspase-3, Bcl-2, and Bcl-XL in transfection group when compared with control group. From left to right: $CD90^-$ HepG2 group; control group; transfection group; (B) Quantification of caspase-3, bcl-2, and bcl-xl after miR-548c-5p transfection normalized to β-actin. Protein expression of caspase-3, Bcl-2, and Bcl-XL decreased significantly in transfected cells (*P<0.05).

was no significant difference in the expression of *p53*, *p65*, *β-catenin*, *Tg737* and *bcl-XL* (P>0.05) (Figures 1B).

Expression of p65, ß-catenin, p53, Tg737, bcl-2, bcl-XL, caspase-3 and caspase-8 in $CD90^+$ cells following miR-548c-5p transfection

The miR-548c-5p expression in the $CD90^+$ cells following transfection with miR-548c-5p mimics was increased by 80 fold as compared to untransfected cells (P<0.05). In the miR-548c-5p transfected $CD90^+$ cells, the expression of *β-catenin*, *Tg737*, *bcl-2*, *bcl-XL* and *caspase-3* was down-regulated significantly (P<0.05) when compared with untransfected cells. There was no marked difference in the expression of *p65*, *p53* and *caspase-8* between $CD90^+$ cells before and after the transfection (P>0.05) (Figures 1C).

Protein expression of caspase-3, bcl-2 and bcl-xl in $CD90^+$ cells following miR-548c-5p transfection

The western blot assay showed that protein expression of caspase-3, Bcl-2, and Bcl-XL decreased significantly in $CD90^+$ cells transfected with miR-548c-5p when compared with untransfected $CD90^+$ cells (Figures 2A, B).

miR-548c-5p inhibits $CD90^+$ cell proliferation

MTT assay was performed to examine the IR of $CD90^+$ HepG2 cell proliferation after miR-548c-5p transfection. In miR-548c-5p transfected cells, the OD was decreased at 24 h, 48 h, and 72 h after the transfection (Figures 3A, B, C). IR of $CD90^+$ HepG2 cells following the transfection increased markedly as compared to untransfected $CD90^+$ HepG2 cells and the IR increased over time (Figures 3D).

miR-548c-5p inhibits migration and invasion of $CD90^+$ cells

The wound healing assay showed that the migration ability of $CD90^+$ HepG2 cells was significantly compromised at 48 h after miR-548c-5p transfection when compared with untransfected $CD90^+$ HepG2 cells (Figures 4A, B).

The transwell invasion assay revealed that the number of $CD90^+$ HepG2 cells penetrating the membrane decreased at 48 h after miR-548c-5p transfection as compared to the control group (Figures 4C). The number of cells penetrating the membrane was markedly lower in the transfected cells as compared to untransfected cells (P<0.05) (Figures 4D).

Apoptosis of $CD90^+$ cells following transfection with miR-548c-5p

The apoptosis of $CD90^+$ HepG2 cells was observed under a fluorescence microscope. Propidium iodide staining showed the increased number of late apoptotic $CD90^+$ HepG2 cells at 48 h after miR-548c-5p transfection as compared to the un-transfected cells (Figures 5A1 and B1). Annexin V-FITC staining also revealed the increased number of apoptotic $CD90^+$ HepG2 cells after the transfection (Figures 5C1 and D1).

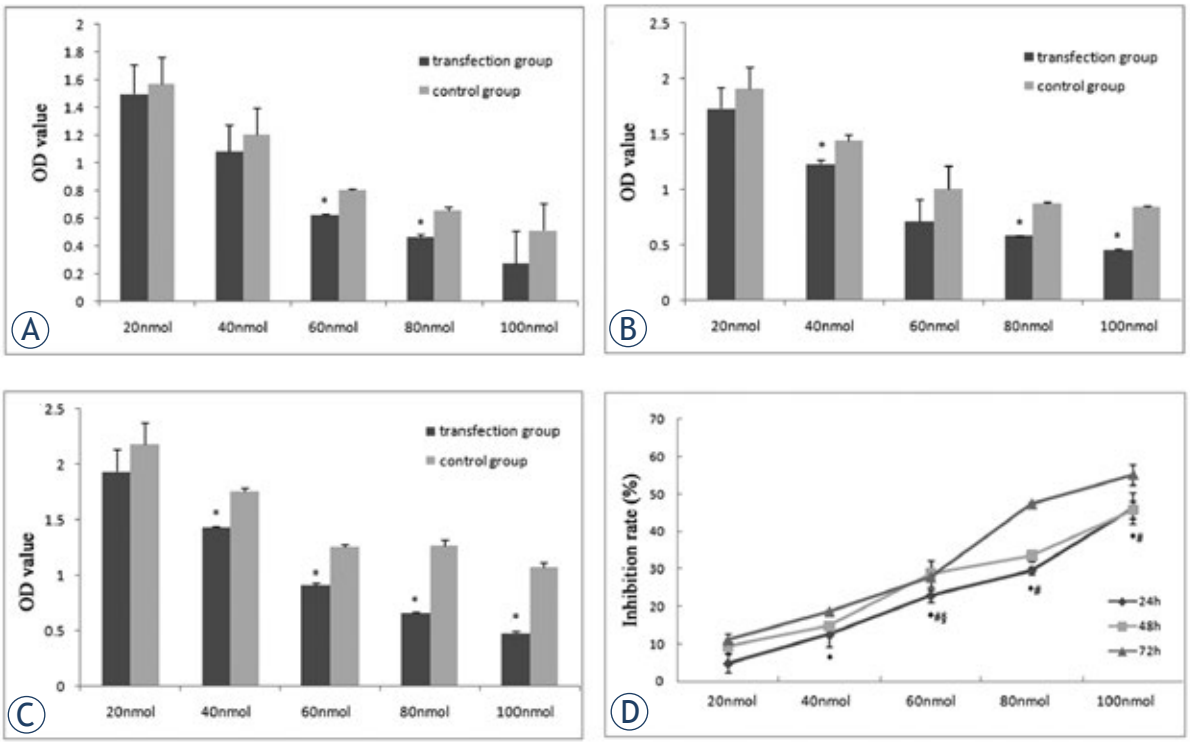

FIGURE 3. miR-548c-5p inhibits CD90+ cell proliferation. IR of CD90+ HepG2 cells increased markedly following transfection and the IR increased over time. (A) OD at 24 h after miR-548c-5p transfection. OD decreased at 24 h after miR-548c-5p transfection in MTT assay; (B) OD at 48 h after miR-548c-5p transfection. OD decreased at 48 h after miR-548c-5p transfection in MTT assay; (C) OD at 72 h after miR-548c-5p transfection. OD decreased at 72 h after miR-548c-5p transfection in MTT assay; (D) IR after transfection with miR-548c-5p mimics (MTT). IR of CD90+ HepG2 cells increased markedly following transfection with miR-548c-5p mimics and IR increased over time.* 72h verses 24h, P<0.05; # 72h verses 48h, P<0.05; 48h verses 24h, P<0.05

Discussion

Our study showed that miR-548c-5p could down-regulate the expression of *β-catenin, Tg737, bcl-2, bcl-XL*, and *caspase-3*, inhibit the proliferation, migration, and invasion and promote apoptosis of CD90+ HepG2 cells. miR-548c-5p might be a suppressor of LCSC-like cells.

miR-548c-5p had a potential influence on apoptosis. miR-548c-5p may be a regulator of *caspase-3, bcl-2* and *bcl-XL* in the CD90+ HepG2 cells. In the present study, *caspase-3, bcl-2*, and *bcl-XL* were down-regulated in the CD90+ HepG2 cells after the transfection with miR-548c-5p mimics. The relationship between apoptosis and tumours is one of the focuses in recent years. The increase of anti-apoptosis is an important process in the development and progression of tumors.[18] The caspase family is one of the key participants in the apoptosis.[20] Caspase-3 is activated through either extrinsic or intrinsic signalling pathway and is a key effector caspase for proteolysis of other effector caspases and cellular proteins. Many apoptosis-triggering factors have a relationship with caspase-3.[21,22] Vaishnav *et al*. reported JNK Interacting Protein-1(JIP1) to be a target for caspase-3 mediated cleavage in response to both chemical and receptor mediated apoptotic stimuli.[22] Caspase-3 cleaves JIP1 at two sites leading to the disassembly of the JNK/JIP signalling complex thought to be required for JNK activation. Cleavage of both ERK and JNK scaffold proteins by caspases suggests a general mechanism for the regulation MAPK signalling during apoptotic cell death. In the present study, caspase-3 was down-regulated in the CD90+ HepG2 cells, which may influence the caspase-3 dependent signal transduction pathway. Although down-regulation of caspase-3 was inconsistent with the findings that the reduction of proliferation, we postulated that there might be other mechanisms related to caspase-3 affecting the apoptosis following the transfection.

The Bcl-2 family was first discovered among multiple genes of programmed cell death-regulating families. In recent years, the Bcl-2 family has aroused special attention.[23] Bcl-2 and bcl-XL can inhibit the apoptosis. Kim *et al*. found that Bcl-2 was highly expressed in the gastrointestinal tumors.[24]

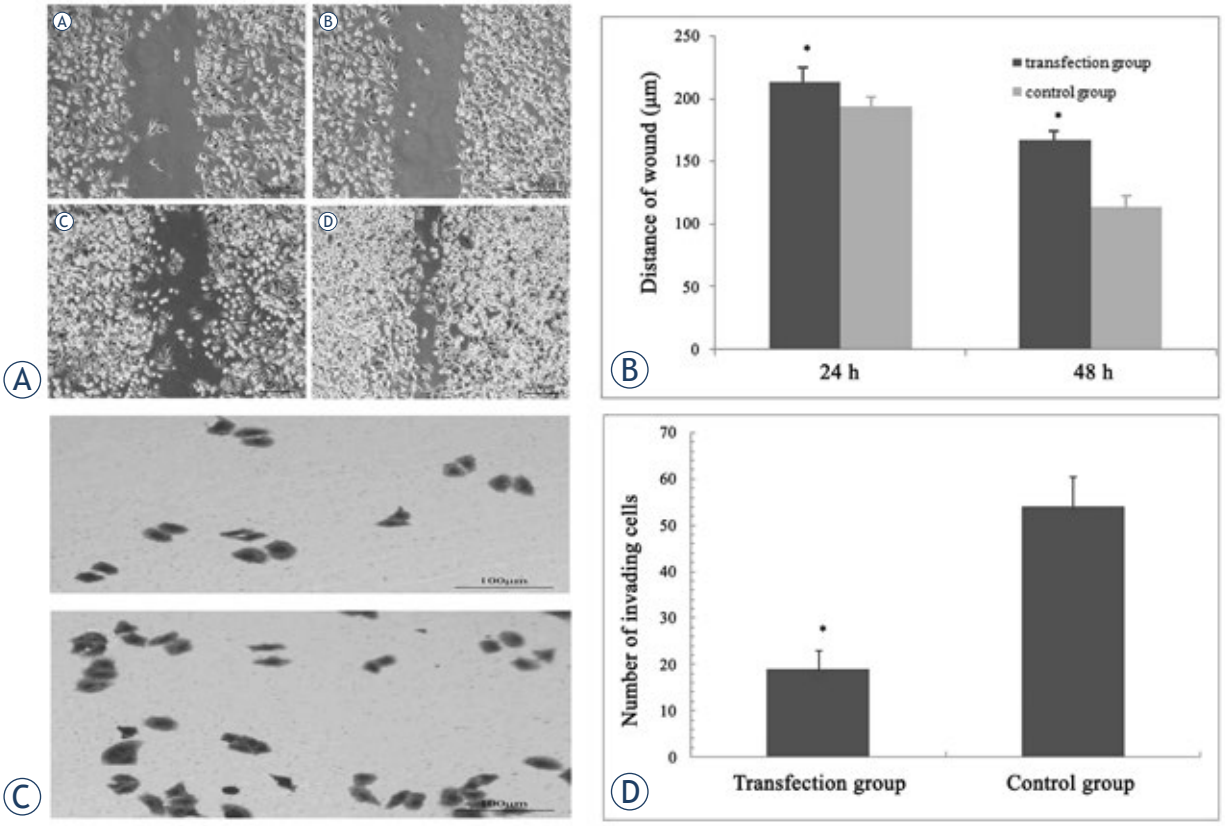

FIGURE 4. Wound healing assay (A, B) and transwell invasion assay (C, D). (A) Wound healing assay (1): miR-548c-5p transfection group (24 h); (2): control group (24 h); (3): miR-548c-5p transfection group (48 h); (4): control group (48 h); (B) Distance of wound was correlated to cell migration ability. Results showed that cell migration was inhibited in transfection group at 24 h and 48 h after miR-548c-5p transfection ($P<0.05$); (C) Cells penetrating the membrane in transwell invasion assay. The number of CD90+ HepG2 cells penetrating the membrane decreased at 48 h after miR-548c-5p transfection, upper: transfection group; lower: control group; (D) Changes in the number of cells penetrating the membrane in transwell invasion assay. The number of cells penetrating the membrane was lower in the transfection group than that in the control group. *P<0. 05 *vs* control group.

As apoptosis was inhibited, the cancer growth increased, resulting in poor prognosis and poor response to the treatment.[25] We found in the present study that *bcl-2* and *bcl-XL* were down-regulated in the CD90+ HepG2 cells. It is well known that *bcl-2* is an anti-apototic gene, and the inhibitory effect of *bcl-2* on apoptosis may be exerted through regulating the intracellular signal transduction by preventing Ca^{2+} from entering cells.[26] As bcl-2 can inhibit apoptosis, we postulate that miR-548c-5p may promote the apoptosis and inhibit the proliferation of CD90+ HepG2 cells partly through down-regulating bcl-2. It is predicted by TargetScan (http://www.targetscan.org), miRanda (http://www.microrna.org/microrna/home.do) and PicTar (http://pictar.bio.nyu.edu/) methods that *bcl-2* and *bcl-XL* may be possible downstream regulating genes of miR-548c-5p, but whether miRNA directly acts on the *bcl-2* and *bcl-XL*, or regulates them through other pathways is needed to be further confirmed in more studies. Our study showed that miR-548c-5p could promote apoptosis of CD90+ HepG2 cells and the *β-catenin* expression was decreased. It has been reported that β-catenin is an important mediator of the classical Wnt pathway and plays an important role in the tumour growth.[27] Lee *et al*. reported that inhibitor of DNA binding 3 mediated X-ray-induced apoptosis of keratinocytes through down-regulation of endogenous β-catenin level in HaCaT keratinocytes.[28] Selenite could induce apoptosis through reactive oxygen species (ROS)-dependent inhibition of AKT/b-catenin signaling pathway.[29] We speculate that the increased apoptosis of CD90+ HepG2 cells may be attributed to the decreased β-catenin following miR-548c-5p transfection. Whether the increased apoptosis of CD90+ HepG2 cells following miR-548c-5p transfection is mediated by other pathways is required to be further investigated.

Apoptosis-related genes were differentially expressed in the CD90+ HepG2 cells, including down-regulation of *caspase-3* and *bcl-2*, and up-regulation

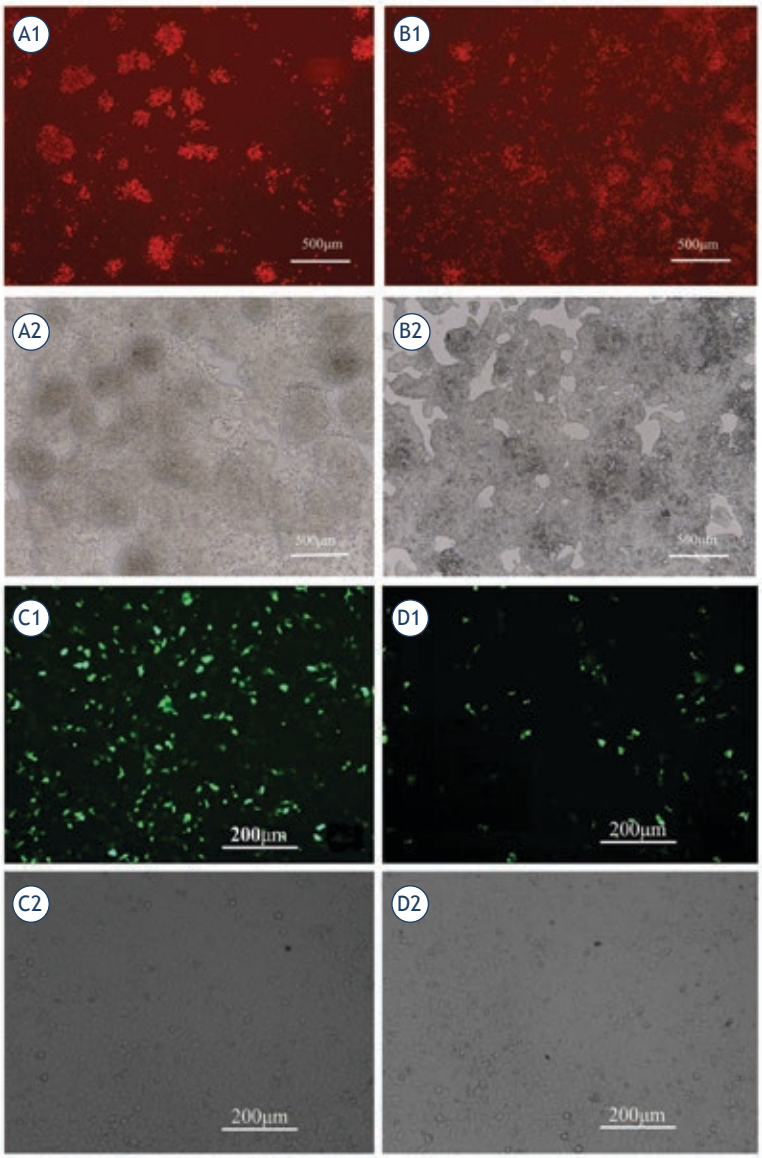

FIGURE 5. Apoptosis of CD90+ HepG2 cells after miR-548c-5p transfection. PI staining (A1, B1) showed apoptosis of CD90+ HepG2 cells increased in the transfection group at 48 h after miR-548c-5p transfection as compared to the control group. (A1) PI positive cells in the transfection group; (A2) cells under normal light in the transfection group; (B1) PI positive cells in the control group; (B2) cells under normal light in the control group. Annexin V-FITC staining (C1, D1) showed the apoptotic CD90+ HepG2 cells increased in the transfection group. (C1) Annexin V-FITC positive cells in the transfection group; (C2) cells under normal light in the transfection group; (D1) Annexin V-FITC positive cells in the control group; (D2) cells under normal light in the control group.

of *caspase-8*, though *bcl-XL* and *p53* remained unchanged. This may attribute to the imbalance between apoptotic and anti-apoptotic processes in the CD90+ HepG2 cells, affecting the development and progression of CD90+ HepG2 cells. Nevertheless, apoptosis is an extremely complex process, and ultimately depends on various apoptosis-related genes.

miRNAs are new groups of carcinogenic genes or tumour suppressor genes, playing important roles in the carcinogenesis.[30-32] Significant differences in the miRNA expression have been reported between liver cancer and para-liver cancer tissues.[33,34] Some studies have shown that miR-200a is related to the β-catenin and tumour growth factor.[35,36] Silencing of miR-200a gene could promote the occurrence of liver cancer.[36] Our results showed the expression of miR-548c-5p, miR-145, miR-375 and miR-874 were decreased in the CD90+ HepG2 cells, while that of miR-155, miR-198 and miR-1289 increased. These changes indicate that CD90+ HepG2 cells may differ from CD90- HepG2 cells in miRNAs expression, of which miR-548c-5p affects proliferation and invasion of CD90+ HepG2 cells demonstrated on our study. What roles other miRNAs play in the CD90+ HepG2 cells remain still unclear.

In summary, the *caspase-3* and *bcl-2* in the CD90+ HepG2 cells are down-regulated and *caspase-8* up-regulated, while *bcl-XL* remains unchanged. It is postulated that there is an imbalance between apoptosis and anti-apoptosis in the LCSC-like cells, resulting in the alteration of biological features of LCSC-like cells. Levels of several miRNAs are also changed in the CD90+ HepG2 cells, of which miR-548c-5p is found to affect several apoptosis-related genes including *bcl-2*, *bcl-XL* and *caspase-3*, indicating miR-548c-5p plays an important role in the apoptosis of LCSC-like cells. miR-548c-5p also affects the proliferation, migration, and invasion of CD90+ HepG2 cells and may thus act as a suppressor of LCSC-like cells. As a whole, miR-548c-5p plays a regulatory role in the primary liver cancer. Although increasing studies on cancer cells and LCSC-like cells have emerged, more efforts are needed to elucidate them in an in-depth way.

Acknowledgement

This study was supported by National Natural Science Foundation of China (No: 30940034).

References

1. Mishra L, Banker T, Murray J, Byers S, Thenappan A, He AR, et al. Liver stem cells and hepatocellular carcinoma. *Hepatology* 2009; **49:** 318-29.
2. Marquardt JU, Factor VM, Thorgeirsson SS. Epigenetic regulation of cancer stem cells in liver cancer: Current concepts and clinical implications. *J Hepatol* 2010; **53:** 568-77.
3. Lingala S, Cui YY, Chen X, Ruebner BH, Qian XF, Zern MA, et al. Immunohistochemical staining of cancer stem cell markers in hepatocellular carcinoma. *Exp Mol Path* 2010; **89:** 27-35.
4. Park JR, Kim RJ, Lee YK, Kim SR, Roh KJ, Oh SH, et al. Dysadherin can enhance tumorigenesis by conferring properties of stem-like cells to hepatocellular carcinoma cells. *J Hepatol* 2011; **54:** 122-31.
5. Ardebili SY, Zajc I, Gole B, Campos B, Herold-Mende C, Drmota S, et al. CD133/prominin1 is prognostic for GBM patient's survival, but inversely correlated with cysteine cathepsins' expression in glioblastoma derived spheroids. *Radiol Oncol* 2011; **45:** 102-15.
6. Yang ZF, Ngai P, Ho DW, Yu WC, Ng MN, Lau CK, et al. Identification of local and circulating cancer stem cells in human liver cancer. *Hepatology* 2008; **47:** 919-28.
7. Yang ZF, Ho DW, Ng MN, Lau CK, Yu WC, Ngai P, et al. Significance of $CD90^+$ cancer stem cells in human liver cancer. *Cancer Cell* 2008; **13:** 153-66.
8. Tomuleasa C, Soritau O, Rus-Ciuca D, Pop T, Todea D, Mosteanu O, et al. Isolation and characterization of hepatic cancer cells with stem-like properties from hepatocellular carcinoma. *J Gastrointestin Liver Dis* 2010; **19:** 61-7.
9. Kohga K, Tatsumi T, Takehara T, Tsunematsu H, Shimizu S, Yamamoto M, et al. Expression of CD133 confers malignant potential by regulating metalloproteinases in human hepatocellular carcinoma. *J Hepatol* 2010; **52:** 872-9.
10. Ma S, Chan KW, Lee TK, Tang KH, Wo JY, Zheng BJ, et al. Aldehyde dehydrogenase discriminates the CD133 liver cancer stem cell populations. *Mol Cancer Res* 2008; **6:** 1146-53.
11. Na DC, Lee JE, Yoo JE, Oh BK, Choi GH, Park YN. Invasion and EMT-associated genes are up-regulated in B viral hepatocellular carcinoma with high expression of CD133-human and cell culture study. *Exp Mol Pathol* 2011; **90:** 66-73.
12. Chiba T, Kita K, Zheng YW, Yokosuka O, Saisho H, Iwama A, et al. Side population purified from hepatocellular carcinoma cells harbors cancer stem cel1-1ike properties. *Hepatology* 2006; **44:** 240-51.
13. Cui F, Wang J, Chen D, Chen YJ. CD133 is a temporary marker of cancer stem cells in small cell lung cancer, but not in non-small cell lung cancer. *Oncol Rep* 2011; **25:** 701-8.
14. Kim CF, Jackson EL, Woolfenden AE, Lawrence S, Babar I, Vogel S, et al. Identification of bronchioalveolar stem cells in normal lung and lung cancer. *Cell* 2005; **121:** 823-35.
15. Yin S, Li J, Hu C, Chen X, Yao M, Yan M, et al. CD133 positive hepatocellular carcinoma cells possess high capacity for tumorigenicity. *Int J Cancer* 2007; **120:** 1444-50.
16. Suetsugu A, Nagaki M, Aoki H, Motohashi T, Kunisada T, Moriwaki H. Characterization of $CD133^+$ hepatocel1u1ar carcinoma cells as cancer stem/progenitor cells. *Biochem Biophys Res Commun* 2006; **351:** 820-4.
17. Ma S, Chan KW, Hu L, Lee TK, Wo JY, Ng IO, et al. Identification and characterization of tumorigenic liver cancer stem/progenitor cells. *Gastroenterology* 2007; **132:** 2542-56.
18. Khan MS, Halagowder D, Devaraj SN. Methylated chrysin induces co-ordinated attenuation of the canonical Wnt and NF-kB signaling pathway and upregulates apoptotic gene expression in the early hepatocarcinogenesis rat model. *Chem Bio Interact* 2011; **193:** 12-21.
19. Hwang HW, Mendell JT. MicroRNAs in cell proliferation, cell death, and tumorigenesis. *Br J Cancer* 2006; **94:** 776-80.
20. Hashimoto T, Kikkawa U, Kamada S. Contribution of caspase(s) to the cell cycle regulation at mitotic phase. *PLoS One* 2011; **6:** e18449.
21. Depraetere V, Golstein P. Dismantling in cell death: molecular mechanisms and relationship to caspase activation. *Scand J Immunol* 2005; **47:** 523-31.
22. Vaishnav M, MacFarlane M, Dickens M. Disassembly of the JIP1/JNK molecular scaffold by caspase-3-mediated cleavage of JIP1 during apoptosis. *Exp Cell Res* 2011; **317:** 1028-39.
23. Rudner J, Elsaesser SJ, Jendrossek V, Huber SM. Anti-apoptotic Bcl-2 fails to form efficient complexes with pro-apoptotic Bak to protect from Celecoxib-induced apoptosis. *Biochemical Pharmacol* 2011; **81:** 32-42.
24. Kim R, Emi M, Matsuura K, Tanabe K. Therapeutic potential of antisense Bcl-2 as a chemosensitizer for patients with gastric carcinoma. *Gan To Kagaku Ryoho*. 2005; **32:** 1540-5.
25. Barrezueta LF, Oshima CT, Lima FO, De Oliveira Costa H, Gomes TS, Neto RA, et al. The intrinsic apoptotic signaling pathway in gastric adenocarcinomas of Brazilian patients: Immunoexpression of the Bcl-2 family (Bcl-2, Bcl-x, Bak, Bax, Bad) determined by tissue microarray analysis. *Mol Med Report* 2010; **3:** 261-7.
26. Chami M, Prandini A, Campanella M, Pinton P, Szabadkai G, Reed JC, et al. Bcl-2 and bax exert opposing effects on Ca^{2+} signaling,which do not depend on their putative pore-forming region. *J Biol Chem* 2004; **279:** 54581-9.
27. Samuel MS, Lopez JI, McGhee EJ, Croft DR, Strachan D, Timpson P, et al. Actomyosin-mediated cellular tension drives increased tissue stiffness and β-catenin activation to induce epidermal hyperplasia and tumor growth. *Cancer Cell* 2011; **19:** 776-91.
28. Lee YS, Mollah ML, Sohn KC, Shi G, Kim DH, Kim KH, et al. Ki-Hwan Kim ID3 mediates X-ray-induced apoptosis of keratinocytes through the regulation of β-catenin. *J Dermatol Sci* 2010; **60:** 138-42.
29. Luo H, Yang Y, Huang F, Li F, Jiang Q, Shi K, et al. Selenite induces apoptosis in colorectal cancer cells via AKT-mediated inhibition of β-catenin survival axis. *Cancer Lett* 2012; **315:** 78-85.
30. Chan JA, Krichevsky AM, Kosik KS. MicroRNA-21 is an antiapoptotic factor in human glioblastoma cells. *Cancer Res* 2005; **65:** 6029-33.
31. Bachour T, Bennett K. The role of microRNAs in breast cancer. *J Assoc Genet Technol* 2011; **37:** 21-8.
32. Lin Z, Flemington EK. miRNAs in the pathogenesis of oncogenic human viruses. *Cancer Lett* 2011; **305:**186-99.
33. Kerr TA, Korenblat KM, Davidson NO. MicroRNAs and liver disease. *Transl Res* 2011; **157:** 241-52.
34. Huang YS, Dai Y, Yu XF, Bao SY, Yin YB, Tang M, et al. Microarray analysis of microRNA expression in hepatocellular carcinoma and non-tumorous tissues without viral hepatitis. *J Gastroenterol Hepatol* 2008; **23:** 87-94.
35. Gregory PA, Bert AG, Paterson EL, Barry SC, Tsykin A, Farshid G, et al. The miR-200 family and miR-205 regulate epithelial to mesenchymal transition by targeting ZEB1 and SIP1. *Nat Cell Biol* 2008; **10:** 593-601.
36. Feitelson MA, Lee J. Hepatitis B virus integration, fragile sites, and hepatocarcinogenesis. *Cancer Lett* 2007; **252:** 157-70.

research article

Comparison of 3D MRI with high sampling efficiency and 2D multiplanar MRI for contouring in cervix cancer brachytherapy

Primoz Petric[1], Robert Hudej[1], Peter Rogelj[2], Mateja Blas[3], Barbara Segedin[1], Helena Barbara Zobec Logar[1], Johannes Carl Athanasios Dimopoulos[4]

[1] Department of Radiotherapy, Institute of Oncology Ljubljana, Ljubljana, Slovenia
[2] University of Primorska, Faculty of Mathematics, Natural Sciences and Information Technologies, Koper, Slovenia
[3] Institute of Oncology Ljubljana, Research Sector, Unit for Biostatistics, Ljubljana, Slovenia
[4] Metropolitan Hospital, Department of Radiotherapy, Athens, Greece

Radiol Oncol 2012; 46(3): 242-251.

Received 1 January 2012
Accepted 17 February 2012

Correspondence to: Primož Petrič, MD,MSc, Department of Radiotherapy, Institute of Oncology Ljubljana, Zaloška 2, 1000 Ljubljana, Slovenia. Phone: +386 1 5879 206; Fax: +386 1 5879 400; E-mail: ppetric@onko-i.si

Disclosure: No potential conflicts of interest were disclosed.

Background. MRI sequences with short scanning times may improve accessibility of image guided adaptive brachytherapy (IGABT) of cervix cancer. We assessed the value of 3D MRI for contouring by comparing it to 2D multi-planar MRI.

Patients and methods. In 14 patients, 2D and 3D pelvic MRI were obtained at IGABT. High risk clinical target volume (HR CTV) was delineated by 2 experienced radiation oncologists, using the conventional (2D MRI-based) and test (3D MRI-based) approach. The value of 3D MRI for contouring was evaluated by using the inter-approach and inter-observer analysis of volumetric and topographic contouring uncertainties. To assess the magnitude of deviation from the conventional approach when using the test approach, the inter-approach analysis of contouring uncertainties was carried out for both observers. In addition, to assess reliability of 3D MRI for contouring, the impact of contouring approach on the magnitude of inter-observer delineation uncertainties was analysed.

Results. No approach- or observer - specific differences in HR CTV sizes, volume overlap, or distances between contours were identified. When averaged over all delineated slices, the distances between contours in the inter-approach analysis were 2.6 (Standard deviation (SD) 0.4) mm and 2.8 (0.7) mm for observers 1 and 2, respectively. The magnitude of topographic and volumetric inter-observer contouring uncertainties, as obtained on the conventional approach, was maintained on the test approach. This variation was comparable to the inter-approach uncertainties with distances between contours of 3.1 (SD 0.8) and 3.0 (SD 0.7) mm on conventional and test approach, respectively. Variation was most pronounced at caudal HR CTV levels in both approaches and observers.

Conclusions. 3D MRI could potentially replace multiplanar 2D MRI in cervix cancer IGABT, shortening the overall MRI scanning time and facilitating the contouring process, thus making this treatment method more widely employed.

Key words: cervix cancer; brachytherapy; contouring; MRI

Introduction

Image guided adaptive brachytherapy (IGABT) enables individualized irradiation, applying high doses to the target volume while respecting organs at risk (OAR) dose constraints.[1,2] Accurate contouring of these regions is a precondition for treatment success and consistent reporting in brachytherapy as well as in external beam irradiation.[3] Various imaging modalities have been employed in gynaecological IGABT.[4-23] T2 weighted fast spin echo (T2w FSE) MRI currently represents the modality of choice due to its high soft tissue depiction quality.[16-28] Favourable reports on diagnostic and

dosimetric outcome of MRI based approach are reflected in encouraging clinical results.[18-24,29,30]

However, limited access to MRI precludes its widespread adoption in this field. Until the role of low cost modalities (CT and US) is systematically evaluated, implementation of high resolution MRI sequences with short scanning times may make IGABT available to a wider population of patients. Currently, assessment of multiplanar post-insertion 2D T2w FSE MRI is required for accurate contouring.[1,2,27] However, majority of treatment planning systems (TPS) do not enable import of non-resampled images in multiple planes. Classically, only (para)transverse images are imported and used for delineation, while other planes are resampled by the TPS from the (para)transverse set. Due to the slice thickness of 3-5 mm, the resampled images have poor resolution and are not useful for evaluation of patho-anatomical structures (Figure 1A). Non-resampled high-resolution (para)sagittal and (para)coronal 2D MR images have to be obtained in addition. As a result, 2D multiplanar MRI is characterized by long scanning time and the need for a separate DICOM-viewer to integrate findings from different planes during contouring.[1,2,27,28] This approach is currently used at the Institute of Oncology Ljubljana. In addition, a 3D T2w FSE sequence with high sampling efficiency, 1 mm isotropic voxel size and large field of view (SPACE) is obtained at our department (Figure 1B). 3D MRI is co-registered with 2D para-transverse images in the TPS to reduce applicator reconstruction uncertainties.[31] Due to the small voxel size, high resolution images in multiple planes can be resampled by the TPS from the 3D data-set (Figure 1C).

The aim of our study was to assess whether the 3D SPACE sequence could potentially replace multiplanar 2D MRI for contouring of high risk clinical target volume (HR CTV). By omitting multiplanar 2D MRI, the scanning time would be shortened. In addition, utilizing high-resolution images, resampled in multiple planes from the 3D data-set by the TPS, the separate DICOM viewer would no longer be required and fusion of multiple image series with its inherent uncertainties could be avoided.

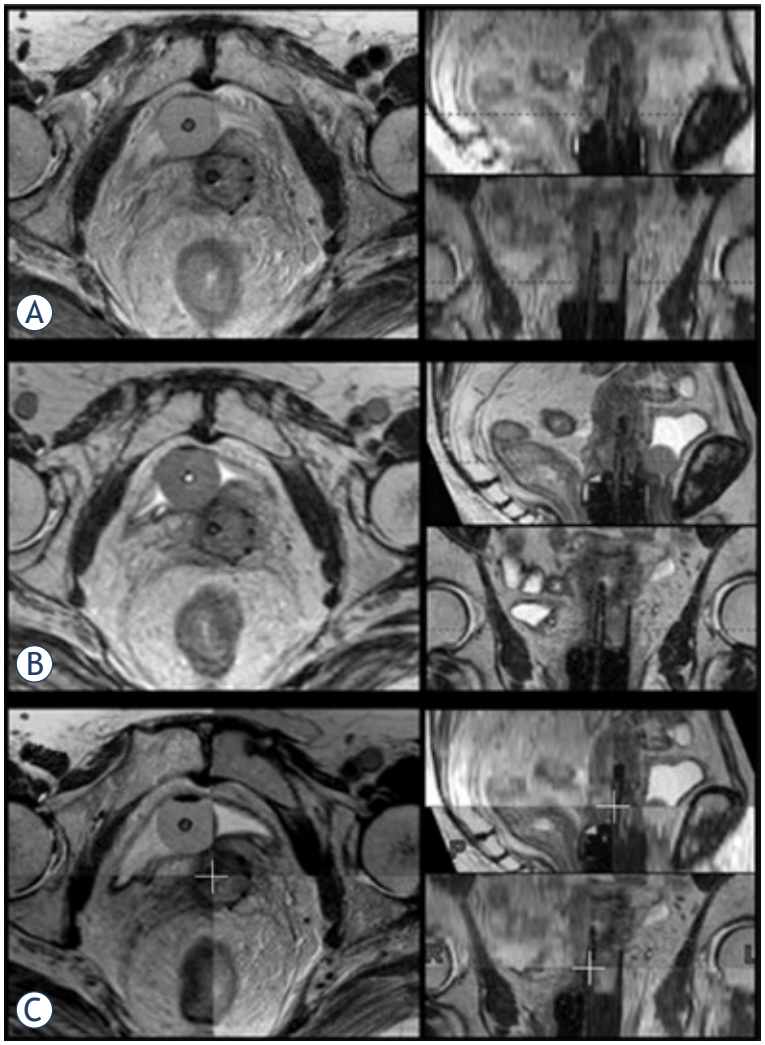

FIGURE 1. Post-insertion pelvic MRI. (A) Para-transverse 2D T2w FSE MR images were imported into the TPS (left). Para-sagittal and -coronal images were resampled from this data-set (right): due to the 3.9 mm slice thickness, their resolution is poor. (B) 3D MRI data-set was imported into the TPS. High resolution para-transverse (left), -sagittal and -coronal images (right) were resampled due to an isotropic voxel size of 1 mm. (C) Co-registration of the 2D para-transverse and 3D MRI data-sets.

Patients and methods

The value of 3D MRI for contouring was evaluated by using the inter-approach and inter-observer analysis of volumetric and topographic contouring uncertainties. In addition, to assess reliability of 3D MRI for contouring, the impact of contouring approach on the magnitude of inter-observer delineation uncertainties was analysed.

To assess the magnitude of deviation from the conventional approach when using the test approach, the inter-approach analysis of contouring uncertainties was performed for both observers.

The study was carried out according to the Helsinki Declaration.

Patients and tumours

Fourteen consecutive patients with biopsy proven cervix cancer (8 FIGO stage IIB and 6 stage IIIB), treated at our department with radical MRI-based

IGABT between December 2006 and September 2007, were included. Mean tumour width, thickness and height, measured from the MRI at diagnosis, were 51 (Standard deviation (SD 11), 41 (SD 10) and 45 (SD 16) mm, respectively. Treatment consisted of 3D conformal CT-based external beam radiotherapy +/- concurrent chemotherapy, followed by 2 fractions of MRI-based pulsed dose rate IGABT. Details of our treatment strategy were presented elsewhere.[32] First IGABT fraction from each case was used for analysis.

Post-insertion MRI and image registration

Planning MRI was obtained after applicator insertion at a 1.5 T scanner (Siemens Magnetom Avanto© 2006, Siemens AG, Erlangen, Germany), using a pelvic surface phased-array coil. 2D T2w FSE images (slice thickness 3 mm, interslice gap 0.9 mm, in-plane pixel size 0.6 × 0.6 mm, field of view 20 × 20 cm, matrix size 288 × 320, echo time 98 ms, repetition time 5700 ms, flip angle 150°, acquisition time ≈12 minutes), were obtained in para-transverse (perpendicular to cervical canal), para-coronal and para-sagittal (parallel to cervical canal) plane. In addition, 3D isotropic T2w FSE sequence with high sampling efficiency (SPACE, a vendor-specific sequence) was performed (176 slices, isotropic voxel size of 1 mm, field of view 40 × 40 cm, matrix size 384 × 386, echo time 131 ms, repetition time 1500 ms, flip angle 150°, acquisition time ≈7 minutes). Para-transverse 2D images and 3D data set were transferred to the TPS (Brachyvision, version 8.5, Copyright© 1996-2008 Varian Medical Systems Inc., Palo Alto, USA) and co-registered, using shared DICOM coordinates. Manual registration corrections were applied where patient movement occurred between sequences. From the 3D data-set, para-transverse, para-coronal and para-sagittal images were resampled within the TPS to match the slice thickness and acquisition planes of the 2D images (Figure 1C).

Contouring

HR CTV was outlined independently by 2 experienced radiation oncologists, respecting the GEC-ESTRO recommendations, using two different approaches.[1] (1) *Conventional approach:* contouring on non-resampled para-transverse 2D MRI; during delineation, non-resampled para-sagittal and para-coronal 2D images were available on a separate DICOM viewer to assess topographical relations between the target, applicator and normal anatomical structures in 3 dimensions. This information was taken into account and integrated on para-transverse images in the TPS, where contouring was performed. (2) *Test approach:* contouring on para-transverse images, resampled from the 3D MRI; resampled high resolution para-sagittal and para–coronal images were available in the TPS contouring windows (Figure 1B), enabling direct incorporation of spatial information on patho-anatomical structures and interactive assessment of contours in all planes, without the use of an additional DICOM viewer. Contours, obtained in this study, were used for the purpose of analysis only, not for actual treatment. The interval between conventional and test contouring was at least one month.

Volumetric and topographic analysis

Using a dedicated software tool (Contour Analysis Tool – CAT, version 2), developed at our departments, inter–approach (intra-observer) and inter-observer contouring variation was assessed for each observer and approach, respectively. In volumetric analysis, HR CTV sizes were compared. In addition, volumetric conformity index (VCI) was computed for pairs of HR CTVs as the ratio between the common and encompassing volume[33], and compared within the inter-approach and inter-observer analysis. The common volume is defined as the intersection of two contoured volumes, while the encompassing volume is their union. In topographic analysis of inter-approach variations, the shortest 2D distance between conventional and test contour was calculated for each contour point on each slice for both observers. In inter-observer assessment, corresponding distances between delineations of the two observers were measured for both approaches. In order to identify eventual dependence of the variation magnitude on cranio-caudal level of the contoured volume, the analysis was carried out for all slices and, in addition, for the following HR CTV levels: (1) caudal-most two, (2) mid-level, and (3) cranial-most two slices.

Statistical analysis

Continuous numerical variables were presented as mean values and standard deviations. Inter-approach and inter-observer variation was assessed by calculating Bland-Altman limits of agreement[34,35], and Lin's concordance correlation coefficient.[36,37] We used the bootstrap method to obtain a more reliable 95% confidence interval for the cor-

TABLE 1. Inter-approach and inter-observer differences in HR CTV sizes

	Diff. in HR CTV [cm^3] (mean (SD))	Limits of agreement (mean +/- 2SD) [cm^3]	95% CI [cm^3]	CCC	95% boot CI
Inter-approach analysis					
Observer 1	-1.2 (2.3)	-5.8, 3.4	-8.0, 5.7	0.97	0.94, 0.99
Observer 2	1.4 (2.8)	-4.3, 7.1	-7.1, 10.0	0.96	0.88, 0.99
Inter-observer analysis					
Conventional approach	2.8 (4.5)	-6.2, 11.9	-10.8, 16.4	0.87	0.75, 0.96
Test approach	0.3 (4.5)	-8.7, 9.2	-13.2, 13.7	0.91	0.84, 0.96

SD = standard deviation of differences; 95% CI = limits of 95% confidence interval for lower and upper limit; CCC = Lin's concordance correlation coefficient; 95% boot CI = 95% bootstrap confidence interval for CCC

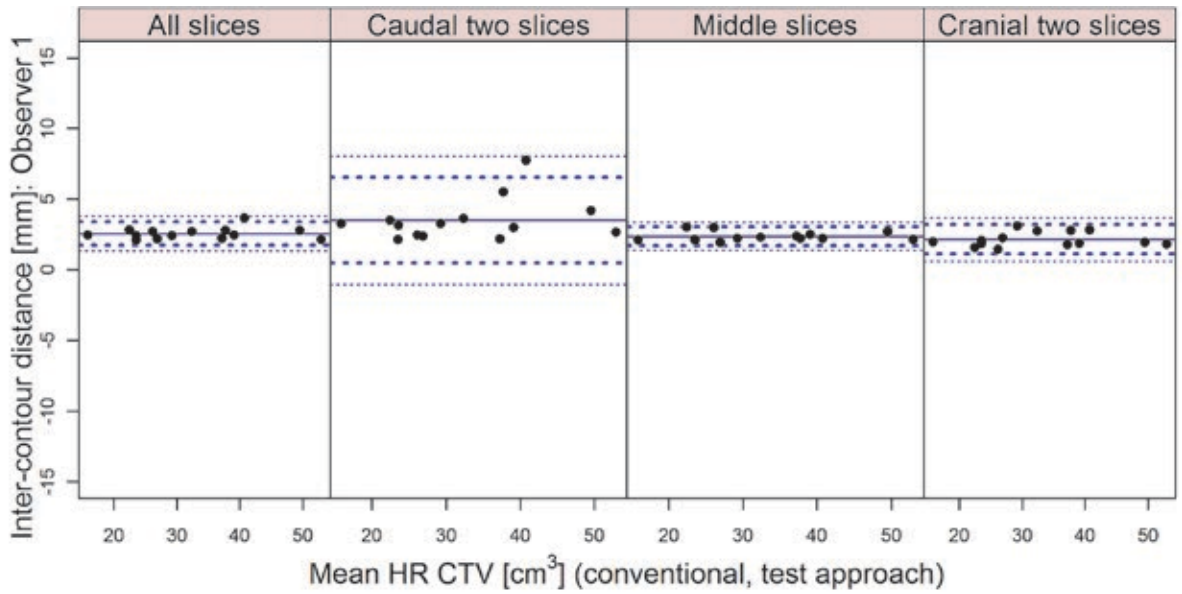

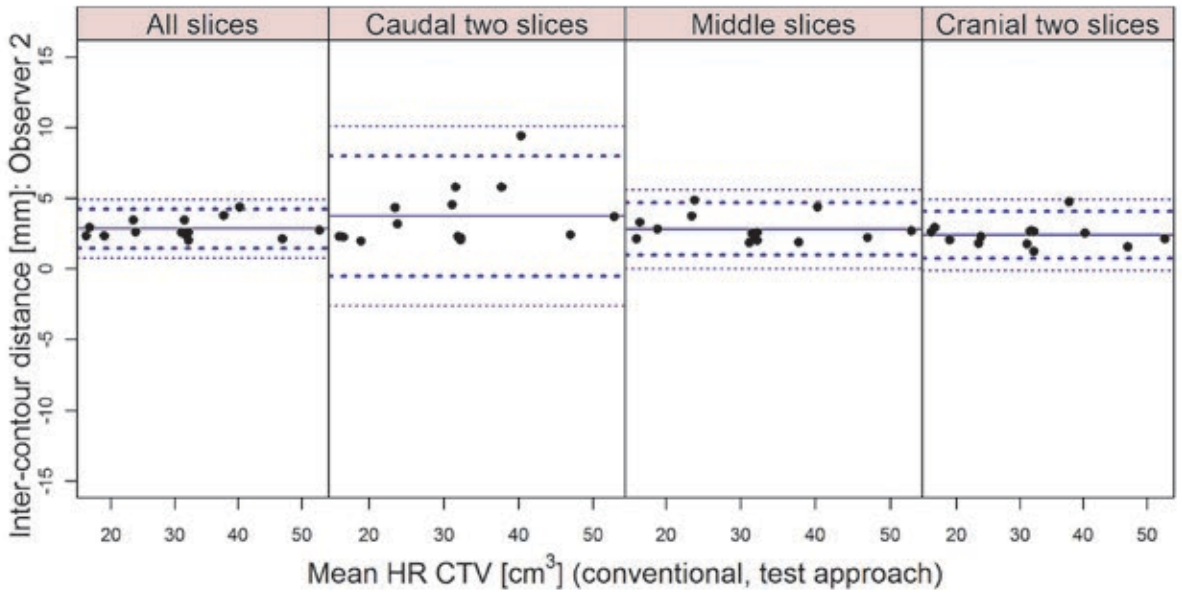

FIGURE 2. Bland-Altman inter-approach analysis of the distances between contours for observer 1 (A) and 2 (B) and for different levels of the contoured volume (all, caudal two, middle and cranial two slices). Full circles: mean values (mm) of the individual distances. Thick dotted lines: limits of agreement (mean ± 2 standard deviations). Thin dotted lines: 95% confidence limits.

relation coefficient. All analyses and graphs were performed using a statistical program R (version 2.11.1., R Foundation for Statistical Computing, Vienna, Austria).

Results

No approach- or observer - specific differences in HR CTV sizes, VCI, or distances between contours were identified. The magnitude of topographic and volumetric inter-observer contouring uncertainties, as obtained on the conventional approach, was maintained on the test approach. This variation was comparable to the inter-approach uncertainties from both observers. Variation was most pronounced at caudal HR CTV levels in both approaches and observers. Detailed results of our analysis are presented below.

Using the conventional approach, mean HR CTVs of 32 (Standard deviation (SD) 10.5) cm^3 and 31.8 (SD 10.8) cm^3 were obtained for observer 1 and 2, respectively. Using the test approach, the respective HR CTV sizes were 33.2 (SD 11.0) cm^3 and 30.4 (SD 11.2) cm^3.

Using the inter-approach Bland-Altman analysis, high agreement in HR CTV sizes was found for both observers (Table 1). A favourable mean VCI of 0.8 (SD 0.03) and 0.79 (SD 0.04) was obtained for observer 1 and 2, respectively. The results of the Bland-Altman analysis of the inter-approach distances between contours were comparable for both observers and are presented in Table 2 and Figure 2. When averaged over all slices of the HR CTV, mean inter-approach distances were 2.6 mm (SD 0.4 mm) for observer 1 and 2.8 mm (SD 0.7 mm) for observer 2. Inter-approach contouring variation was most pronounced at the caudal level of the HR CTV (observer 1: 3.5 mm, SD 1.5 mm; observer 2: 3.7 mm; SD 2.1 mm). At the mid and cranial levels of the HR CTV, the inter-approach distances between contours were smaller (Table 2, Figure 2).

On the inter-observer analysis, high agreement in HR CTV sizes was found for both approaches (Table 1). Favourable mean VCI on conventional approach of 0.76 (SD 0.05) was maintained on test approach (mean VCI: 0.75; SD 0.05). The results of the Bland-Altman analysis of the inter-observer distances between contours were comparable for both approaches and are presented in Table 2 and Figure 3. When averaged over all slices of the HR CTV, mean inter-observer distances between contours of 3.1 mm (SD 0.8 mm) were found on conventional and 3.0 mm (SD 0.7 mm) on test approach. Similar to the inter-approach analysis, highest inter-observer distances were obtained at the caudal level of the HR CTV on the inter-observer assessment and were comparable for both contouring approaches (conventional: 5.4 mm, SD 3.1 mm; test: 4.4 mm, SD 3.0 mm). At the mid and cranial levels of the HR CTV, the inter-observer distances were smaller (Table 2, Figure 3).

Discussion

The dose conformity in IGABT exceeds any other radiotherapy modality and even minimal contouring variation can result in significant uncertainties of optimized dose distribution.[37] This may have important clinical consequences and compromise treatment recording and reporting, undermining overall IGABT efficacy. One of the potential sources of systematic contouring variations is the choice of imaging modality.

High resolution 3D T2w FSE isotropic MRI with high sampling efficiency, small voxel size, large field of view and sufficient signal to noise ratio was introduced for diagnostic imaging of the pelvis and other anatomical regions, potentially improving the diagnostic possibilities of MRI.[38-46] Nevertheless, it seems that further improvements of 3D MRI are required before it could be considered as a replacement for 2D multiplanar imaging in local staging.[38,40] As far as imaging for gynaecological IGABT treatment planning is concerned, 2D T2w FSE multi-planar MRI is currently considered the modality of choice.[1,2] Results of the MRI-based IGABT have been published by several groups, demonstrating improved chance of cure and reduced morbidity rates when compared to conventional radiography-based method.[20-23,47] Nevertheless, in spite of these favourable reports, widespread utilization of MRI and IGABT remains impeded by limited resources.[48-50] The innovative approach to 3D MRI-based contouring, evaluated in our study, may make IGABT more easily employed. By omitting post-insertion multi-planar 2D MRI and by using 3D SPACE sequence both for applicator reconstruction and contouring, the MRI scanning time was reduced from approximately 19 to 7 minutes in our study. The achieved reduction is comparable to other strategies that could be proposed to improve IGABT availability (i.e. combination of MRI for the first application and CT, ultrasound or radiography for subsequent application(s)). Importantly, by applying a single sequence, uncertainties due to eventual patient mo-

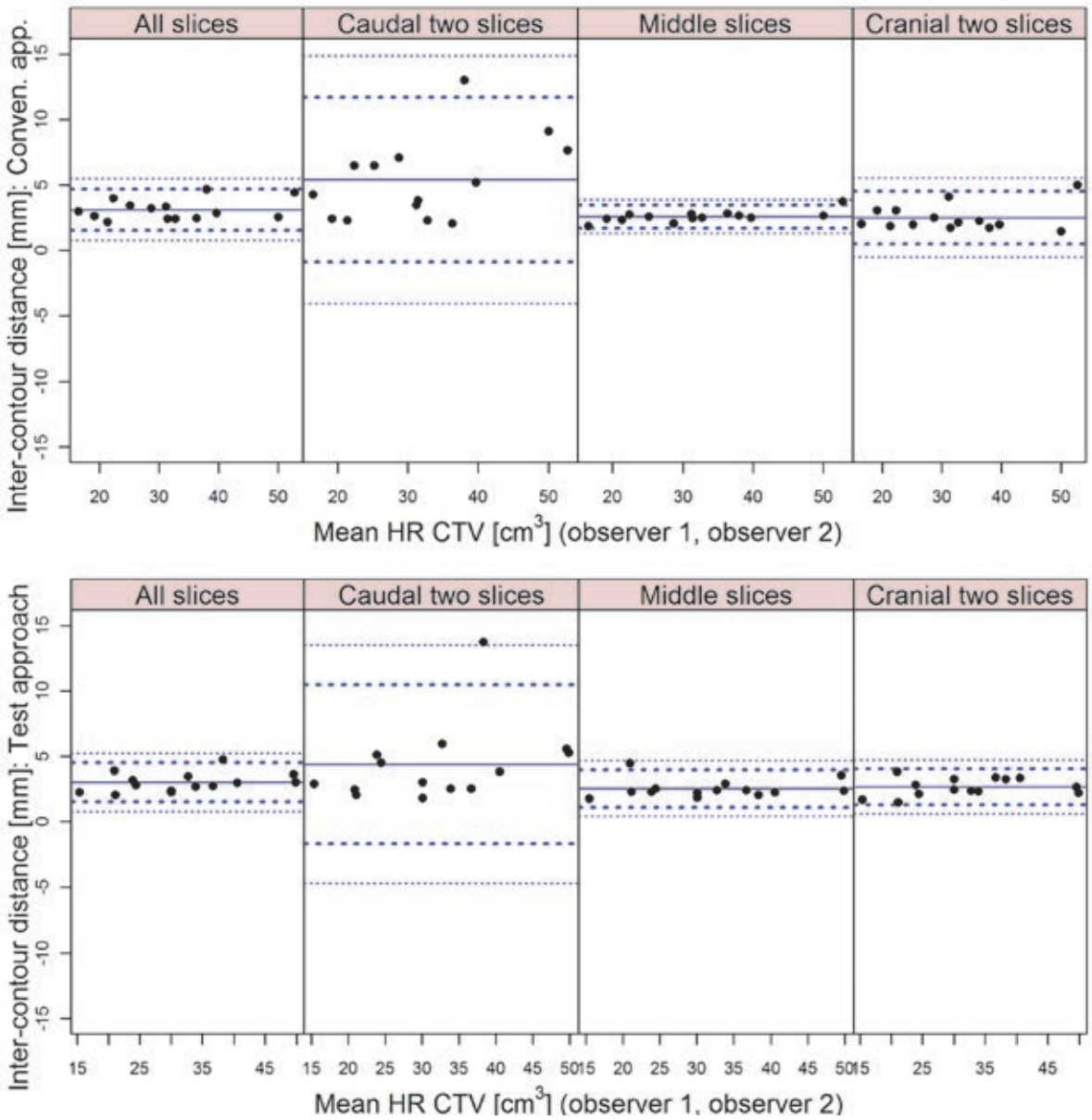

FIGURE 3. Bland-Altman inter-observer analysis of the distances between contours for conventional (A) and test (B) approach and for different levels of the contoured volume (all, caudal two, middle and cranial two slices). Full circles: mean values (mm) of the individual distances. Thick dotted lines: limits of agreement (mean ± 2 standard deviations). Thin dotted lines: 95% confidence limits.

tion between sequences were reduced. However, the introduction of a new imaging approach could result in sequence-specific observer's interpretation of findings and systematic deviations from our standard technique. No such deviations could be found in our study. In addition, no observer-specific deviations were identified and the magnitude of intra-observer uncertainties was comparable to inter-observer variation.

VCI is one of the commonly used measures of volumetric similarity between delineated objects. Poor agreement is indicated by a low VCI. As the agreement increases, VCI approaches 1. Small differences in HR CTV sizes (Table 1) and favourable results on VCI, obtained in our study, indicate high level of volumetric agreement between the conventional and test delineations. An inter-approach VCI of around 0.8 compares favourably with results of similar studies both in the field of EBRT and BT.[51-57] In addition, high inter-observer VCI of the conventional 2D MRI approach was maintained for 3D MRI-based contouring. However, the sensitivity of VCI to contouring deviations increases with decreasing size of analysed volumes: contouring

TABLE 2. Inter-approach and inter-observer distances between contours at different cranio-caudal levels of the HR CTV

	Inter-contour distance [mm] (mean (SD))	Limits of agreement [mm]	95% CI [mm]
All slices			
Inter-approach analysis			
Observer 1	2.6 (0.4)	1.8, 3.4	1.3, 3.8
Observer 2	2.8 (0.7)	1.5, 4.2	0.8, 4.9
Inter-observer analysis			
Conventional approach	3.1 (0.8)	1.5, 4.7	0.8, 5.5
Test approach	3.0 (0.7)	1.5, 4.5	0.8, 5.2
Caudal two slices			
Inter-approach analysis			
Observer 1	3.5 (1.5)	0.5, 6.5	-1.0, 8.0
Observer 2	3.7 (2.1)	-0.5, 8.0	-2.6, 10.1
Inter-observer analysis			
Conventional approach	5.4 (3.1)	-0.9, 11.7	-4.0, 14.9
Test approach	4.4 (3.0)	-1.7, 10.5	-4.7, 13.5
Middle slices			
Inter-approach analysis			
Observer 1	2.4 (0.3)	1.7, 3.0	1.7, 3.3
Observer 2	2.8 (0.9)	0.9, 4.7	0.0, 5.6
Inter-observer analysis			
Conventional approach	2.6 (0.4)	1.7, 3.5	1.3, 3.9
Test approach	2.5 (0.7)	1.1, 4.0	0.4, 4.7
Cranial two slices			
Inter-approach analysis			
Observer 1	2.1 (0.5)	1.1, 3.2	0.6, 3.7
Observer 2	2.4 (0.8)	0.7, 4.1	-0.1, 4.9
Inter-observer analysis			
Conventional approach	2.5 (1.0)	0.5, 4.5	-0.5, 5.5
Test approach	2.7 (0.7)	1.3, 4.0	0.6, 4.7

SD = standard deviation of differences; 95% CI = limits of 95% confidence interval for lower and upper limit.

deviation of a given absolute magnitude will be reflected in a more favourable VCI when analysing large, compared to small volumes. This makes direct comparisons of results between EBRT (typically large volumes) and BT (typically small volumes) studies challenging. In addition, the possibility to directly compare studies is limited due to differences in formalisms applied and the number of observers/cases analysed.[51-53] Nevertheless; our results indicate that the implementation of 3D MRI for contouring introduced no volumetric uncertainties when compared to the conventional approach.

VCI gives no information on the absolute magnitude of contouring variations and their topography. However, brachytherapy is characterized by an inhomogeneous dose distribution with a steep dose gradient. Consequently, the magnitude and topography of contouring uncertainties have a direct impact on treatment. In our study, quantitative assessment of variability revealed mean distances of up to 2.8 (SD 0.9) mm and 2.7 (SD 0.7) mm between analysed pairs of contours for the middle and cranial parts of the HR CTV, respectively. In caudal parts of the contoured volumes, mean inter-approach and inter-observer distances between delineations of up to 3.7 (SD 2.1) and 5.4 (SD 3.1) mm, respectively, were found (Table 2, Figures 2, 3). Therefore, higher variability was present in those

parts of the HR CTV, which are typically located in the close proximity of the ring source-channel. It has to be noted that up to approximately 4% deviation of commonly reported DVH parameters for the HR CTV can be expected per mm relative displacement of the contours with respect to the applicator.[58] In addition, relatively large standard deviations of inter-contour distances reflect a considerable spread of individual values, in particular in the caudal regions of the HR CTV (Table 2, Figures 2, 3). Assessment of the effects of these variations on the commonly evaluated dose-volume parameters was not a subject of our investigation and will deserve special attention in the future. Contouring variation should be considered as one of the most important sources of uncertainties in IGABT.

Due to a 1 mm isotropic voxel size, 3D MRI allowed for a high-resolution image resampling in any plane within the TPS (Figure 1B). In this way, the need for an additional DICOM viewer during delineation could be omitted, reducing the infrastructural requirements of the department and facilitating contouring.

There are some limitations of our study. We evaluated the capability of 3D MRI to replace conventional 2D multi-planar MRI for delineation of HR CTV. The value of this approach for contouring of the gross tumour volume and intermediate risk CTV was not assessed. However, since the HR CTV is currently the most widely used volume for dose prescription and optimisation in IGABT, our results can be considered practically relevant.[20,22,23,29] Next, since the inter-observer analysis was chosen to assess the inter-approach variations it could be argued that the number of observers (2) may be suboptimal and that the reported differences in inter-observer comparison could be attributed to the variability caused by particular case and not the observer. However, due to the specific expertise, required for the competence of a radiation oncologist in the field of cervix cancer IGABT, it is very challenging to obtain a higher number of observers for this purpose in a mono-institutional setting. Our results should be regarded as an indication of the value of the 3D MRI in gynaecological IGABT. However, further studies with higher number of observers may be required to confirm this. Finally, the SPACE sequence is vendor-specific. Before extrapolating the findings of our study to sequences from other vendors, additional work may be required.

It has to be noted that the pixel dimensions are larger on the para-transverse images, resampled from the 3D MRI (1 x 1 mm) when compared to the conventional para-transverse 2D MRI (0.6 x 0.6 mm). This results in a lower resolution and image quality in the main contouring plane. Eventual improvements of the 3D MRI are expected to further enhance the capability to use these sequences for treatment planning. Nevertheless, our results demonstrate that the described limitation did not result in an increase of contouring uncertainties.

Potential impact of MRI characteristics on the applicator reconstruction uncertainties deserves special mention. The procedure of defining the source channels on the images is a crucial step in IGABT, since the dose calculation is based on the geometry of source positions.[59] Imaging with small slice thickness or the use of 3D sequences with isotropic voxel size has been recommended by the Gyn GEC-ESTRO working group to reduce the applicator reconstruction uncertainties. In addition, contouring and reconstruction should be performed preferably in the same image series to avoid fusion uncertainties.[30] 3D MRI, evaluated in our study, therefore seems particularly suitable for gynaecological IGABT. Due to a small voxel size it enables an accurate applicator reconstruction, while the uncertainties related to image registration and fusion (Figure 1C) are avoided by using a single sequence for contouring and applicator reconstruction.[31]

Conclusions

3D MRI-based contouring of HR CTV introduced no systematic deviations from the conventional 2D multi-planar MRI-based approach. By omitting multi-planar MRI and employing a single 3D sequence for treatment planning, total image acquisition time was shortened for more than 50 %, when compared to our conventional technique. In addition, uncertainties due to patient motion between sequences were reduced. The use of additional DICOM viewer was no longer required during delineation, facilitating the contouring process. By employing a single 3D MRI sequence with 1 mm isotropic voxel size both for contouring and applicator reconstruction, uncertainties of image registration and fusion are avoided and the applicator reconstruction facilitated. 3D MRI could be considered as an alternative to conventional 2D multi-planar MRI in cervix cancer IGABT, making this treatment method potentially more widely employed.

References

1. Haie-Meder C, Pötter R, Van Limbergen E, Briot E, De Brabandere M, Dimopoulos J, et al. Recommendations from Gynaecological (GYN) GEC-ESTRO Working Group (I): concepts and terms in 3D image based 3D treatment planning in cervix cancer brachytherapy with emphasis on MRI assessment of GTV and CTV. *Radiother Oncol* 2005; **74:** 235-45.
2. Pötter R, Haie-Mader C, Van Limbergen E, Barillot I, De Brabandere M, Dimpoulos J, et al. Recommendations from gynaecological (GYN) GEC-ESTRO Working Group: (II): concepts and terms of 3D imaging, radiation physics, radiobiology, and 3D dose volume parameters. *Radiother Oncol* 2006; **78:** 67-77.
3. Yadav P, Ramasubramanian V, Paliwal BR. Feasibility study on effect and stability of adaptive radiotherapy on kilovoltage cone beam CT. *Radiol Oncol* 2011; **45:** 220-6.
4. Mayr NA, Montebello JF, Sorosky JI, Daugherty JS, Nguyen DL, Mardirossian G, et al. Brachytherapy management of the retroverted uterus using ultrasound-guided implant applicator placement. *Brachytherapy* 2005; **4:** 24-9.
5. Sahinler I, Cepni I, Colpan D, Cepni K, Koksal S, Koca A, et al. Tandem application with transvaginal ultrasound guidance. *Int J Radiat Oncol Biol Phys* 2004; **59:** 190-6.
6. Davidson MT, Yuen J, D'Souza D, Radwan JS, Hammond JA, Batchelar DL. Optimization of high-dose-rate cervix brachytherapy applicator placement: the benefits of intraoperative ultrasound guidance. *Brachytherapy* 2008; **7:** 248-53.
7. Stock RG, Chan K, Terk M, Dewyngaert JK, Stone NN, Dottino P. A new technique for performing Syed –Neblett template interstitial implants for gynecologic malignancies using transrectal-ultrasound guidance. *Int J Radiat Oncol Biol Phys* 1997; **37:** 819-25.
8. Weitmann HD, Knocke TH, Waldhäusl C, Pötter R. Ultrasound-guided interstitial Brachytherapy in the treatment of advanced vaginal recurences from cervical and endometrial carcinoma. *Strahlenther Onkol* 2006; **182:** 86-95.
9. Van Dyk S, Narayan K, Fisher R, Bernshaw D. Conformal brachytherapy planning for cervical cancer using transabdominal ultrasound. *Int J Radiat Oncol Biol Phys* 2009; **75:** 64-70.
10. Datta NR, Srivastava A, Maria Das KJ, Gupta A, Rastogi N. Comparative assessment of doses to tumor, rectum, and bladder as evaluated by orthogonal radiographs vs. computer enhanced computed tomography-based intracavitary brachytherapy in cervical cancer. *Brachytherapy* 2006; **5:** 223-9.
11. Shin KH, Kim TH, Cho JK, Kim JY, Park SY, Park SY, et al. CT-guided intracavitary radiotherapy for cervical cancer: Comparison of conventional point A plan with clinical target volume-based three-dimensional plan using dose volume parameters. *Int J Radiat Oncol Biol Phys* 2006; **64:** 197-204.
12. Mai J, Rownd J, Erickson B. CT-guided high-dose-rate dose prescription for cervical carcinoma: the importance of uterine wall thickness. *Brachytherapy* 2002; **1:** 27-35.
13. Weitmann HD, Pötter R, Waldhäusl C, Nechvile E, Kirisits C, Knocke TH. Pilot study in the treatment of endometrial carcinoma with 3D image-based high-dose-rate brachytherapy using modified Heyman Packing: clinical experience and dose-volume histogram analysis. *Int J Radiat Oncol Biol Phys* 2005; **62:** 468-78.
14. Pelloski CE, Palmer M, Chronowski GM, Jhingran A, Horton J, Eifel PJ. Comparison between CT-based volumetric calculations and ICRU reference-point estimates of radiation doses delivered to bladder and rectum during intracavitary radiotherapy for cervical cancer. *Int J Radiat Oncol Biol Phys*. 2005; **62:** 131-7.
15. Sun LM, Huang EY, Ko SF, Wang CJ, Leung SW, Lin H, et al. Computer-tomography-assisted three-dimensional technique to assess rectal and bladder wall dose in intracavitary brachytherapy for uterine cervical cancer. *Radiother Oncol* 2004; **71:** 333-7.
16. Schoeppel SL, Ellis JH, LaVigne ML, Schea RA, Roberts JA. Magnetic resonance imaging during intracavitary gynecologic brachytherapy. *Int J Radiat Oncol Biol Phys* 1992; **23:** 169-74.
17. Tardivon AA, Kinkel K, Lartigau E, Masselot J, Gerbaulet AP, Vanel D. MR imaging during intracavitary brachytherapy of vaginal and cervical cancer: preliminary results. *Radiographics* 1996; **16:** 1363-70.
18. Viswanathan AN, Cormack R, Holloway CL, Tanaka C, O'Farrell D, Devlin PM, et al. Magnetic resonance-guided interstitial therapy for vaginal recurrence of endometrial cancer. *Int J Radiat Oncol Biol Phys* 2006; **66:** 91-9.
19. Wachter-Gerstner N, Wachter S, Reinstadler E, Fellner C, Knocke TH, Wambersie A, et al. Bladder and rectum dose defined from MRI based treatment planning for cervix cancer brachytherapy: comparison of dose-volume histograms for organ contours and organ wall, comparison with ICRU rectum and bladder reference point. *Radiother Oncol* 2003; **68:** 269-76.
20. Pötter R, Dimopoulos J, Georg P, Lang S, Waldhäusl C, Wachter-Gerstner N, et al. Clinical impact of MRI assisted dose volume adaptation and dose escalation in brachytherapy of locally advanced cervix cancer. *Radiother Oncol* 2007; **83:** 148-55.
21. Haie-Meder C, Chargari C, Rey A, Dumas I, Morice P, Magné N, et al. MRI-based low dose-rate brachytherapy experience in locally advanced cervical cancer patients initially treated by concomitant chemoradiotherapy. *Radiother Oncol* 2010; **96:** 161-5.
22. De Brabandere M, Mousa AG, Nulens A, Swinnen A, Van Limbergen E. Potential of dose optimisation in MRI-based PDR brachytherapy of cervix carcinoma. *Radiother Oncol* 2008; **88:** 217-26.
23. Lindegaard JC, Tanderup K, Nielsen SK, Haack S, Gelineck J. MRI-Guided 3D Optimization Significantly Improves DVH Parameters of Pulsed-Dose-Rate Brachytherapy in Locally Advanced Cervical Cancer. *Int J Radiat Oncol Biol Phys* 2008; **71:** 756-64.
24. Boss EA, Barentsz JO, Massuger LF, Boonstra H. The role of MR imaging in invasive cervical carcinoma. *Eur Radiol* 2000; **10:** 256-70.
25. Subak LL, Hricak H, Powell CB, Azizi L, Stern JL. Cervical carcinoma: computed tomography and magnetic resonance imaging for preoperative staging. *Obstet Gynecol* 1995; **86:** 43-50.
26. Hricak H, Gatsonis C, Coakley FV, Snyder B, Reinhold C, Schwartz LH, et al. Early invasive cervical cancer: CT and MR imaging in preoperative evaluation – ACRIN/GOG comparative study of diagnostic performance and interobserver variability. *Radiology* 2007; **245:** 491-8.
27. Mitchell DG, Snyder B, Coakley F, Reinhold C, Thomas G, Amendola M, et al. Early invasive cervical cancer: tumor delineation by magnetic resonance imaging, computed tomography, and clinical examination, verified by pathologic results, in the ACRIN 6651/GOG 183 Intergroup Study. *J Clin Oncol* 2006; **24:** 5687-94.
28. Dimopoulos JC, Schard G, Berger D, Lang S, Goldner G, Helbich T, et al. Systematic evaluation of MRI findings in different stages of treatment of cervical cancer: potential of MRI on delineation of target, patho-anatomical structures and organs at risk. *Int J Radiat Oncol Biol Phys* 2006; **64:** 1380-8.
29. Podobnik J, Kocijancic I, Kovac V, Sersa I. 3T MRI in evaluation of asbestos-related thoracic diseases - preliminary results. *Radiol Oncol* 2010; **44:** 92-6.
30. Sofic A, Beslic S, Sehovic N, Caluk J, Sofic D. MRI in evaluation of perianal fistulae. *Radiol Oncol* 2010; **44:** 220-7.
31. Dimopoulos JC, Schirl G, Baldinger A, Helbich TH, Pötter R, et al. MRI assessment of cervical cancer for adaptive radiotherapy. *Strahlenther Onkol* 2009; **185:** 282-7.
32. Hellebust TP, Kirisits C, Berger D, Pérez-Calatayud J, De Brabandere M, De Leeuw A, et al. Recommendations from Gynaecological (GYN) GEC-ESTRO Working Group: Considerations and pitfalls in comissioning and applicator reconstruction in 3D image-based treatment planning of cervix cancer brachytherapy. *Radiother Oncol* 2010; **96:** 153-60.
33. Petric P, Hudej R, Music M. MRI assisted cervix cancer brachytherapy preplanning, based on insertion of the applicator in para-cervical anaesthesia: preliminary results of a prospective study. *J Contemp Brachyther* 2009; **1:** 163-9.
34. Kouwenhoven E, Giezen M, Struikmans H. Measuring the similarity of target volume delineations independent of the number of observers. *Phys Med Biol* 2009; **54:** 2863-73.
35. Bland JM, Altman DG. Statistical methods for assessing agreement between two methods of clinical measurements. *Lancet* 1986; **1:** 307-10.
36. Bland JM, Altman DG. Measuring agreement in method comparison studies. *Stat Methods Med Res* 1999; **8:** 135-60.
37. Lin LI. A concordance correlation coefficient to evaluate reproducibility. *Biometrics* 1989; **45:** 255-68.

38. Georg D, Kirisits C, Hillbrand M, Dimopoulos J, Pötter R. Image-guided radiotherapy for cervix cancer: high-tech external beam therapy versus high-tech brachytherapy. *Int J Radiat Oncol Biol Phys* 2008; **71:** 1272-8.

39. Lichy MP, Wietek BM, Mugler JP 3rd, Horger W, Menzel MI, Anastasiadis A, et al. Magnetic resonance imaging of the body trunk using a single-slab, 3-dimensional, T2-weighted turbo-spin-echo sequence with high sampling efficiency (SPACE) for high spatial resolution imaging: initial clinical experiences. *Invest Radiol* 2005; **40:** 754-60.

40. Fütterer JJ, Yakar D, Strijk SP, Barentsz JO. Preoperative 3T MR imaging of rectal cancer: local staging accuracy using a two-dimensional and three-dimensional T2-weighted turbo spin echo sequence. *Eur J Radiol* 2008; **65:** 66-71.

41. Kim H, Lim JS, Choi JY, Park J, Chung YE, Kim MJ, et al. Rectal cancer: comparison of accuracy of local-regional staging with two- and three-dimensional preoperative 3-T MR imaging. *Radiology* 2010; **254:** 485-92.

42. Rosenkrantz AB, Neil J, Kong X, Melamed J, Babb JS, Taneja SS, et al. Prostate cancer: Comparison of 3D T2-weighted with conventional 2D T2-weighted imaging for image quality and tumor detection. *AJR Am J Roentgenol* 2010; **194:** 446-52.

43. Arizono S, Isoda H, Maetani YS, Hirokawa Y, Shimada K, Nakamoto Y, et al. High-spatial-resolution three-dimensional MR cholangiography using a high-sampling-efficiency technique (SPACE) at 3T: Comparison with the conventional constant flip angle sequence in healthy volunteers. *J Magn Res Imaging* 2008; **28:** 685-90.

44. Arizono S, Isoda H, Maetani YS, Hirokawa Y, Shimada K, Nakamoto Y, et al. High spatial resolution 3D MR cholangiography with high sampling efficiency technique (SPACE): Comparison of 3 T vs. 1.5 T. *Eur J Radiol* 2010; **73:** 114-8.

45. Baumert B, Wörtler K, Steffinger D, Schmid GP, Schmidt GP, Reiser MF, Baur-Melnyk A. Assessment of the internal craniocervical ligaments with a new magnetic resonance imaging sequence: three dimensional turbo spin echo with variable flip-angle distribution (SPACE). *Magn Res Imaging* 2009; **27:** 954-60.

46. Young JY, Yoon YC, Kwon JW, Ahn JH, Choe BK. Diagnosis of internal derangement of the knee at 3.0 T MR imaging: 3D isotropic intermediate-weighted versus 2D sequences. *Radiology* 2009; **253:** 780-7.

47. Young JY, Yoon YC, Choi SH, Kwon JW, Yoo J, Choe BK. Three-dimensional isotropic shoulder MR arthrography for the diagnosis of labral lesions at 3.0 T. *Radiology* 2009; **250:** 498-505.

48. Gerbaulet A, Pötter R, Haie-Meder C. Cervix cancer. In: Gerbaulet A, Pötter R, Mazeron JJ, Meertens H, Van Limbergen E, editors. *The GEC ESTRO handbook of brachytherapy*. Brussels: European Society of Therapeutic Radiology and Oncology; 2002. p 301-63.

49. Guedea F, Ellison T, Venselaar J, Borras JM, Hoskin P, Poetter R, et al. Overview of brachytherapy resources in Europe: a survey of patterns of care study for brachytherapy in Europe. *Radiother Oncol* 2007; **82:** 50-4.

50. Guedea F, Venselaar J, Hoskin P, Hellebust TP, Peiffert D, Londres B, et al. Patterns of care for brachytherapy in Europe: updated results. *Radiother Oncol* 2010; **97:** 514-20.

51. Viswanathan AN, Erickson BA. Three-dimensional imaging in gynaecological brachytherapy: a survey of the American Brachytherapy Society. *Int J Radiat Oncol Biol Phys* 2010; **76:** 104-9.

52. Dimopoulos JC, De Vos V, Berger D, Dumas I, Kirisits C, Shenfield CB, et al. Inter-observer comparison of target delineation for MRI-assisted cervical cancer brachytherapy: application of the GYN GEC-ESTRO recommendations. *Radiother Oncol* 2009; **91:** 166-72.

53. Lang S, Nulens A, Briot E, Kirisits C, De Brabandere M, Dumas I, Dimopoulos J, et al. Intercomparison of treatment concepts for MR image assisted brachytherapy of cervical carcinoma based on GYN GEC-ESTRO recommendations. *Radiother Oncol* 2006; **78:** 185-93.

54. Petric P, Dimopoulos J, Kirisits C, Berger D, Hudej R, Pötter R. Inter- and intraobserver variation in HR-CTV contouring: Intercomparison of transverse and paratransverse image orientation in 3D-MRI assisted cervix cancer brachytherapy. *Radiother Oncol* 2008; **89:** 164-71.

55. Rasch C, Barillot I, Remeijer P, Touw A, van Herk M, Lebesque JV. Definition of the prostate in CT and MRI: a multiobserver study. *Int J Radiat Oncol Biol Phys* 1999; **43:** 57-66.

56. Struikmans H, Warlam-Rodenhuis C, Stam T, Stapper G, Tersteeg RJ, Bol GH, et al. Interobserver variability of clinical target volume delineation of glandular breast tissue and of boost volume in tangential breast irradiation. *Radiother Oncol* 2005; **76:** 293-9.

57. Hurkmans CW, Borger JH, Pieters BR, Russell NS, Jansen EP, Mijnheer BJ. Variability in target volume delineation on CT scans of the breast. *Int J Radiat Oncol Biol Phys* 2001; **50:** 1366-72.

58. Weiss E, Richter S, Krauss T, Metzelthin SI, Hille A, Pradier O, et al. Conformal radiotherapy planning of cervix carcinoma: differences in the delineation of target volume. A comparison between gynaecologic and radiation oncologists. *Radiother Oncol* 2003; **67:** 87-95.

59. Tanderup K, Hellebust TP, Lang S, Granfeldt J, Pötter R, Lindegaard JC, et al. Consequences of random and systematic reconstruction uncertainties in 3D image based brachytherapy in cervical cancer. *Radiother Oncol* 2008; **98:** 156-63.

research article

Cetuximab in preoperative treatment of rectal cancer - term outcome of the XERT trial

Vaneja Velenik[1], Janja Ocvirk[2], Irena Oblak[1], Franc Anderluh[1]

[1] Department of Radiotherapy, Institute of Oncology Ljubljana, Ljubljana, Slovenia
[2] Department of Medical Oncology, Institute of Oncology Ljubljana, Ljubljana, Slovenia

Radiol Oncol 2012; 46(3): 252-257.

Received 10 February 2012
Accepted 19 March 2012

Correspondence to: Assist. Prof Vaneja Velenik, MD, PhD, Institute of Oncology Ljubljana, Zaloska 2, 1000 Ljubljana, Slovenia. Phone: +38615879661; Fax: +38615879400; E-mail: vvelenik@onko-i.si

Disclosure: No potential conflicts of interest were disclosed.

Background. Preoperative capecitabine-based chemoradiotherapy (CRT) is feasible for the treatment of resectable locally advanced rectal cancer (LARC). To try to improve efficacy, we conducted a phase II study in which the epidermal growth factor receptor-targeting monoclonal antibody cetuximab was added to capecitabine-based CRT. The results for long-term survival and for an analysis investigating the relationship between survival and patient and disease characteristics, including tumour *KRAS* mutation status, and surgery type, are presented.

Patients and methods. Patients with resectable LARC received capecitabine (1250 mg/m^2 twice daily, orally) for 2 weeks followed by cetuximab alone (400 mg/m^2 for 1 week) and then with CRT (250 mg/m^2/week) comprising capecitabine (825 mg/m^2 twice daily) and radiotherapy to the small pelvis (45 Gy in 25 1.8-Gy fractions), five days a week for five weeks. Surgery was conducted six weeks following CRT, with post-operative chemotherapy with capecitabine (1250 mg/m^2 twice daily for 14 days every 21 days) three weeks later.

Results. Forty-seven patients were enrolled and 37 underwent treatment. Twenty-eight of the patients (75.7%) had T3N+ disease. Thirty-six patients were evaluable for efficacy. The median follow-up time was 39.0 months (range 5.0--87.0). The three-year local control, disease-free survival, relapse-free survival and overall survival rates were 96.9% (95% CI 90.0--100), 72.2% (57.5--86.9), 74.3% (95% CI 59.8--88.8) and 68.1% (95% CI 36.7--99.4), respectively. There was no significant association between survival and gender, age, tumour location in the rectum, type of surgery, pathological T or N status, tumour regression grade or tumour *KRAS* mutation status, although sample sizes were small.

Conclusions. Preoperative cetuximab plus capecitabine-based CRT was feasible in patients with resectable LARC and was associated with an impressive three-year local control rate. The use of tumour *KRAS* mutation status as a biomarker for the efficacy of cetuximab-based regimens in this setting requires further investigation.

Key words: rectal cancer; radio-chemotherapy; cetuximab

Introduction

Preoperative concurrent chemoradiotherapy (CRT) is associated with improved local tumour control compared with preoperative radiotherapy[1,2] and is a commonly used approach for the treatment of stage II/III locally advanced rectal cancer (LARC). Since the initial observation of the clinical advantages of CRT over radiotherapy, methods of further improving outcomes have been investigated.

In a previous phase II study, we reported that the use of preoperative capecitabine-based CRT was feasible for the treatment of resectable LARC.[3] We then attempted to improve the efficacy of this regimen by adding the epidermal growth factor receptor (EGFR)-targeting monoclonal antibody, cetuximab. The rationale for the use of this combination was based on the radiosensitizing effects observed with cetuximab in *in vivo* model systems[4,5], supported by clinical evidence from a randomized phase III trial investigating the combination of cetuximab and radiotherapy in the treatment of locally advanced squamous cell carcinoma of the head and neck.[6,7] In the phase III trial, the combination of

cetuximab and radiotherapy was significantly more beneficial, in terms of both locoregional control and survival, than radiotherapy alone.

In 2007, we designed a prospective, non-randomized, open label phase II study to investigate the impact of adding cetuximab to preoperative capecitabine-based CRT for the treatment of 37 patients with resectable LARC. The primary endpoint of the trial was pathological complete response (pCR). Results reported in 2010 showed a pCR of 8% (3 patients) with overall-, T- and N-downstaging rates of 73%, 57% and 81%, respectively. The total sphincter preservation rate was 76%.[8]

The identification of biomarkers to tailor treatment to patients most likely to benefit has become an integral part of the investigation of novel treatments and regimens.[9,10] Retrospective analyses of data from randomized trials demonstrated significant improvements in survival when cetuximab was added to standard chemotherapy regimens for the treatment of patients with metastatic CRC not harbouring *KRAS* mutations.[11,12] While the reported incidence rates of tumour *KRAS* mutations in rectal cancer are lower than those for CRC, with rates ranging between 13% and 48%[13-17] compared with the 55-70% reported for metastatic colorectal cancer (mCRC), the presence of such mutations may still have a significant impact on treatment outcome.

We report here the results of the long-term follow-up of our phase II study[8], with three-year survival results, together with findings from an analysis conducted to investigate any relationship between survival and baseline patient and disease characteristics, including tumour *KRAS* mutation status, and the type of surgery conducted.

Patients and methods

Details of the study design, eligibility criteria, treatment and assessments have been reported in detail previously.[8] The study was approved by the relevant ethics committees and was conducted in accordance with the Declaration of Helsinki. It was registered at ClinicalTrials.gov (NCT00689702). All patients provided written informed consent.

Patients and study design

Briefly, patients with histologically-confirmed International Union Against Cancer (UICC) stage II/III adenocarcinoma of the rectum and a World Health Organization (WHO) performance status (PS) of ≤2 and who had not previously received radiotherapy and/or chemotherapy for their disease were included in the study.[8] The extent of locoregional disease was determined by magnetic resonance imaging (MRI).

Patients were scheduled to receive eight weeks of treatment, at the end of which the primary tumour was re-evaluated with pelvic MRI and response evaluated according to Response Evaluation Criteria In Solid Tumours (RECIST). Definitive surgery was scheduled to take place four to six weeks after the completion of CRT. A decision on the type of surgery to be conducted was taken prior to the start of preoperative CRT. Three cycles of postoperative chemotherapy, each lasting three weeks, were recommended to start within six weeks of surgery. After the operation the post-treatment surveillance was regularly done.[18]

Treatment

Capecitabine (1250 mg/m^2 twice daily orally) was administered for two weeks, followed, on day 1 of week 3, by cetuximab IV (400 mg/m^2). Starting on day 1 of week 4, patients received cetuximab (250 mg/m^2/week) plus CRT with capecitabine (825 mg/m^2 twice daily) and radiotherapy to the small pelvis (45 Gy in 25 1.8-Gy fractions), five days a week for five weeks. Radiation was delivered using three-dimensional conformal computed tomography (CT)-based treatment planning. The chemotherapy component of CRT was initiated on the first day and finished on the last day of radiotherapy (including weekends). Surgery was to be sphincter-sparing where possible. Post-operative chemotherapy comprised capecitabine (1250 mg/m^2 twice daily for two weeks every three weeks days).

Assessments

During treatment patients were monitored weekly for safety. Tumour response was assessed five weeks after the end of preoperative treatment. After surgery, histological examination of excised tissue was performed to determine the degree of pathological tumour response. Histological regression of the primary tumour was evaluated using a previously described tumour regression grading (TRG) system: TRG 0=no regression, TRG 1=minimal regression, TRG 2=moderate regression, TRG 3=good regression and TRG 4=total regression.[19,20]

Tumour KRAS mutation analysis

Tumour tissue for *KRAS* analysis was obtained prior to neoadjuvant treatment and at surgery. After

microdissection, intratumoural gene expression levels and analysis of seven *KRAS* mutations (codon 12 and codon 13) was carried out using a proprietary procedure, the ResponseDX: Colon™ system (Response Genetics Inc., Los Angeles, California, USA) referred to in previous publications.[21,22]

Statistical methods and considerations

The primary endpoint of the study was the pathological complete response (pCR) rate (defined as the complete disappearance of all tumour cells in surgically excised tissue), results for which have been reported in a separate publication.[8] Secondary endpoints reported here are: locoregional control (defined as the time from inclusion to documentation of tumour recurrence in the pelvis. It is emphasized that the development, or progression, of metastatic disease did not constitute local failure), relapse-free survival (defined as the time from inclusion to the first occurrence of disease relapse [local or distant], death or date of last follow-up), disease-free survival (defined as the time to relapse, second cancer, or death from any cause, whichever came first) and overall survival (defined as time from inclusion to the date of death from any cause or to the date of last follow-up).

The Kaplan-Meier method was used to estimate the rates of overall, relapse-free, disease-free and local relapse-free survival. A univariate analysis was performed to investigate any association between relapse-free and disease-free survival and parameters including gender, age, tumour location in the rectum (low, middle, upper third), type of surgery (abdominoperineal amputation, sphincter sparing), pathological T or N status, TRG and tumour *KRAS* mutation status. The log-rank test was used to test the significance between the subgroups for this endpoint. The cumulative incidence approach was used to estimate the rates for disease-specific mortality, local recurrence and distant metastasis. Statistical analysis was performed using the SPSS statistical software package, version 12 (SPSS Inc., Chicago, IL, USA).

Results

Patients

Between February 2007 and September 2008, 43 patients were recruited into the study. Thirty-seven of these patients subsequently received preoperative treatment with cetuximab plus capecitabine-based CRT. Median age was 55 years, 81.1% were males, and 90.9% presented with stage III disease. The median distance of tumour from the anal verge was 6.0 cm (range 1.0-11.0 cm).

Preoperative treatment, surgery and postoperative chemotherapy

Cetuximab administration was discontinued after the first dose in four patients due to hypersensitivity reactions: these patients continued to receive capecitabine and radiotherapy. All 37 patients received the planned dose of radiation. Only two patients (5.4%) received less than 90% of the planned dose of capecitabine, one due to grade 3 hepatotoxicity and one due to grade 3 diarrhoea.

All 37 patients underwent surgery. Sphincter-sparing surgery was performed in 26 patients (70.3%) and abdominoperineal amputation in 11 patients (29.7%). One patient experienced back pain a few months after surgery and, on re-examination of the pretreatment MRI scan, was found to have had sacral bone metastasis prior to treatment. This patient was excluded from the survival and *KRAS* analyses. Tumour tissue from 32 patients was available for *KRAS* analysis and *KRAS* mutations were detected in the tumour tissue of 13 patients (40.6%).

Postoperative chemotherapy was administered to 34 patients. Thirty-two were able to receive all three planned cycles at the recommended dose: among these patients, one developed grade 3 leukopenia and one had grade 2 vomiting. The remaining two patients received two cycles of capecitabine due to the development of grade 2 diarrhoea.

Treatment outcome

The median follow-up time for all 36 patients was 39.0 months (range 5.0-87.0 months). The median time to disease recurrence was 35.0 months (range 5.0-87.0 months). Local failure occurred in one patient (2.8%), 11.5 months after the end of treatment. The three-year local control rate was 96.9% (95% CI 90.9-100). Disease dissemination was observed in nine patients (25.0%) with the following pattern of distribution: liver (n=3; 8.3%), lung (n=3; 8.3%), suprarenal gland (n=1; 2.8%), bones (n=1; 2.8%) and synchronous lung plus retroperitoneum (n=1; 2.8%). The latest distant failure was observed 26 months after the end of treatment. No secondary malignancies were observed. The three-year relapse-free survival rate was 74.3% (95% CI 59.8-88.8) (Figure 1) and the three-year disease-free survival rate was 72.2% (95% CI 57.5-86.9) (Figure 2).

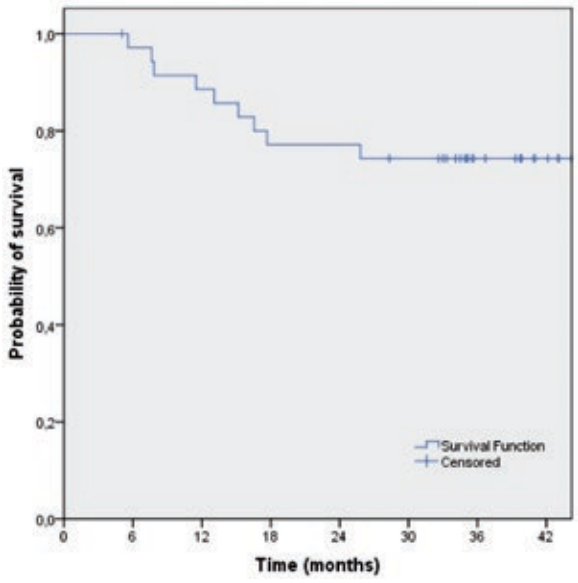

FIGURE 1. Relapse-free survival of patients treated with preoperative capecitabine-base chemotherapy and cetuximab (n=36).

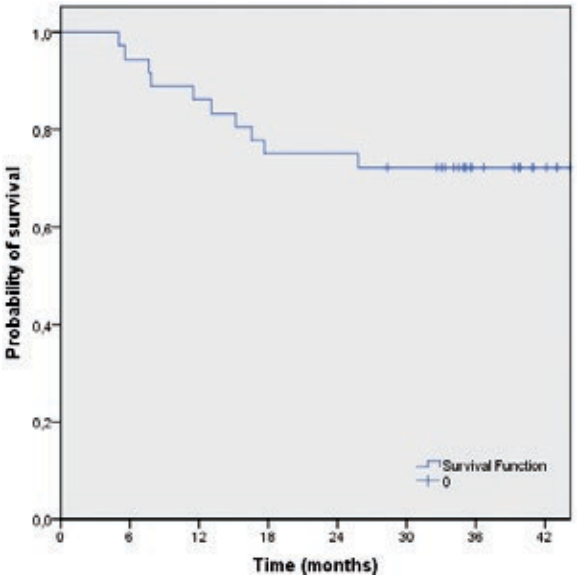

FIGURE 2. Disease-free survival of patients treated with preoperative capecitabine-base chemotherapy and cetuximab (n=36).

The median survival has not yet been reached. The three-year survival rate was 68.1% (95% CI 36.7-99.4) (Figure 3).

There was no significant association between relapse- or disease-free survival and gender, age, tumour location in the rectum, type of surgery, pathological T or N status, TRG or tumour *KRAS* mutation status (Table 1).

Deaths

As of September 2011, six of the 36 patients had died due to the following causes: rectal cancer (n=4), preoperative complications (n=1) and non-disease or treatment-related cause (accident at work) (n=1).

Discussion

The results of this trial demonstrated that the addition of cetuximab to preoperative capecitabine-based CRT led to a pCR rate of 8%[8] with long-term results showing a three-year local control rate of 96.9%, a three-year disease-free survival rate of 72.2% and a three-year overall survival rate of 68.1%. The treatment regimen was well tolerated.

Since the results of the landmark randomized trial reported by the German Rectal Cancer Study Group in 2004, which confirmed the local control and reduced toxicity benefits of preoperative fluorouracil-based CRT over post-operative

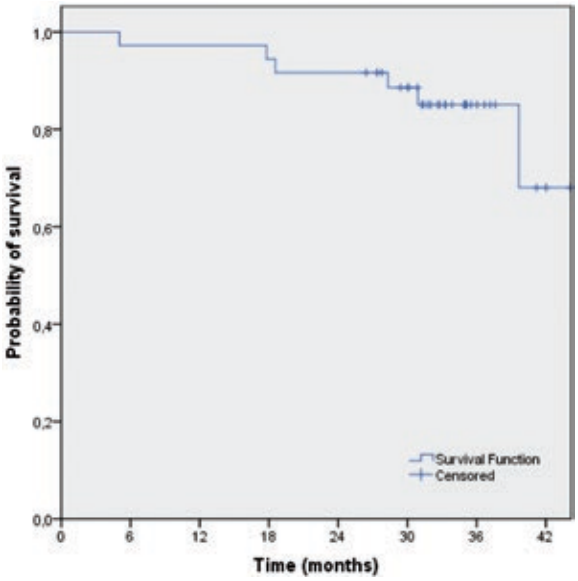

FIGURE 3. Overall survival of patients treated with preoperative capecitabine-base chemotherapy and cetuximab (n=36).

CRT for LARC[1], ways to improve the efficacy of preoperative CRT regimens have been investigated. In the study conducted by the German Rectal Cancer Study Group, the preoperative treatment comprised 5 Gy (in fractions of 1.8 Gy per day, five days per week) and fluorouracil (1000 mg/m^2/day 120-hour continuous infusion in the first and fifth weeks of radiotherapy). Four five-day cycles of fluorouracil (500 mg/m^2) were administered one month after surgery. By five years, 6% of patients receiving preoperative therapy had relapsed.

TABLE 1. Univariate analysis of disease-free survival according to patient, disease and treatment characteristics

Parameter	Chi-squared	Degrees of freedom	p value*
Gender	0.010	1	0.919
Age	1.061	1	0.303
Tumor location in the rectum (lower, middle or upper third)	5.396	2	0.067
Type of surgery (abdominoperineal amputation or sphincter-sparing)	2.311	2	0.315
Pathohistology			
Node	0.275	2	0.872
Tumor	0.973	1	0.324
Dworak regression grade			
1-4	7.966	4	0.093
3–4 vs 0–2	0.254	1	0.614
Tumour KRAS **mutation status**	1.903	2	0.386

* Log-rank test. Number of patients = 36.

In an earlier study from our group, we reported on the use of a capecitabine-based preoperative CRT regimen without cetuximab.[3] The study used the same preoperative CRT regimen as that described in the present study but followed by four, rather than three, cycles of post-operative fluorouracil chemotherapy. Among 56 patients completing CRT and surgery, 55 had R0 resection. The pCR rate of 9.1% was similar to that reported in our current study with cetuximab and the five-year local control rate was 87.4% (95% CI 75.0-99.8%).

The original German Rectal Cancer Study Group trial reported a five-year overall survival rate of 76% for the use of preoperative CRT in LARC.[1] In a recently reported randomized phase II study, the use of a dual chemotherapy combination of capecitabine and oxaliplatin in CRT followed by surgery and four cycles of post-operative capecitabine/oxaliplatin was reported to be associated with a three-year overall survival rate of 90%[23], although the acute grade 3/4 toxicity associated with this regimen was fairly high: during CRT, 29% of patients experienced grade 3/4 toxicity, mainly diarrhea.[24] The three-year overall survival results reported in our current study was 68.1%, which may in part reflect the single-agent composition of the chemotherapy component of the CRT regimen. In a phase II study in 40 patients, the addition of irinotecan to capecitabine and cetuximab in the preoperative CRT regimen was associated with a three-year overall survival rate of 94.7%.[17]

It is now well established that patients with mCRC who have tumour *KRAS* mutations are unlikely to benefit from the addition of cetuximab to standard chemotherapy.[25,26] However, in rectal cancer, the influence of *KRAS* mutation status on tumour response in the presence of radiation is unclear. Data from a number of studies have suggested both no association[13,14,16] and a negative association[27] between the presence of tumour *KRAS* mutations and tumour regression and/or survival in patients with rectal cancer receiving preoperative CRT. In our study, no association between tumour *KRAS* mutation status and survival following preoperative cetuximab/capecitabine-based CRT could be found. Our findings support those from another analysis of data from 57 patients receiving CRT containing cetuximab plus irinotecan and capecitabine, in which tumour *KRAS* mutation status did not appear to influence tumour regression or disease-free survival.[15] However, in a pooled analysis of data from 130 patients taking part in a number of phase II trials, including our own study, the presence of tumour *KRAS* mutations was significantly associated with pathologic nonresponse.[21] It is possible, therefore, that tumour *KRAS* mutation status may be important in predicting outcome to cetuximab in this setting, but this would require larger scale analyses. Another study demonstrated that it was not *KRAS* mutation status that predicted achievement of a pCR following cetuximab-based neoadjuvant CRT, but rather the presence of *EGF* A+61G gene polymorphism, independent of *KRAS* mutation status.[22] These data warrant additional investigation.

Our current study also reported relapse- and disease-free survival to be independent of gender, age, tumour location within the rectum, type of surgery, pathological T or N status and TRG, although, as for the *KRAS* analysis, the numbers of patients involved in the analysis are small. In a previous study, there was indication from a univariate

analysis that post-operative parameters, including pathologic T or N status and TRG, were associated with disease-free survival.[28] In multivariate analysis, however, only the association between pN and TRG and disease-free survival remained.

In conclusion, our study demonstrates that the addition of cetuximab to capecitabine-based preoperative CRT is feasible and is associated with an impressive three-year local control rate of 97%. The use of tumour *KRAS* mutation status as a biomarker to identify which patients are most likely to respond to cetuximab-based CRT requires further, larger scale investigation.

Acknowledgements

The authors declare that they have no conflict of interests. Merck KGaA provided support as study drug (cetuximab) donation. Merck KGaA has reviewed the publication. The views and opinions described in the publication do not necessarily reflect those of Merck KGaA

References

1. Sauer R, Becker H, Hohenberger W, Rodel C, Wittekind C, Fietkau R, et al. Preoperative versus postoperative chemoradiotherapy for rectal cancer. *N Engl J Med* 2004; **351:** 1731-40.
2. Conde S, Borrego M, Teixeira T, Teixeira R, Corbal M, Sá A, et al. Impact of neoadjuvant chemoradiation on pathologic response and survival of patients with locally advanced rectal cancer. *Rep Pract Oncol Radiother* 2010; **15:** 51-9.
3. Velenik V, Oblak I, Anderluh F. Long-term results from a randomized phase II trial of neoadjuvant combined-modality therapy for locally advanced rectal cancer. *Radiat Oncol* 2010; **5:** 88.
4. Milas L, Mason K, Hunter N, Petersen S, Yamakawa M, Ang K, et al. In vivo enhancement of tumor radioresponse by C225 antiepidermal growth factor receptor antibody. *Clin Cancer Res* 2000; **6:** 701-8.
5. Nasu S, Ang KK, Fan Z, Milas L. C225 antiepidermal growth factor receptor antibody enhances tumor radiocurability. *Int J Radiat Oncol Biol Phys* 2001; **51:** 474-7.
6. Bonner JA, Harari PM, Giralt J, Azarnia N, Shin DM, Cohen RB, et al. Radiotherapy plus cetuximab for squamous-cell carcinoma of the head and neck. *N Engl J Med* 2006; **354:** 567-78.
7. Bonner JA, Harari PM, Giralt J, Cohen RB, Jones CU, Sur RK, et al. Radiotherapy plus cetuximab for locoregionally advanced head and neck cancer: 5-year survival data from a phase 3 randomised trial, and relation between cetuximab-induced rash and survival. *Lancet Oncol* 2010; **11:** 21-8.
8. Velenik V, Ocvirk J, Oblak I, Anderluh F. A phase II study of cetuximab, capecitabine and radiotherapy in neoadjuvant treatment of patients with locally advanced resectable rectal cancer. *Eur J Surg Oncol* 2011; **36:** 244-50.
9. Zhou Y, Boardman LA, Miller RC. Genetic testing for young-onset colorectal cancer: case report and evidence-based clinical guidelines. *Radiol Oncol* 2010; **44:** 57-61.
10. Lewander A, Gao J, Adell G, Zhang H, Sun XF. Expression of NF-kappa B p65 phosphorylated at serine-536 in rectal cancer with or without preoperative radiotherapy. *Radiol Oncol* 2011; **45:** 279-84.
11. Bokemeyer C, Bondarenko I, Hartmann JT, de Braud F, Schuch G, Zubel A, et al. Efficacy according to biomarker status of cetuximab plus FOLFOX-4 as first-line treatment for metastatic colorectal cancer: the OPUS study. *Ann Oncol* 2011; **22:** 1535-46.
12. Van Cutsem E, Kohne CH, Lang I, Folprecht G, Nowacki MP, Cascinu S, et al. Cetuximab plus irinotecan, fluorouracil, and leucovorin as first-line treatment for metastatic colorectal cancer: updated analysis of overall survival according to tumor KRAS and BRAF mutation status. *J Clin Oncol* 2011; **29:** 2011-9.
13. Bengala C, Bettelli S, Bertolini F, Sartori G, Fontana A, Malavasi N, et al. Prognostic role of EGFR gene copy number and KRAS mutation in patients with locally advanced rectal cancer treated with preoperative chemoradiotherapy. *Br J Cancer* 2010; **103:** 1019-24.
14. Davies JM, Trembath D, Deal AM, Funkhouser WK, Calvo BF, Finnegan T, et al. Phospho-ERK and AKT status, but not KRAS mutation status, are associated with outcomes in rectal cancer treated with chemoradiotherapy. *Radiat Oncol* 2011; **6:** 114.
15. Erben P, Strobel P, Horisberger K, Popa J, Bohn B, Hanfstein B, et al. KRAS and BRAF mutations and PTEN expression do not predict efficacy of cetuximab-based chemoradiotherapy in locally advanced rectal cancer. Int J *Radiat Oncol Biol Phys* 2011; **81:** 1032-8.
16. Gaedcke J, Grade M, Jung K, Schirmer M, Jo P, Obermeyer C, et al. KRAS and BRAF mutations in patients with rectal cancer treated with preoperative chemoradiotherapy. *Radiother Oncol* 2010; **94:** 76-81.
17. Kim SY, Hong YS, Kim DY, Kim TW, Kim JH, Im SA, et al. Preoperative chemoradiation with cetuximab, irinotecan, and capecitabine in patients with locally advanced resectable rectal cancer: a multicenter Phase II study. *Int J Radiat Oncol Biol Phys* 2011; **81:** 677-83.
18. Velenik V. Post-treatment surveillance in colorectal cancer. *Radiol Oncol* 2010; **44:** 135-41.
19. Dworak O, Keilholz L, Hoffmann A. Pathological features of rectal cancer after preoperative radiochemotherapy. *Int J Colorectal Dis* 1997; **12:** 19-23.
20. Mihaylova I, Parvanova V, Velikova C, Kurteva G, Ivanova D. Degree of tumor regression after preoperative chemo-radiotherapy in locally advanced rectal cancer – Preliminary results. *Rep Pract Oncol Radiother* 2011; **16:** 237-42.
21. Grimminger PP, Danenberg P, Dellas K, Arnold D, Rodel C, Machiels JP, et al. Biomarkers for cetuximab-based neoadjuvant radiochemotherapy in locally advanced rectal cancer. *Clin Cancer Res* 2011; **17:** 3469-77.
22. Hu-Lieskovan S, Vallbohmer D, Zhang W, Yang D, Pohl A, Labonte MJ, et al. EGF61 polymorphism predicts complete pathologic response to cetuximab-based chemoradiation independent of KRAS status in locally advanced rectal cancer patients. *Clin Cancer Res* 2011; **17:** 5161-9.
23. Fernández-Martos C, Pericay C, Salud A, Massuti B, Alonso V, Safont M, et al. Three-year outcomes of GCR-3: a phase II randomized trial comparing conventional preoperative chemoradiation (CRT) followed by surgery and postoperative adjuvant chemotherapy (CT) with induction CT followed by CRT and surgery in locally advanced rectal cancer. [Abstract]. *J Clin Oncol* 2011; **29(15S):** Abstract 3552.
24. Fernández-Martos C, Pericay C, Aparicio J, Salud A, Safont M, Massuti B, et al. Phase II, randomized study of concomitant chemoradiotherapy followed by surgery and adjuvant capecitabine plus oxaliplatin (CAPOX) compared with induction CAPOX followed by concomitant chemoradiotherapy and surgery in magnetic resonance imaging-defined, locally advanced rectal cancer: Grupo Cáncer de Recto 3 study. *J Clin Oncol* 2010; **28:** 859-65.
25. Bokemeyer C, Bondarenko I, Makhson A, Hartmann JT, Aparicio J, de Braud F, et al. Fluorouracil, leucovorin, and oxaliplatin with and without cetuximab in the first-line treatment of metastatic colorectal cancer. *J Clin Oncol* 2009; **27:** 663-71.
26. Van Cutsem E, Kohne CH, Hitre E, Zaluski J, Chang Chien CR, Makhson A, et al. Cetuximab and chemotherapy as initial treatment for metastatic colorectal cancer. *N Engl J Med* 2009; **360:** 1408-17.
27. Garcia-Aguilar J, Chen Z, Smith DD, Li W, Madoff RD, Cataldo P, et al. Identification of a biomarker profile associated with resistance to neoadjuvant chemoradiation therapy in rectal cancer. *Ann Surg* 2011; **254:** 486-93.
28. Vecchio FM, Valentini V, Minsky BD, Padula GD, Venkatraman ES, Balducci M, et al. The relationship of pathologic tumor regression grade (TRG) and outcomes after preoperative therapy in rectal cancer. *Int J Radiat Oncol Biol Phys* 2005; **62:** 752-60.

research article

Inguinal or inguino-iliac/obturator lymph node dissection after positive inguinal sentinel lymph node in patients with cutaneous melanoma

Nebojsa Glumac[1], Marko Hocevar[1], Vesna Zadnik[2], Marko Snoj[1]

[1] Department of Surgical Oncology, Institute of Oncology, Ljubljana, Slovenia
[2] Cancer Registry, Institute of Oncology, Ljubljana, Slovenia

Radiol Oncol 2012; 46(3): 258-264.

Received 22 August 2011
Accepted 11 September 2011

Correspondence to: Nebojša Glumac, MD, PhD, Department of Surgical Oncology, Institute of Oncology, Zaloška 2, 1000 Ljubljana, Slovenia. Phone: +386 41 437 890; Fax: +386 1 5879 407; E-mail: nglumac@onko-i.si

Disclosure: No potential conflicts of interest were disclosed.

Background. The aim of the study was to determine whether the presence of inguinal sentinel lymph node (SLN) metastases smaller than 2 mm (micrometastases) subdivided according to the number of micrometastases predicts additional, non-sentinel inguinal, iliac or obturator lymph node involvement in completion lymph node dissection (CLND).

Patients and methods. Positive inguinal SLN was detected in 58 patients (32 female, 26 male, median age 55 years) from 743 consecutive and prospectively enrolled patients with primary cutaneous melanoma stage I and II who were treated with SLN biopsy between 2001 and 2007.

Results. Micrometastases in inguinal SLN were detected in 32 patients, 14 were single, 2 were double, and 16 were multiple. Twenty-six patients had macrometastases.

Conclusions. No patient with any micrometastases or a single SLN macrometastasis in the inguinal region had any iliac/obturator non-sentinel metastases after CLND in our series. Furthermore, no patient with single SLN micrometastasis in the inguinal region had any non-sentinel metastases at all after CLND in our series. In these cases respective CLND might be omitted.

Key words: melanoma; inguinal; sentinel lymph node biopsy; micrometastases; lymphadenectomy

Introduction

Since its introduction by Morton in 1992, sentinel lymph node biopsy (SLNB) is now becoming a standard of care for staging of patients with clinical stage I and II cutaneous melanoma or breast cancer.[1-3] Sentinel lymph node (SLN) predicts the status of regional nodal basin and its surgical recovery nears 100%.[4] The standard of treatment for positive SLN is completion lymph node dissection (CLND).[5] Specifically, in the inguinal region the extent of CLND is not yet clearly defined. Both inguinal and inguino-iliac/obturator lymph node dissection are being performed.

Before the introduction of SLNB the standard of treatment for palpable metastatic inguinal lymph nodes in patients with cutaneous melanoma was inguino-iliac/obturator lymph node dissection. This was due to the fact that up to 40% of patients with palpable metastatic inguinal lymph nodes had metastases in the iliac or obturator nodes.[6]

Nowadays, the situation has changed. The metastatic deposits found in the SLN are much smaller than previously detected palpable metastases and thus the chance of iliac or obturator node metastasis is considerably lower. Frequently, the CLND after positive inguinal SLN is completely negative thus adding the patient only additional complica-

tions and morbidity, and no benefit.[4,5,7] Namely, only 10-30% of patients with SLN metastases in any region have additional metastases in non-sentinel lymph nodes.[8] There are even fewer patients with iliac or obturator metastases after positive inguinal SLN.[9] Therefore, inguinal dissection might be radical enough procedure after positive inguinal SLN. However, at present time, it is difficult to predict in which subset of inguinal SLN positive patients the iliac/obturator lymph node dissection would not present with any further positive lymph nodes. Through the literature review we did not find any author who dealt specifically with the pattern of non-sentinel metastasis after a positive inguinal SLN.

The aim of our study was to determine the predictive value of inguinal SLN micrometastases subdivided according to the number of micrometastases in predicting non-sentinel inguinal, iliac or obturator lymph node involvement in CLND. In addition, we reviewed files of melanoma patients who were surgically treated for palpable inguinal metastases in the same time period.

Patients and methods

Patients

The files of all 743 consecutive and prospectively enrolled patients with primary cutaneous melanoma stage I and II who were treated with SLNB at the Institute of Oncology, Ljubljana, Slovenia between January 2001 and December 2007 were reviewed retrospectively in our study. Positive inguinal SLN was detected in 58 patients (32 female, 26 male, median age 55 years). In addition, we reviewed files of 94 stage III melanoma patients who were surgically treated for palpable inguinal metastases at our department in the same time period.

The investigators strictly followed recommendations of the Helsinki declaration and of the European Council Convention on Protection of Human Rights in Bio-Medicine.

TABLE 1. Patients' clinicopathological characteristics after positive inguinal SLNB

Characteristic	SLNB group
Total, n	58
Sex, n (%)	
Female	32 (55.2%)
Male	26 (44.8%)
Age, years	
Median	55
Range	7.6-87.1
Primary site, n (%)	
Trunk	11 (19%)
Lower extremity	47 (81%)
Unknown	0 (0%)
Breslow, mm	
Mean	3.66
Median	3.2
Range	1.1-13
0-1, n (%)	0 (0%)
1.01-2, n (%)	14 (24.1%)
2.01-4, n (%)	30 (51.8%)
>4.01, n (%)	14 (24.1%)
Unknown	0 (0%)
Clark, n (%)	
III	11 (19%)
IV	36 (62%)
V	4 (6.9%)
Unknown	7 (12.1%)
Ulceration, n (%)	
Yes	30 (51.7%)
No	21 (36.2%)
Unknown	7 (12.1%)
SLN removed, n	
Mean	1.86
Range	1-4
SLN status, n (%)	
1 micrometastasis	14 (24.1%)
2 micrometastases	2 (3.5%)
2+ micrometastases	16 (27.6%)
Macrometastases	26 (44.8%)
CLND nodes removed, n (mean)	
Inguinal dissection	10.1
Inguino-iliac dissection	19.3

SLNB = sentinel lymph node biopsy; SLN = sentinel lymph node; CLND = completion lymph node dissection

Methods

Preoperatively, ultrasound of the inguinal region was performed in most patients. Criteria for SLNB were as follows: cutaneous melanoma stage I or II thicker than 1 mm or thinner than 1 mm, but with signs of gross regression, ulceration or Clark level IV/V. SLNB and wide local excision were performed using the standard triple technique of preoperative lymphoscintigraphy using ^{99m}Tc radiolabelled nano-colloid, followed by perioperative intradermal injection of Patent blue dye and intraoperative use of a hand-held sterile gamma probe.[10] SLN was defined as the only hot and/or blue node, the hot and/or blue node receiving afferent lymphatic channel from the tumour and the hot and/or blue node which was the first one in sequential pattern.

The SLN was examined histopatologically by using routine HE and immunohistochemical stain-

TABLE 2. Patients' clinicopathological characteristics after palpable inguinal metastases

Characteristic	Palpable metastases
Total, n	93
Sex, n (%)	
Female	53 (57%)
Male	40 (43%)
Age, years	
Median	66
Range	18-75
Primary site, n (%)	
Trunk	9 (10%)
Lower extremity	71 (76%)
Unknown	13 (14%)
Breslow, mm	
Mean	4.58
Median	3.45
Range	0.5 - 25
0-1, n (%)	7 (7%)
1.01-2, n (%)	12 (13%)
2.01-4, n (%)	22 (24%)
>4.01, n (%)	26 (28%)
Unknown	26 (28%)
Clark, n (%)	
III	14 (15%)
IV	34 (37%)
V	7 (7%)
Unknown	33 (36%)
Ulceration, n (%)	
Yes	26 (28%)
No	9 (10%)
Unknown	58 (62%)
Palpable nodes positive, n	
Mean	3.45
Range	2-26
LND nodes removed, n (mean)	
Inguinal dissection	12.9
Inguino-iliac dissection	16.7

LND = lymph node dissection

ing for S-100 protein and HMB-45 antigen as previously reported.[10] Briefly, SLN were bisected, fixed in formalin and embedded in paraffin. A maximum of 8 sections of each half were made, odd sections were stained with routine HE and even sections were immunohistochemically stained for S-100 except for the section 6 which was immunohistochemically stained for HMB45. For the purpose of our study the definitions of micrometastases and macrometastases are metastatic deposits within SLN smaller or equal to (≤) 2 mm and larger than (>) 2 mm, respectively. We acknowledge that this is in contrast to the current TNM classification where micrometastases and macrometastases are defined as clinically non palpable and palpable metastatic nodes respectively.[11] A cluster of cells (10 - 30 grouped cells) or isolated tumour cells (up to 20 individual cells) were also defined as micrometastasis.[12] The number of micrometastases and macrometastases was also recorded.

Every patient with metastatic inguinal LN underwent a (C)LND of the involved nodal basin regardless of the metastasis size (palpable or non-palpable, identified at the SLNB) or number. Inguinal or inguino-iliac/obturator lymph node dissection was performed depending on surgeon's personal decision, guided mostly by the age and performance status of the patient. The metastatic involvement of non-sentinel inguinal, iliac or obturator lymph nodes was recorded. The nodes in the CLND specimens were evaluated by the routine HE technique. Adjuvant radiotherapy was given to the patients with more than 3 cm metastatic nodes, with more than 3 metastatic nodes or with metastatic extra capsular extension.

Statistical analysis

Numerical variables are presented by its mean, median, followed by minimum and maximum values. Attributive data are described as the absolute numbers with corresponding relative frequencies. The overall survival rates were analysed using Kaplan-Meier method.[13] Log-rank test was used to test the equality of the overall survival curves from the time of diagnosis until death of any cause. Chi-squared test was used to determine the statistical significance of the association between inguinal SLN histology and CLND status. All tests were two-sided. A p value of less than 0.05 was considered statistically significant. The statistical analysis was performed using the SPSS/PC software package (version 13.0. for Windows).

Results

Inguinal metastases detected after SLNB

Between January 2001 and December 2007, all lymphatic basins SLNB were performed in 743 patients. Overall, positive inguinal SLN was detected in 58 cases. Median follow-up of these SLN positive patients was 1.87 years (range 0.76-7.17). Clinicopathological characteristics of the patients with positive inguinal SLN are given in Table 1 and additional data for 93 patients with palpable inguinal metastases are given in Table 2.

Twenty-six (44.8%) patients had macrometastases in the inguinal SLN. Micrometastases (includ-

TABLE 3. Association between CLND negative and positive patients divided according to micrometastases and macrometastases

	CLND negative	CLND positive	Total
micrometastases	31	1	32
macrometastases	16	10	26
Total	47	11	58

Chi-square, $p = 0.01$; CLND = completion lymph node dissection

TABLE 4. Studies reporting on SLN characteristics predictive for the absence of additional metastases in non-sentinel lymph nodes

Author	N	SLN characteristic(s)
Carlson *et al.* 2003[14]	104	Not found
Cochran *et al.* 2004[17]	90	Tumour area <1%
Dewar *et al.* 2004[18]	146	Subcapsular location
Vuylsteke *et al.* 2005[19]	71	Breslow <2.5mm, tumour load <0.3mm^2
van Akkooi *et al.* 2006[16]	77	Micrometastases <0.1mm
Glumac *et al*. 2008[7]	74	Single micrometastasis <2mm

N = Number of patients with positive SLN; SLN = sentinel lymph node

ing clusters of cells and isolated tumour cells) in inguinal SLN were detected in 32 (55.2 %) patients.

The patients with micrometastases were divided into three groups on the basis of the micrometastases number in the inguinal SLN: there were 14 patients with single micrometastasis, 2 patients with double micrometastases in one node, and 16 patients with more than two micrometastases in one or more lymph nodes (Table 1). Inguinal or inguino-iliac/obturator CLND was performed in all patients depending on surgeon's personal decision, guided mostly by the age and performance status of the patient.

Out of 14 patients with solitary and 2 patients with double micrometastases, all were without additional metastases in non-sentinel lymph nodes regardless of the type of CLND performed. Out of 16 patients with 3 or more micrometastases, only 1 had additional positive non-sentinel lymph nodes. Altogether, there were 11 patients with metastases in non-sentinel lymph nodes; 1 had multiple micrometastases in the inguinal SLN and 10 had macrometastases in the inguinal SLN. The difference between CLND negative and positive groups of patients, divided according to inguinal SLN tumour burden, was statistically significant with Chi-square p value of 0.01 (Table 3).

Inguinal CLND was performed in 40/58 (69%) patients. The median follow up in this group was 1.59 years (range 0.76-5.69). Seven patients had positive non-sentinel nodes (5 patients had 1 positive non-sentinel node, 1 patient had 2 and 1 patient had 4 positive non-sentinel nodes). Out of those 7 patients, 6 were disease free upon follow up and 1 died with gross melanosis of the leg without systemic progress.

Inguino-iliac/obturator CLND was performed in 18/58 (31%) patients. The median follow up of these patients was 2.71 years (range 0.83-7.17). Four patients had positive non-sentinel nodes (3 patients had 1 positive non-sentinel node and 1 patient had 5 positive non-sentinel nodes). Out of those 4 patients, 3 were disease free upon follow up and 1 died from systemic progress.

Adjuvant postoperative radiotherapy was given to 2 patients (3.5%). Additional 17 patients (29.3%) received palliative radiotherapy later in time due to disease progression.

Not surprisingly, the log rank test of Kaplan-Meier survival curves showed a statistically significant better survival (Figure 1, $p = 0.032$) for patients with SLN micrometastases (91.5% overall survival at 2 years, CI 84.1 % - 98.9%, median follow up 2.5 years) compared to patients with SLN macrometastases (64.0% overall survival at 2 years, CI 50.3% - 77.7%, median follow up 1.6 years).

On the other hand, there was no statistical difference after log rank test of Kaplan-Meier survival curves ($p = 0.604$) for patients after inguinal CLND compared to patients after inguino-iliac/obturator CLND.

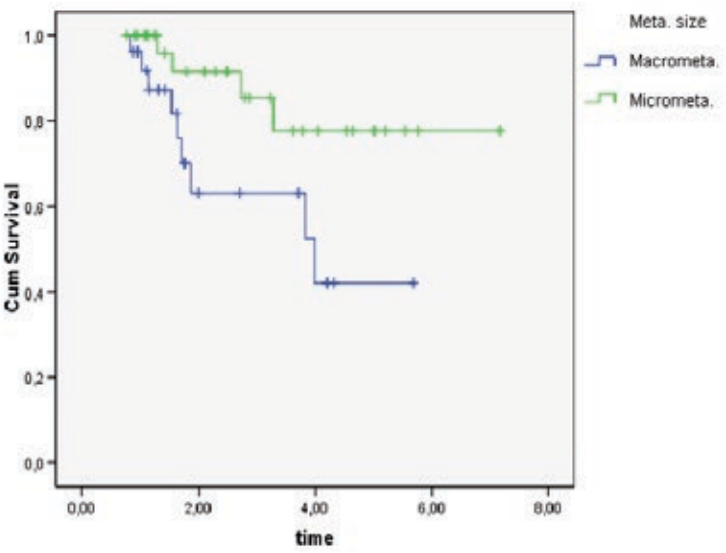

SLN = sentinel lymph node

FIGURE 1. The log rank test of Kaplan-Meier overall survival curves for patients with SLN micrometastases compared to patients with SLN macrometastases (p = 0.032).

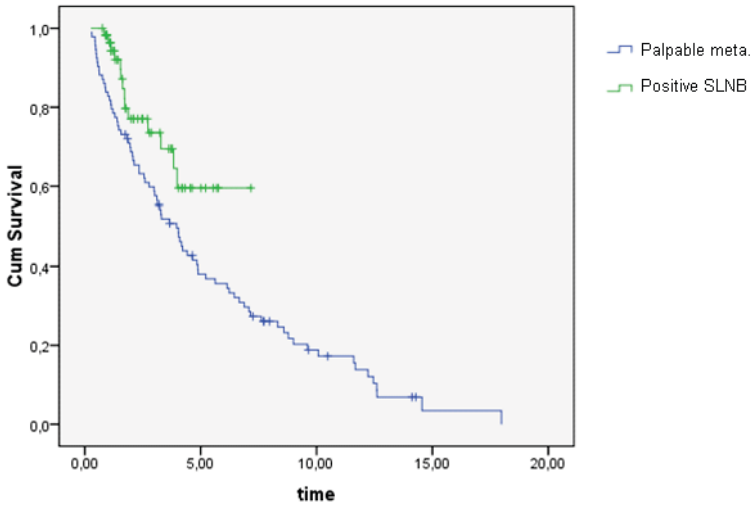

SLN = sentinel lymph node

FIGURE 2. The log rank test of Kaplan-Meier overall survival curves for patients after positive inguinal SLN compared to patients after palpable inguinal metastases (p = 0.028).

Palpable inguinal metastases

In addition, there were 93 stage III melanoma patients who were surgically treated for palpable inguinal metastasis in the same time period. Inguinal LND was performed in 21/93 (23%) patients while inguino-iliac/obturator LND was performed in 72/93 (77%). There was not any statistical difference in the log rank test of Kaplan-Meier survival curves (p = 0.420) between patients when comparing the type of dissection performed after palpable inguinal metastases.

On average, there were 3.45 positive LN after palpable inguinal metastases while there were only 1.28 positive LN after positive inguinal SLNB (Tables 1 and 2). There were 21/93 (22.6%) patients with positive iliac/obturator LN after palpable inguinal metastases while there were only 3/58 (5.2%) patients with positive iliac/obturator LN after positive inguinal SLNB.

The log rank test of Kaplan-Meier survival curves showed a statistically significant better overall survival (Figure 2, p = 0.028) for patients with positive inguinal SLNB (77.1% survival at 2 years, CI 64.4% - 89.8%, median follow up 1.9 years) than for patients with palpable inguinal metastases (70.5% survival at 2 years, CI 60.3% - 807%, median follow up 3.3 years).

Discussion

As we have shown in our previous study, metastases in non-sentinel lymph nodes in patients with micrometastases in SLN are a rare event regardless of the lymphatic region. In fact, no patient with a single SLN micrometastasis in any region had metastases in CLND.[7]

Our study focused on the rates of inguinal, iliac and obturator non-sentinel metastatic involvement in relation to micrometastases, macrometastases and number of micrometastases in the inguinal SLN.

Due to CLND associated morbidity, such as scarring, limb oedema, seroma formation, paresthesias and deterioration of pre-existing medical co-morbidities, identification of patients without non-sentinel lymph node involvement would be of great clinical importance. Specifically in the inguinal region, the pattern of non-sentinel lymph node involvement of inguinal, iliac and obturator nodes is of great interest, due to possibility of omitting the iliac/obturator part of the CLND.

We observed that more than half (55.2%) of the positive SLN were micrometastatic, which presents a rather high percentage, yet similar to the results reported by other authors.[14] This fact might be explained by the selection of patients because the majority of our patients underwent preoperative ultrasound of the inguinal region, thus detecting at least some larger metastases that are otherwise too small to be palpated.

In 14 cases, SLN micrometastases were single, while in 2 they were double, and in 16 multiple. We observed that no patient with any microme-

tastases or a single SLN macrometastasis had any iliac/obturator non-sentinel metastases after CLND. Furthermore, no patient with single SLN micrometastasis had any non-sentinel metastases at all after CLND. Statistically, the difference in finding additional positive nodes after CLND between the groups with inguinal SLN micrometastases and macrometastases was statistically significant (p = 0.01) confirming the fact that the obvious difference between the mentioned groups is not a coincidence.

Iliac/obturator CLND might be avoided after detecting a single macrometastasis or any micrometastases in the inguinal SLN and CLND of any type might be avoided after detecting a single micrometastasis in the inguinal SLN. These statements are additionally supported (although clearly not proven) by the absence of statistically significant survival difference between Kaplan-Meier survival curves (p = 0.604) for patients after inguinal CLND compared to patients after inguino-iliac/obturator CLND in the SLNB positive patients and even in patients with palpable inguinal melanoma metastases. Another fact supporting our proposal for omitting the iliac/obturator part of CLND after micrometastases in SLN is that out of 7 patients with additional metastases after only inguinal CLND, 6 were disease free upon last follow up and 1 died with gross melanosis of the leg without systemic progress.

On the other hand, we found iliac/obturator metastases in 21% of patients with palpable inguinal melanoma metastases and there was statistical difference in survival between patients with positive inguinal SLNB and palpable inguinal metastases (Figure 2). Hence, full inguino-iliac/obturator LND is still recommended after finding palpable inguinal metastases.

One of the first researchers to deal with the subject of non-sentinel metastases was Starz *et al.* in 2001.[15] His group tried to predict non-sentinel node involvement by creating so called ''S classification'' using two morphometric parameters: the number of tumour-involved, 1-mm slices of the SLN and the centripetal depth of metastatic cell invasion. Their otherwise quite complicated system of classification has shown that there are no further metastases when SLN metastasis is less or equal to 1 mm and located peripherally. The Eggermont study revealed a group of patients with sub-micrometastases (< 0.1 mm) that had no non-sentinel metastases and are thus unlikely to benefit from CLND.[16] Similarly, other authors are trying to determine which SLN characteristics prognosticate no further metastases to non-sentinel lymph nodes (Table 4). Vuylsteke *et al.* found this to be primary cutaneous melanoma with Breslow thickness of 2.5 mm or less and the surface of metastases in SLN of 0.3 mm^2 or less.[19] Dewar *et al.* described it as only subcapsular localisation of metastases in SLN[18] and Cochran *et al.* reported it as a relative metastases surface to SLN surface of 1% or less.[17] In contrast, Carlson *et al.* were unable to predict no involvement to non-sentinel lymph nodes by any known parameter.[14] The difference between Carlson's study and ours is that we subdivided micrometastases to single, double or multiple micrometastases that yielded the group of single micrometastasis that had no additional metastases in non-sentinel lymph nodes. Through the literature review we did not find any author who dealt specifically with the pattern of non-sentinel metastasis after a positive inguinal SLN.

At present, we feel that, after micrometastases in the inguinal SLN are detected, iliac/obturator CLND can be omitted. However, this question needs to be addressed in a properly designed prospective trial.

References

1. Morton DL, Wen DR, Wong JH, Economou JS, Cagle LA, Storm FK, et al. Technical details of intraoperative lymphatic mapping for early stage melanoma. *Arch Surg* 1992; **127:** 392-9.
2. Momennezhad M, Zakavi SR, Kakhki VRD, Jangjoo A, Ghavamnasiri MR, Sadeghi R. Scatterogram: a method for outlining the body during lymphoscintigraphy without using external flood source. *Radiol Oncol* 2011; **45:** 184-8.
3. Polom K, Murawa D, Michalak M, Murawa P. Sentinel node biopsy in breast cancer using infrared laser system first experience with PDE camera. *Rep Pract Oncol Radiother* 2011; **16:** 82-6.
4. Cochran AJ, Balda BR, Starz H, Bachter D, Krag DN, Cruse CW, et al. The Augsburg Consensus. Techniques of lymphatic mapping, sentinel lymphadenectomy, and completion lymphadenectomy in cutaneous malignancies. *Cancer* 2000; **89:** 236-41.
5. Pilko G, Zgajnar J, Music M, Hocevar M. Lower tumour burden and better overall survival in melanoma patients with regional lymph node metastases and negative preoperative ultrasound. *Radiol Oncol* 2012; 46(3): 258-264.; **46:** 60-8.
6. Hughes TM, A'Hern RP, Thomas JM. Prognosis and surgical management of patients with palpable inguinal lymph node metastases from melanoma. *Br J Surg* 2000; **87(7):** 892-901.
7. Glumac N, Hocevar M, Zadnik V, Snoj M. Sentinel lymph node micrometastasis may predict non-sentinel involvement in cutaneous melanoma patients. *J Surg Oncol* 2008; **98:** 46-8.
8. McMasters KM, Wong SL, Edwards MJ, Chao C, Ross MI, Noyes RD, et al. Frequency of nonsentinel lymph node metastasis in melanoma. *Ann Surg Oncol* 2002; **9:** 137-41.
9. van der Ploeg IM, Kroon BB, Valdés Olmos RA, Nieweg OE. Evaluation of lymphatic drainage patterns to the groin and implications for the extent of groin dissection in melanoma patients. *Ann Surg Oncol* 2009; **16:** 2994-9.
10. Hocevar M, Bracko M, Pogacnik A, Vidergar-Kralj B, Besic N, Zgajnar J. Role of imprint cytology in the intraoperative evaluation of sentinel lymph nodes for malignant melanoma. *Eur J Cancer* 2003; **39:** 2173-8.

11. Balch CM, Buzaid AC, Soong SJ, Atkins MB, Cascinelli N, Coit DG, et al. Final version of the American Joint Committee on Cancer staging system for cutaneous melanoma. *J Clin Oncol* 2001; **19:** 3635-48.

12. Hermanek P, Hutter RV, Sobin LH, Wittekind C. International Union Against Cancer. Classification of isolated tumor cells and micrometastasis. *Cancer* 1999; **86:** 2668-73.

13. Kaplan EL, Meier P. Non-parametric estimation for incomplete observations. *J Am Stat Assoc* 1958; **53:** 457-81.

14. Carlson GW, Murray DR, Lyles RH, Staley CA, Hestley A, Cohen C. The amount of metastatic melanoma in a sentinel lymph node: does it have prognostic significance? *Ann Surg Oncol* 2003; **10:** 575-81.

15. Starz H, Balda BR, Krämer KU, Büchels H, Wang H. A micromorphometry-based concept for routine classification of sentinel lymph node metastases and its clinical relevance for patients with melanoma. *Cancer* 2001; **91:** 2110-21.

16. van Akkooi AC, de Wilt JH, Verhoef C, Schmitz PI, van Geel AN, Eggermont AM, et al. Clinical relevance of melanoma micrometastases (<0.1 mm) in sentinel nodes: are these nodes to be considered negative? *Ann Oncol* 2006; **17:** 1578-85.

17. Cochran AJ, Wen DR, Huang RR, Wang HJ, Elashoff R, Morton DL. Prediction of metastatic melanoma in nonsentinel nodes and clinical outcome based on the primary melanoma and the sentinel node. *Mod Pathol* 2004; **17:** 747-55.

18. Dewar DJ, Newell B, Green MA, Topping AP, Powell BW, Cook MG. The microanatomic location of metastatic melanoma in sentinel lymph nodes predicts nonsentinel lymph node involvement. *J Clin Oncol* 2004; **22:** 3345-9.

19. Vuylsteke RJ, Borgstein PJ, van Leeuwen PA, Gietema HA, Molenkamp BG, Statius Muller MG, et al. Sentinel lymph node tumor load: an independent predictor of additional lymph node involvement and survival in melanoma. *Ann Surg Oncol* 2005; **12:** 440-8.

case report

Intensity modulated radiation therapy (IMRT) for the treatment of unicentric Castlemans disease: a case report and review of the use of radiotherapy in the literature

Chance Matthiesen, Rajeev Ramgopol, Jonathan Seavey, Salahuddin Ahmad, Terence Herman

Department of Radiation Oncology, University of Oklahoma Health Sciences Center, Oklahoma City, OK, USA

Radiol Oncol 2012; 46(3): 265-270.

Received 25 September 2011
Accepted 17 October 2011

Correspondence to: Chance Matthiesen M.D., Department of Radiation Oncology, Peggy and Charles Stephenson Oklahoma Cancer Center, 800 N.E. 10th Street, OKCC L100, Oklahoma City, OK 73104, USA. Phone: +1 405-271-3016; Fax: +1 405-271-8297; E-mail: chance-matthiesen@ouhsc.edu

Disclosure: No potential conflicts of interest were disclosed.

Background. Surgical resection is considered standard therapy for cases of resectable unicentric Castleman's disease (UCD). Unresectable cases of UCD do not have a consensus regarding the optimal treatment approach, but have utilized steroids, observation, chemotherapy, and radiotherapy. Here we discuss a patient presentation of UCD treated with an advanced radiotherapy technique, IMRT.

Case report. A 47 year old female was found to have an intra-thoracic posterior UCD and was determined not to be a good surgical candidate. She was referred for radiotherapy and was treated using IMRT to a total dose of 4320 cGy in 180 cGy fractions including a scheduled 10 day break. Following the break, the patient's treatment was replanned at which the initial treatment volume was reduced by 50.9% for the duration of the treatment course. Radiation Therapy Oncology Group (RTOG) grade III pneumonitis developed which was managed medically. Neither disease progression nor late effects have occurred.

Conclusions. The use of IMRT and planned treatment break was successful in the treatment of a case of UCD, and should be considered for other unresectable cases.

Key words: Castleman's disease; IMRT

Introduction

Castleman's Disease (CD) was first described in 1954 and further characterized in 1956 by Benjamin Castleman when he reported on 13 cases of localized mediastinal lymphoid hyperplasia.[1] CD, also known as angiofollicular lymph node hyperplasia or giant lymph node hyperplasia, is a rare disorder of unknown etiology. As originally described, CD was a localized disease limited to a single lymph node, which is now referred to as Unicentric Castleman's Disease (UCD). In 1978, Gaba *et al.* recognized the multicentric Castleman's disease manifestation (MCD).[2] Little is understood regarding the pathogenesis of CD. An association was noted between human herpes virus 8 (HHV-8), human immunodeficiency virus (HIV), and MCD. This association has fueled theories as to the pathology of MCD, but has contributed little to the understanding of UCD or HHV-8 negative MCD.[3-5]

Clinically, UCD tends to be asymptomatic and is frequently diagnosed incidentally. MCD frequently presents with systemic manifestations at presentation such as fever, weight loss, diaphoresis, and fatigue. The disease progression of CD has been described as ranging from indolent to fulminant.[6] Additionally, CD has been associated with increased risk of lymphoma, amyloidosis,

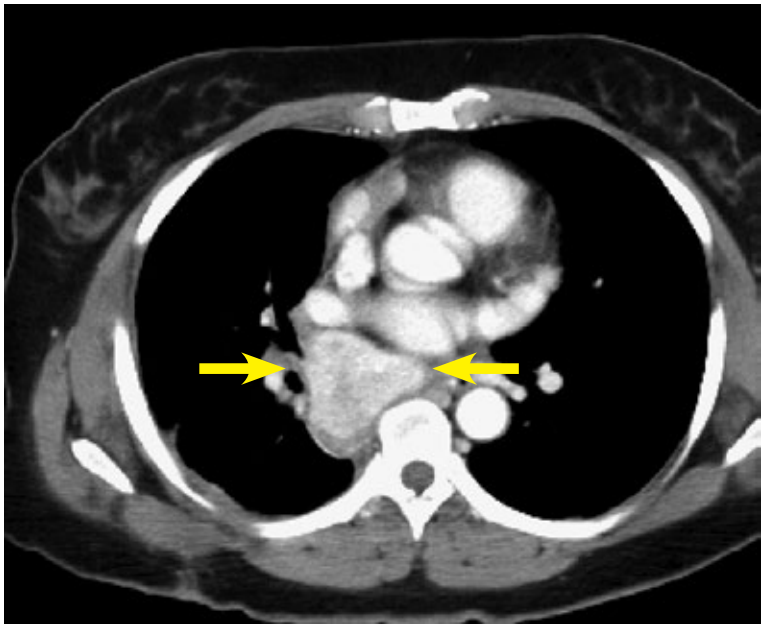

FIGURE 1. CT of patient at initial presentation with a mass noted in the posterior right mediastinum.

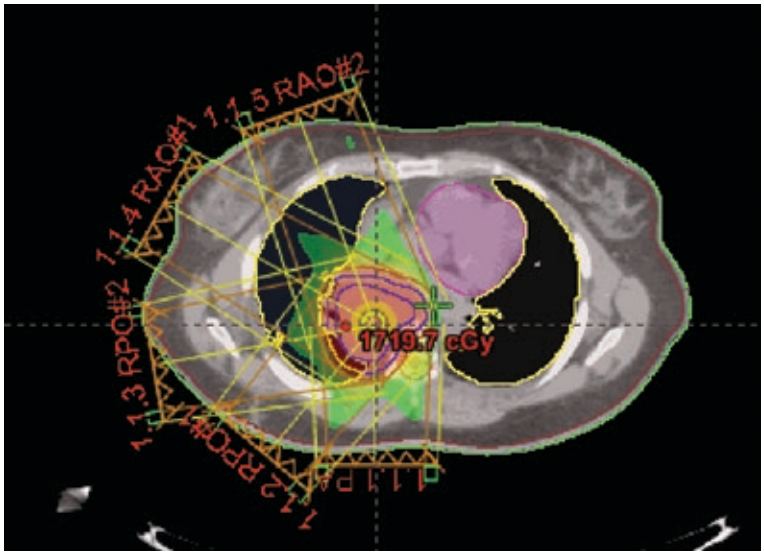

FIGURE 2. Illustration of the contoured mass and five field (1.1.1-1.1.5) coplanar beam arrangements for the IMRT treatment plan.

renal insufficiency, and POEMS (polyneuropathy, organomegaly, endocrinopathy, monoclonal gammopathy, skin changes) syndrome which has sometimes guided treatment decisions.[6,7]

Standard treatment guidelines are lacking, and there is a paucity of evidence owing to the rarity and heterogeneity of the disease. Literature has been limited to mostly case reviews and a few small case-series. Surgery is considered standard therapy for resectable UCD with several case reports and retrospective series reporting excellent local control and cure rates.[8-10] An alternative successful treatment approach for UCD has included the use of radiotherapy.[11-14] Other treatment approaches have included steroids, observation, chemotherapy, and combinations of the above mentioned modalities.[13,15] Unresectable cases of UCD do not have a consensus regarding the optimal treatment approach.[14] The treatment for MCD is even less understood and is beyond the scope of this paper. This paper reviews and illustrates a case of UCD that was incidentally found and treated with primary radiotherapy, specifically intensity modulated radiation therapy (IMRT). Furthermore, we aim to review and summarize prior reports regarding the use of radiotherapy.

Case report

Patient presentation

The patient is a 47 year old Native American female without significant past medical history or known CD risk factors who presented after being critically injured in a motor vehicle accident. During her trauma evaluation and stabilization, a posterior mediastinal mass was noted as shown in Figure 1. She was taken to the operating room for multiple internal injuries necessitating surgical repair. Visualization of the mass was noted but was not attended to at that time. After a several month recovery, she returned to the thoracic surgeon for follow-up and further workup of the mass. Biopsy was performed via mediastinoscopy and pathology results revealed angiofollicular lymph node hyperplasia, consistent with CD. CT and PET-CT scans were performed which showed the mass to be 5.5 cm x 4.6 cm with a peak SUV of 5.3. Due to the location of the mass and history of recent prior surgery, she was determined not to be a good candidate for complete surgical resection. She was then referred to consider radiotherapy treatment options.

Treatment

Treatment simulation was performed in the supine position and immobilization via a vac-lock. Treatment planning was performed on Eclipse External Beam Planning 7.5.51 (Varian Medical Systems, Palo Alto CA). Given the midline, posterior location of the mass, IMRT was utilized to reduce the dose gradient and toxicity to the surrounding normal tissues. The gross tumor volume (GTV) was

contoured and expanded 5 mm to create the planning target volume (PTV). The patient was treated to a total dose of 4320 cGy. RT was delivered in nine initial once daily fractions of 180 cGy to a total dose of 1620. She was then placed on a 10 day break followed by re-simulation and treatment planning. She then completed the total 4320 cGy dose prescription without interruption in 180 cGy once daily fractions. Radiation therapy (RT) beam arrangements are shown in Figure 2. The initial PTV volume was 235.7 cm^3 and the re-CT PTV following treatment break was reduced to 120 cm^3, a reduction of approximately 50.9%. Cumulative dose volume constraints allowed the mean total lung dose to be limited to 961 cGy and the 20% volume to be limited to 1706 cGy. The heart was limited to a mean dose of 939 cGy, and the expanded cord mean to 1163 cGy. Dose volume histograms of each plan (pre and post treatment break) and a cumulative plan sum are shown in Figures 3, 4, and 5. A summary of mean and max dose statistics is shown in Table 1. No acute side effects were noted during treatment.

Follow-up

At a follow-up of ten months, the patient has had no disease progression. She did develop RTOG grade III pneumonitis at three months follow-up which was managed by steroids. Follow-up PET-CT (Figure 6) showed the mass to be stable at 3.9 cmx 5.1 cm and SUV values to be at background. No late effects have occurred.

Discussion

Consensus suggests that the optimal treatment approach for patients presenting with UCD has been surgical resection, as cure rates following this approach are near 100%.[8-10] The most well-known evidence for this is from a retrospective report of sixty-one patients with UCD treated with surgery and followed for twenty years.[16] This report illustrated that complete resection offered the best chance of cure. Other reports have shown that partial resections can ameliorate constitutional manifestations in symptomatic patients; however, documented recurrences did occur more than nine years post resection so continued follow-up is necessary.[12,13]

The approach and treatment of unresectable UCD is not standardized, as methods including combinations of observation, steroids, surgery, chemotherapy, and radiotherapy in multiple set-

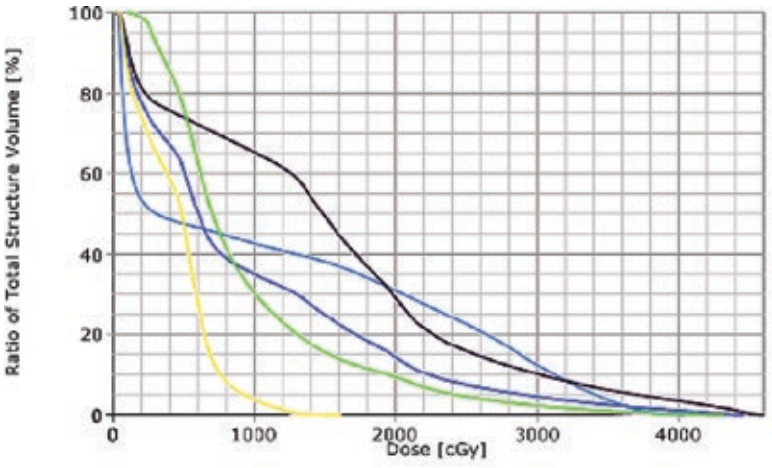

FIGURE 3. DVH of initial IMRT treatment plan. Line colors as follows: Orange - Spinal Cord, Pink - Heart, Yellow - Total Lung, Green - Right Lung, Blue - Left Lung.

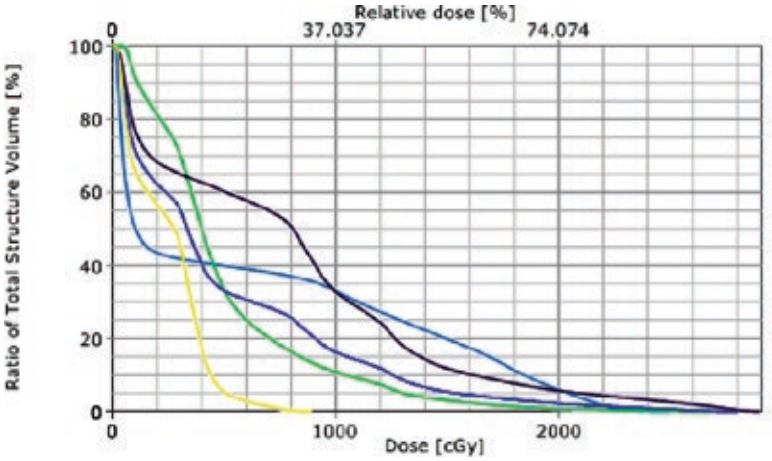

FIGURE 4. DVH of post treatment break IMRT treatment plan. Line colors as follows: Orange - Spinal Cord, Pink - Heart, Yellow - Total Lung, Green - Right Lung, Blue - Left Lung.

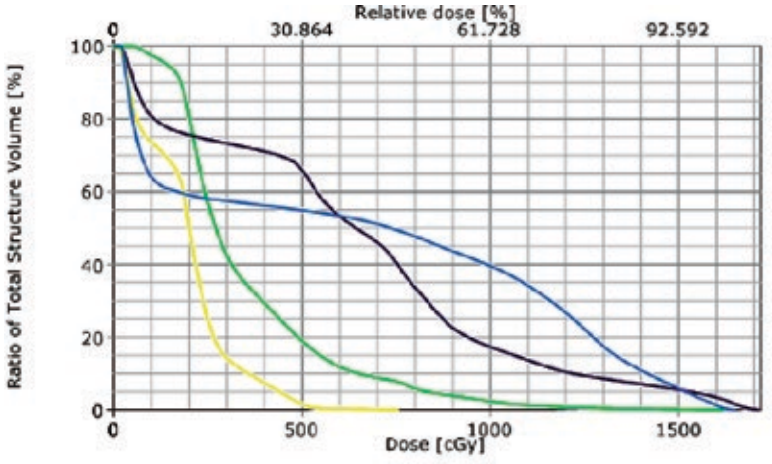

FIGURE 5. DVH of Cumulative IMRT treatment plans. Line colors as follows: Orange - Spinal Cord, Pink - Heart, Yellow - Total Lung, Green - Right Lung, Blue - Left Lung.

Table 1. Organs at risk and the mean and max dose values for each individual treatment plan and cumulative plan.

Organ	Initial Plan Dose (cGy)	Replan Dose (cGy)	Cumulative Dose (cGy)
Spinal Cord	Mean (672), Max(1656)	Mean (633), Max(2493)	Mean (1163), Max(4057)
Right Lung	Mean (638), Max(1717)	Mean (780), Max(2908)	Mean (1496), Max(4609)
Left Lung	Mean (196), Max(761)	Mean (246), Max(895)	Mean (447), Max(1617)
Total Lung	Mean (394), Max(1663)	Mean (504), Max(2813)	Mean (961), Max(4476)
Heart	Mean (355), Max(1622)	Mean (501), Max(2686)	Mean (939), Max(4335)

FIGURE 6. CT at four months post-RT. The mass is noted to be smaller.

tings have been utilized.[14] Additional reports have commented on the use of radiotherapy.[11-14,17,18] To the best of our knowledge, no previous reports have commented on the use of IMRT, which is now used routinely for diseases involving the thorax such as lymphoma and cancers of the lung and esophagus as well as for other localisations.[19-24]

In our report we illustrated the successful use of IMRT for a case of unresectable UCD. Previous reports have utilized cumulative doses ranging from 12 to 50 Gy[11,12], with lower doses resulting in disease remission in some cases,[25-28] but failure in others.[2,16,29] A prior review of the literature[14], showed no correlation between dose and response when using primary radiotherapy.

Neuhof and Debus reported on five patients treated with radiotherapy with doses ranging from 40-46 Gy.[11] Four patients were alive at analysis and all four achieved disease stabilization, or a partial / complete response to radiotherapy. Treatment was well tolerated with the exception of one patient who developed acute grade III skin reactions, followed by stenosis of the trachea, esophagus, and bronchus. Treatment technique in this patient was 3D conformal planning.

Chronowski *et al.* reported on 21 CD patients.[12] Twelve had UCD of which four were treated with radiotherapy. All four responded favorably to treatment, with three complete responses to radiotherapy and one partial response. At analysis, two were disease free and the other two had died of unrelated causes. Radiotherapy doses ranged from 39.6 to 40 Gy at 1.8 and 2 Gy fractionation. No comments of toxicity were reported.

De Vries *et al.* reported the use of neoadjuvant radiotherapy for a case of unresectable UCD.[14] In their technique, they used a conventional approach for a lesion in the abdomen treated in 2 Gy fractions to 40 Gy. A 10 Gy intraoperative boost was applied at the time of surgery. No radiotherapy complications were reported. They concluded a neoadjuvant approach could be applied to other cases of UCD.

In our report, we describe the use of IMRT for UCD. To our knowledge, no previous reporting of this technique for CD is in the literature. IMRT has been well studied and known to be effective for diseases involving the chest to allow radiotherapy dose escalation with minimization of normal tissue toxicity.[20,21,30,31] Additionally, we introduce the application of a treatment break during radiotherapy to allow for tumor size reduction. Given the lymphoid nature of CD, and the known apoptotic response of lymphoid tissues to radiotherapy[32], a reduction of tumor size in CD could reasonably be expected. In our case, we treated the tumor mass to 1620 cGy, then allowed a for10 day break followed by re-simulation and treatment planning. As a result, the initial PTV was reduced by approximately 50.9%. This PTV volume reduction resulted in further dose minimization to the normal lungs, esophagus, and spinal cord following IMRT

treatment replan. Although a dosimetric comparison of radiotherapy techniques is not the intent of this discussion, it should be understood that the use of IMRT is more optimal versus 3D conformal techniques to achieve these results. Furthermore, it should be noted that IMRT can allow greater dose escalation for such tumors; though no evidence is available supporting such a decision. Other modern photon techniques which could be considered include arc therapy and tomotherapy, as in certain situations these techniques may be able to provide an improved normal tissue toxicity dose reduction or more rapid treatment administration. As proton therapy becomes more available, such patients and lesion locations may be most optimally treated by this method to benefit from the proton beam dose characteristics of the Bragg peak. Since unicentric CD often appears in younger patients[11], methods and techniques to limit normal tissue dose should always be taken into consideration.

Conclusions

The dosimetric advantages of IMRT make it a suitable treatment approach for unresectable UCD. A treatment break during therapy should also be considered depending upon lesion location and patient characteristics to further reduce treatment target volumes and improve the dose gradients to the normal tissue.

Clinical practice points

The approach and treatment of unresectable UCD is not defined, as methods including combinations of surgery, chemotherapy, and radiotherapy in multiple settings have been utilized. Additional reports have commented on the successful use of radiotherapy. No previous reports have commented on the use of IMRT, which is now used routinely for diseases involving the thorax such as lymphoma and of the lung and esophagus. The dosimetric advantages of IMRT make it a suitable treatment approach for unresectable UCD. In our report, we highlighted the successful use of IMRT for an unresectable mediastinal mass in a younger patient with UCD. We also described the application of a planned treatment break followed by resimulation and replan of the treatment course. Such an approach allowed the planning treatment volume to be reduced by 50.9% which subsequently allowed greater normal tissue sparing and dose reduction. At follow-up, the patient has had a partial response to radiotherapy and disease stabilization. Therefore, we suggest that the use of IMRT should be considered for unresectable unicentric Castleman's disease and the implementation of a treatment break should be considered.

References

1. Castleman B, Iverson L, Menendez VP. Localized mediastinal lymphnode hyperplasia resembling thymoma. *Cancer* 1956; **9:** 822-30.
2. Gaba AR, Stein RS, Sweet DL, Variakojis D. Multicentric giant lymph node hyperplasia. *Am J Clin Pathol* 1978; **69:** 86-90.
3. Soulier J, Grollet L, Oksenhendler E, Miclea JM, Cacoub P, Baruchel A, et al. Molecular analysis of clonality in Castleman's disease. *Blood* 1995; **86:** 1131-8.
4. Soulier J, Grollet L, Oksenhendler E, Cacoub P, Cazals-Hatem D, Babinet P, et al. Kaposi's sarcoma-associated herpesvirus-like DNA sequences in multicentric Castleman's disease. *Blood* 1995; **86:** 1276-80.
5. Gessain A, Sudaka A, Brière J, Fouchard N, Nicola MA, Rio B, et al. Kaposi sarcoma-associated herpes-like virus (human herpesvirus type 8) DNA sequences in multicentric Castleman's disease: is there any relevant association in non-human immunodeficiency virus-infected patients? *Blood* 1996; **87:** 414-6.
6. Herrada J, Cabanillas F, Rice L, Manning J, Pugh W. The clinical behavior of localized and multicentric Castleman disease. *Ann Intern Med* 1998; **128:** 657-62.
7. Casper C. The aetiology and management of Castleman disease at 50 years: translating pathophysiology to patient care. *Br J Haematol* 2005; **129:** 3-17.
8. Seco JL, Velasco F, Manuel JS, Serrano SR, Tomas L, Velasco A. Retroperitoneal Castleman's disease. *Surgery* 1992; **112:** 850-5.
9. McCarty MJ, Vukelja SJ, Banks PM, Weiss RB. Angiofollicular lymph node hyperplasia (Castleman's disease). *Cancer Treat Rev* 1995; **21:** 291-310.
10. Shahidi H, Myers JL, Kvale PA. Castleman's disease. *Mayo Clin Proc* 1995; **70:** 969-77.
11. Neuhof D, Debus J. Outcome and late complications of radiotherapy in patients with unicentric Castleman disease. *Acta Oncol* 2006; **45:** 1126-31.
12. Chronowski GM, Ha CS, Wilder RB, Cabanillas F, Manning J, Cox JD. Treatment of unicentric and multicentric Castleman disease and the role of radiotherapy. *Cancer* 2001; **92:** 670-6.
13. Bowne WB, Lewis JJ, Filippa DA, Niesvizky R, Brooks AD, Burt ME, et al. The management of unicentric and multicentric Castleman's disease: a report of 16 cases and a review of the literature. *Cancer* 1999; **85:** 706-17.
14. de Vries IA, van Acht MM, Demeyere TB, Lybeert ML, de Zoete JP, Nieuwenhuijzen GA. Neoadjuvant radiotherapy of primary irresectable unicentric Castleman's disease: a case report and review of the literature. *Radiat Oncol* 2010; **5:** 7.
15. Peterson BA, Frizzera G. Multicentric Castleman's disease. *Semin Oncol* 1993; **20:** 636-47.
16. Keller AR, Hochholzer L, Castleman B. Hyaline-vascular and plasma-cell types of giant lymph node hyperplasia of the mediastinum and other locations. *Cancer* 1972; **29:** 670-83.
17. Ye B, Gao SG, Li W, Yang LH, Zhao SH, Ma K, et al. A retrospective study of unicentric and multicentric Castleman's disease: a report of 52 patients. *Med Oncol* 2010; **27:** 1171-8.
18. Lin CY, Chang YL. Castleman's disease in the head and neck region: Meta-analysis of reported cases in Taiwan and literature review. *J Formos Med Assoc* 2010; **109:** 913-20.
19. Paumier A, Ghalibafian M, Beaudre A, Ferreira I, Pichenot C, Messai T, et al. Involved-node radiotherapy and modern radiation treatment techniques in patients with Hodgkin lymphoma. Int *J Radiat Oncol Biol Phys* 2011; **80:** 199-205.

20. Welsh J, Gomez D, Palmer MB, Riley BA, Mayankkumar AV, Komaki R, Dong L, et al. Intensity-modulated proton therapy further reduces normal tissue exposure during definitive therapy for locally advanced distal esophageal tumors: A dosimetric study. *Int J Radiat Oncol Biol Phys* 2011 Apr 4. [Epub ahead of print]

21. Lievens Y, Nulens A, Gaber MA, Defraene G, De Wever W, Stroobants S, et al. Intensity-modulated radiotherapy for locally advanced non-small-cell lung cancer: a dose-escalation planning study. *Int J Radiat Oncol Biol Phys* 2011; **80:** 306-13.

22. Banu A, Enis O, Kaan G, Gungor G. Intensity modulated radiotherapy (IMRT) in bilateral retinoblastoma. *Radiol Oncol* 2010; **44:** 194-8.

23. Bailey DW, Lalith K; Podgorsak MB. A fully electronic intensity-modulated radiation therapy quality assurance (IMRT) process implemented in a network comprised of independent treatment planning, record and verify, and delivery systems. *Radiol Oncol* 2010; **44:** 124-30.

24. Śladowska A, Hetnał M, Dymek P, Kabat D, Kisielewicz K, Wawrzak M, et al. Application of IMRT in adjuvant treatment of soft tissue sarcomas of the thigh – preliminary results. *Reports of Practical Oncology and Radiotherapy* 2011; **16:** 110-4.

25. Weisenburger DD, DeGowin RL, Gibson P, Armitage JO. Remission of giant lymph node hyperplasia with anemia after radiotherapy. *Cancer* 1979; **44:** 457-62.

26. Nordstrom DG, Tewfik HH, Latourette HB. Plasma cell giant lymph node hyperplasia responding to radiation therapy. *AJR Am J Roentgenol* 1978; **130:** 169-71.

27. Marti S, Pahissa A, Guardia J, Moragas A, Bacardi R. Multicentric giant follicular lymph node hyperplasia. Favorable response to radiotherapy. *Cancer* 1983; **51:** 808-10.

28. Veldhuis GJ, van der Leest AH, de Wolf JT, de Vries EG, Vellenga E. A case of localized Castleman's disease with systemic involvement: treatment and pathogenetic aspects. *Ann Hematol* 1996; **73:** 47-50.

29. Beck JT, Hsu SM, Wijdenes J, Bataille R, Klein B, Vesole D, et al. Brief report: alleviation of systemic manifestations of Castleman's disease by monoclonal anti-interleukin-6 antibody. *N Engl J Med* 1994; **330:** 602-5.

30. Li X, Wang X, Li Y, Zhang X. A 4D IMRT planning method using deformable image registration to improve normal tissue sparing with contemporary delivery techniques. *Radiat Oncol* 2011; **6:** 83.

31. Chapet O, Fraass BA, Ten Haken RK. Multiple fields may offer better esophagus sparing without increased probability of lung toxicity in optimized IMRT of lung tumors. *Int J Radiat Oncol Biol Phys* 2006; **65:** 255-65.

32. Suciu D. Cellular death by apoptosis in some radiosensitive and radioresistant mammalian tissues. *J Theor Biol* 1983; **105:** 391-401.

Radiol Oncol 2012; 46(3): 179-188.
doi:10.2478/v10019-012-0034-y

PET/CT primarnega prostatičnega raka s 11C-holinom. Povezava s stadijem, z razvrstitvijo po Gleasonu in z biološkimi pokazatelji tumorske agresivnosti

Chen J, Zhao Y, Li X, Sun P, Wang M, Wang R, Jin X

Izhodišča. Vrednosti standardiziranega privzema (VSP) 11C-holina se prekrivajo pri raku prostate in pri benigni prostatični hiperplaziji, zato so mnenja o klinični uporabnosti 11C-holina PET/CT-ja v diagnostiki prostatičnega raka nasprotujoča. V raziskavi smo izmerili maksimalne VSP v prostatičnih spremembah (P) in v medeničnih mišicah (M) ter izračunali razmerje VSPmax P/M. Nato smo želeli ugotoviti, ali obstaja povezava med VSPmax P/M razmerjem za označevalec 11C-holin in stadijem tumorja, razvrstitvijo po Gleasonu in nivojem nekaterih bioloških označevalcev tumorske agresivnosti.

Metode. Pri 26 bolnikih s primarnim prostatičnim rakom smo naredili PET/CT z 11C-holinom. Obenem so bili v tumorskih vzorcih teh bolnikov določeni histopatološki gradusi ter imunohistokemično izražanje Ki-67, CD31, androgenih receptorjev (AR), Her-2/neu, Bcl-2 in PTEN.

Rezultati. Vrednosti VSPmax in razmerja VSPmax P/M niso pokazale statistično značilnih razlik med bolniki s stadijem II in III, pač pa so bile pri bolnikih s stadijem IV značilno višja. Vrednosti razmerja VSPmax P/M so bila značilno višja v spremembah, ki so imela Gleasonov gradus 4+3 ali več od tistih z gradusom nižjim ali enakim 3+4. Razmerje VSPmax P/M je bilo statistično značilno povezano z izražanjem Ki-67, CD31, ob tem pa je bilo višje v skupini bolnikov, katerih tumorske celice so izražali HER-2/neu. Med gradusom tumorja oz. izražanjem bioloških označevalcev in VSPmax pa ni bilo statističnih povezav.

Zaključki. 11C-holin PET/CT z določitvijo razmerja VSPmax P/M bi lahko bila dragocena neinvazivna slikovna metoda v diagnostiki in oceni stadija primarnega prostatičnega raka.

Radiol Oncol 2012; 46(3): 189-197.
doi:10.2478/v10019-012-0020-4

Kombinirana uporaba CT in MR pri ohranjajoči kirurgiji okončin

Xu J, Shen J, Ding Y, Shen HY, Zeng ZP, Ma RF, Li CH, Barden B

Izhodišča. Namen prospektivne klinične raziskave je bil ovrednotiti vrednost kombinirane slikovne uporabe MR in večreznega spiralnega CT pri ohranjajoči kirurgiji okončin onkoloških ortopedskih bolnikov.

Bolniki in metode. Devet bolnikov z malignimi kostnimi tumorji zgornjih ali spodnjih okončin (7 osteosarkomov in 2 hondrosarkoma) smo zdravili z ohranjajočo kirurgijo okončin. Bolnikom smo preoperativno določili nivoje osteotomij in premere protez na osnovi preoperativnih CT in MR slikanj. Histopatološki izvid smo upoštevali kot standardni diagnostični kriterij za vrednotenje natančnosti CT in MR, s katerima smo predhodno določili razširjenost tumorja.

Rezultati. Razširitev tumorja izmerjena z MR je bila primerljiva z dejansko razširitvijo ($p>0,05$, parni Student t test), razširitev izmerjena s CT pa je bila manjša kot dejanska. Dolžina, doslednost in poravnava prizadete okončine so bili pravilno rekonstruirani po operaciji. Pri vseh bolnikih smo dosegli odlično funkcijo.

Zaključki. V raziskavi smo ugotovili, da je MR boljša metoda kot CT za določitev tumorske razširitve, kombinirana uporaba merjenj z MR in CT pa omogoča visoko natančnost za prileganje proteze in odlične funkcionalne rezultate.

Radiol Oncol 2012; 46(3): 198-206.
doi:10.2478/v10019-012-0028-9

Valujoča portalna hitrost z ritmiziranjem: ultrazvočna diferencialna diagnoza in klinična značilnost

Meng Q, Lv L, Yang B, Fu N, Lu G

Izhodišča. Namen raziskave je bil ugotoviti koristnost rutinske ultrazvočne ocene valujoče portalne hitrosti ter jetrnih ven pri diagnozi arterioportalne fistule (APF) in kardiogenega transsinusoidnega šanta (KTŠ).

Bolniki in metode. Pri 282 osebah smo pregledali portalno veno z barvnim in pulznim ultrazvokom Doppler. Za diagnosticiranje APF in KTŠ smo določali krivulje zapisov hitrosti v deblu portalne vene in njenih vejah. V primeru dopplerske diagnoze APF in KTŠ smo za potrditev naredili še ultrazvok srca, ultrazvok srca z uporabo kontrastnega sredstva, CT ali digitalno subtrakcijsko angiografijo. Za oceno hemodinamike smo uporabili največjo hitrost v portalni veni (V_{max}), najmanjšo hitrost (V_{min}), V_{max}/V_{min}, arterijsko največjo sistolno hitrost in indeks upora ter vensko retrogradno in anterogradno hitrost.

Rezultati. Krivulja zapisov hitrosti drenažne portalne vene pri APF je bila tipično arterijska ali bifazna, v obliki sistolnega hepatofugalnega zobca in diastolne hepatopetalne nizke izravnane oblike. Pretok v prizadeti portalni veni je bil pri bolnikih z intrahepatalnim APF vedno hepatofugalen, pri tistih z ekstrahepatalnim APF pa hepatopetalen. Krivulja zapisov hitrosti portalne vene pri bolnikih s KTŠ, zlasti v intrahepatalnih vejah, je pokazala tipično grbasto oblik, z ali brez prehodne hepatofugalne oblike. Rezultati pulzne Doppler preiskave so pokazali povečanje retrogradne faze pretoka v jetrnih venah, s povečanjem hitrosti v dveh fazah.

Zaključki. Krivulje hitrosti pretoka v portalni veni je v primeru suma na APF in KTS potrebno rutinsko ocenjevati, zlasti pri bolnikih z gastrointestinalnimi motnjami.

Radiol Oncol 2012; 46(3): 207-212.
doi:10.2478/v10019-012-0040-0

Katepsin X v serumu bolnikov z rakom črevesja: povezanost z napovedjo poteka bolezni

Vižin T, Christensen IJ, Nielsen HJ, Kos J

Izhodišča. Povečano izražanje lizosomske cisteinske proteaze katepsina X je povezano z motnjami imunskega sistema in nevrodegenerativnimi boleznimi, vloga katepsina X pri nastanku in napredovanju raka pa je manj poznana. Pri malignih procesih so ugotovili povečano izločanje prokatepsina X, zato predpostavljamo, da nivo celokupnega serumskega katepsina X bolje odseva napredovanje bolezni kot pa nivo aktivnega katepsina X.

Bolniki in metode. V retrospektivno študijo smo vključili 77 bolnikov z rakom črevesja. Vzorce krvi smo zbirali pred zdravljenjem. Vrednosti celokupnega katepsina X smo določili s testom ELISA. Kot kontrolne skupine smo vključili zdrave osebe (n=77), bolnike z adenomom (n=77) in bolnike brez neoplastičnih sprememb (n=77).

Rezultati. Nismo dokazali statistično značilnih razlik med bolniki z rakom črevesja ter kontrolnimi skupinami zdravih oseb, bolnikov z adenomom in bolnikov brez neoplastičnih sprememb (p=0,89). Pri bolnikih z rakom črevesja so bile višje vrednosti celokupnega katepsina X značilno povezane s krajšim celokupnim preživetjem (razmerje obetov = 2.08, 95%, interval zaupanja: 1.07-4.05, p=0.028).

Zaključki. Celokupni serumski katepsin X bi lahko služil kot napovedni dejavnik za celokupno preživetje pri bolnikih z rakom črevesja. Njegove povišane vrednosti odražajo bolj agresiven tumorski fenotip in kažejo na vlogo v kasnejših stopnjah napredovanja raka.

Radiol Oncol 2012; 46(3): 213-225.
doi:10.2478/v10019-012-0037-8

Nasproten vpliv rekombinantnega humanega eritropoetina na odgovor celic raka dojk na citotoksične učinke cisplatina

Trošt N, Juvan P, Serša G, Debeljak N

Izhodišča. Humani rekombinantni eritropoetin (rHuEpo) v klinični onkologiji uporabljamo za zdravljenje anemij, ki se razvijejo kot posledica kemoterapije. Ustreznost rHuEpo terapije pri rakavih bolnikih je postala vprašljiva, potem ko so nekatere klinične študije pokazale njene negativne učinke za preživetje bolnikov. Namen raziskave je bil določiti občutljivost celic raka dojk na rHuEpo oziroma opredeliti njegovo vlogo na izražanje genov po izpostavitvi na cisplatin (cDDP).

Meteriali in metode. Celični liniji MCF-7 in MDA-MB-231, ki se razlikujeta glede na izražanje estrogenskega (ER) in progesteronskega (PR) receptorja ter v statusu *p53*, smo izpostavili rHuEpo za 24 ur in pa v 9 zaporednih tednih. Analizirali smo njihov odziv na cisplatin. S testom klonogenosti smo določili proliferacijski nivo celic ter delež njihovega preživetja po izpostavitvi na cDDP. Odzivnost celic na rHuEpo in cDDP smo preverili tudi na nivoju izražanja genov signalne poti *p53*.

Rezultati. 24-urna izpostavitev na rHuEpo je zmanjšala proliferacijo celic raka dojk, a jih je hkrati zaščitila pred citotoksičnostjo cDDP. Dolgotrajna izpostavitev je povečala nivo proliferacije celic MCF-7 ter njihovo občutljivost na cDDP, vendar ni imela nobenega učinka na celice MDA-MB-231. Pri tej celični liniji smo pokazali spremembe v nivoju fosforilacije proteina ERK, kar je nakazovalo na vlogo signalne poti MAPK. Razlike med učinki kratkotrajne in dolgotrajne izpostavitve celic na rHuEpo smo potrdili tudi na nivoju izražanja od *p53*-odvisnih genov ter genov iz družine *bcl-2*; najbolj očitne so bile razlike v izražanju genov *BCL2* in *BAD*.

Zaključki. Proliferacija in preživetje MCF-7 celic sta negativno regulirana z dolžino izpostavitve celic na rHuEpo, medtem ko so MDA-MB-231 celice pri enakih pogojih skorajda neodzivne na rHuEpo. Slednje imajo mutiran p53 in so model ER(+)/PR(-) raka dojk, za katerega so značilni agresivnejši fenotipi. Receptorski (ER/PR^{++}) ter p53 status torej lahko napovesta celični odziv na rHuEpo in cDDP.

RadiolOncol 2012; 46(3): 226-232.
doi:10.2478/v10019-012-0035-x

Protitumorska učinkovitost kombinirane elektrokemoterapije in obsevalnega zdravljenja na tumorskem modelu raka dojke

Raeisi E, Reza Aghamiri SM, Bandi A, Rahmatpour N, Firoozabadi SM, Kafi-abad SA, Mir LM

Izhodišče. Namen študije je bil ugotoviti učinkovitost kombiniranega zdravljenja tumorjev z elektrokemoterapijo in obsevalnim zdravljenjem, pri nizkih dozah obsevanja. Radisensitizacija tumorjev je bila preučevana na velikih duktalnih karcinomskih tumorjih na Balb/c miših.

Materiali in metode. Tumorji, povpečne velikosti 630 mm^3 so bili zdravljeni s cisplatinom, električnimi pulzi, radioterapijo, elektrokemoterapijo, kot samostojne modelitete zdravljenja in v različnih kombinacijah. V kombiniranem zdravljenju z elektrokemoterapiji s cisplatinom so bili tumorji obsevani s Kobalt-60 γ-žarki pri dozah 3 in 5 Gy. V kontrolne skupine so bile vključene tudi kombinacije obsevanja z aplikacijo električnih pulzov, kot tudi s cisplatinom. Protitumorska učinkovitost je bila vrednotena z zaostankom rasti tumorjev, časom podvojitve velikosti tumorjev, indeksa inhibicije rasti tumorjev, kot tudi stopnjo objektivnih in popolnih odgovorov tumorjev.

Rezultati. Kot pričakovano, je bila protitumorska učinkovitost elektrokemoterapije večja kot zdravljenja s cisplatinom ali aplikacijo električnih pulzov. Pri kombiniranem zdravljenju tumorjev z obsevanjem (3 ali 5 Gy), se je kombinacija z elektrokemoterapijo izkazala za najučinkovitejšo. In sicer, pri obsevanju s 5 Gy so 2/8 tumorjev bili v popolnem odgovoru 100 dni po začetku zdravljenja.Tudi pri ostalih parametrih odgovora tumorjev, je bil kombinacija s 5 Gy bolj učinkovita, kot nižja obsevalna doza (3 Gy).

Zaključki. Rezultati študije kažejo, da je obsevanje tumorjev po elektrokemoterapiji učinkovito, tudi pri nizkih, enkratnih dozah 3 Gy ali 5 Gy. Ti rezultati so bili pridobljeni na modelu invazivnega duktalnega carcinoma miši, ki so bili veliki in zato predstavljajo klinično primerljivo situacijo.

RadiolOncol 2012; 46(3): 233-241.
doi:10.2478/v10019-012-0025-z

miR-548c-5p zavirajo proliferacijo in migracijo ter spodbujajo apoptozo v celicah CD90+ HepG2

Fang L, Zhang HB, Li H, Fu Y, Yang GS

Izhodišča. S pojavom teorije tumorskih izvornih celic so eno od žarišč raziskav raka jeter postale celice, podobne izvornim celicam raka jeter (LCSC).

Materiali in metode. V raziskavi smo uporabili CD90+ HepG2 celice kot možne celice, podobne LCSC, ter smo analizirali izražanje miRNA in genov. Začetna raziskava je pokazala, da imajo molekule miR-548c-5p možen učinek na CD90+ HepG2 celice, zaradi česar smo jih vključili v nadaljnje raziskave. Celice CD90+ HepG2 smo razdelili na skupino, transfecirano z miR-548c-5p molekulami, in na kontrolno skupino. S testom MTT smo spremljali proliferacijo celic CD90+ HepG2. Sposobnost migracije in invazije celic smo določili s testom celjenja rane *('wound healing')* in testom migracije celic '*transwell*'. Apoptozo smo določali s fluorescenčno mikroskopijo.

Rezultati. Rezultati so pokazali, da je izražanje *kaspaze-3* in *bcl-2* zmanjšano, izražanje *kaspaze-8* pa povečano v celicah CD90+ HepG2. Poleg tega transfekcija z miR-548c-5p zmanjša izražanje *β-katenina, Tg737, bcl-2, bcl-XL* in *kaspaze-3*, zavira proliferacijo, migracijo in invazijo celic ter spodbuja apoptozo celic CD90+ HepG2.

Zaključki. Ugotovitve raziskave nakazujejo neravnovesje med apoptozo in antiapoptozo v LCSC-podobnih celicah, kar vpliva na biološke lastnosti teh celic. Molekule miRNA imajo regulatorsko vlogo v LCSC-podobnih celicah, pri čemer molekule miR-548c-5p delujejo zaviralno.

RadiolOncol 2012; 46(3): 242-251.
doi:10.2478/v10019-012-0023-1

Primerjava 3D in 2D MR slikanja za konturiranje pri brahiterapiji raka materničnega vratu

Petrič P, Hudej R, Rogelj P, Blas M, Šegedin B, Zobec Logar HB, Dimopoulos JCA

Izhodišča. Namen naše raziskave je bil opredeliti uporabnost 3D MR sekvence za vrisovanje tarčnih volumnov. MR sekvence s kratkim časom slikanja bi lahko izboljšale dostopnost 3D slikovno vodene brahiterapije raka materničnega vratu (angl. *Image Guided Adaptive Brachytherapy* – IGABT).

Bolniki in metode. Pri 14 bolnicah, zdravljenih z IGABT smo po vstavitvi aplikatorja opravili 2D in 3D MR slikanje male medenice. Dva izkušena radioterapevta (opazovalca) sta na MR slike vrisala visoko rizični tarčni volumen (angl. *High Risk Clinical Target Volume* – HR CTV) z uporabo dveh različnih pristopov: konvencionalnega (na podlagi 2D MR sekvenc) in testnega (na podlagi 3D MR sekvence). Opravili smo volumetrično in topografsko analizo razlik med vrisanimi konturami, da bi opredelili morebitno variabilnost vrisovanja, ki bi nastala zaradi opazovalca ali različnega pristopa. Opredelili smo velikost odstopanj med testno vrisanimi konturami in konturami, vrisanimi s konvencionalnim pristopom pri obeh opazovalcih. Za oceno zanesljivosti uporabe testnega pristopa pri vrisovanju smo opravili analizo vpliva konvencionalnega in testnega pristopa na variabilnost vrisovanja med opazovalcema.

Rezultati. Analiza ni odkrila opazovalcu ali pristopu lastne volumetrične ali topografske variabilnosti vrisovanja HR CTV. Variabilnost vrisanih področij je bila primerljiva pri obeh analizah. Povprečna razdalja med konturama, vrisanima z uporabo konvencionalnega in testnega pristopa, je znašala 2,6 (standardna deviacija (SD) 0,4) mm pri prvem in 2,8 (SD 0,7) mm pri drugem opazovalcu. Pri obeh opazovalcih se je razdalja med konturama, vrisanima s konvencionalnim pristopom (3,1 mm; SD 0,8 mm), ohranila na testnem pristopu (3 mnm; SD 0,7 mm). Variabilnost je bila najbolj izrazita v kavdalnih delih HR CTV pri obeh opazovalcih in pristopih.

Zaključki. 3D MR sekvenca bi lahko nadomestila multiplanarno 2D MR slikanje za potrebe IGABT. S skrajšanjem celokupnega časa delovanja MR naprave in poenostavitvijo procesa vrisovanja bi takšen pristop lahko omogočil večjo dostopnost IGABT za zdravljenje raka materničnega vratu.

RadiolOncol 2012; 46(3): 252-257.
doi:10.2478/v10019-012-0030-2

Predoperativna radioterapija, kapecitabin in cetuksimab pri zdravljenju lokalno napredovalega raka danke. Rezultati klinične raziskave XERT II. faze

Velenik V, Ocvirk J, Oblak I, Anderluh F

Izhodišča. Predoperativna radiokemoterapija s kapecitabinom je standardno zdravljenje operabilnega lokalno napredovalega raka danke. Da bi izboljšali učinkovitost zdravljenja smo naredili klinično raziskavo II. faze, v kateri smo standardnemu predoperativnemu zdravljenju dodali tarčno zdravilo za epidermalni rastni faktor cetuksimab. Želeli smo ugotoviti dejavnike preživetja in njihovo odvisnost od značilnosti bolezni, vključno stanje mutiranosti KRAS in tipa operacije.

Bolniki in metode. Bolniki z operabilnim lokalno napredovalim rakom danke (LARC) so prejemali kapecitabin 14 dni (1250 mg/m^2/12 ur), cetuksimab 15. dan (400 mg/m^2) in nato 250 mg/m^2 tedensko v času kemoradioterapije. Obsevali smo jim področje medenice do skupne doze 45 Gy (v dnevnih odmerkih po 1,8 Gy) v 5 tednih. Od prvega do zadnjega dne obsevanja (vključno s sobotami in nedeljami) so sočasno prejemali kapecitabin 825 mg/m/12 ur. Operirali smo jih 6 tednov po končanem obsevanju. Pooperativno so prejemali še kemoterapijo s kapecitabinom 14 dni (1250 m^2/12 ur) v tritedenskih krogih.

Rezultati. V raziskavo smo vključili 43 bolnikov, 37 smo jih zdravili po predvideni shemi. 28 (75,7%) je imelo bolezen v stadiju T3N+. Učinkovitost zdravljenja smo lahko analizirali pri 36 bolnikih. Srednji čas sledenja je bil 39 mesecev (5-87). Triletna lokalna kontrola bolezni je bila 96,9% (95%, interval zaupanja (IZ) 90,0-100.0), preživetje brez bolezni 72,2% (95% IZ 57,5-86,9), preživetje brez ponovitve bolezni 74,3% (95% 59,8-88,8) in celokupno preživetje 68,1% (95% IZ 36,7-99,4). Odvisnosti preživetja od spola, starosti, lege tumorja v danki, tipa operacije, patohistološkega stadija T ali N, stopnje regresa bolezni ali stanja mutacije KRAS nismo ugotovili.

Zaključki. Predoperativna kemoradioterapija raka danke s kapecitabinom in cetuksimabom je povezana z odlično 3-letno lokalno kontrolo. Ugotovitev KRAS mutiranosti tumorja je lahko označevalec učinkovitosti zdravljenja raka danke s cetuksimabom, zato bodo potrebne nadaljnje raziskave.

RadiolOncol 2012; 46(3): 258-264.
doi:10.2478/v10019-012-0041-z

Ingvinalna ali ingvino-iliako/obturatorna disekcija po pozitivni ingvinalni varovalni bezgavki pri bolnikih s kožnim melanomom

Glumac N, Hočevar M, Zadnik V, Snoj M

Izhodišča. Standardno zdravljenje po pozitivni varovalni bezgavki je disekcija bezgavčne lože. V ingvinalnem predelu tip disekcije ni povsem določen. Zasevki v ingvinalni varovalni bezgavki so mnogo manjši, kot so bili, ko so bolniki prihajali s tipnimi zasevki. Zato je tudi možnost zasevkov v preostalih ingvinalnih, iliakalnih ali obturatornih bezgavkah toliko manjša. Po pozitivni ingvinalni varovalni bezgavki izvajamo tako ingvinalno kot ingvino-iliako/obturatorno disekcijo. Namen raziskave je bil določiti pomen števila zasevkov v ingvinalni varovalni bezgavki manjših od 2 mm (mikrozasevki) glede na prisotnost zasevkov v preostalih odstranjenih bezgavkah.

Bolniki in metode. Pozitivna ingvinalna varovalna bezgavka je bila prisotna pri 58 bolnikih od 743, ki smo jih zaporedno zdravili zaradi kožnega melanoma v stadiju I ali II med leti 2001 in 2007.

Rezultati. Mikrozasevke smo ugotovili pri 32 bolnikih; 14 je bilo solitarnih, 2 sta bila dvojna in 16 je bilo multiplih. Šestindvajset bolnikov je imelo makrozasevke.

Zaključki. Noben bolnik z mikrozasevkom ali solitarnim makrozasevkom v ingvinalni varovalni bezgavki ni imel nadaljnjih zasevkov iliakalno ali obturatorno. Še več, noben bolnik s solitarnim mikrozasevkom v ingvinalni varovalni bezgavki ni imel kakršnihkoli nadaljnjih zasevkov iliakalno, obturatorno ali ingvinalno. V teh primerih bi lahko opustili obsežnejšo limfadenektomijo.

Radiol Oncol 2012; 46(3): 265-270.
doi: 10.2478/v10019-012-0008-0

Intenzitetno modulirana radioterapija (IMRT) za zdravljenje unicentrične oblike Castlemanove bolezni. Prikaz primera in pregled literature o uporabi radioterapije

Matthiesen C, Ramgopol R, Seavey J, Ahmad S, Herman T

Izhodišča. Standardna terapija unicentrične oblike Castlemanove bolezni (UCD) ostaja kirurška resekcija. Za enkrat ni enotnega mnenja, kako najbolje zdraviti tiste bolnike, ki zaradi različnih razlogov ne morejo biti operirani. Izbiramo med kortikosteroidi, samoopazovanjem, kemoterapijo in obsevanjem. V članku predstavljamo primer UCD, ki smo jo zdravili z moderno tehniko obsevanja, intenzitetno modulirano radioterapijo (IMRT).

Prikaz primera. Pri 47-letni bolnici smo v zadnjem delu mediastinuma naključno odkrili UCD. Ker zaradi spremljajočih bolezni ni bila primerna za kirurško zdravljenje, smo se odločili, da jo bomo zdravili z radioterapijo. Uporabili smo tehniko IMRT do skupne tumorske doze 43,2 Gy v frakcijah po 1,8 Gy in z 10-dnevno pavzo. Med pavzo smo naredili nov plan obsevanja, ker se je prvotni volumen tumorja zmanjšal za 50,9%. Po končanem obsevanju se je razvil pneumonitis 3. stopnje po oceni RTOG (Radiation Therapy Oncology Group), ki smo ga učinkovito zdravili s kortikosteroidi. Ob zadnjem pregledu bolnica ni imela znakov ponovitve bolezni in znakov poznih stranskih učinkov obsevanja.

Zaključki. Uporaba IMRT z načrtovano pavzo je lahko uspešna pri zdravljenju UCD in je ena od možnosti zdravljenja neresektabilnih oblik bolezni.

November 18-24, 2012
Ljubljana, Slovenia

cost

Electroporation based Technologies and Treatments

International SCIENTIFIC WORKSHOP and POSTGRADUATE COURSE

Cell membrane electroporation, its mechanisms and applications in biology, medicine and biotechnology.
The basis of the phenomena, current applications and future prospects.

Invitation:

The postgraduate course is intended both for novices and experts in electroporation, including PhD students, researchers and users. You are all kindly invited to attend the workshop and the course on electroporation based technologies and treatments. In order to apply, please submit your abstract and registration form. Abstract submission is strongly encouraged and is necessary if credits (5 ECTS) are sought for. Each participant submitting an abstract will also be required to give a short oral presentation of the work. The forms and instructions can be obtained from www.ebtt.org. This course has been accredited also by the Medical Chamber of Slovenia, so active and passive participants receive 20 CME credits.

Faculty members and lecturers:

Damijan Miklavčič, University of Ljubljana, Slovenia
Lluis M. Mir, CNRS and Institute Gustave Roussy, Villejuif, France
Eberhard Neumann, University of Bielefeld, Germany
Véronique Préat, Catholic University of Louvain, Brussels, Belgium
Gregor Serša, Institute of Oncology, Ljubljana, Slovenia
Justin Teissié, CNRS and IPBS, Toulouse, France
P. Thomas Vernier, University of Southern California, USA

Invited lecturers:

Rafael Davalos, Virginia Tech, School of Biomedical Engineering and Sciences, USA
David A. Dean, University of Rochester, Department of Pediatrics, USA
Julie Gehl, Copenhagen University Hospital, Herlev, Denmark
Tadej Kotnik, University of Ljubljana, Slovenia
Marie-Pierre Rols, CNRS and IPBS, Toulouse, France
Mounir Tarek, Université Henri-Poincaré, Nancy, France
Stefan Töpfel, DIL-e.V. Institute of Food Technologies, Quakenbrück, Germany

Tuition fee:

Tuition fee (630 EUR) includes: Attendance to lectures, book of abstracts and course material, lunches and social events, certificate of attendance and examination (5 ECTS credits, 20 CME). A limited number of grants for students are available from COST and BEMS. Members of EBEA and BES have reduced fee.

Key lectures and content of the course:

- Electrical properties of cells and tissues in electric field
- Physical chemistry of membrane electroporation
- Electroporation *in vitro* and *in vivo* - protocols
- Development of devices and electrodes
- Electrochemotherapy of tumors
- Application of electroporation in gene transfection
- Electroporation in transdermal drug delivery

Additional topics

- Molecular dynamics simulations of lipid bilayers electroporation, **Mounir Tarek**
- Non-thermal irreversible electroporation as a tissue ablation therapy, **Rafael Davalos**
- Cell-specific targeting strategies for electroporation-mediated gene delivery in the lung, **David A. Dean**
- Safety and toxicity of electroporation, **Julie Gehl**
- Electroporation in food processing, **Stefan Töpfel**

Laboratory and practical work

- Gene electrotransfer using different electrical pulse parameters
- Monitoring cell membrane electropermeabilization with ratiometric fluorescence dye FURA-2AM
- Electropermeabilization detection of attached cells with propidium iodide
- Measurements of the induced transmembrane voltage with fluorescent dye di-8-ANEPPS
- Electroporation of bacteria
- Electroporation of planar lipid bilayers
- Cell electrofusion
- Pulsed electric field - induced cryoprotection of spinach leaves
- Analysis of pulse parameters on gene electrotransfer – efficiency and visualization on a membrane level
- Skin electroporation
- Electrochemotherapy treatment planning: optimization of voltage and electrode position

www.ebtt.org

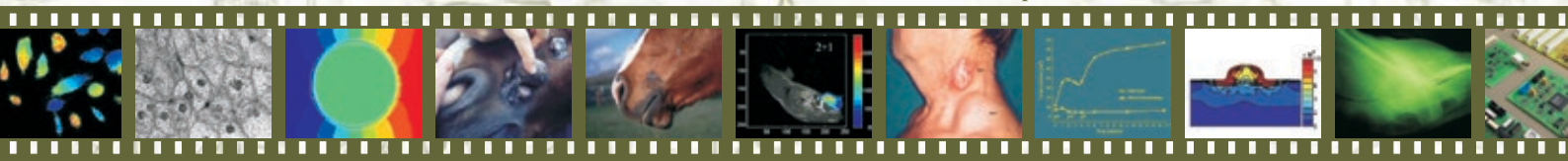

Fundacija "Docent dr. J. Cholewa"
je neprofitno, neinstitucionalno in nestrankarsko
združenje posameznikov, ustanov in organizacij, ki želijo
materialno spodbujati in poglabljati raziskovalno
dejavnost v onkologiji.

Dunajska 106
1000 Ljubljana

ŽR: 02033-0017879431

Activity of "Dr. J. Cholewa" Foundation for Cancer Research and Education – a report for the second quarter of 2012

The Dr. J. Cholewa Foundation for Cancer Research and Education aims to search for and support novel initiatives and forward thinking in all of the activities in any way associated with cancer. It is a non-profit, non-government and non-political association of experts, institutions and organisations associated with cancer research, cancer education, cancer treatment and prevention.

The Foundation continues to support the publication of "Radiology and Oncology", an international medical scientific journal that is edited, published and printed in Ljubljana, Slovenia. "Radiology and Oncology" publishes scientific articles, reviews, case reports, short reports and letters to the editor about problems in experimental and clinical research in radiology, radiophyics, experimental and clinical oncology, supportive therapy, prevention and early diagnostics of different types of cancer. Radiology and Oncology is an open access journal with a Science Citation Index impact factor. In the first and the second quarter of 2012 the Foundation gave its support to a number of lay associations and organizations that are involved in the fight against cancer in Slovenia. The Foundation also supports a number of activities with long term effect and is thus involved in activities in all three levels of prevention of cancer.

The Dr. J. Cholewa Foundation for Cancer Research and Education helps professional and other associations in Slovenia to organise scientific and other meetings of specific interest in different fields of advanced cancer research and education.

The Foundation has continued with its activities throughout the first and second quarter of 2012 with the aim to spread as much knowledge as possible about cancer and related problems in Slovenia, an important part of this activities being the education and information of the lay public.

Borut Štabuc, MD, PhD
Andrej Plesničar, MD, MSc
Tomaž Benulič, MD

Prvi na poti individualnega zdravljenja bolnikov z napredovalim nedrobnoceličnim pljučnim rakom.

Iressa je prva in edina tarčna monoterapija, ki dokazano podaljša preživetje brez napredovanja bolezni v primerjavi z dvojno kemoterapijo kot zdravljenje prvega reda pri bolnikih z napredovalim nedrobnoceličnim pljučnim rakom z mutacijo EGFR.

IRESSA® (GEFITINIB)
SKRAJŠAN POVZETEK GLAVNIH ZNAČILNOSTI ZDRAVILA

Sestava: Filmsko obložene tablete vsebujejo 250 mg gefitiniba.
Indikacije: zdravljenje odraslih bolnikov z lokalno napredovalim ali metastatskim nedrobnoceličnim pljučnim rakom z aktivacijskimi mutacijami EGFR-TK
Odmerjanje in način uporabe: Zdravljenje z gefitinibom mora uvesti in nadzorovati zdravnik, ki ima izkušnje z uporabo zdravil proti raku. Priporočeno odmerjanje zdravila IRESSA je ena 250-mg tableta enkrat na dan. Tableto je mogoče vzeti s hrano ali brez nje, vsak dan ob približno istem času.
Kontraindikacije: preobčutljivost za zdravilno učinkovino ali katerokoli pomožno snov, dojenje
Opozorila in previdnostni ukrepi: Pri 1,3 % bolnikov, ki so dobivali gefitinib, so opažali intersticijsko bolezen pljuč (IBP). Ta se lahko pojavi akutno in je bila v nekaterih primerih smrtna. Če se bolniku poslabšajo dihalni simptomi, npr. dispneja, kašelj in zvišana telesna temperatura, morate zdravljenje z zdravilom IRESSA prekiniti in bolnika takoj preiskati. Če je potrjena IBP, morate terapijo z zdravilom IRESSA končati in bolnika ustrezno zdraviti. Opažene so bile nepravilnosti testov jetrnih funkcij, občasno zabeležene kot hepatitis. Opisani so bili posamezni primeri odpovedi jeter. Zato so priporočljive redne kontrole delovanja jeter. V primeru blagih do zmernih sprememb v delovanju jeter je treba zdravilo IRESSA uporabljati previdno. Če so spremembe hude, pride v poštev prekinitev zdravljenja. Zdravilo IRESSA vsebuje laktozo. Bolniki z redko dedno intoleranco za galaktozo, laponsko obliko zmanjšane aktivnosti laktaze ali malabsorpcijo glukoze/galaktoze ne smejo jemati tega zdravila. Bolnikom naročite, da morajo takoj poiskati zdravniško pomoč, če se jim pojavijo kakršnikoli očesni simptomi, huda ali dolgotrajna driska, navzea, bruhanje ali anoreksija, ker lahko vse te posredno povzročijo dehidracijo.
Medsebojno delovanje zdravil: Sočasna uporaba močnih zaviralcev CYP3A4 lahko poveča koncentracijo gefitiniba v plazmi. Močni zaviralci CYP2D6 lahko pri izrazitih metabolizatorjih CYP2D6 povečajo koncentracijo gefitiniba v plazmi za približno 2-krat. Induktorji CYP3A4 lahko povečajo presnovo gefitiniba in zmanjšajo njegovo koncentracijo v plazmi. Zato lahko sočasna uporaba induktorjev CYP3A4 zmanjša učinkovitost zdravljenja in se ji je treba izogniti. Snovi, ki občutno in dolgotrajno zvišajo pH v želodcu, lahko zmanjšajo koncentracijo gefitiniba v plazmi in tako zmanjšajo njegovo učinkovitost. Veliki odmerki kratkodelujočih antacidov, uporabljenih blizu časa jemanja gefitiniba, imajo lahko podoben učinek. Pri nekaterih bolnikih, ki so jemali varfarin skupaj z gefitinibom, so se pojavili zvišanje internacionalnega normaliziranega razmerja (INR) in/ali krvavitve. Bolnike, ki sočasno jemljejo varfarin in gefitinib, morate redno kontrolirati glede sprememb protrombinskega časa (PČ) ali INR.
Neželeni učinki: V kumulativnem naboru podatkov kliničnih preskušanj III. faze so bili najpogosteje opisani neželeni učinki, ki so se pojavili pri več kot 20 % bolnikov, driska in kožne reakcije (vključno z izpuščajem, aknami, suho kožo in srbenjem). Neželeni učinki se ponavadi pojavijo prvi mesec zdravljenja in so praviloma reverzibilni. Ostali pogostejši neželeni učinki so: anoreksija, konjunktivitis, blefaritis in suho oko, krvavitev, npr. epistaksa in hematurija, intersticijska bolezen pljuč (1,3 %), navzea, bruhanje, stomatitis, dehidracija, suha usta, nepravilnosti testov jetrnih funkcij, bolezni nohtov, alopecija, asimptomatično laboratorijsko zvišanje kreatinina v krvi, proteinurija, cistitis, astenija, pireksija.
Vrsta in vsebina ovojnine: škatla s 30 tabletami po 250 mg gefitiniba
Način izdajanja zdravila: samo na recept
Datum priprave besedila: januar 2011
Imetnik dovoljenja za promet: AstraZeneca AB, S-151 85, Sodertalje, Švedska
Pred predpisovanjem, prosimo, preberite celoten povzetek glavnih značilnosti zdravila.
Dodatne informacije so na voljo pri:
AstraZeneca UK Limited, Podružnica v Sloveniji, Verovškova 55, 1000 Ljubljana, telefon: 01/51 35 600.

Samo za strokovno javnost.
Informacija pripravljena: avgust 2011

AstraZeneca
ONKOLOGIJA

IRESSA®
gefitinib

Merck Serono Onkologija | ključ je v kombinaciji

Erbitux 5 mg/ml raztopina za infundiranje (Skrajšan povzetek glavnih značilnosti zdravila)

Sestava: En ml raztopine za infundiranje vsebuje 5 mg cetuximaba in pomožne snovi. Cetuksimab je himerno monoklonsko IgG1 protitelo. **Terapevtske indikacije:** Zdravilo Erbitux je indicirano za zdravljenje bolnikov z metastatskim kolorektalnim rakom z ekspresijo receptorjev EGFR in nemutiranim tipom KRAS v kombinaciji s kemoterapijo na osnovi irinotekana, kot primarno zdravljenje v kombinaciji s FOLFOX in kot samostojno zdravilo pri bolnikih, pri katerih zdravljenje z oksaliplatinom in irinotekanom ni bilo uspešno ter pri bolnikih, ki ne prenašajo irinotekana. Zdravilo Erbitux je indicirano za zdravljenje bolnikov z rakom skvamoznih celic glave in vratu v kombinaciji z radioterapijo za lokalno napredovalo bolezen in v kombinaciji s kemoterapijo na osnovi platine za ponavljajočo se in/ali metastatsko bolezen. **Odmerjanje in način uporabe:** Zdravilo Erbitux pri vseh indikacijah infundirajte enkrat na teden. Pred prvo infuzijo mora bolnik prejeti premedikacijo z antihistaminikom in kortikosteroidom. Začetni odmerek je 400 mg cetuksimaba na m^2 telesne površine. Vsi naslednji tedenski odmerki so vsak po 250 mg/m^2. **Kontraindikacije:** Zdravilo Erbitux je kontraindicirano pri bolnikih z znano hudo preobčutljivostno reakcijo (3. ali 4. stopnje) na cetuksimab. Kombinacija zdravila Erbitux s kemoterapijo, ki vsebuje oksaliplatin, je kontraindicirana pri bolnikih z metastatskim kolorektalnim rakom z mutiranim tipom KRAS ali kadar status KRAS ni znan. **Posebna opozorila in previdnostni ukrepi:** Če pri bolniku nastopi blaga ali zmerna reakcija, povezana z infundiranjem, lahko zmanjšate hitrost infundiranja. Priporočljivo je, da ostane hitrost infundiranja na nižji vrednosti tudi pri vseh naslednjih infuzijah. Če se pri bolniku pojavi huda kožna reakcija (≥ 3. stopnje po kriterijih US NCI-CTC), morate prekiniti terapijo s cetuksimabom. Z zdravljenjem smete nadaljevati le, če se je reakcija izboljšala do 2. stopnje. Zaradi možnosti pojava znižanja nivoja magnezija v serumu se pred in periodično med zdravljenjem priporoča določanje koncentracije elektrolitov. Če se pojavi sum na nevtropenijo, je potrebno bolnika skrbno nadzorovati. Potrebno je upoštevati kardiovaskularno stanje bolnika in sočasno dajanje kardiotoksičnih učinkovin kot so fluoropirimidini. Cetuksimab je treba uporabljati previdno pri bolnikih z anamnezo keratitisa, ulcerativnega keratitisa ali zelo suhih oči. **Interakcije:** Farmakokinetične značilnosti cetuksimaba ostanejo nespremenjene po sočasni uporabi enkratnega odmerka irinotekana, tudi farmakokinetika irinotekana je nespremenjena pri sočasni uporabi cetuksimaba. Pri kombinaciji s fluoropirimidini se je povečala pogostnost srčne ishemije, vključno z miokardnim infarktom in kongestivno srčno odpovedjo ter pogostnost sindroma dlani in stopal. V kombinaciji s kemoterapijo na osnovi platine se lahko poveča pogostnost hude levkopenije ali hude nevtropenije. **Neželeni učinki:** Zelo pogosti (≥ 1/10): hipomagneziemija, povečanje ravni jetrnih encimov, kožne reakcije, blage ali zmerne reakcije povezane z infundiranjem, blag do zmeren mukozitis. Pogosti (≥ 1/100, < 1/10): dehidracija, hipokalciemija, anoreksija, glavobol, konjunktivitis, driska, navzeja, bruhanje, hude reakcije povezane z infundiranjem, utrujenost. **Posebna navodila za shranjevanje:** Shranjujte v hladilniku (2 °C - 8 °C). **Pakiranje:** 1 viala z 20 ml ali 100 ml raztopine. **Način in režim izdaje:** H. **Imetnik dovoljenja za promet:** Merck KGaA, 64271 Darmstadt, Nemčija. **Datum zadnje revizije besedila:** Januar 2012.

Pred predpisovanjem zdravila natančno preberite celoten Povzetek glavnih značilnosti zdravila.

Podrobnejše informacije so na voljo pri predstavniku imetnika dovoljenja za promet z zdravilom: Merck d.o.o., Ameriška ulica 8, 1000 Ljubljana, tel.: 01 560 3810, faks: 01 560 3830, el. pošta: info@merck.si

www.merckserono.net

www.Erbitux-international.com

Merck Serono

Merck Serono is a division of Merck.

MERCK

Samo za strokovno javnost PM-ONC-1/12-30.01.2012

SKRAJŠAN POVZETEK GLAVNIH ZNAČILNOSTI ZDRAVILA

Samo za strokovno javnost.

Ime zdravila: Tarceva 25 mg/100 mg/150 mg filmsko obložene tablete

Kakovostna in količinska sestava: Ena filmsko obložena tableta vsebuje 25 mg, 100 mg ali
150 mg erlotiniba (v obliki erlotinibijevega klorida).

Terapevtske indikacije: Nedrobnocelični rak pljuč: Zdravilo Tarceva je indicirano za prvo linijo zdravljenja bolnikov z lokalno napredovalim ali metastatskim nedrobnoceličnim rakom pljuč z EGFR-aktivirajočimi mutacijami. Zdravilo Tarceva je indicirano tudi za samostojno vzdrževalno zdravljenje bolnikov z lokalno napredovalim ali metastatskim nedrobnoceličnim rakom pljuč s stabilno boleznijo po 4 ciklih standardne kemoterapije na osnovi platine v prvi liniji zdravljenja. Zdravilo Tarceva je indicirano tudi za zdravljenje bolnikov z lokalno napredovalim ali metastatskim nedrobnoceličnim rakom pljuč po neuspehu vsaj ene predhodne kemoterapije. Pri predpisovanju zdravila Tarceva je treba upoštevati dejavnike, povezane s podaljšanim preživetjem. Koristnega vpliva na podaljšanje preživetja ali drugih klinično pomembnih učinkov zdravljenja niso dokazali pri bolnikih z EGFR-negativnimi tumorji (glede na rezultat imunohistokemije). Rak trebušne slinavke: Zdravilo Tarceva je v kombinaciji z gemcitabinom indicirano za zdravljenje bolnikov z metastatskim rakom trebušne slinavke. Pri predpisovanju zdravila Tarceva je treba upoštevati dejavnike, povezane s podaljšanim preživetjem. Koristnega vpliva na podaljšanje preživetja niso dokazali za bolnike z lokalno napredovalo boleznijo.

Odmerjanje in način uporabe: Zdravljenje z zdravilom Tarceva mora nadzorovati zdravnik z izkušnjami pri zdravljenju raka. Pri bolnikih z lokalno napredovalim ali metastatskim nedrobnoceličnim rakom pljuč, ki še niso prejeli kemoterapije, je treba testiranje za določanje mutacij EGFR opraviti pred začetkom zdravljenja z zdravilom Tarceva. Zdravilo Tarceva vzamemo najmanj eno uro pred zaužitjem hrane ali dve uri po tem. Kadar je potrebno odmerek prilagoditi, ga je treba zmanjševati v korakih po 50 mg. Pri sočasnem jemanju substratov in modulatorjev CYP3A4 bo morda potrebna prilagoditev odmerka. Pri dajanju zdravila Tarceva bolnikom z jetrno okvaro je potrebna previdnost. Če se pojavijo hudi neželeni učinki, pride v poštev zmanjšanje odmerka ali prekinitev zdravljenja z zdravilom Tarceva. Uporaba zdravila Tarceva pri bolnikih s hudo jetrno ali ledvično okvaro ter pri otrocih ni priporočljiva. Bolnikom kadilcem je treba svetovati, naj prenehajo kaditi, saj so plazemske koncentracije erlotiniba pri kadilcih manjše kot pri nekadilcih. Nedrobnocelični rak pljuč: Priporočeni dnevni odmerek zdravila Tarceva je 150 mg. Rak trebušne slinavke: Priporočeni dnevni odmerek zdravila Tarceva je 100 mg, v kombinaciji z gemcitabinom. Pri bolnikih, pri katerih se kožni izpuščaj v prvih 4 do 8 tednih zdravljenja ne pojavi, je treba ponovno pretehtati nadaljnje zdravljenje z zdravilom Tarceva.

Kontraindikacije: Preobčutljivost na erlotinib ali katero koli pomožno snov.

Posebna opozorila in previdnostni ukrepi: Pri določanju bolnikovega statusa mutacij EGFR je pomembno izbrati dobro validirano in robustno metodologijo, da se izognemo lažno negativnim ali lažno pozitivnim rezultatom. *Kadilci:* Bolnikom, ki kadijo, je treba svetovati, naj prenehajo kaditi, saj so plazemske koncentracije erlotiniba pri kadilcih zmanjšane v primerjavi s plazemskimi koncentracijami pri nekadilcih. Verjetno je, da je velikost zmanjšanja klinično pomembna. *Intersticijska bolezen pljuč:* Pri bolnikih, pri katerih se akutno pojavijo novi in/ali poslabšajo nepojasnjeni pljučni simptomi, kot so dispneja, kašelj in vročina, je treba zdravljenje z zdravilom Tarceva prekiniti, dokler ni znana diagnoza. Bolnike, ki se sočasno zdravijo z erlotinibom in gemcitabinom, je treba skrbno spremljati zaradi možnosti pojava toksičnosti, podobni intersticijski bolezni pljuč. Če je ugotovljena intersticijska bolezen pljuč, zdravilo Tarceva ukinemo in uvedemo ustrezno zdravljenje. *Driska, dehidracija, neravnovesje elektrolitov in ledvična odpoved:* Pri približno polovici bolnikov, ki so se zdravili z zdravilom Tarceva, se je pojavila driska (vključno z zelo redkimi primeri, ki so se končali s smrtnim izidom). Zmerno do hudo drisko zdravimo z loperamidom. V nekaterih primerih bo morda potrebno zmanjšanje odmerka. V primeru hude ali dolgotrajne driske, navzeje, anoreksije ali bruhanja, povezanih z dehidracijo, je treba zdravljenje z zdravilom Tarceva prekiniti in dehidracijo ustrezno zdraviti. O hipokaliemiji in ledvični odpovedi so poročali redko. Posebno pri bolnikih z dejavniki tveganja (sočasno jemanje drugih zdravil, simptomi, bolezni ali drugi dejavniki, vključno z visoko starostjo) moramo, če je driska huda ali dolgotrajna oziroma vodi v dehidracijo, zdravljenje z zdravilom Tarceva prekiniti in bolnikom zagotoviti intenzivno intravensko rehidracijo. Dodatno je treba pri bolnikih s prisotnim tveganjem za razvoj dehidracije spremljati ledvično delovanje in serumske elektrolite, vključno s kalijem. *Hepatisis, jetrna odpoved*: Pri uporabi zdravila Tarceva so poročali o redkih primerih jetrne odpovedi (vključno s smrtnimi). K njenemu nastanku je lahko pripomogla predhodno obstoječa jetrna bolezen ali sočasno jemanje hepatotoksičnih zdravil. Pri teh bolnikih je treba zato premisliti o rednem spremljanju jetrnega delovanja. Dajanje zdravila Tarceva je treba prekiniti, če so spremembe jetrnega delovanja hude. *Perforacije v prebavilih*: Bolniki, ki prejemajo zdravilo Tarceva, imajo večje tveganje za razvoj perforacij v prebavilih, ki so jih opazili občasno (vključno z nekaterimi primeri, ki so se končali s smrtnim izidom). Pri bolnikih, ki sočasno prejemajo zdravila, ki zavirajo angiogenezo, kortikosteroide, nesteroidna protivnetna zdravila (NSAID) in/ali kemoterapijo na osnovi taksanov, ali so v preteklosti imeli peptični ulkus ali divertikularno bolezen, je tveganje večje. Če pride do tega, je treba zdravljenje z zdravilom Tarceva dokončno ukiniti. *Kožne bolezni pri katerih so prisotni mehurji in luščenje kože:* Poročali so o primerih kožnih bolezni z mehurji in luščenjem kože, vključno z zelo redkimi primeri, ki so nakazovali na Stevens-Johnsonov sindrom/toksično epidermalno nekrolizo in so bili v nekaterih primerih smrtni. Zdravljenje z zdravilom Tarceva je treba prekiniti ali ukiniti, če se pri bolniku pojavijo hude oblike mehurjev ali luščenja kože. *Očesne bolezni:* Bolniki, pri katerih se pojavijo znaki in simptomi, ki nakazujejo na keratitis in so lahko akutni ali se poslabšujejo: vnetje očesa, solzenje, občutljivost na svetlobo, zamegljen vid, bolečine v očesu in/ali rdeče oči, se morajo takoj obrniti na specialista oftalmologije. V primeru, da je diagnoza ulcerativnega keratitisa potrjena, je treba zdravljenje z zdravilom Tarceva prekiniti ali ukiniti. V primeru, da se postavi diagnoza keratitisa, je treba skrbno razmisliti o koristih in tveganjih nadaljnega zdravljenja. Zdravilo Tarceva je pri bolnikih, ki so v preteklosti imeli keratitis, ulcerativni keratitis ali zelo suhe oči, uporabljati previdno. Uporaba kontaktnih leč je prav tako dejavnik tveganja za keratitits in ulceracijo. Med uporabo zdravila Tarceva so zelo redko poročali o primerih perforacije ali ulceracije roženice. *Medsebojno delovanje z drugimi zdravili:* Močni induktorji CYP3A4 lahko zmanjšajo učinkovitost erlotiniba, močni zaviralci CYP3A4 pa lahko povečajo toksičnost. Sočasnemu zdravljenju s temi zdravili se je treba izogibati. Tablete vsebujejo laktozo in jih ne smemo dajati bolnikom z redkimi dednimi stanji: intoleranco za galaktozo, laponsko obliko zmanjšane aktivnosti laktaze ali malabsorpcijo glukoze/galaktoze.

Medsebojno delovanje z drugimi zdravili in druge oblike interakcij: Erlotinib se pri ljudeh presnavlja v jetrih z jetrnimi citokromi, primarno s CYP3A4 in v manjši meri s CYP1A2. Presnova erlotiniba zunaj jeter poteka s CYP3A4 v črevesju, CYP1A1 v pljučih in CYP1B1 v tumorskih tkivih. Z zdravilnimi učinkovinami, ki se presnavljajo s temi encimi, jih zavirajo ali pa so njihovi induktorji, lahko pride do interakcij. Erlotinib je srednje močan zaviralec CYP3A4 in CYP2C8, kot tudi močan zaviralec glukuronidacije z UGT1A1 *in vitro*. Pri kombinaciji ciprofloksacina ali močnega *zaviralca CYP1A2* (npr. fluvoksamina) z erlotinibom je potrebna previdnost. V primeru pojava neželenih učinkov, povezanih z erlotinibom, lahko odmerek erlotiniba zmanjšamo. Predhodno ali sočasno zdravljenje z zdravilom Tarceva ni spremenilo očistka prototipov *substratov CYP3A4*, midazolama in eritromicina. Inhibicija glukoronidacije lahko povzroči interakcije z zdravili, ki so *substrati UGT1A1* in se izločajo samo po tej poti. Močni *zaviralci aktivnosti CYP3A4* zmanjšajo presnovo erlotiniba in zvečajo koncentracije erlotiniba v plazmi. Pri sočasnem jemanju erlotiniba in močnih zaviralcev CYP3A4 je zato potrebna previdnost. Če je treba, odmerek erlotiniba zmanjšamo, še posebno pri pojavu toksičnosti. Močni *spodbujevalci aktivnosti CYP3A4* zvečajo presnovo erlotiniba in pomembno zmanjšajo plazemske koncentracije erlotiniba. Sočasnemu dajanju zdravila Tarceva in induktorjev CYP3A4 se je treba izogibati. Pri bolnikih, ki potrebujejo sočasno zdravljenje z zdravilom Tarceva in močnim induktorjem CYP3A4, je treba premisliti o povečanju odmerka do 300 mg ob skrbnem spremljanju njihove varnosti. Zmanjšana izpostavljenost se lahko pojavi tudi z drugimi induktorji, kot so fenitoin, karbamazepin, barbiturati ali šentjanževka. Če te zdravilne učinkovine kombiniramo z erlotinibom, je potrebna previdnost. Kadar je mogoče, je treba razmisliti o drugih načinih zdravljenja, ki ne vključujejo močnega spodbujanja aktivnosti CYP3A4. Bolnikom, ki jemljejo *kumarinske antikoagulante*, je treba redno kontrolirati protrombinski čas ali INR. Sočasno zdravljenje z zdravilom Tarceva in *statinom* lahko poveča tveganje za miopatijo, povzročeno s statini, vključno z rabdomiolizo; to so opazili redko. Sočasna uporaba *zaviralcev P-glikoproteina*, kot sta ciklosporin in verapamil, lahko vodi v spremenjeno porazdelitev in/ali spremenjeno izločanje erlotiniba. Za erlotinib je značilno zmanjšanje topnosti pri pH nad 5. *Zdravila, ki spremenijo pH v zgornjem delu prebavil*, lahko spremenijo topnost erlotiniba in posledično njegovo biološko uporabnost. Učinka antacidov na absorpcijo erlotiniba niso proučevali, vendar je ta lahko zmanjšana, kar vodi v nižje plazemske koncentracije. Kombinaciji erlotiniba in zaviralca protonske črpalke se je treba izogibati. Če menimo, da je uporaba antacidov med zdravljenjem z zdravilom Tarceva potrebna, jih je treba jemati najmanj 4 ure pred ali 2 uri po dnevnem odmerku zdravila Tarceva. Če razmišljamo o uporabi ranitidina, moramo zdravili jemati ločeno: zdravilo Tarceva je treba vzeti najmanj 2 uri pred ali 10 ur po odmerku ranitidina. V študiji faze Ib ni bilo pomembnih učinkov *gemcitabina* na farmakokinetiko erlotiniba, prav tako ni bilo pomembnih učinkov erlotiniba na farmakokinetiko gemcitabina. Erlotinib poveča koncentracijo platine. Pomembnih učinkov *karboplatina* ali paklitaksela na farmakokinetiko erlotiniba ni bilo. *Kapecitabin* lahko poveča koncentracijo erlotiniba. Pomembnih učinkov erlotiniba na farmakokinetiko kapecitabina ni bilo.

Neželeni učinki: *Zelo pogosti neželeni učinki* so kožni izpuščaj in driska, kot tudi utrujenost, anoreksija, dispneja, kašelj, okužba, navzea, bruhanje, stomatitis, bolečina v trebuhu, pruritus, suha koža, suhi keratokonjunktivitis, konjunktivitis, zmanjšanje telesne mase, depresija, glavobol, nevropatija, dispepsija, flatulenca, alopecija, okorelost, pireksija, nenormalnosti testov jetrne funkcije. *Pogosti neželeni učinki* so krvavitve v prebavilih, epistaksa, keratitis, paronihija, folikulitis, akne/akneiformni dermatitis, fisure na koži. *Občasno* so poročali o perforacijah v prebavilih, hirzutizmu, spremembah obrvi, krhkih nohtih, odstopanju nohtov od kože, blagih reakcijah na koži (npr. hiperpigmentacija), spremembah trepalnic, hudi intersticijski bolezni pljuč (vključno s smrtnimi primeri). *Redko* pa so poročali o jetrni odpovedi. *Zelo redko* so poročali o Stevens-Johnsonovem sindromu/toksični epidermalni nekrolizi ter o ulceracijah in perforacijah roženice.

Režim izdaje zdravila: H/Rp. **Imetnik dovoljenja za promet:** Roche Registration Limited, 6 Falcon Way, Shire Park, Welwyn Garden City, AL7 1TW, Velika Britanija. **Verzija:** 1.0/12. **Informacija pripravljena:** Julij 2012.

025-12-TAR

DODATNE INFORMACIJE SO NA VOLJO PRI:
Roche farmacevtska družba d.o.o., Vodovodna cesta 109, 1000 Ljubljana.
Povzetek glavnih značilnosti zdravila je dosegljiv na
www.roche.si ali www.onkologija.si.

Tarceva®
erlotinib

ČAS ZA ŽIVLJENJE.

DOKAZANO PODALJŠA PREŽIVETJE PRI BOLNIKIH:

- z lokalno napredovalim ali metastatskim nedrobnoceličnim rakom pljuč[1]
- z metastatskim rakom trebušne slinavke[1]

[1] Povzetek glavnih značilnosti zdravila TARCEVA, www.ema.europa.eu

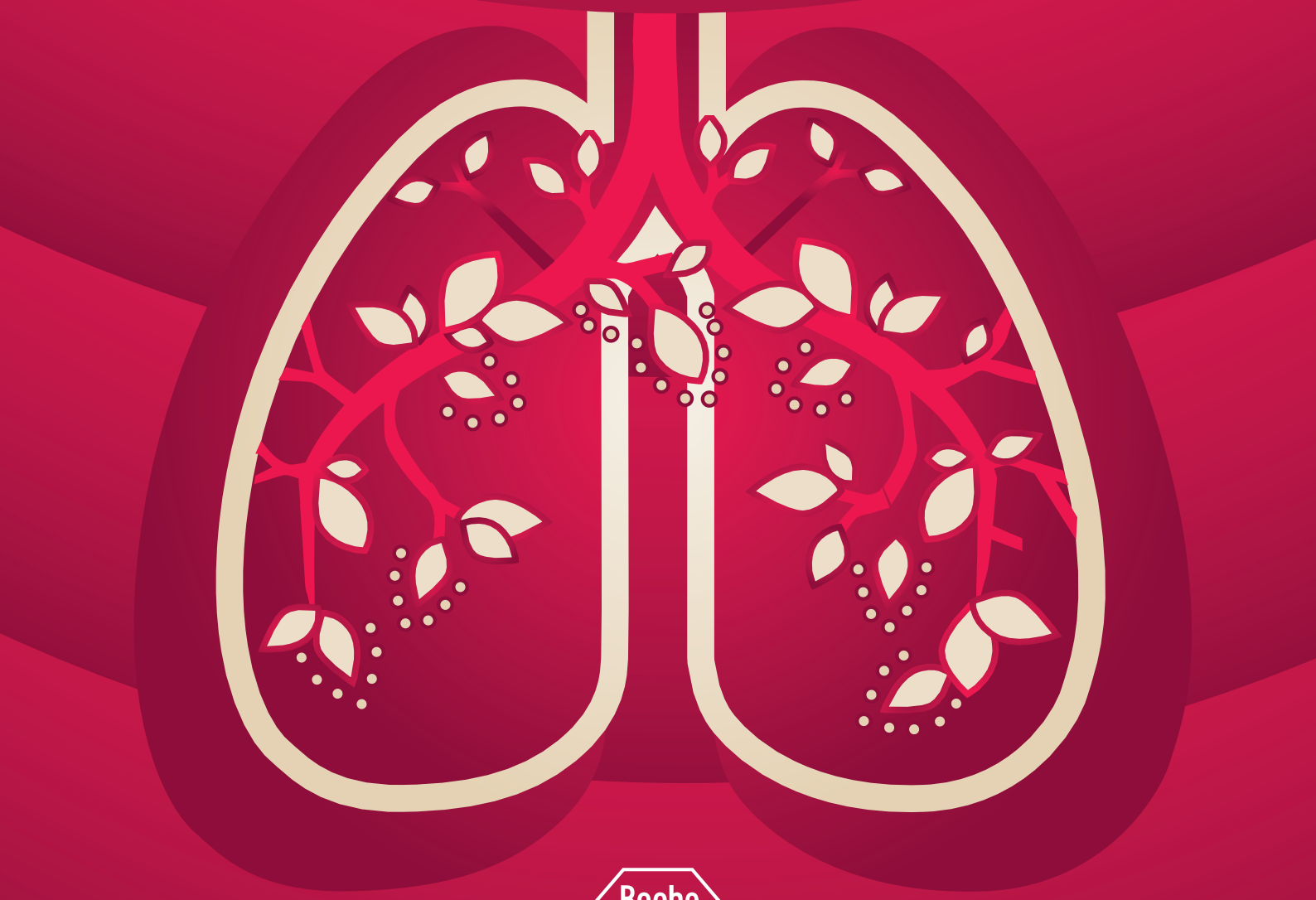

Roche

odprto

Novartis Oncology prinaša spekter inovativnih zdravil, s katerimi poskuša spremeniti življenje bolnikov z rakavimi in hematološkimi obolenji.

Ta vključuje zdravila kot so Glivec® (imatinib), Tasigna® (nilotinib), Afinitor® (everolimus), Zometa® (zoledronska kislina), Femara® (letrozol), Sandostatin® LAR® (oktreotid/i.m. injekcije) in Exjade® (deferasiroks).

Novartis Oncology ima tudi obširen razvojni program, ki izkorišča najnovejša spoznanja molekularne genomike, razumskega načrtovanja in tehnologij za odkrivanje novih učinkovin.

glivec imatinib

Tasigna nilotinib

AFINITOR (everolimus) tablete

ZOMETA zoledronska kislina

Femara letrozol

Sandostatin LAR oktreotid/i.m. injekcije

EXJADE deferasiroks

NOVARTIS ONCOLOGY

Novartis Pharma Services Inc. • Podružnica v Sloveniji • Verovškova 57 • 1000 Ljubljana

Samo za strokovno javnost.

NV-JA-08/11-SI

Kakovost • Izbira • Zadovoljstvo

THE

Natrelle™

COLLECTION

Prsni vsadki in ekspanderji tkiv

Individualne ženske

Individualen izbor

ALLERGAN

DISTRIBUCIJA IN PRODAJA:
SANOLABOR, d.d.,
Leskoškova 4, 1000 Ljubljana, Slovenija
Tel:+386 (0)1 585-42-11
Fax:+386 (0)1 585-42-98
www.sanolabor.si

Sanolabor

PROMOCIJA, MARKETING IN STROKOVNA PODPORA:
EWOPHARMA d.o.o., Cesta 24.junija 23, 1000 Ljubljana, Slovenija
Jurij Pivka, vodja poslovne enote -Medicinska estetika
Tel: +386 (0) 59 084 845, mobilnik: +386 (0) 51 326 058
Fax: +386 (0) 59 084 849

Novo, učinkovito zdravilo

za zdravljenje metastatskega raka prostate, odpornega na kastracijo pri odraslih bolnikih, z napredovalo obliko bolezni ali po osnovni kemoterapevtski shemi z docetakselom[1]

V placebo-nadzorovani klinični raziskavi III. faze so imeli bolniki, ki so prejeli zdravilo ZYTIGA® v kombinaciji z prednizonom:

- 35,4% manjše tveganje za smrt (HR=0,65)[2]
- 33% manjše tveganje za radiografsko potrjeno napredovanje bolezni[2]
- pomembno manj bolečin[2]
- primerljiv pojav neželenih učinkov kot v skupini, ki je prejemala placebo[2]
- možnost jemanja zdravila na domu (peroralno zdravljenje)[1]

Samo za strokovno javnost

Zdravilo je v postopku pridobitve financiranja s strani ZZZS.

SKRAJŠANO NAVODILO ZA PREDPISOVANJE ZDRAVILA:

Ime zdravila: ZYTIGA® 250 mg tablete **Kakovostna in količinska sestava:** 250 mg abirateronacetata; pomožne snovi: laktoza monohidrat, mikrokristalna celuloza, premreženi natrijev karmelozat, povidon, natrijev lavrilsulfat, magnezijev stearat in koloidni silicijev dioksid. **Indikacije:** uporaba skupaj s prednizonom ali prednizolonom za zdravljenje metastatskega raka prostate, rezistentnega na kastracijo pri odraslih bolnikih, z napredovalo obliko bolezni ali po osnovni kemoterapevtski shemi z docetakselom. **Odmerjanje:** priporočeni odmerek: 1.000 mg (štiri 250 mg tablete v enem odmerku), 10 mg prednizona ali prednizolona/dan, najmanj dve uri po obroku. Pri bolnikih s hudo okvaro jeter ali ledvic je potrebna previdnost. **Kontraindikacije:** preobčutljivost za zdravilno učinkovino ali katerokoli pomožno snov, uporaba zdravila pri ženskah. **Posebna opozorila:** Pri uporabi zdravila pri bolnikih z anamnezo kardiovaskularne bolezni je potrebna previdnost. Pri bolnikih z iztisnim deležem levega prekata < 50% ali s srčnim popuščanjem razreda III ali IV po NYHA varnost uporabe zdravila ni dokazana. Pred začetkom zdravljenja je treba urediti hipertenzijo in odpraviti hipokaliemijo. Če kadarkoli med zdravljenjem pride do pojava hude hepatotoksičnosti je treba z zdravljenjem prenehati in se ga ne sme ponovno uvesti. Pri bolnikih, ki prejemajo prednizon ali prednizolon in so v stresni situaciji, je lahko pred in med stresno situacijo ter po njej indiciran zvečan odmerek kortikosteroidov. Pri bolnikih z napredovanim metastatskim rakom prostate (rezistentnim na kastracijo) lahko pride do zmanjšanja kostne gostote. Jemanje zdravila v kombinaciji z glukokortikoidi lahko ta učinek poveča. Pri bolnikih z rakom prostate, zdravljenih s ketokonazolom, lahko pričakujemo nižjo stopnjo odziva na zdravljenje. Bolniki z redko dedno intoleranco za galaktozo, laponsko obliko zmanjšane aktivnosti laktaze ali malabsorpcijo glukoze/galaktoze ne smejo jemati tega zdravila. Zdravilo vsebuje tudi več kot 1 mmol (oziroma 27,2 mg) natrija na odmerek (v štirih tabletah), kar je treba upoštevati pri bolnikih na dieti z nadzorovanim vnosom natrija. **Interakcije:** zdravila se ne sme jemati s hrano, ker se bistveno poveča absorpcija abirateronacetata. Pri sočasni uporabi z zdravili, ki jih aktivira ali presnavlja CYP2D6, zlasti tistih z majhno terapevtsko širino je potrebna previdnost. In vitro podatki kažejo, da je zdravilo substrat CYP3A4. Med zdravljenjem se uporabi močnih zaviralcev in induktorjev CYP3A4 izogibajte ali bodite še posebej previdni. **Nosečnost in dojenje:** Ženske, ki so noseče in ženske, ki bi lahko bile noseče, morajo v primeru stika ali rokovanja z zdravilom, nositi zaščitne rokavice. **Neželeni učinki:** periferni edemi, hipokaliemija, hipertenzija, okužbe sečil, adrenalna insufucienca, hipertrigliceridemija, srčno popuščanje, angina pektoris, aritmija, atrijska fibrilacija, tahikardija, hepatotoksičnost z zvišanimi vrednostmi ALT, AST in celokupnega bilirubina. **Imetnik dovoljenja za promet:** Janssen-Cilag International NV, Turnhoutseweg 30, 2340 Beerse, Belgija, Predstavnik v Sloveniji: Johnson & Johnson d.o.o., Šmartinska 53, Ljubljana **Režim izdajanja zdravila:** Rp.Spec. **Datum zadnje revizije besedila:** 05.09.2011

Viri:

1. ZYTIGA® – Povzetek glavnih značilnosti zdravila: 05. 09. 2011
2. de Bono JS et al. Abiraterone and increased survival in metastatic prostate cancer. N Engl J Med 2011; 364: p1995-2005.

janssen
PHARMACEUTICAL COMPANIES OF Johnson&Johnson

ZYT-SLO-A-015-051011

Zytiga®
abirateronacetat

TANTUM® VERDE
Benzidamin

Lajšanje bolečine in oteklin pri vnetju v ustni votlini in žrelu, ki nastanejo zaradi okužb in stanj po operaciji in kot posledica radioterapije (t.i. radiomukozitis).

CSC ANGELINI

Imetnik dovoljenja za promet
CSC Pharma d.o.o.
Jana Husa 1a
1000 Ljubljana

www.tantum-verde.si

Tantum Verde 1,5 mg/ml oralno pršilo, raztopina

Kakovostna in količinska sestava
1 ml raztopine vsebuje 1,5 mg benzidaminijevega klorida, kar ustreza 1,34 mg benzidamina. V enem razpršku je 0,17 ml raztopine. En razpršek vsebuje 0,255 mg benzidaminijevega klorida, kar ustreza 0,2278 mg benzidamina. En razpršek vsebuje 13,6 mg 96 odstotnega etanola, kar ustreza 12,728 mg 100 odstotnega etanola, in 0,17 mg metilparahidroksibenzoata (E218).

Terapevtske indikacije
Samozdravljenje: lajšanje bolečine in oteklin pri vnetju v ustni votlini in žrelu, ki so lahko posledica okužb in stanj po operaciji. Po nasvetu in navodilu zdravnika: lajšanje bolečine in oteklin v ustni votlini in žrelu, ki so posledica radiomukozitisa.

Odmerjanje in način uporabe
Uporaba 2- do 6-krat na dan (vsake 1,5 do 3 ure). Odrasli: 4 do 8 razpršk 2- do 6-krat na dan. Otroci od 6 do 12 let: 4 razprški 2- do 6-krat na dan. Otroci, mlajši od 6 let: 1 razpršek na 4 kg telesne mase; do največ 4 razprške 2 do 6-krat na dan.

Kontraindikacije
Znana preobčutljivost za zdravilno učinkovino ali katerokoli pomožno snov.

Posebna opozorila in previdnostni ukrepi
Pri manjšini bolnikov lahko resne bolezni povzročijo ustne/žrelne ulceracije. Če se simptomi v treh dneh ne izboljšajo, se mora bolnik posvetovati z zdravnikom ali zobozdravnikom, kot je primerno. Zdravilo vsebuje aspartam (E951) (vir fenilalanina), ki je lahko škodljiv za bolnike s fenilketonurijo. Zdravilo vsebuje izomalt (E953) (sinonim: izomaltitol (E953)). Bolniki z redko dedno intoleranco za fruktozo ne smejo jemati tega zdravila. Uporaba benzidamina ni priporočljiva za bolnike s preobčutljivostjo za salicilno kislino ali druga nesteroidna protivnetna zdravila. Pri bolnikih, ki imajo ali so imeli bronhialno astmo, lahko pride do bronhospazma. Pri takih bolnikih je potrebna previdnost.

Medsebojno delovanje z drugimi zdravili in druge oblike interakcij
Pri ljudeh raziskav o interakcijah niso opravljali.

Nosečnost in dojenje
Tantum Verde z okusom mentola 3 mg pastile se med nosečnostjo in dojenjem ne smejo uporabljati.

Vpliv na sposobnost vožnje in upravljanja s stroji
Uporaba benzidamina lokalno v priporočenem odmerku ne vpliva na sposobnost vožnje in upravljanja s stroji.

Neželeni učinki
Bolezni prebavil Redki: pekoč občutek v ustih, suha usta.
Bolezni imunskega sistema Redki: preobčutljivostna reakcija.
Bolezni dihal, prsnega koša in mediastinalnega prostora Zelo redki: laringospazem.
Bolezni kože in podkožja Občasni: fotosenzitivnost. Zelo redki: angioedem.

Rok uporabnosti
4 leta. Zdravila ne smete uporabljati po datumu izteka roka uporabnosti, ki je naveden na ovojnini. Posebna navodila za shranjevanje Za shranjevanje pastil niso potrebna posebna navodila. Plastenko z raztopino shranjujte v zunanji ovojnini za zagotovitev zaščite pred svetlobo. Shranjujte pri temperaturi do 25°C. Shranjujte v originalni ovojnini in nedosegljivo otrokom.

CLINIPORATOR

LEADING CLINICAL ELECTROPORATION

Electrochemotherapy

Effective, safe, simple.

For local tumours control

Before electrochemotherapy

10 weeks after electrochemotherapy

Gehl J, EJC Supplements, Volume 4, N° 11:35-37, 2006

Before electrochemotherapy

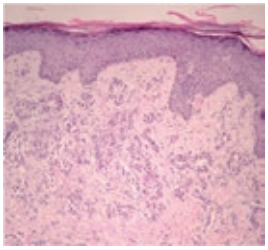

60 days after electrochemotherapy

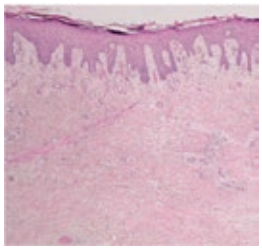

Quaglino P, Annals Of Surgical Oncology. 15 (8):2215-2222. 2008

CLINICAL INDICATIONS
Melanoma and other skin tumors
Local recurrences and cutaneous metastases from breast cancer
Head and neck cancers

High response rate
Preservation of normal tissue and organ function
Efficacy in areas previously treated with radiation therapy
Palliation of painful, ulcerated or bleeding lesions
Improved quality of life and cosmetic results

IGEA SpA, Carpi, Italy | www.igeamedical.com | info@igeamedical.com

IGEA®
CLINICAL BIOPHYSICS

Instructions for authors

The editorial policy

Radiology and Oncology is a multidisciplinary journal devoted to the publishing original and high quality scientific papers, professional papers, review articles, case reports and varia (editorials, short communications, professional information, book reviews, letters, etc.) pertinent to diagnostic and interventional radiology, computerized tomography, magnetic resonance, ultrasound, nuclear medicine, radiotherapy, clinical and experimental oncology, radiobiology, radiophysics and radiation protection. Therefore, the scope of the journal is to cover beside radiology the diagnostic and therapeutic aspects in oncology, which distinguishes it from other journals in the field.

The Editorial Board requires that the paper has not been published or submitted for publication elsewhere; the authors are responsible for all statements in their papers. Accepted articles become the property of the journal and, therefore cannot be published elsewhere without the written permission of the editors.

Submission of the manuscript

The manuscript written in English should be submitted to the journal via online submission system Editorial Manager available for this journal at: www.radioloncol.com.

In case of problems, please contact Sašo Trupej at saso.trupej@computing.si or the Editor of this journal at gsersa@onko-i.si

All articles are subjected to the editorial review and the review by independent referees.

Authors are requested to suggest persons competent to review their manuscript. However, please note that this will be treated only as a suggestion, the final selection of reviewers is exclusively the Editor's decision. The authors' names are revealed to the referees, but not vice versa.

Manuscripts which do not comply with the technical requirements stated herein will be returned to the authors for the correction before peer-review. The editorial board reserves the right to ask authors to make appropriate changes of the contents as well as grammatical and stylistic corrections when necessary. Page charges will be charged for manuscripts exceeding the recommended page number, as well as additional editorial work and requests for printed reprints.

All articles are published printed and on-line as the open access. To support the open access policy of the journal, the authors are encouraged to pay the open access charge of 500 EUR.

Manuscripts submitted under multiple authorship are reviewed on the assumption that all listed authors concur in the submission and are responsible for its content; they must have agreed to its publication and have given the corresponding author the authority to act on their behalf in all matters pertaining to publication. The corresponding author is responsible for informing the coauthors of the manuscript status throughout the submission, review, and production process.

Preparation of manuscripts

Radiology and Oncology will consider manuscripts prepared according to the Uniform Requirements for Manuscripts Submitted to Biomedical Journals by International Committee of Medical Journal Editors (www.icmje.org). The manuscript should be typed double-spaced with a 3-cm margin at the top and left-hand side of the sheet. The manuscript should be written in grammatically and stylistically correct language. Abbreviations should be avoided. If their use is neccessary, they should be explained at the first time mentioned. The technical data should conform to the SI system. The manuscript, including the references, must not exceed 15 typewritten pages, and the number of figures and tables is limited to 8. If appropriate, organize the text so that it includes: Introduction, Materials and methods, Results and Discussion. Exceptionally, the results and discussion can be combined in a single section. Start each section on a new page, and number each page consecutively with Arabic numerals.

The Title page should include a concise and informative title, followed by the full name(s) of the author(s); the institutional affiliation of each author; the name and address of the corresponding author (including telephone, fax and E-mail), and an abbreviated title. This should be followed by the abstract page, summarizing in less than 250 words the reasons for the study, experimental approach, the major findings (with specific data if possible), and the principal conclusions, and providing 3-6 key words for indexing purposes. Structured abstracts are preferred. Slovene authors are requested to provide title and the abstract in Slovene language in a separate file. The text of the research article should then proceed as follows:

Introduction should summarize the rationale for the study or observation, citing only the essential references and stating the aim of the study.

Materials and methods should provide enough information to enable experiments to be repeated. New methods should be described in detail.

Results should be presented clearly and concisely without repeating the data in the figures and tables. Emphasis should be on clear and precise presentation of results and their significance in relation to the aim of the investigation.

Discussion should explain the results rather than simply repeating them and interpret their significance and draw conclusions. It should discuss the results of the study in the light of previously published work.

Charts, Illustrations, Photographs and Tables must be numbered and referred to in the text, with the appropriate location indicated. Charts, illustrations and photographs, provided electronically, should be of appropriate quality for good reproduction. Illustrations and charts must be vector image, created in CMYK colour space, used font familie are encouraged "Century Gothic" and saved as .AI, .EPS or .PDF format. Color charts, illustrations and photographs are encouraged. Picture (image) size must be 2.000 pixels on the longer side and saved as .JPG (maximum quality) format. In photographs, mask the identities of the patients. Tables should be typed double-spaced, with a descriptive title and, if appropriate, units of numerical measurements included in the column heading. The files with the figures can be uploaded as separate files.

References must be numbered in the order in which they appear in the text and their corresponding numbers quoted in the text. Authors are responsible for the accuracy of their references. References to the Abstracts and Letters to the Editor must be identified as such. Citation of papers in preparation or submitted for publication, unpublished observations, and personal communications should not be included in the reference list. If essential, such material may be incorporated in the appropriate place in the text. References follow the style of Index Medicus. All authors should be listed when their number does not exceed six; when there are seven or more authors, the first six listed are followed by "et al.". The following are some examples of references from articles, books and book chapters:

Dent RAG, Cole P. *In vitro* maturation of monocytes in squamous carcinoma of the lung. *Br J Cancer* 1981; **43:** 486-95.

Chapman S, Nakielny R. *A guide to radiological procedures.* London: Bailliere Tindall; 1986.

Evans R, Alexander P. Mechanisms of extracellular killing of nucleated mammalian cells by macrophages. In: Nelson DS, editor. *Immunobiology of macrophage.* New York: Academic Press; 1976. p. 45-74.

Authorization for the use of human subjects or experimental animals

Manuscripts containing information related to human or animal use should clearly state that the research has complied with all relevant national regulations and institutional policies and has been approved by the authors' institutional review board or equivalent committee. These statements should appear in the Materials and methods section (or for contributions without this section, within the main text or in the captions of relevant figures or tables).

When reporting experiments on human subjects, authors should indicate whether the procedures followed were in accordance with the Helsinki Declaration. Patients have the right to privacy; therefore the identifying information (patient's names, hospital unit numbers) should not be published unless it is essential. In such cases the patient's informed consent for publication is needed, and should appear as an appropriate statement in the article.

The research using animal subjects should be conducted according to the EU Directive 2010/63/EU and following the Guidelines for the welfare and use of animals in cancer research (*Br J Cancer 2010;* **102:** 1555 – 77). Authors must identify the committee approving the experiments, and must confirm that all experiments were performed in accordance with relevant regulations.

Transfer of copyright agreement

For the publication of accepted articles, authors are required to send the Transfer of Copyright Agreement to the publisher on the address of the editorial office. A properly completed Transfer of Copyright Agreement, signed by the Corresponding Author on behalf of all the authors, must be provided for each submitted manuscript. The non-commercial use of each article will be governed by the Creative Commons Attribution-NonCommercial-NoDerivs license.

Conflict of interest

When the manuscript is submitted for publication, the authors are expected to disclose any relationship that might pose real, apparent or potential conflict of interest with respect to the results reported in that manuscript. Potential conflicts of interest include not only financial relationships but also other, non-financial relationships. In the Acknowledgement section the source of funding support should be mentioned. The Editors will make effort to ensure that conflicts of interest will not compromise the evaluation process of the submitted manuscripts; potential editors and reviewers will exempt themselves from review process when such conflict of interest exists. The statement of disclosure must be in the Cover letter accompanying the manuscript or submitted on the form available on www.icmje.org/coi_disclosure.pdf

Page proofs will be sent by E-mail or faxed to the corresponding author. It is their responsibility to check the proofs carefully and return a list of essential corrections to the editorial office within three days of receipt. Only grammatical corrections are acceptable at this time.

Reprints: The electronic version of the published papers will be available on www.versitaopen.com/ro free of charge.

AROMASIN®
eksemestan

ENDOKRINO ZDRAVLJENJE BOLNIC Z RAKOM DOJK PO MENOPAVZI

BISTVENI PODATKI IZ POVZETKA GLAVNIH ZNAČILNOSTI ZDRAVILA

AROMASIN 25 mg obložene tablete
Sestava in oblika zdravila: Ena obložena tableta vsebuje 25 mg eksemestana. **Indikacije:** Adjuvantno zdravljenje žensk po menopavzi, ki imajo invazivnega zgodnjega raka dojke s pozitivnimi estrogenskimi receptorji in so se uvodoma vsaj 2 do 3 leta zdravile s tamoksifenom. Zdravljenje napredovalega raka dojke pri ženskah z naravno ali umetno povzročeno menopavzo, pri katerih je bolezen napredovala po antiestrogenskem zdravljenju. Učinkovitost še ni bila dokazana pri bolnicah, pri katerih tumorske celice nimajo estrogenskih receptorjev. **Odmerjanje in način uporabe:** 25 mg enkrat na dan, najbolje po jedi. Pri bolnicah z zgodnjim rakom dojke je treba zdravljenje nadaljevati do dopolnjenega petega leta adjuvantnega hormonskega zdravljenja (tamoksifen, ki mu sledi eksemestan) oz. do recidiva tumorja. Pri bolnicah z napredovalim rakom dojke je treba zdravljenje nadaljevati, dokler ni razvidno napredovanje tumorja. **Kontraindikacije:** Preobčutljivost na zdravilno učinkovino ali na katerokoli pomožno snov, ženske pred menopavzo, nosečnice in doječe matere. **Posebna opozorila in previdnostni ukrepi:** Ne sme se predpisovati ženskam s predmenopavznim endokrinim statusom. Previdna uporaba pri jetrni ali ledvični okvari. Po uporabi so poročali o zmanjšanju mineralne gostote kosti ter večji pogostnosti zlomov. Ženskam z osteoporozo ali tveganjem zanjo je treba na začetku adjuvantnega zdravljenja izmeriti mineralno kostno gostoto s kostno denzitometrijo. Čeprav še ni dovolj podatkov, kako učinkujejo zdravila za zdravljenje zmanjšane mineralne kostne gostote, ki jo povzroča Aromasin, je treba pri bolnicah s tveganjem uvesti zdravljenje ali profilakso osteoporoze ter bolnice natančno spremljati. Zdravilo vsebuje saharozo, zato ga ne smejo jemati bolniki z redko dedno intoleranco za fruktozo, malabsorpcijo glukoze/galaktoze ali pomanjkanjem saharoza-izomaltaze. Vsebuje tudi metilparahidroksibenzoat, ki lahko povzroči alergijske reakcije (lahko zapoznele) in izjemoma bronhospazem. **Medsebojno delovanje z drugimi zdravili:** Sočasna uporaba zdravil – npr. rifampicina, antiepileptikov (npr. fenitoina ali karbamazepina) ali zdravil rastlinskega izvora s šentjaževko – ki inducirajo CYP3A4, lahko zmanjša učinkovitost zdravila Aromasin. Uporabljati ga je treba previdno z zdravili, ki se presnavljajo s pomočjo CYP3A4 in ki imajo ozek terapevtski interval. Kliničnih izkušenj s sočasno uporabo zdravila Aromasin in drugih zdravil proti raku ni. Ne sme se jemati sočasno z zdravili, ki vsebujejo estrogen, saj bi ta izničila njegovo farmakološko delovanje. **Vpliv na sposobnost vožnje in upravljanja s stroji:** Po uporabi zdravila je lahko psihofizična sposobnost za upravljanje s stroji ali vožnjo avtomobila zmanjšana. **Neželeni učinki:** Neželeni učinki so bili v študijah, v katerih so uporabljali standardni odmerek 25 mg na dan, ponavadi blagi do zmerni. ***Zelo pogosti (> 1/10):*** nespečnost, glavobol, vročinski oblivi, navzea, močnejše znojenje, bolečine v sklepih, mišicah in kosteh, utrujenost. **Način in režim izdajanja:** Predpisovanje in izdaja zdravila je le na recept zdravnika specialista ustreznega področja medicine ali od njega pooblaščenega zdravnika. **Imetnik dovoljenja za promet:** Pfizer Luksembourg SARL, 51, Avenue J. F. Kennedy, L-1855, Luksemburg. **Datum zadnje revizije besedila:** 31.8.2011
Pred predpisovanjem se seznanite s celotnim povzetkom glavnih značilnosti zdravila.

"SAMO ZA STROKOVNO JAVNOST"

ARO-01-12

Pfizer

Pfizer Luxembourg SARL, Grand Duchy of Luxembourg, 51, Avenue J.F. Kennedy, L-1855,
PFIZER, Podružnica za svetovanje s področja farmacevtske dejavnosti, Ljubljana, Letališka 3c, 1000 Ljubljana, SLOVENIJA

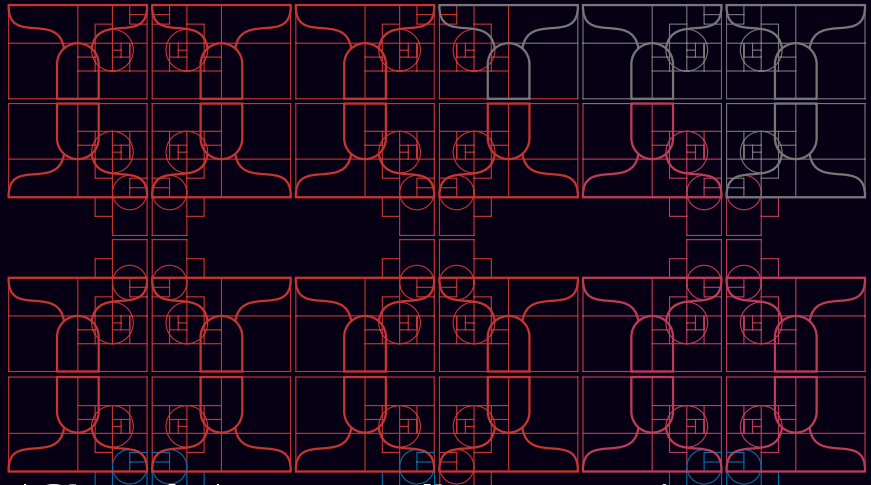

Radiology and Oncology | Ljubljana | Slovenia | www.versitaopen.com/ro

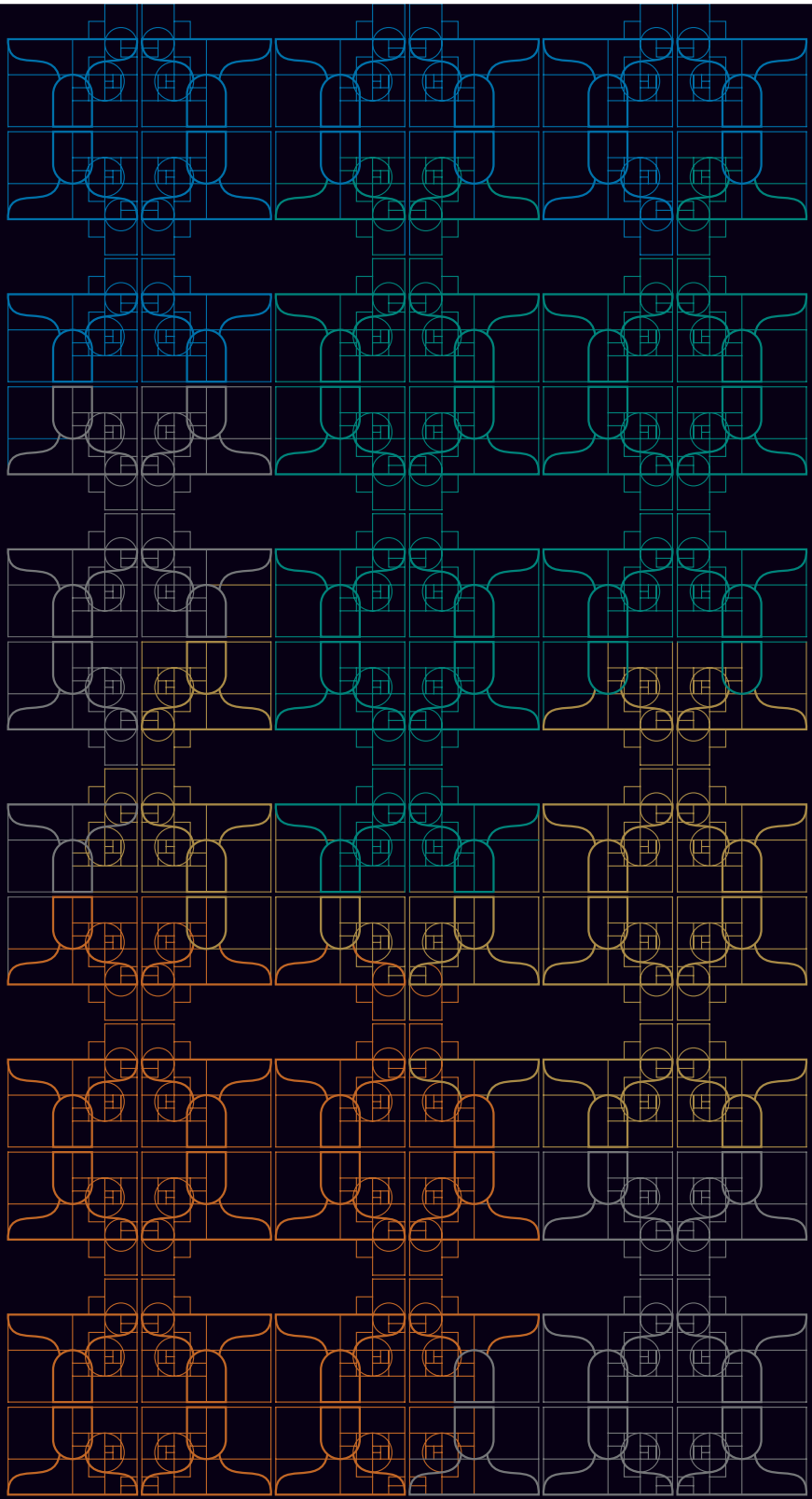

ISSN 1318 - 2099